

ES322 Geomorphology Fall 2023

Oregon Coast Field Trip

Mapleton-Florence-Sunset Bay-Scottsburg Loop

Tectonic Geomorphology - Seismic History - Coast Range Geomorphology

Steve Taylor, Ph.D.
Earth and Physical Sciences Dept.
Western Oregon University
Monmouth, OR 97361

Table of Contents

Adams (1984), Active Deformation of the Oregon Coast	1-7
McInelly and Kelsey (1990), Tectonic Deformation Cape Arago	8-22
Komar (1992), Ocean Processes and Hazards	23-26
Mitchell et al (1994) Vertical Deformation	27-31
Kelsey et al (1994) Coast Range Topography and Deformation	32-36
Kelsey et al (1996) Quaternary Plate Deformation in Oregon	37-42
Dariento and Peterson (1990), Tectonic Subsidence and Buried Marshes	43-49
Hart (1997), Buried Forests of Oregon	50-54
Armentrout (198X), Geologic Field Guide to Cape Arago-Coos Bay	55-64C

Class Notes and Exercises

Fluvial Notes	65-82
Paleoflood Hydrology, Fluvial Process	83-104
Soils and Mass Wasting	105-118
Surficial Mapping Methodology	119-122
Field Maps / Site Resources	
Geologic Map of Cape Arago / Garden Valley Areas	123
Cape Arago-Sunset Bay Maps	124-127
Garden Valley Maps	128-130A
Soil Survey Cape Arago / Coos County	131-157
Geomorphic Mapping Exercise (Sunset Bay)	158-163
Oregon Coast Tectonic Geomorphology Exercise	164-176
Conversion Charts	177-182
Blank Pages for Field Notes, Graph Paper	183+

ACTIVE DEFORMATION OF THE PACIFIC
NORTHWEST CONTINENTAL MARGIN

John Adams

Earth Physics Branch, Energy, Mines and
Resources, Ottawa, Canada K1A 0Y3

Abstract. Tilted and uplifted marine terraces in southern Oregon show progressive landward tilting of the coastal ranges at about $5 - 16 \times 10^{-8}$ rad. yr^{-1} for the last 0.25 m.y. Tide gauges in Washington and British Columbia, and ten resurveyed leveling lines running inland from the coast, indicate contemporary landward (down-to-the-east) tilt rates of about $1-12 \times 10^{-8}$ rad. yr^{-1} averaged over periods of from 10 to 50 years. The leveling lines traverse, and the terraces cut across, dipping Cenozoic strata: Pleistocene (dips to 3°), Miocene (dips to 30°) and Eocene (dips to 60°). Southern Oregon from Cape Blanco to the Siletz River shows geodetic or terrace tilting in the same direction as the underlying stratal dips. Hence present-day deformation continues past deformation of the coastal ranges and is most likely related to active subduction of the Juan de Fuca plate. The steep stratal dips, lack of major active faults and historic earthquakes, and presence of very young bedding-plane faults suggest that much of the onshore deformation and shortening within the overlying North American plate is taken up by folding rather than thrust faulting. Present shortening rates across

north-trending folds near the coast are between 0.02 and 1.9×10^{-7} yr^{-1} . The rate of shortening decreases rapidly eastwards from the Juan de Fuca - North American plate boundary. A total of about 25 mm yr^{-1} of permanent shortening could be occurring within the North American plate; most of it in the westernmost 40 km. The landward tilt and shortening rates are similar to those above many other subduction zones that have experienced great thrust earthquakes. While a high strain rate measured near Seattle, Washington, has been interpreted as elastic strain accumulation before a thrust earthquake, the low level of historic seismicity and the similarity of short- and long-term deformation rates suggest alternatively that the subduction beneath Washington is aseismic. The issue has considerable implications for seismic hazard evaluation in the Pacific Northwest and could be resolved by a search for the effects (or lack of effects) of prehistoric great earthquakes.

INTRODUCTION

The Pacific coast of Oregon and Washington lies close to the boundary between the North American and Juan de Fuca plates. South of Vancouver Island marine magnetic anomalies indicate present convergence at 35 mm yr^{-1} between the two plates [Riddihough and Hyndman, 1976; Riddihough, 1977]. The calc-alkaline vol-

Copyright 1984
by the American Geophysical Union.

Paper number 4T0560.
0278-7407/84/004T-0560\$10.00

canic rocks of the Cascade Range, the morphology of the sea floor and the deformation of young offshore sediments, all suggest subduction of the Juan de Fuca plate beneath the North American plate, but present-day underthrusting is unproven.

The case for active subduction has been well presented by Riddiough and Hyndman [1976], who explained the absence of a deep, well-defined Benioff Zone in terms of the low plate-convergence rate and the young age (and hence hot and more plastic nature) of the underthrust sea floor. Recently, Ando and Balazs [1979] showed a simple landward tilt for the Olympic Peninsula of northwest Washington from both repeated geodetic level surveys and tide gauge records. They compared the simple tilt with the well-documented and complex pattern of pre-, co-, and post-seismic movements observed in Japan, and interpreted the Washington data to indicate contemporary, though aseismic, subduction.

An earlier paper [Reilinger and Adams, 1982], closely related to the present one, analyzed leveling and tide gauge data for Oregon and Washington, showed that there was a well-defined landward tilting of the 600-km-long coastal ranges at about 3×10^{-8} rad. yr⁻¹ and noted that the tilting agreed with studies in progress on the deformation rate of marine terraces in Oregon (now published in the present paper). Although the agreement between long- and short-term deformation rates suggests that the subduction is occurring by aseismic creep as hypothesized by Ando and Balazs, recent measurements of horizontal deformation on northwest Washington, interpreted as elastic strain accumulation by Savage et al. [1981], seem to be incompatible with aseismic subduction. Further contemporary deformation studies seemed needed before the correct alternative--aseismic subduction, or subduction with large, infrequent thrust earthquakes--might be determined.

In this paper I describe coastal terraces in Oregon and Washington and quantify their deformation. By analysis of east-west geodetic leveling lines and tide gauge records I show that contemporary deformation rates are similar to the rates for the last 0.25 m.y. and by extrapolation of terrace tilts to the dip on the underlying strata that the pattern of deformation in the coastal ranges of the Pacific Northwest has remained substantially the same over the last half

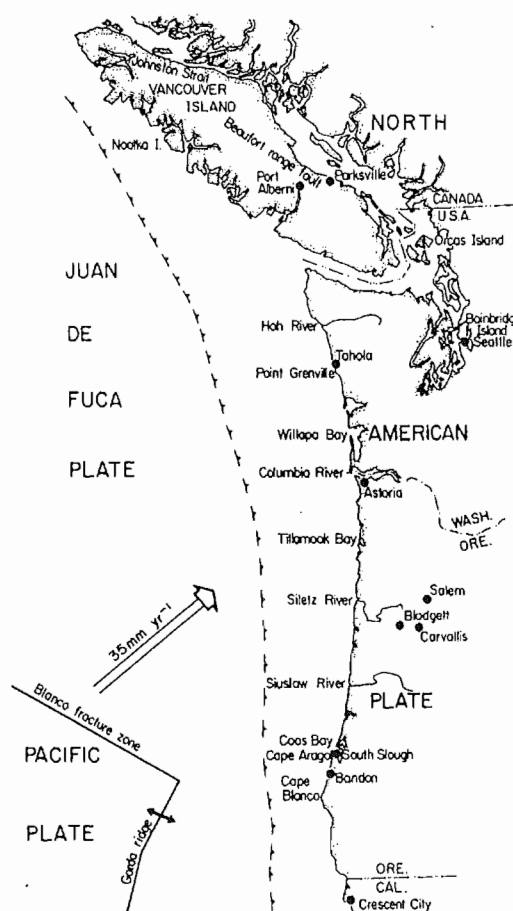


Fig. 1. Map of Pacific Northwest coast showing localities mentioned in the text, inferred trench position (broken barbed line), and compression vector representing motion of the Juan de Fuca plate relative to North America [Riddiough, 1977].

million years. Both the rates and the persistence of deformation patterns argue that subduction continues beneath Oregon and Washington despite the lack of shallow thrust earthquakes.

GEOMORPHIC EVIDENCE FOR LANDWARD TILT OF THE COASTAL RANGES

Marine Terraces in Oregon and Washington

Along much of the Oregon coast (Figure 1) there are emerged wave-cut surfaces and terraces that demonstrate coastal uplift. The highest and most spectacular terraces are to the south between Cape Arago and Cape Blanco, and have

TABLE 1. Uplift and Tilt of Marine Terraces Near Coos Bay, Oregon

Terrace	Assigned Age, yr	Elevation, ^a m	Eustatic Correction, m	Uplift ^a Rate, mm yr ⁻¹	Tilt, rad.	Average Tilt Rate, 10 ⁻⁸ rad. yr ⁻¹
A Cape Arago						
Metcalf	230,000	150	0	0.65	0.019	8
Seven Devils	124,000	85	-6	0.64	0.006	5
Pioneer	103,000	55	+15	0.68	0.005	5
Whisky Run	83,000	21	+13	0.41	0.004	5
B Trig 691						
Metcalf	230,000	230	0	1.0	0.037	16
Seven Devils	124,000	123	-6	0.94	0.017	14
Pioneer	103,000	44	+15	0.57	0.0098	10

^aRelative to sea level at longitude 124.376 degrees west.

of sea level rise approximates that of the land uplift, as is well explained by Bloom [1980]. In regions of slow uplift the youngest emerged feature is the Holocene (~6000 yr) bench, the next, the bench or benches that correspond to high sea levels about 100,000 yr (at 82,000, 103,000, and 124,000 yr ago), and above that a bench 230,000 yr old. In regions of more rapid uplift there may be additional benches cut during periods 28,000, 42,000 and 60,000 yr ago when sea level was relatively high but still lower than the present [Bloom et al., 1974].

Radiocarbon dating of wood and shells from the Whisky Run and Pioneer terraces near Bandon gives ages between 36,000 and 45,000 yr [Janda, 1972, p. 63], but are probably minimum ages. A more definite age for the Whisky Run terrace at Bandon is a Th/U date of $72,200 \pm 5300$ yr on solitary corals [Kennedy et al., 1982]; G.L. Kennedy (personal communication, 1982) infers the terrace to represent the 82,000-yr sea level maximum. This plausible age of 82,000 yr for the Whisky Run and consideration of the known sea level history leads to the following ages for the terraces near Cape Arago: Whisky Run, 82,000; Pioneer, 103,000; Seven Devils, 124,000; and Metcalf 230,000 years. When these ages are applied to the tilted terraces near Cape Arago, they indicate approximately constant tilt and uplift rates for the last 230,000 years (Table 1), a geologically reasonable result given the tectonic environment.

At Cape Blanco, Cl^{37} and Th/U dating

of shells on the main wave-cut surface (widely considered to correlate with the Pioneer, e.g., Beaulieu and Hughes [1976]), gave ages of 35,000 yr, but in view of carbonate-closure problems supply only a minimum age [Richards and Thurber, 1966]. More recently, Wehmiller et al. [1977] have determined an amino acid racemization date of $50,000 \pm 20,000$ yr for shells from the same place, considered the terrace to represent either the 42,000 or 60,000 yr sea level maxima of Bloom et al. [1974], and hence calculated an uplift rate of either 2.75 or 1.5 mm yr⁻¹. If the dates for both the Whisky Run and main Cape Blanco terrace are correct, the Blanco terrace cannot correlate with the Pioneer as widely thought, but must instead represent a post-Whisky Run terrace.

Above the main terrace at Cape Blanco, there are three named terraces: the Silver Butte (about 60 m elevation), the Indian Creek (170 m), and the Poverty Ridge (270 m) [Janda, 1972; Beaulieu and Hughes, 1976]. It is not possible to assign terrace ages unambiguously, but the elevations and Janda's [1972] correlation of the Indian Creek and Seven Devils terraces are more consistent with a 60,000 yr age for the main Blanco terrace rather than 42,000 yr.

The present uncertainty in the absolute ages of the terraces at Cape Arago and at Cape Blanco does not detract from the evidence they provide for progressive tilting and uplift. At worst, the adopted ages could be wrong by a factor of 2 (e.g.,

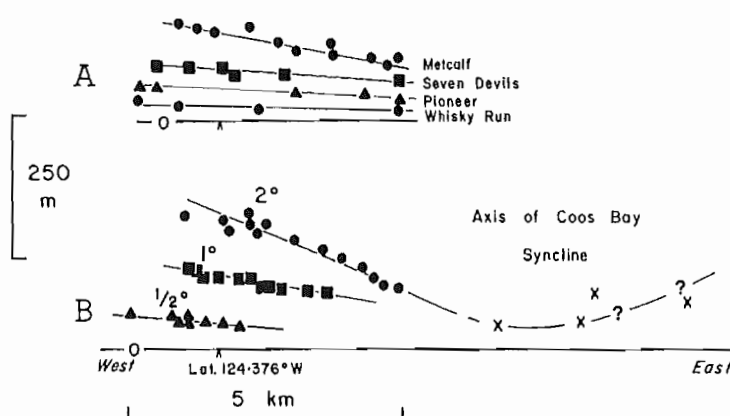


Fig. 3. East-west cross section of terrace elevations north (A) and south (B) of Cape Arago showing the landward tilt of the terraces and demonstrating the progressive nature of the deformation. Elevations are of the terrace surface and not the wave-cut platform and are taken from Griggs [1944, plate 42]. Note that individual terraces cannot be distinguished on the east side of South Slough, but the highest remnants appear to rise above sea level on the east flank of the Coos Bay Syncline.

the youngest plausible age for the Whiskey Run terrace is 42,000 yr) and so the derived rates, even if in error by this factor, still represent rapid deformation.

Landward Tilting of Marine Terraces, Coastal Oregon

Because the Oregon coast is nearly parallel to the subduction trench, there are only a few places where irregularities allow marine terraces to demonstrate tilting normal to the trench.

Wave-cut surfaces that form today in California have an initial seaward slope of 0.3° – 1.0° [Bradley and Griggs, 1976], and it is therefore likely that the newly emerged wave-cut surfaces in Oregon had similar seaward slopes. Hence their present landward tilt represents not only tilting from the horizontal but also back-tilting of the initial seaward slope. For an initial seaward slope of 0.3° , surfaces of 42,000, 60,000, 100,000 and 230,000 years would need to be tilted landward at 12 , 8 , 5 , and 2×10^{-8} rad. yr^{-1} , respectively, to be horizontal, and any present tilt in the landward direction increases the total tilt rate. Therefore tilt rates calculated assuming a horizontal surface may be low by a factor of 2 or more, the error being greatest for the youngest terraces. The seaward slope correction applies only to surfaces cut

across wide platforms parallel to the tilt direction and is not applicable at Cape Arago because those platforms were cut perpendicular to the tilt direction. At Cape Blanco, however, the main terrace is 6 km wide, probably 60,000 years old, and cut parallel to the tilt direction, so that although it has a landward tilt of 0.10° (see map of Cape Blanco in the work of Beaulieu and Hughes [1976]), and also Janda [1972, p. 48], the total amount of landward tilting, including removal of an initial seaward tilt, could be as much as 0.4° , corresponding to a mean tilt rate of 11×10^{-8} rad. yr^{-1} .

The terraces near Cape Arago have a distinct landward (down-to-the-east) dip [Baldwin, 1966]. For example, Janda [1972, p. 28] gives the elevation of the Whiskey Run wave-cut surface at Cape Arago as 29 m, but as less than 5 m at Charleston, 5.5 km to the east. Ideally, the elevation of the wave-cut surface for every terrace should be plotted against distance normal to the trench, but, in general, only the elevations of the terrace cover beds are known. The terrace cover beds lie on the wave-cut surface and may be 15–20 m thick; to determine tilt of the terraces from elevation of the cover beds, it is necessary to assume that their thickness is constant. When terrace elevations (taken from Griggs [1945, plate 42]) are plotted as two east-west pro-

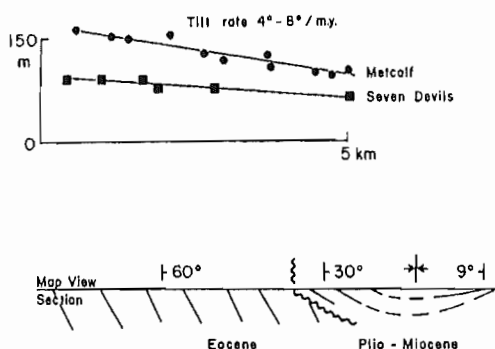


Fig. 4. Relationship between tilted marine terraces (top) and underlying geologic structure (bottom), Coos Bay Syncline, Oregon. The terraces are tilted down toward the axis of the syncline.

files, one north (A) and one south (B) of Cape Arago, they show simple eastward tilt with the amount of tilt being greatest for the oldest and highest surface (Figure 3). The simple pattern for each surface suggests that in each case a single surface has been identified (Table 1).

For the oldest surface, the maximum dip is about 2° on profile B. From an assigned age of 230,000 years, the average landward tilt rate is 16×10^{-8} rad. yr $^{-1}$ (9° per million years). Profile A gives 8×10^{-8} rad. yr $^{-1}$, and both profiles indicate progressive tilting of surfaces of successive age. Two further profiles (not shown) to the south give rates of 6 and 7×10^{-8} rad. yr $^{-1}$ from the tilt of the Metcalf terrace. A few kilometers to the south of all four profiles a geodetic tilt rate of $(12 \pm 7) \times 10^{-8}$ rad. yr $^{-1}$ between Bandon and Coquille (see below) suggests that tilting in the region has continued at substantially its present rate for 230,000 years.

The easterly tilting of the Cape Arago terraces is related to the tightening of the underlying north trending syncline (Figure 4). Volume constraints require bedding-plane slip during the tightening of folds, the fault throws being opposite in sense to the tilt trend (Figure 5). Hence the apparently smooth landward tilt of the terraces shown in Figure 3 may in fact be interrupted by successive faults.

Youthful Faulting in the Coastal Ranges

Faults with throws of less than 10 m would not show on the 50-foot contour interval map [Griggs, 1945, plate 42] used

to construct Figure 3, but are observed in the coastal section east of Cape Arago where there has been an extensive study of the structure and stratigraphy of the Coos Bay Coalfield. Fault displacements probably occur at many places on terraces throughout coastal Oregon and Washington but have been inadequately studied.

At Mussel Reef (Yokam Point), near Cape Arago, a reverse bedding-plane fault which dips east at 70° displaces the Whisky Run terrace surface by 5 m, west side down [Baldwin, 1966, p. 199]. Across Sunset Bay, the Whisky Run Terrace is 6 m lower to the east than the west and may well be offset by a concealed fault [Beaulieu and Hughes, 1975, p. 43]. A further fault has displaced the wave-cut platform by a meter and formed a ridge on the sand [Allen and Baldwin, 1944, p. 40].

At the Seven Devils Mine, on the Seven Devils terrace and 8 km southeast of Cape Arago, a southeast-striking fault in the terrace cover beds displaces the bedrock by more than 3 m, with the northeast side being upthrown [Griggs, 1945]. Along the Whisky Run terrace north of Bandon there are several offsets in the Eocene bedrock, and faulting of the terrace is illustrated by Murphy et al. [1979]. The illustrated fault is one of several faults within the cover beds of the Whisky Run terrace. It strikes $N42^\circ W$, dips $30^\circ W$ and has 0.3 m of thrust displacement (P.J. Murphy, Stone and Webster Corp., written communication, 1981).

Further south at Cape Blanco, Dott [1971, p. 52, 56] notes "youthful

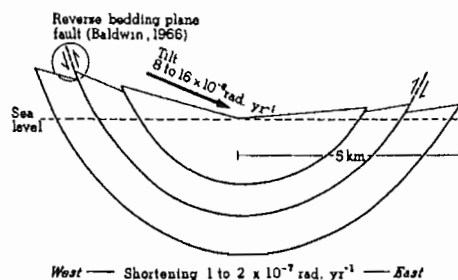


Fig. 5. Schematic cross section across the Coos Bay Syncline showing slip on reverse bedding-plane faults as a consequence of compression across the syncline. Tilt on the flanks is superimposed on a lesser landward tilt (see Figure 9) and produces greater uplift on the western (Cape Arago) flank than on the eastern flank.

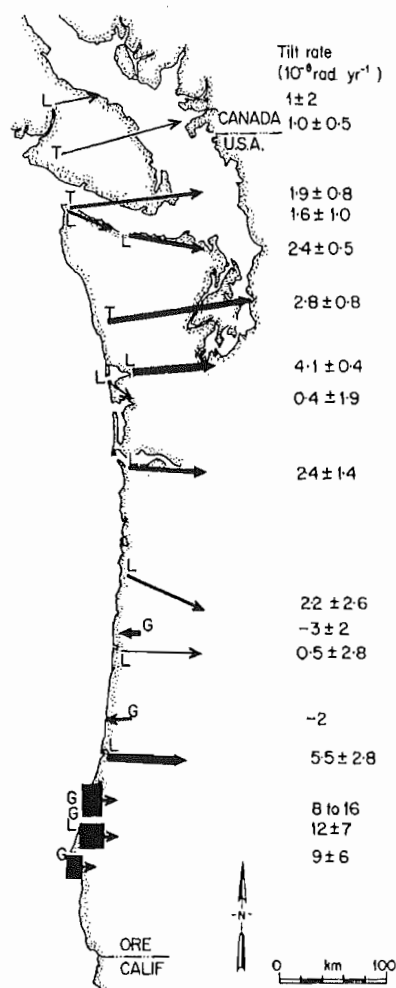


Fig. 10. Summary of tilt rates and directions derived from geodetic, tide gauge, and terrace deformation data. Arrow lengths represent spatial extent of data, arrow widths represent magnitude of tilt rate. Negative rates represent seaward tilting. Letters beside arrows represent nature of evidence for rate: G, geomorphic, L, leveling, T, tide gauge. Note the consistent direction and similar magnitude of tilting in the coast ranges. The exceptions are the short coastal profiles in the south, which are controlled by local structure.

most cases fortuitous and need not represent the true tilt direction, they are uniformly down to the east, and overall suggest an easterly or east-northeasterly tilt. Further, although the rates are determined for periods as short as 10 yr and as long as 230,000 yr, there are no

serious differences in magnitude among them. The rates are most rapid in the south where they are determined for the flanks of individual folds, but where they span the entire width of the coast range the rates are consistently about 3×10^{-8} rad. yr^{-1} south of Vancouver Island, and on rather scant evidence perhaps half that rate to the north. The general agreement between the rates and their consistency with stratal dips and geologic structure suggest that deformation has continued in the coastal ranges at the contemporary rate for about the last half million years; the rates are similar to those observed near other active subduction zones that are associated with earthquakes.

ONSHORE LANDWARD TILTING AND ITS RELATION TO SUBDUCTION ELSEWHERE

Landward tilting of the coastal ranges is a distinctive component of onshore deformation in the Pacific Northwest, and similar tilting occurs adjacent to subduction zones elsewhere. Away-from-trench tilting is usually easily documented for island arcs, as the islands have shorelines that are normal to the trench. Thus tilting has been established for the Ryukyu Islands [Ota and Yoshikawa, 1978], and for the New Hebrides [Taylor et al., 1980]; rate about 10×10^{-8} rad. yr^{-1} .

Landward tilting of coastal ranges is commonly more difficult to quantify as the coasts themselves are parallel to the trench, and measurements must be made at fortuitous places where peninsulas or reentrants occur. Thus in Costa Rica, landward tilting across the Nicoya Peninsula is indicated by drowned shorelines to the east and elevated terraces to the west [Alt et al., 1980] and by bioerosion morphology on coastal platforms [Fischer, 1980]. In Chile, marine terraces on the Arauco Peninsula and adjacent islands are tilted 1° - 3° down the east (landward) at inferred rates of 5 to 60×10^{-8} rad. yr^{-1} [Kaizuka et al., 1973, Table 3]. The landward tilt rate from the terraces is very nearly the same as the rate of 10 - 40×10^{-8} rad. yr^{-1} deduced from the uplift pattern caused by historic earthquakes and their probable frequency.

The North Island of New Zealand is being obliquely underthrust by the Pacific plate at 50 mm yr^{-1} [Cole and Lewis, 1981] and the complexity of deformation decreases along the east coast

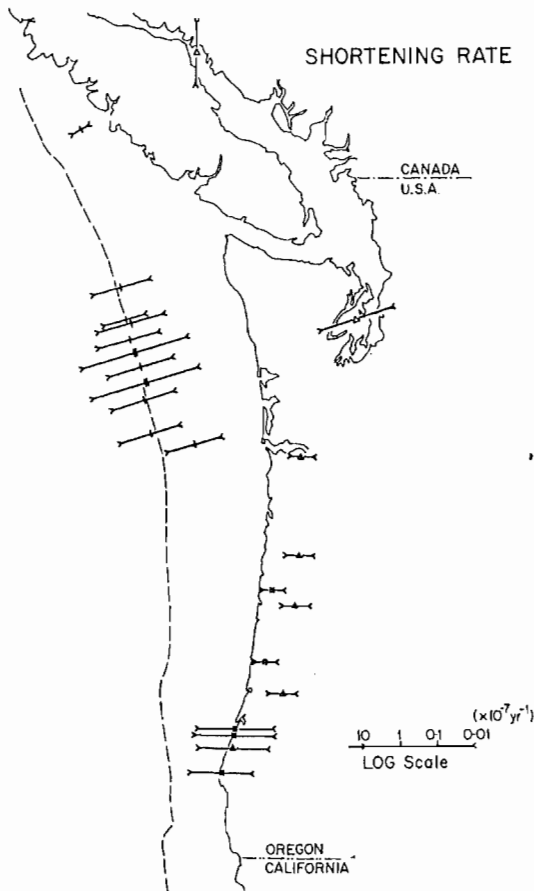


Fig. 11. Summary of contemporary shortening rates and directions derived from trilateration (open triangles), leveling (filled triangles), terrace tilting (squares), stratal folding (single bars), folding and faulting (double bars) as discussed in the text. In order to plot the large range of rates, arrow lengths are proportional to the logarithm of the rate.

The straight line on Figure 12 represents an exponential decay of shortening rate away from the plate boundary. Obviously, the exact decay relationship is poorly defined, but the one on the figure is equivalent to total shortening across the margin of 25 mm yr^{-1} , 80% of which occurs in the most westerly 40 km. The total shortening rate could be a sizeable fraction of the plate convergence rate. For the slope, shelf, and the immediate coast, the young geologic structures indicate contemporary shortening in a direction approximately parallel to the

Juan de Fuca-North American plate compression vector.

SHORTENING AND STRESS DIRECTIONS IN THE PACIFIC NORTHWEST

For the central part of the Pacific Northwest continental margin, the analysis of magnetic anomalies indicates relative convergence between the Juan de Fuca and North American plates of 35 mm yr^{-1} along $N50^\circ E$, or 32 mm yr^{-1} normal to the continental margin [Riddiough, 1977]. The convergence rate has decreased sharply in the last 4.5 m.y. Two fragments of the Juan de Fuca plate appear to be moving independently of the main plate. North of the Nootka Fault Zone, the Explorer plate is moving $N6^\circ E$ at 19 mm yr^{-1} relative to North America and 14 mm yr^{-1} normal to the Vancouver Island continental margin [Riddiough, 1977]. South of $42^\circ N$ the Gorda plate is moving north, parallel to

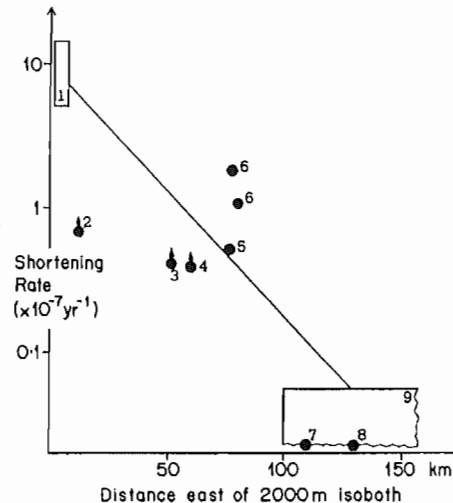


Fig. 12. Composite profile of shortening rate eastwards from the Juan de Fuca-North American plate boundary (represented by the 2000 m isobath). Note logarithmic scale. Straight line (with equation $y = 10^{-6} \exp(-0.04 x)$) represents suggested rapid decay of shortening rate eastwards. Data are 1, folding and thrusting of marginal folds [Barnard, 1978]. 2, folding of marginal folds [Carson et al., 1974]. 3, folded unconformity on shelf. 4, tilted terrace at Cape Blanco. 5, leveling near Bandon. 6, tilted terraces at Cape Arago. 7, terrace on Siuslaw River. 8, terrace on Siletz River. 9, range of values for leveling across coast ranges.

7

Late Quaternary Tectonic Deformation in the Cape Arago-Bandon Region of Coastal Oregon as Deduced From Wave-Cut Platforms

GALAN W. MCINNELLY¹ AND HARVEY M. KELSEY

Department of Geology, Western Washington University, Bellingham

The Cape Arago region of south central Oregon sits on the upper plate of the Cascadia subduction zone about 80 km east of the base of the continental slope. The style of late Pleistocene deformation along the Cascadia forearc near Cape Arago is well expressed by the altitudinal variation of a set of five uplifted wave-cut platforms. These platforms record open folding, with a half wavelength of about 6-7 km, as well as late Quaternary offset on flexural-slip reverse faults that parallel bedding in the underlying bedrock. The folds have produced both landward and seaward tilts to the uplifted wave-cut platforms. Because the folds cut obliquely across the coastline, the magnitude of coastal uplift is variable. In the case of the lowest, 80 ka wave-cut platform, this variable uplift has resulted in coastal deformation ranging from subsidence to a maximum uplift rate of 0.8 m/kyr. Quantitative analysis of the mechanism of flexural slip folding for the South Slough syncline near Cape Arago indicates that the late Quaternary strain rate has decreased in the last 200 kyr. Evidence of past great subduction-style earthquakes, such as regional uplift and regional landward tilting of wave-cut platforms, or regional submergence of coastlands, is lacking in the Cape Arago region. Instead, the deformational style is controlled by folding. Though localized folding is dominant, the occurrence of great subduction-style earthquakes is not precluded because localized folding could occur concurrently with regional coseismic deformation.

INTRODUCTION

Late Pleistocene marine terraces, formed by wave abrasion during interglacial and interstadial eustatic high stands of sea, are preserved in several localities along the Cascadia forearc [Griggs, 1945; Adams, 1984; West and McCrumb, 1988; R. J. Janda, Field guide to Pleistocene sediments and landforms and soil development in the Cape Arago-Cape Blanco area of Coos and Curry Counties, southern coastal Oregon, Friends of the Pleistocene, hereinafter referred to as unpublished guidebook, 1970]. Such platforms represent spatial and temporal reference surfaces from which the style, rates, and mechanisms of supracrustal tectonic deformation may be deduced [Lajoie, 1986].

One of the best areas within the Cascadia forearc for analysis of tectonic deformation of marine terraces is the Cape Arago region of southwestern Oregon (Figure 1). At Cape Arago a flight of five marine terraces, four of which are extensively preserved, have been uplifted and deformed [Griggs, 1945; Baldwin, 1945, 1966; Lund, 1973; Ehlen, 1967; Beaulieu and Hughes, 1975; Armentrout, 1980; Adams, 1984; R. J. Janda, unpublished guidebook, 1970]. Cape Arago is 52 km north of Cape Blanco in the southern portion of the Cascadia subduction zone and lies within 80 km east of the Cascadia trench (Figure 1, inset). The three youngest terraces at Cape Arago are the Whisky Run, Pioneer, and Seven Devils terraces, respectively [Griggs, 1945]. The fourth terrace is the Metcalf terrace [Adams, 1984]. The fifth and oldest terrace is herein informally designated as the Arago Peak terrace.

The marine terraces are cut into sediments that range in age from Eocene to Pliocene [Baldwin, 1966; Armentrout, 1980]. Most of the rocks are part of an Eocene and Oligocene

overlap assemblage in the Oregon coast ranges and consist of arkosic sandstones, siltstones, and mudstones. Sediments of the "Miocene beds" and the Pliocene Empire Formation [Armentrout, 1980] overlie the Eocene and Oligocene bedrock on the margins of Coos Bay near Charleston.

The northern portion of the study area (Figure 1) is underlain by the north plunging South Slough syncline. The syncline is an asymmetric fold, steeper on the west limb, with an axis that coincides with South Slough [Baldwin, 1966] (Figures 1 and 2). Initiation of folding began at least by pre-Miocene time based on the angular discordance between Oligocene and Miocene sediments [Armentrout, 1980; Baldwin, 1966].

On the basis of marine terrace tilting and geodetic leveling surveys, Adams [1984] reported shortening rates of as much as 25 mm/yr within the westernmost continental margin in the vicinity of Cape Arago. Adams [1984] suggested that the eastward (landward) tilt of the terraces at Cape Arago is, in large part, due to progressive tightening of the underlying South Slough syncline. On the basis of volumetric considerations of a growing fold, Adams predicted interruptions of the smooth eastward tilt of the Cape Arago terraces by successive bedding-plane flexural-slip faults. One such bedding-plane fault displaces the Whisky Run terrace platform at Yoakam Point [Baldwin, 1966; Adams, 1984] (Figure 2).

The purpose of our paper is to document late Pleistocene and Holocene deformation along the Cascadia subduction zone in the Cape Arago to Bandon portion of the Oregon coast (Figure 1). We analysed deformation by mapping the distribution, structure, and altitudinal variation of uplifted wave-cut platforms. In light of the uncertainty surrounding the response of the Cascadia forearc to subduction [Heaton and Kanamori, 1984; Atwater, 1987; Spence, 1989] the distinction between a deformation event restricted to a few folds near Cape Arago and a more regional deformation event that includes local folds is significant. Therefore a second purpose of our paper is to comment on the role of local folds in subduction tectonics, using the late Quaternary

¹Now at Geo Engineers, Bellevue, Washington.

Copyright 1990 by the American Geophysical Union.

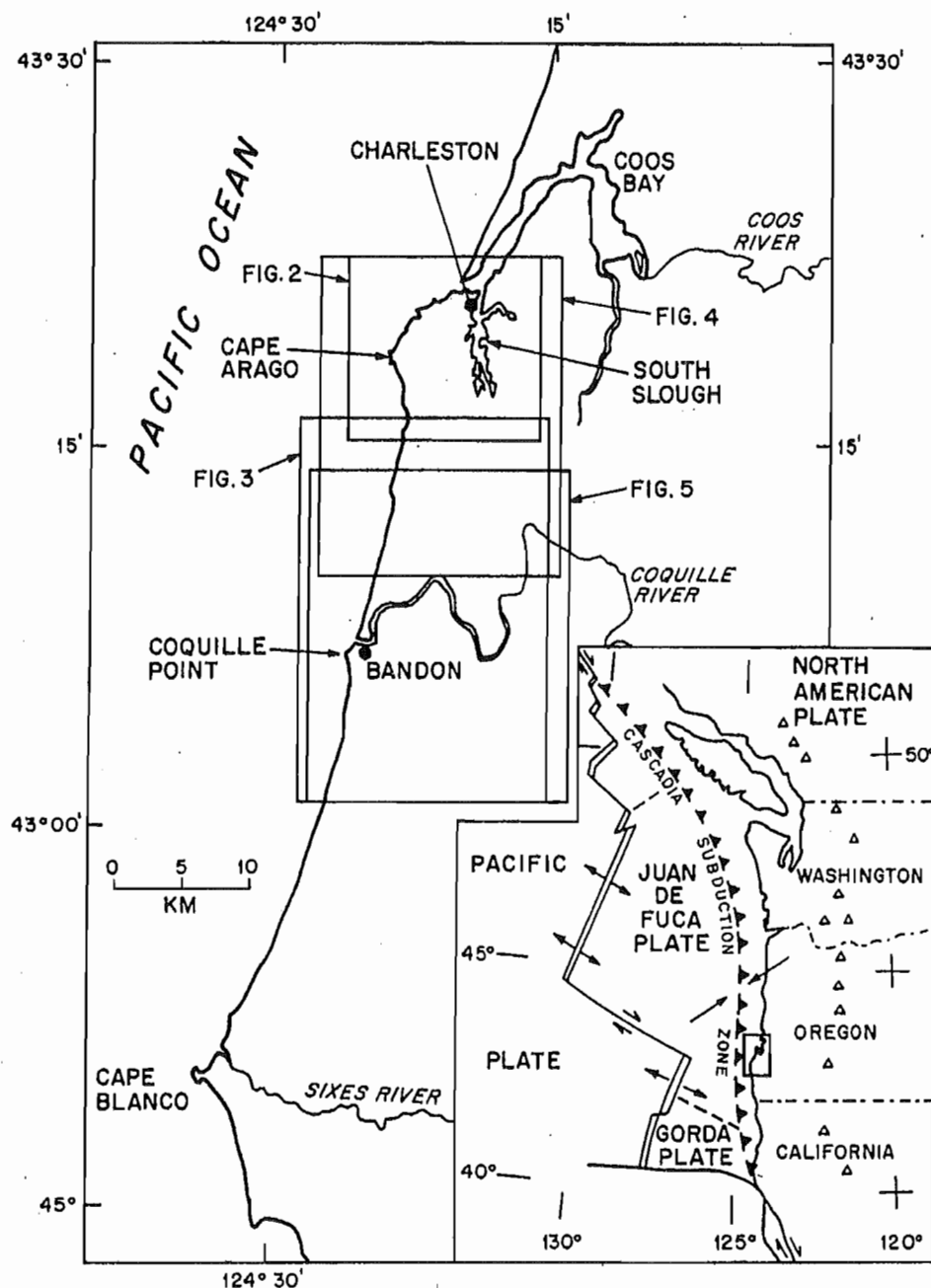


Fig. 1. Location map of the study area (boxes locate Figures 2-5) within the context of the regional tectonic setting of the Pacific Northwest and the Cascadia subduction zone (inset). Triangles are volcanoes of the Cascade Range.

folds in the Cape Arago-Bandon region as a basis of discussion.

DISTRIBUTION OF MARINE TERRACES

We differentiated marine terraces on the basis of elevation and degree of erosional dissection. Marine terrace distribution in all cases except for the area immediately east of South Slough closely follows terrace distribution as originally mapped by Griggs [1945]. For these terraces, platform elevations were obtained by altimeter survey (error of ± 2 m) or well log data (error of ± 6 m). All altimeter surveys were closed on either a U.S. Geological Survey bench mark or point of known altitude. We obtained platform altitudes along the coast exclusively by altimeter survey. Quantitative

analysis of uplift history and strain rate (see below) used only elevation data obtained by the more accurate altimeter method.

East of South Slough, marine terraces were previously undifferentiated. In this area we mapped terrace distribution exclusively by aerial photograph interpretation. With the exception of coastal exposures we obtained relatively limited and poorer quality platform altitude data in this area.

The four younger terraces (Whisky Run, Pioneer, Seven Devils, and Metcalf) are regionally extensive and extend from Coos Bay to about 12 km south of Bandon (Figures 2 and 3). Highly dissected remnants of the fifth and oldest terrace (Arago Peak terrace) are found only at higher elevations on the Cape Arago headlands (Figure 2). The terrace

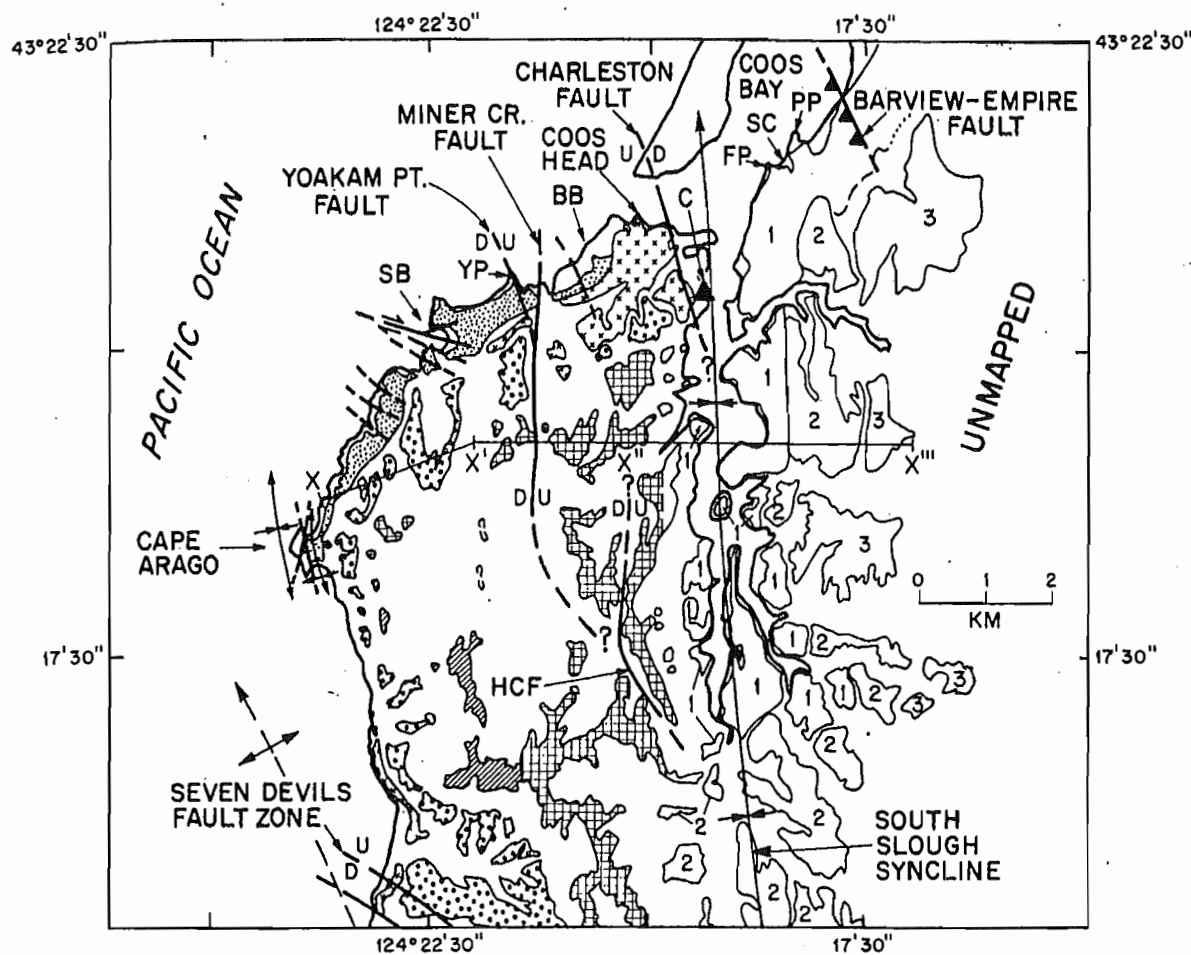


Fig. 2. Map showing distribution of late Pleistocene marine terrace sediments for the five uplifted surfaces in northern portion of study area. Map units for cover sediments on Quaternary wave-cut platforms: solid circles, Whisky Run; crosses, Pioneer; open circles, Seven Devils; checked pattern, Metcalf; diagonal shading, Arago Peak. Map units for cover sediments on Quaternary wave-cut platforms east of South Slough: 1, lowest surface; 2, middle surface; 3, upper surface. SB, Sunset Bay; YP, Yoakam Point; BB, Bastendorff Beach; CH, Coos Head; C, Charleston; FP, Fossil Point; SC, Stinky Cove; PP, Pigeon Point; HCF, Hayward Creek fault. Onshore structural data in part from Baldwin [1966], Ehlen [1967], R. J. Janda (unpublished guidebook, 1970), and Armentrout [1980]. Offshore data from Newton *et al.* [1980] and Clarke *et al.* [1985].

surfaces are moderately to well dissected in the northern portion of the study area (Figure 2). In contrast, in the southern portion of the study area the lower three terraces form a relatively undissected, broad coastal plain at lower elevations (Figure 3).

The Whisky Run and Pioneer terraces are younger and therefore, in general, better preserved than the Seven Devils and Metcalf terraces (Figures 2 and 3). Between Cape Arago and Charleston the Whisky Run terrace forms a prominent, nearly continuous surface.

We recognize three distinct surfaces to the east and northeast of South Slough (Figure 2). Individual surfaces are less apparent because relatively low uplift rates east of the South Slough syncline have minimized spacial separation of Pleistocene wave-cut platforms [Adams, 1984]. There is presently no basis, other than altitude, for correlation of these surfaces with surfaces across South Slough to the west.

We follow previous workers and tentatively correlate the lowest surface east of South Slough with Whisky Run terrace [Baldwin, 1966; R. J. Janda, unpublished guidebook,

1970]. However, the presence of the Charleston fault (Figure 2) raises the possibility that the platform underlying this lowest surface may be correlative with the Pioneer platform. Alternatively, the platform may have been cut in Pioneer or Seven Devils time and reoccupied by the Whisky Run eustatic sea level high stand. We retain the Whisky Run terrace designation for the lowest surface but acknowledge that the surface may be older than Whisky Run.

Marine cover sediments of the Metcalf, Seven Devils, Pioneer, and Whisky Run terraces vary in thickness from about 2.5 to 20 m (Table 1). Sediments on terraces in the Cape Arago area are generally no thicker than about 6 m, although the sediments of the Pioneer terrace are about 15 m thick near Coos Head (Figure 2). South of the Cape Arago headland, sediment thicknesses for the three lower terraces increase to about 20 m. The variation in sediment thickness on the modern wave-cut platforms in the Cape Arago area is consistent with the variation in sediment thickness on late Pleistocene wave-cut platforms, as described by Peterson *et al.* [1987]. The present coastline to the northeast of the Cape Arago headland is generally stripped of sand, while beaches

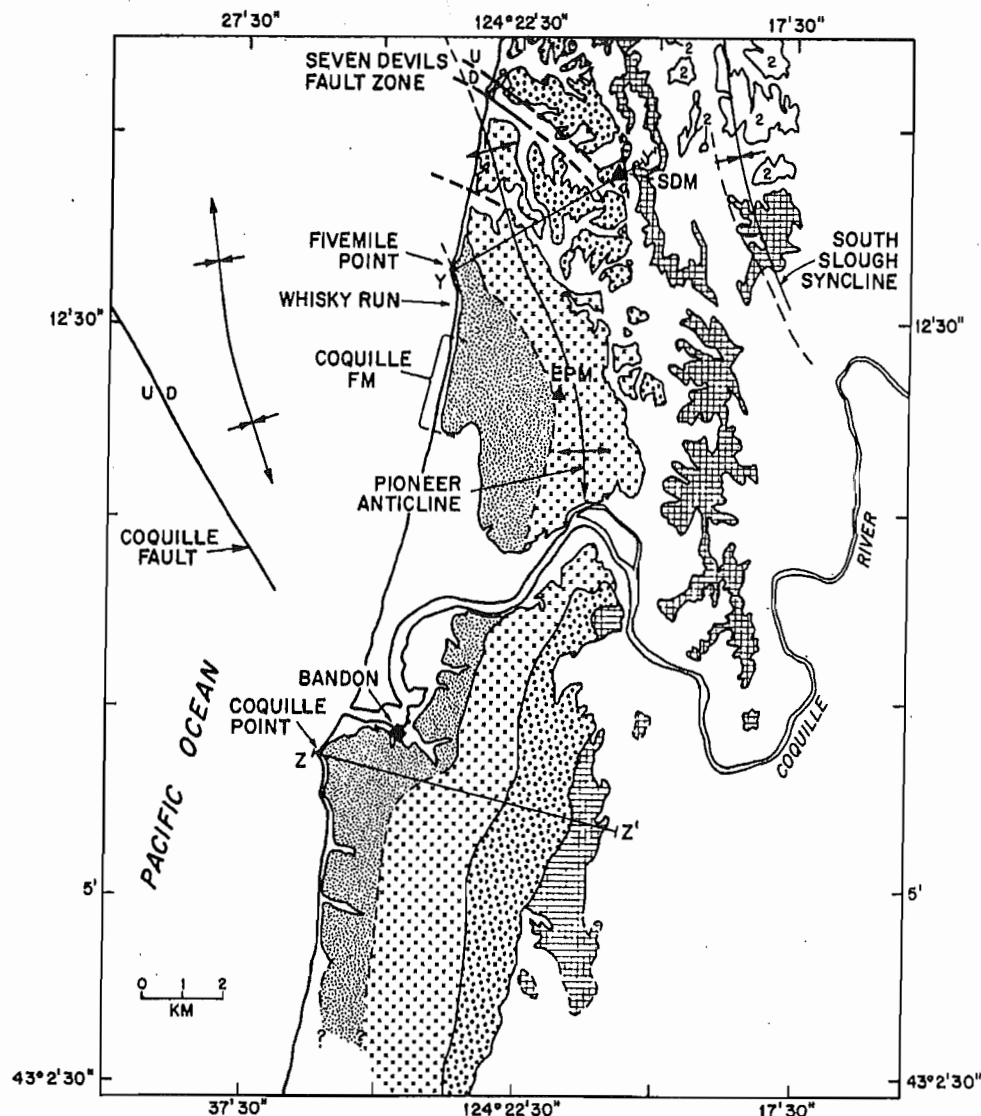


Fig. 3. Map showing distribution of late Pleistocene marine terrace sediments for the four extensively preserved surfaces in southern portion of study area. For explanation of map units, see caption for Figure 2. Triangles locate placer mines: SDM, Seven Devils Mine; EPM, Eagle-Pioneer Mine. Offshore data from Newton *et al.* [1980] and Clarke *et al.* [1985].

to the south of the headland have relatively thick accumulations of sand; cover sediments on the uplifted terraces show the same pattern.

DEFORMATION OF WAVE-CUT PLATFORMS

Overview

Differential uplift of wave-cut platforms along the coast reflects late Quaternary folding and faulting of the underlying bedrock. Platforms west of South Slough rise to the southwest from Coos Head to maximum elevations in the vicinity of Cape Arago, where the oldest platform is uplifted to 212 m (Figures 2 and 4). The platforms also descend gradually to the south from Cape Arago and reach elevation minimums 12–15 km south of Bandon (Figures 4 and 5). The Whisky Run platform descends from a high point at Cape Arago (35 m) to sea level just north of the Coquille River (Figures 4 and 5). South of the Coquille River, the Whisky Run platform is

again emergent and again descends to sea level near the southern boundary of the study area (Figure 5).

East of South Slough, terrace cover sediments have been uplifted to about 90 m [Griggs, 1945]. The terrace surfaces slope toward South Slough (Figure 6).

Deformation Associated With South Slough Syncline

Evidence for late Quaternary growth of the South Slough syncline comes from the more steeply dipping and better exposed west limb. On the west limb, wave-cut platforms are back tilted from initial seaward dips of about 1° (seaward dip estimate from Bradley and Griggs [1976]). The back tilted platforms dip toward the axis of the syncline [Griggs, 1945; Adams, 1984; R. J. Janda, unpublished guidebook, 1970]. On the basis of platform elevation data (Figure 4) the Metcalf platform dips about N60°E (downdip) with a slope of 1.0° between Cape Arago and Charleston. The relative north versus east component of tilt for the Seven Devils, Pioneer,

11

TABLE 1. Characteristics of Marine Terraces: Cape Arago Region

Terrace	Radiometric Age, ka	Preservation and Occurrence	Platform Elevation Range, m	Backedge Elevation Range, m	Terrace Sediment Thickness, m	Faults Cutting Terrace Platforms
Whisky Run	80 ^a	well preserved, regionally extensive	0-35	0-31	3-20	Miner Creek Yoakam Point Bastendorf Beach Barview-Empire Sunset Bay Coquille (?)
Pioneer	...	well preserved, regionally extensive	5-60	15-60	4-20	Miner Creek Charleston Yoakam Point (?) Sunset Bay (?)
Seven Devils	...	well preserved, regionally extensive, moderately dissected	43-104	50-91	3-18	Miner Creek Seven Devils
Metcalf	...	moderately well preserved, regionally extensive, highly dissected	87-167	169-?	3-16	Miner Creek Hayward Creek
Arago Peak	...	poorly preserved, extremely limited, highly dissected	212	?	17 (?)	?

^aMuhs et al. [this issue] and Kennedy et al. [1982].

and Whisky Run terraces cannot be resolved from the spatial distribution of altitude data. However, these data are consistent with a N60°E tilt direction (Figure 4). Altitude differences between Cape Arago and the Coos Head-Charleston area for the Metcalf, Seven Devils, Pioneer, and Whisky Run platforms are 82, 47, 36, and 16 m, respectively. The increasing altitudinal difference documents the progressive tilting of the west limb of the syncline in the late Pleistocene.

On the west limb of the syncline, bedding-plane, flexural-slip faults parallel to the bedding planes of the underlying folded strata offset the wave-cut platforms up to the east (Figures 6 and 7). The structural blocks defined by these faults are rotated down to the east and movement on these faults accommodates strain during tightening of the syncline [Adams, 1984; McInnelly et al., 1989]. Three bedding-plane faults cut the Whisky Run platform east of Sunset Bay (Figures 4 and 7). Vertical displacements of the Whisky Run platform on the Yoakam Point [Baldwin, 1966], Miner Creek, and Bastendorf Beach faults are 4, 5, and 4 m, respectively. Flexural-slip faults also cut the Metcalf and/or Seven Devils platforms (Figures 2, 4, and 6) (Table 1). Minimum vertical displacements of the Metcalf wave-cut platform are 25 and 6 m for the Miner Creek (Figure 6) and Hayward Creek faults, respectively. A possible third bedding-plane fault may offset the Seven Devils platform by as much as 12 m (Figure 6, segment X-X').

The Charleston fault (Figure 4) displaces the Pioneer platform by 19 m in a down-to-the-east sense of displacement. Compared to other faults west of South Slough, the Charleston fault has an opposite offset sense, cuts across bedding planes of the Tertiary bedrock and is steeply dipping to subvertical. The main fault plane is not exposed, but mesoscale faults directly adjacent to the main fault are steeply dipping, conjugate normal faults. On the basis of a mapped trend of N15°W, the Charleston fault may be the onshore extension of one of a group of north-northwest trending, up-to-the-west faults that deform seafloor sediments northwest of Coos Bay [Clarke et al., 1985].

The Charleston fault appears to be a more regionally significant fault than the neighboring flexural-slip faults. The fault separates steeply dipping (40°-70°) beds on the west limb of the South Slough syncline from gently dipping (12°-30°) beds on the east limb. In addition, the fault has displaced the Whisky Run wave-cut platform such that if this platform is projected eastward across the Charleston fault to the axis of the South Slough syncline, the platform is approximately 20 m above sea level. In the absence of offset and tilt due to the Charleston fault the Whisky Run platform would probably project below the level of South Slough. The 19 m offset on the Charleston fault may be therefore younger than the Whisky Run platform.

Holocene Deformation on the Shores of Outer Coos Bay

The eastern shoreline of outer Coos Bay (Figure 2) provides evidence for Holocene growth of the South Slough syncline. Along this shore the Whisky Run platform undulates above and below sea level at least twice. At one locality, platform submergence is associated with offset on the low angle Barview-Empire fault (Figures 2 and 4).

The Barview-Empire fault is inferred to be a thrust fault on the basis of mesoscale thrust faults exposed in the overlying terrace cover sediments above the fault trace. Slip indicators for the mesoscale faults show dip-slip motion. The inferred thrust fault is coplanar with bedding (N25°W, 28°SW) of the underlying Miocene beds and we infer that the Barview-Empire fault is a flexural-slip fault similar to bedding-plane faults west of South Slough.

A group of five drowned Sitka spruce stumps occur within the intertidal zone on the downthrown side of the Barview-Empire fault. The stumps are 0.6-1.5 m below the rooting level of adjacent living Sitka spruce trees. The stumps occur only in proximity to the fault and therefore appear to be related to displacement on the fault. Samples from two of the drowned stumps yield ages of 220 ± 50 ¹⁴C years B.P. (Beta

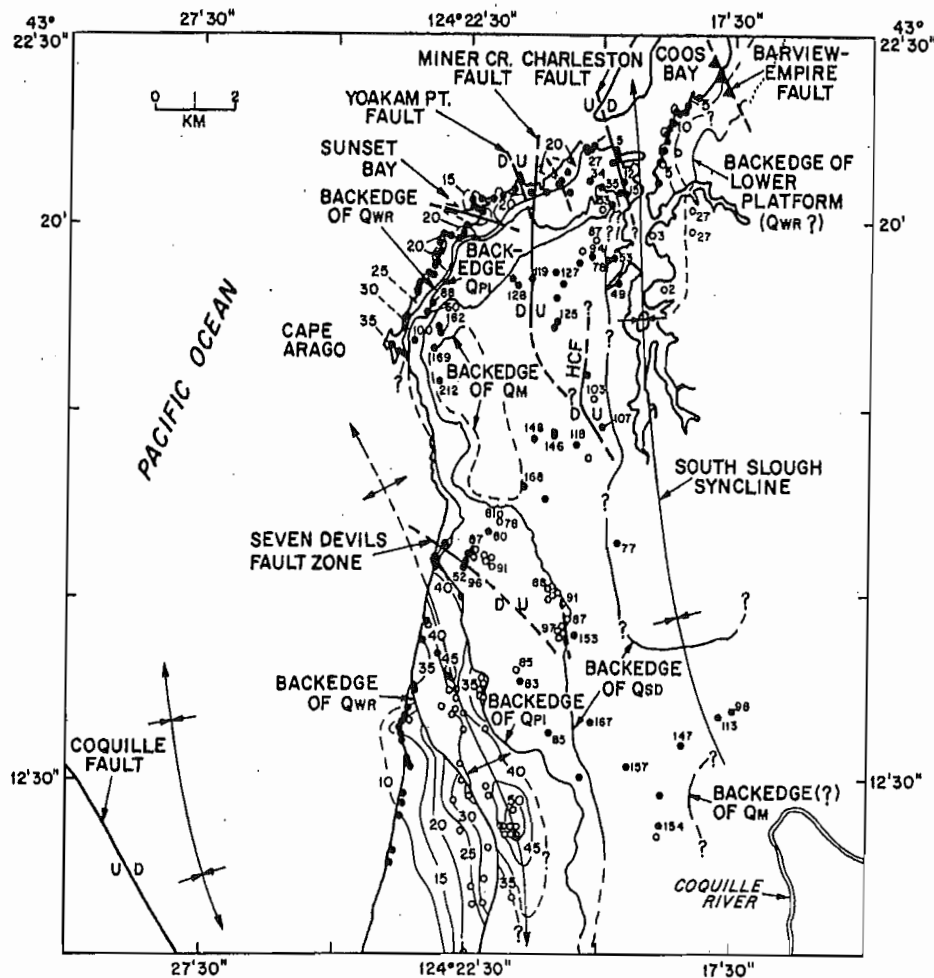


Fig. 4. Wave-cut platform elevation and contour map showing postemergence platform deformation, northern portion of study area. Contour interval is 5 m. Note the northeast dip of all wave-cut platforms on the west limb of the South Slough syncline between Cape Arago and outer Coos Bay. Late Pleistocene to Holocene(?) folding and faulting has warped the wave-cut platforms in the southern portion of the figure. Solid circles are altimeter survey locations, open circles represent platform altitudes calculated from water well logs or minerals exploration boreholes. Labeled backedges on the figure refer to the position of the shoreline angle for the following marine terraces: Qwr, Whisky Run; Qpi, Pioneer; Qsd, Seven Devils; Qm, Metcalf; HCF, Hayward Creek fault. Offshore data from Newton *et al.* [1980] and Clarke *et al.* [1985].

analytic sample Beta-23276) and modern (A. R. Nelson, personal communication; 1988; University of Pittsburgh sample Pitt-185). On the basis of the age of the stumps, we infer late Holocene activity on the Barview-Empire fault. The Whisky Run wave-cut platform is also submerged at Pigeon Point (PP, Figure 2), 1 km southwest of the Barview-Empire fault, and this abrupt change in elevation may be fault controlled as well.

Pioneer Anticline and Coquille Fault

To the southwest and south of the South Slough Syncline, platform warping is controlled mainly by the Pioneer anticline. The northwest trending Pioneer anticline is delineated by the structure contours of the Pioneer wave-cut surface (Figure 4). The half wavelength of the Pioneer anticline is about 6–7 km. The east limb of the Pioneer anticline is cut by high-angle reverse faults of the Seven Devils fault zone (Figure 8). The N50°W strike of the Seven Devils fault zone matches the strike of the underlying Eocene siltstone. Both the reverse sense of slip and the coplanarity of the fault zone

and bedding (Figure 8) lead us to suggest the Seven Devils fault is a bedding-plane flexural-slip fault as well. The Seven Devils fault zone extends to the Seven Devils Mine area (SDM, Figure 3) where Griggs [1945] documents a northwest striking fault which cuts Seven Devils terrace sediments. The fault last moved prior to cutting of the Pioneer terrace, which is not deformed by the fault zone.

Between Fivemile Point and the mouth of the Coquille River the southwest dip of the Whisky Run platform is related to folding of the Pioneer anticline. An abrupt gain in elevation at Coquille Point (Figure 5), however, is accompanied by a distinctive change in platform tilt from southwest to west. This abrupt elevation gain and change in tilt may correspond to an onshore extension of the informally designated Coquille fault (Figure 5). Offshore, the Coquille fault trends N30°W and displaces Pleistocene sediments in a down-to-the-northeast sense [Clarke *et al.*, 1985]. The extrapolated southeast extension of the fault intersects the coast at the mouth of the Coquille River (Figure 5). The wave-cut platforms south of the Coquille River generally dip

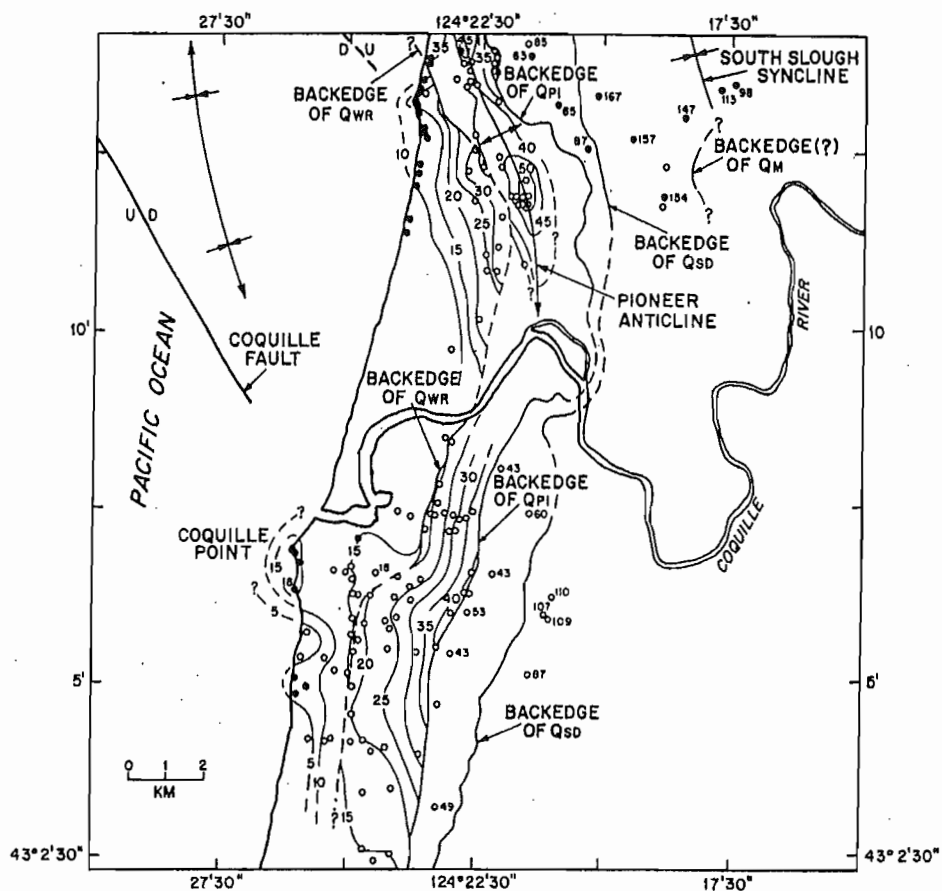


Fig. 5. Wave-cut platform elevation and contour map showing postemergence platform deformation, southern portion of study area. Also shown are offshore structures in this area. Contour interval is 5 m. Note that the Whisky Run platform descends below sea level north of the Coquille River and rises abruptly to 18 m south of the Coquille River. Platforms south of the Coquille River dip seaward in contrast to the back tilted platforms in the vicinity of Cape Arago. Terrace platform elevations gradually descend south of the Coquille River and dip below sea level south of the study area. Symbols and abbreviations are the same as for Figure 4. Offshore data from Newton *et al.* [1980] and Clark *et al.* [1985].

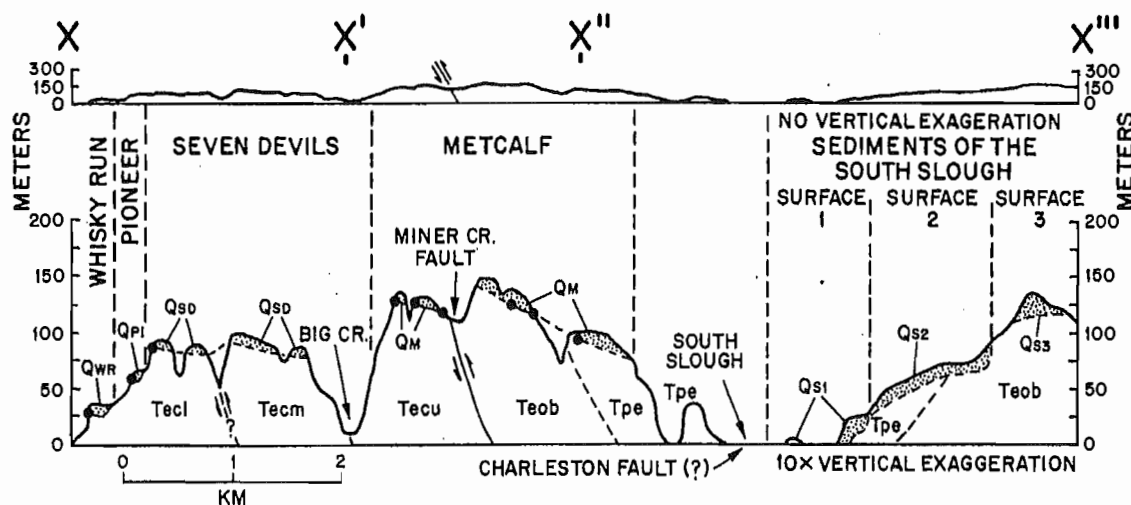


Fig. 6. Northeast to east trending cross section (view to north) showing tilting and faulting of wave-cut platforms near Cape Arago. Differential back tilt of the wave-cut platforms occurs due to offset on flexural-slip faults such as the Miner Creek fault. Surfaces 1, 2, and 3, east of South Slough, slope west toward the syncline axis. Bedrock stratigraphy: Tpe, Pliocene Empire Formation; Totp, Oligocene Tunnel Point Formation; Teob, Eocene-Oligocene Bastendorff Formation; Tecu, Eocene Coaledo Formation, upper member; Tecm, Eocene Coaledo Formation, middle member; Tecl, Eocene Coaledo Formation, lower member; Tees, Eocene Elkton Siltstone Formation. See Figure 2 for location of cross section X to X'''.

14

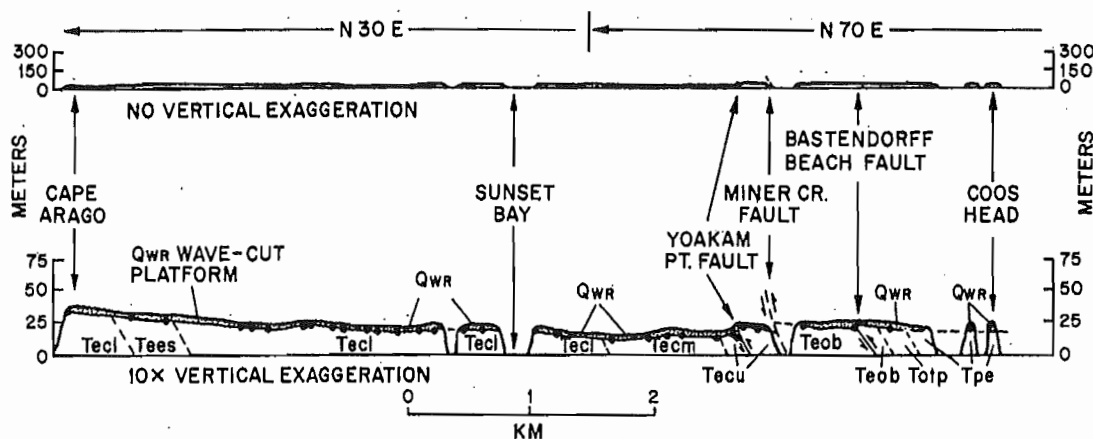


Fig. 7. Post-80 ka deformation of the Whisky Run wave-cut platform is illustrated in this coastwise transect from Cape Arago to Coos Head (view to northwest and north-northwest). Solid circles are altimeter survey locations. Data are projected onto a line that trends N30°E from Cape Arago to Sunset Bay, then N70°E to Coos Head. The gradual descent of the Whisky Run Wave-cut platform from Cape Arago to Coos Head is interrupted repeatedly by flexural-slip faults at Yoakam Point, Miner Creek, and Bastendorff Beach. Geologic units are same as previous figure.

west, except the Whisky Run platform at Coquille Point where it is slightly back tilted (Figures 5 and 9).

TERRACE AGES

We obtained a revised, numerical age estimate for the Whisky Run terrace and a correlation age estimate for the Pioneer terrace. Age assignments for the older terraces are speculative.

To obtain a numerical age estimate for the Whisky Run terrace, we collected fossils for U series, amino acid, and oxygen isotope analyses. Solitary corals (*Balanophyllia ele-*

gans) and bivalve mollusks (*Saxidomus giganteus* and *Mya truncata*) were collected at Coquille Point (U.S. Geological Survey (USGS) locality M2798; Los Angeles County Museum of Natural History (LACMNH) locality 2636), and bivalve mollusks were collected at Cape Blanco (USGS locality M1450 and M1452; LACMNH locality 2641). Analyses of the fossils from both localities are reported by *Muhs et al.* [this issue].

U series analyses of the fossil coral yields an age of 83 ± 5 ka for the Whisky Run terrace at Coquille Point [*Muhs et al.*, this issue]. *Kennedy et al.* [1982] reported a U

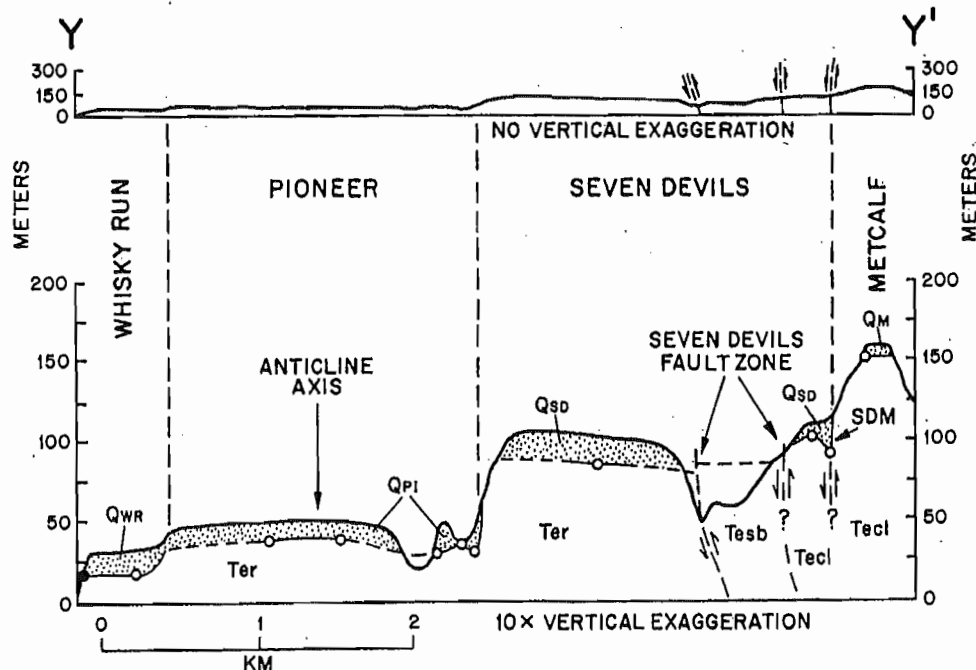


Fig. 8. Cross section Y-Y' (view to northwest) showing anticlinal warping of the Pioneer wave-cut platform. The section is located in the transition zone between wave-cut platforms with eastward tilts (northern portion of study area) and platforms with westward tilts (southern portion of study area). Bedrock stratigraphy: Ter, Eocene Roseburg Formation; Tesb, Eocene Sacchi Beach Beds; Tecu, Eocene Coaledo Formation, lower member. SDM is the Seven Devils placer mine. Displacement of the Seven Devils platform in the Seven Devils fault zone is accommodated either within the siltstone of the Sacchi Beach Beds or along the formation contacts. See Figure 3 for location of cross section.

15

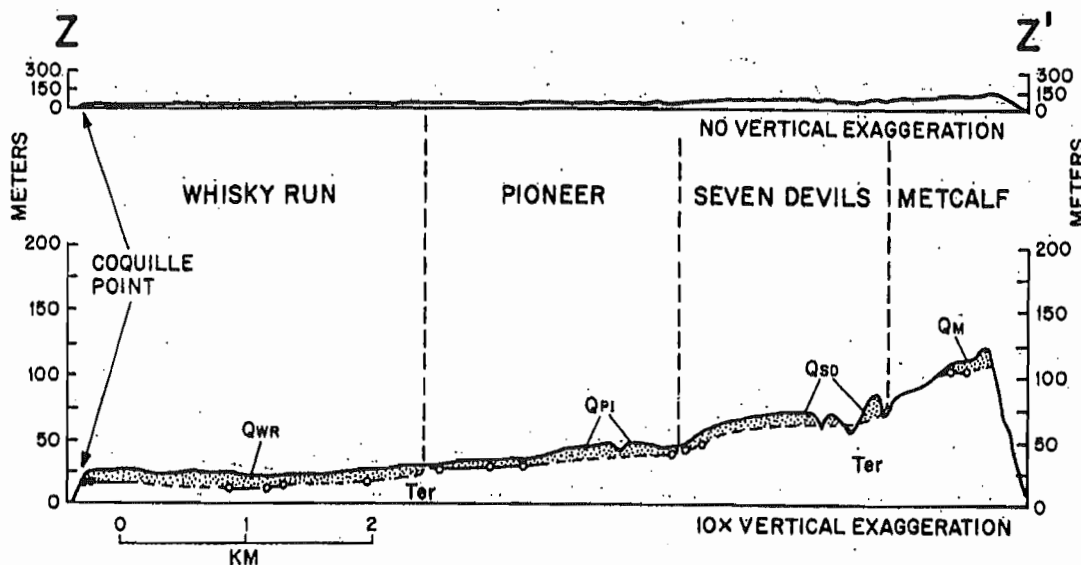


Fig. 9. Cross section Z-Z' (view to north) showing only slightly deformed wave-cut platforms in southern portion of study area. Solid circles are altimeter survey locations; open circles represent altitudes derived from water well logs. Terrace platforms dip seaward, and younger platforms show successively less relief at backedges. A slight downwarping of the Whisky Run platform can be seen east of Coquille Point. See Figure 3 for cross-section location.

series age of approximately 72 ka determined on fossil coral from the same locality but noted isotopic discordance in their fossil corals. *Muhs et al.* [this issue] correlate the Whisky Run wave-cut platform at Coquille Point with the circa 80 ka eustatic high stand of sea level (deep-sea isotope stage 5a) of *Mesolella et al.* [1969] and *Shackleton and Opdyke* [1973]. Amino acid and oxygen isotope data from bivalve shells collected at Cape Blanco suggest that the two lowest terraces at Cape Blanco, the newly designated Cape Blanco terrace [*Muhs et al.*, this issue; *Kelsey*, 1990] and the Pioneer terrace [*Janda*, 1969, also unpublished guidebook, 1970], are probably correlative with the 80 and 105 ka sea level high stands, respectively [*Muhs et al.*, this issue]. Platform elevation data, determined from water well logs, show physical continuity between the 105 ka Pioneer wave-cut platform at Cape Blanco and the Pioneer wave-cut platform at Coquille Point. Therefore the Pioneer platform at Coquille Point was probably formed during the circa 105 ka sea level high stand.

A minimum feasible age for the Seven Devils wave-cut platform is 125 ka, which is the age of the interglacial high stand of sea level that directly preceded the 105 ka high stand. It is possible that the 125 ka terrace was totally removed in the Cape Arago area due to coastal retreat, in which case the Seven Devils terrace is older than 125 ka. We feel our 125 ka age assignment is feasible because the 125 ka sea level was 6 m above present sea level [*Ku et al.*, 1974; *Harmon et al.*, 1983] and platforms attributed to this high stand are present worldwide on both tectonically stable and uplifted coastlines (see review by *Muhs et al.* [this issue]).

The Metcalf terrace must have been cut during a relatively high stand of the sea sometime in the late Pleistocene prior to 125 ka. A minimum age of platform cutting for the Metcalf is about 200 ka (oxygen isotope stage 7 of *Shackleton and Opdyke* [1973]). On the tectonically stable platform of Bermuda, sea level was at 2-m elevation at about 200 ka [*Harmon et al.*, 1983]; and data from Barbados [*Bender et al.*, 1979] and from the tectonically stable New Providence

Islands of the Bahamas [*Muhs and Bush*, 1987; D. R. Muhs, personal communication, 1989] also lead to the conclusion that sea level was a few meters above present at about 200 ka. We recognize, however, that the age of the Metcalf platform could be significantly older than 200 ka.

RATES OF DEFORMATION

Uplift Rates

Maximum rates of uplift for wave-cut platforms at Cape Arago range from 0.5 to 0.8 m/kyr (Table 2). Calculation of maximum uplift rate depends on the age of the platform, the elevation of paleo-sea level (with respect to present sea level) at the time of platform formation, and the present elevation of the platform. In order to calculate alternative uplift rates we employed two different Pleistocene paleo-sea level curves, one for New Guinea [*Bloom et al.*, 1974; *Chappell and Shackleton*, 1986] and one based on data for Japan [*Machida*, 1975] and California and Baja California [*Muhs et al.*, 1988] (Table 2). For platforms that are not landward tilted the shoreline angle (the base of the paleo-sea cliff) is the point of maximum uplift. The shoreline angle is assumed to have been cut during a eustatic sea level high stand and thus represents the paleo-sea level at the time of platform formation. At Cape Arago the wave-cut platforms are tilted landward and the point of maximum uplift for these platforms is seaward of the paleoshoreline angle. Therefore the point of maximum uplift had an initial elevation that was lower than the elevation of paleo-sea level during the time of platform formation. The degree to which the initial elevation is lower than the paleoshoreline angle is dependent on the initial, nontectonic, seaward slope of the wave-cut platform. Modern and ancient wave-cut platforms cut on sandstones similar to the bedrock at Cape Arago have seaward slopes of 20–40 m/km for a 300–600 m wide segment near the backedges and a 7–17 m/km slope farther offshore [*Bradley and Griggs*, 1976]. These seaward slopes are used as a

TABLE 2. Marine Wave-Cut Platforms at Cape Arago: Ages, Uplift Rates, Tilt Rates, and Horizontal Strain Rates

Wave-Cut Platform	Estimated Age, ka	Maximum Elevation, ^a m	Shore-Normal Distance From Shoreline Angle, km	Original Gradient of Platform, m/km	Original Depth of Platform, m	Paleo-Sea Level, m	Sea Level Model ^c	Maximum Uplift Rate, m/kyr	Elevation of Shoreline Angle, m	Uplift Rate at Shoreline angle, m/kyr	Maximum Observed Tilt, ° rad	Tilt Rate rad/yr	Horizontal Strain Rate, yr ⁻¹
Whisky Run	80	35	0.2	20	4	-19 ± 5	NG	0.73 ± 0.07	31	0.63 ± 0.07	2.3 × 10 ⁻³	2.9 × 10 ⁻⁸	0.44 × 10 ⁻⁷
	80	35	0.2	40	8	-19 ± 5	NG	0.78 ± 0.07	31	0.63 ± 0.07			
	80	35	0.2	20	4	-5 ± 2	CA-JP	0.55 ± 0.03	31	0.45 ± 0.03			
	80	35	0.2	40	8	-5 ± 2	CA-JP	0.60 ± 0.03	31	0.45 ± 0.03			
Pioneer	105	68 ^g	0	NA	0	-9 ± 3	NG	0.73 ± 0.03	68	0.73 ± 0.03	5.7 × 10 ⁻³	5.4 × 10 ⁻⁸	0.83 × 10 ⁻⁷
	105	68 ^g	0	NA	0	-2	CA-JP	0.67	68	0.67			
Seven Devils ^h	125	100	0.2	20	4	+6	both	0.78?	98 ^g	0.74?	8.1 × 10 ⁻³ ?	6.5 × 10 ⁻⁸ ?	1.0 × 10 ⁻⁷ ?
	125	100	0.2	40	8	+6	both	0.82?	98 ^g	0.74?			
Metcalf ^h	200?	169	0	NA	0	B+2		0.84?	169	0.84?	17 × 10 ⁻³ ?	8.5 × 10 ⁻⁸	1.3 × 10 ⁻⁷ ?

^aFor Whisky Run and Seven Devils platforms, the maximum elevation near Cape Arago is 200 m seaward (westward) of the paleoshoreline angle. For Pioneer and Metcalf platforms the maximum elevation near Cape Arago is at the paleoshoreline angle. All platforms are landward tilted at Cape Arago.

^bRelative to present sea level.

^cNG, New Guinea model [Chappell and Shackleton, 1986]; CA-JP, California-Japan model [Machida, 1975; Muhs *et al.*, 1988]; B, Bermuda data for 200 ka high stand [Harmon *et al.*, 1983].

^dUncertainties for Whisky Run and Seven Devils wave-cut platforms: (1) paleo-sea level, (2) paleo-water depth during the 80 and 105 ka sea level high stands for the present point of maximum elevation.

^eFor all terrace platforms, tilt is measured from the vicinity of Cape Arago N60°E to the vicinity of South Slough. Tilts measured parallel to the N60°E down-dip direction.

^fSee assumptions for derivation of strain rate in text.

^gElevation is extrapolated from known distance measured in down-tilt direction and using average platform tilt.

^hThe estimated ages of the Seven Devils and Metcalf platforms are minimum ages and not constrained by isotopic data. Therefore all calculated rates based on these ages are maximum rates and are queried because of the large uncertainties.

correction for determining maximum uplift rates on landward tilted platforms (Table 2). For the Whisky Run and Seven Devils wave-cut platforms at Cape Arago, uncertainties in maximum uplift rates are therefore a combination of paleo-sea level uncertainties and the uncertainty as to the paleobathymetry during the 80 and 125 ka sea level high stands at the present points of maximum elevation. Maximum platform elevations on these two terraces are about 200 m westward of the respective terrace shoreline angles, so the correction for landward tilting involves an additional 4–8 m of uplift (Table 2). The maximum elevation of the Pioneer and Metcalf platforms at Cape Arago is at the shoreline angle because these platforms are not extensively preserved at the cape. Therefore no landward tilt correction is necessary for these latter two platforms (Table 2). For the lowest four platforms at Cape Arago we also tabulated uplift rates at the shoreline angle (Table 2) so that we could compare uplift rates among wave-cut platforms. In general, uplift rates increase slightly, within error limits, with increasing age of the terrace (Table 2). However, if the Seven Devils and Metcalf platforms are older than the suggested minimum ages, then there is no consistent trend in uplift rate with increasing age.

Tilt Rates

At Cape Arago the degree of landward tilt increases with increasing age of the wave-cut platform (Table 2). The increasing tilts reflect progressive tilting of platforms on the west limb of the South Slough syncline and also presumably reflects tightening of the syncline throughout late Pleistocene time.

During steady growth of a sinusoidal fold, tilt rates of bedding on the fold limbs decrease as the amount of horizontal shortening increases [Adams, 1984]. If a horizontal surface such as a wave-cut platform is cut across bedding on the limb of such a fold, the wave-cut platform will be tilted at the same rate as the underlying beds. Therefore, as folding progresses, greater amounts of horizontal shortening are required to produce the same degree of tilting for successively younger wave-cut platforms. Constant or decreasing shortening rates will be manifest as a progressive decrease in tilt rates for younger wave-cut platforms. Because tilt rates systematically change with constant shortening rates, horizontal strain rates are more meaningful in terms of analyses of deformation of the fold.

Horizontal Strain Rates

The maximum principal strain direction (direction of maximum contraction) for the South Slough syncline is parallel to the assumed N60°E tilt direction for the tilted wave-cut platforms. The magnitude of the maximum principal strain is

$$\epsilon_z = (L - D)(L^{-1}) \quad (1)$$

where L is the original horizontal length and D is the horizontal length after shortening (Figure 10). The strain rate ϵ'_z is the strain divided by the amount of time over which the strain occurred:

$$\epsilon'_z = (L - D)(L^{-1})(T^{-1}) \quad (2)$$

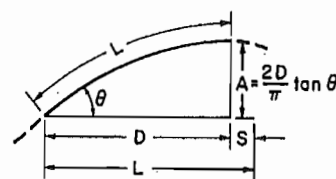


Fig. 10. Geometric relationships for a sinusoidal fold: original length along bedding (L), the horizontal extent across bedding after shortening (D), the amount of horizontal shortening (S), and the maximum flank dip (θ) at the point of inflection of the sinusoidal fold (modified from Rockwell *et al.* [1988]).

In order to calculate horizontal strain rate over time across the South Slough syncline the folded strata of the syncline are assumed to approximate sine curves [Currie *et al.*, 1962], and the syncline is modeled as a flexural-slip, sinusoidal fold using mathematical techniques outlined by Currie *et al.* [1962], Adams [1984], and Rockwell *et al.* [1988]. It is also assumed that original length along bedding is retained during folding, which necessitates that flexural slip must occur along bedding planes. The assumption of a flexural-slip fold mechanism is reasonable because of the occurrence of several flexural-slip faults in the Cape Arago region.

After folding the length L along a geologic stratum (originally a horizontal length) cannot be measured directly and must be calculated from the variable D [Rockwell *et al.*, 1988]:

$$L = (2D/\pi)(E(\theta)/\cos(\theta)) \quad (3)$$

where L is the length along a sine curve or geologic stratum (the original horizontal length) and D is the present horizontal length after shortening measured from the fold axis to the nearest point of inflection. D is therefore one-quarter of a complete sine curve and represents one-quarter of the wavelength of the fold. Theta (θ) is the maximum flank dip of the geologic stratum in the fold (slope of the sine curve), measured at the point of inflection on the fold limb (Figure 10), and $E(\theta)$ is the complete elliptic integral of the second kind (used to approximate the length along a sine curve and described by Weast [1979]). Theta (θ) was measured in the field, and D was measured from a published geologic map [Newton *et al.*, 1980].

To calculate the strain rate, the horizontal shortening rate must be calculated. The horizontal shortening rate is the rate at which the horizontal length D changes with time:

$$\frac{dD}{dt} = \frac{d}{dt} \left[\left(\frac{L\pi}{2} \right) \left(\frac{\cos(\theta)}{E(\theta)} \right) \right] \quad (4)$$

$$\frac{dD}{dt} = \frac{L\pi}{2} \left[\frac{E(\theta) \left(-\sin(\theta) \frac{d\theta}{dt} \right)}{[E(\theta)]^2} \right] - \left[\frac{\cos(\theta) E'(\theta)}{[E(\theta)]^2} \right] \quad (5)$$

$$\frac{dD}{dt} = \frac{L\pi \cos(\theta)}{2 E(\theta)} \left\{ \left[\frac{-E(\theta) \left(\tan(\theta) \frac{d\theta}{dt} \right)}{E(\theta)} \right] - \left[\frac{E'(\theta)}{E(\theta)} \right] \right\} \quad (6)$$

18

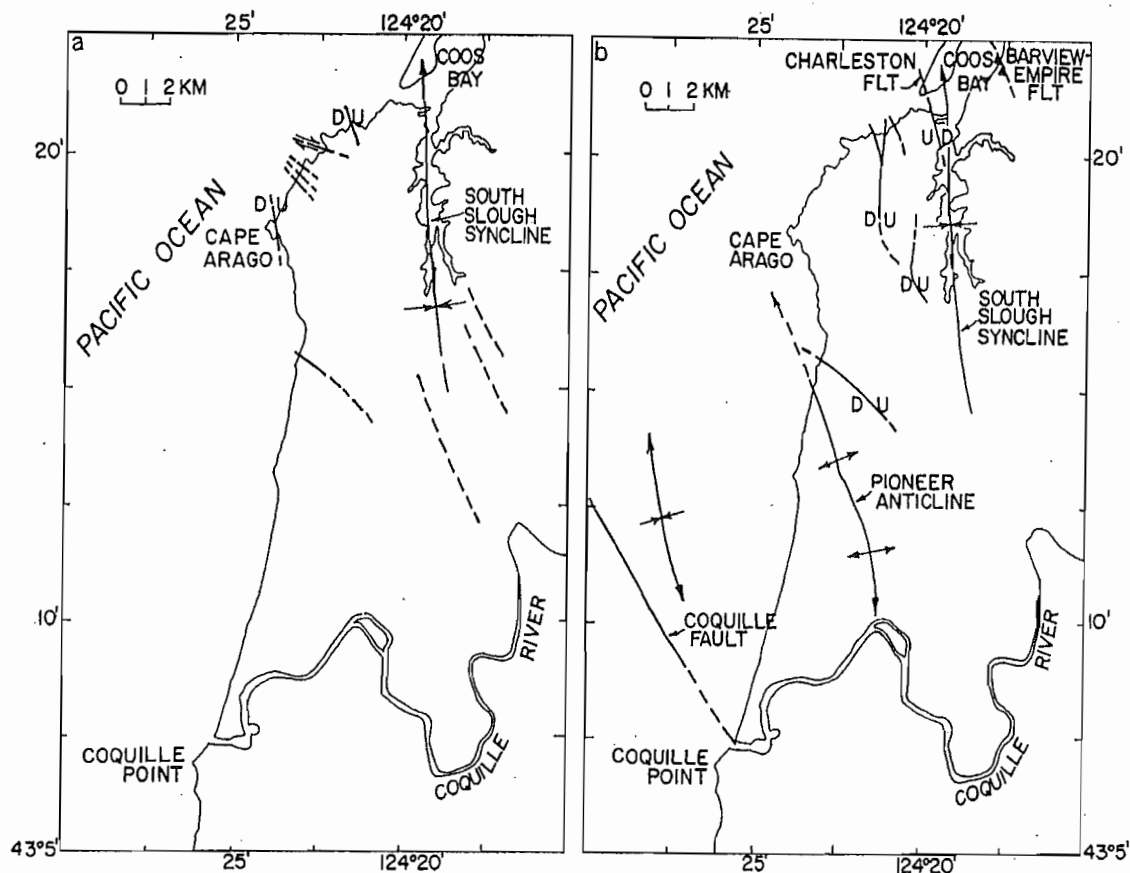


Fig. 11. (a) Tectonic map showing all folds and faults previously mapped in the Eocene to Pliocene bedrock [after Baldwin, 1966; Ehlen, 1967; Newton *et al.*, 1980]. (b) Tectonic map showing folds and faults expressed in late Quaternary wave-cut platforms in the Cape Arago area.

$$\frac{dD}{dt} = -\frac{L\pi \cos(\theta)}{2 E(\theta)} \left\{ \left[\frac{E'(\theta)}{E(\theta)} \right] + \left[\tan(\theta) \frac{d\theta}{dt} \right] \right\} \quad (7)$$

where $E'(\theta)$ is the rate of change of the complete elliptic integral of the second kind for a given change in θ .

Finally, the horizontal strain rate (ϵ'_x , units = yr^{-1}) is calculated by dividing the horizontal shortening rate by the original bedding length L :

$$\epsilon'_x = (dD/dt)(L^{-1}) \quad (8)$$

Application of the above technique to the South Slough syncline requires some relaxation of the assumptions for the model. It is uncertain if the point of inflection actually occurs where maximum flank dip was measured. Thus the measured horizontal distance D may not represent a full one-quarter of the fold wavelength. In addition, the South Slough syncline is not strictly sinusoidal because of the asymmetry of the fold. However, the west limb of the syncline roughly approximates one-quarter of a sine wave.

Recognizing the above uncertainties, evaluation of the deformation of the west limb of the South Slough syncline provides a first-order approximation of late Pleistocene crustal strain rates in the vicinity of Cape Arago. The late Pleistocene strain rates decrease with time (Table 2). In calculating the strain rates we use speculative ages for the Seven Devils and Metcalf platforms. The speculative ages are minimum possible ages, and all alternative ages would yield lower strain rates. Therefore for the two oldest plat-

forms in Table 2, strain rates may not decrease with time. A decrease in strain rate over time would reflect a slowing in the rate of east-west horizontal shortening on the west limb of the South Slough syncline during progressive tightening of the fold. As the total amount of horizontal shortening during folding grows large, horizontal shortening may begin to occur by other mechanisms [Currie *et al.*, 1962]. Therefore the apparent decreasing horizontal strain rates for the west limb of the South Slough syncline may indicate that a component of crustal shortening in the vicinity of Cape Arago is being accommodated elsewhere.

DISCUSSION

Folding: Dominant Style of Deformation

Late Pleistocene deformation of wave-cut platforms in the Cape Arago-Bandon region is dominated by open folds and related flexural-slip, bedding-plane faults. The open folds have half wavelengths of about 6–7 km and subaerially exposed axial lengths of 15–20 km. A comparison of folds and faults that have been previously mapped in the Tertiary bedrock [Ehlen, 1967; Newton *et al.*, 1980] with those that are expressed in the deformed wave-cut platforms (Figure 11) shows that most of the flexural-slip faults are only apparent from offset of late Pleistocene platforms. Furthermore, though the South Slough syncline deforms Eocene strata, the Pioneer anticline is a new fold that has developed in Quaternary sediments but is not apparent in older rocks

(Figure 11). Folding in this region along the Cascadia subduction zone therefore appears to be a persistent style of deformation at least since the late Oligocene, but growth on individual folds can be transitory. Flexural-slip faults are difficult to detect in the Tertiary sediments because they are parallel to bedding planes. The South Slough syncline and the Pioneer anticline are an on-land expression of the landward edge of a fold belt that deforms Cenozoic and Quaternary sediments on the continental shelf of the Cascadia margin [Kulm and Fowler, 1974; Clarke *et al.*, 1985; Peterson *et al.*, 1986].

The folds produce a wide variation in coastal uplift rates where the coastline cuts obliquely across structural trend (Figures 4, 5, and 11). This fold-induced variability in net uplift makes questionable assertions that coastal uplift rate is an indicator of the type of convergent margin [Uyeda and Kanamori, 1979] or the degree of plate interaction [Yonekura, 1983]. To the contrary, local structures can result in a wide range of late Pleistocene coastal uplift rates at any one subduction zone or subduction zone type [Muhs *et al.*, this issue].

While the association of flexural-slip, bedding-plane faults with the open folds is most evident, the folds may also be associated with other faults at depth. The flexural-slip, bedding-plane faults may be seismogenic, but they are not major seismic hazards [Yeats *et al.*, 1981], and such faults are probably not the primary source of seismicity in the Cape Arago-Bandon region. Rather, tightening of the South Slough syncline, subsidence of the axial region, and offset on associated flexural-slip faults may be triggered by reverse faulting on deeper structures.

Though results of our study do not elucidate how the folds grow, from several lines of circumstantial evidence we suggest that these folds may develop during earthquakes. First, in contractional setting similar to the Cape Arago area, earthquakes of magnitude 6.0–7.5 have occurred on blind thrust faults that lie beneath active folds [King and Vita-Finzi, 1981; Stein and King, 1984]. The folds apparently grow episodically during earthquakes generated by movements on these blind faults. Second, several instances of abrupt submergence in the late Holocene are documented in South Slough along the axis of the syncline. Both Nelson [1987, 1988] and Peterson and Darienzo [1989] observed seven to eight instances of abrupt submergence since 4–5 ka in the salt marsh stratigraphy of the slough. At other localities in southwestern Oregon including Coos Bay and the Coquille River estuary (Figure 1), Nelson [1987, 1988] and Peterson and Darienzo [1989] find no evidence of repeated instances of abrupt submergence. Nelson [1988] hypothesized that the local distribution of submerged peat layers in South Slough may record repeated localized Holocene coseismic contraction of the syncline.

We infer that flexural-slip faulting on the wave-cut platforms may occur simultaneously with the postulated coseismic subsidence along the South Slough syncline axis. The best evidence for coseismic flexural-slip faulting is the drowned Sitka spruce stumps in the intertidal zone on the downdropped block of the Barview-Empire fault (Figure 2). The submergence that killed these trees was either a rapid aseismic deformation or, more likely, a coseismic deformation that occurred contemporaneously with abrupt submergence along the syncline axis only 8 km to the southwest. The most recent episode of abrupt submergence of salt

marsh in South Slough, about 200–500 years ago [Nelson, 1988], could have been contemporaneous with the drowning of the Sitka spruce trees on the Barview-Empire fault.

Several observations with regards to the South Slough syncline are open to more than one interpretation. First, the decrease in strain rate on the west limb between 105 ka and the present (Table 2) may reflect a migration of contractional strain to neighboring structures or may reflect that the principal contraction direction is no longer east-west but rather north-south, which is the present direction of regional principal contraction as deduced from historical seismicity [Spence, 1989]. A change to a more northerly direction of principle contraction would result in progressively less contraction of structures with north trending fold axes, such as the South Slough syncline. Second, the role of the Charleston fault is problematic. The fault has the greatest amount of offset (20 m) of all the faults that disrupt the Whisky Run platform. Even though the fault strikes parallel to the syncline axis, the fault does not appear to be a flexural-slip fault because it is steeply dipping and cuts across bedding of the moderately inclined Tertiary strata. One plausible interpretation is that the inferred post-Whisky Run offset on the Charleston fault and the decrease in strain rate on the west limb of the syncline in the last 100 kyr may both be related to changing stress orientations in the Cape Arago region in the late Quaternary.

Regional Vertical Deformation Versus Localized Folding

The Cascadia subduction zone has not experienced historic great earthquakes [Heaton and Kanamori, 1984]. Yet the Cascadia subduction zone has several physical characteristics in common with subduction zones in Alaska, southwest Japan, Chile, and Columbia that have experienced great ($M_w > 8$) subduction-style earthquakes in historic time [Heaton and Kanamori, 1984; Heaton and Hartzell, 1987; Spence, 1989]. In the light of the prevalence of open folding in the forearc of the Cascadia subduction zone in the Cape Arago-Bandon region, as well as in the Cape Blanco region 55 km to the south [Kelsey, 1990], how common are folds along the other subduction zones that have produced great earthquakes?

The most obvious strain that is observed in historic, great subduction-style earthquakes is regional tilting, regional submergence, and regional uplift. For instance, during the 1960 earthquake in Chile and the 1964 earthquake in Alaska, large regions of the forearc (100,000–200,000 km²) underwent coseismic uplift and adjacent regions equally as large (80,000–190,000 km²) underwent coseismic subsidence [Plafker, 1969, 1972]. In southwest Japan, Ota [1986] describes a region of coastal uplift on Muroto Peninsula that developed in response to the 1946 earthquake in the Nankai Trough. The vertical deformation during the earthquake was accompanied by notable landward tilting of a 50-km-wide segment of the coast. Similar landward tilting accompanied coseismic uplift that was associated with the 1964 Alaska and 1960 Chile earthquakes [Plafker, 1972]. Although mapping of the deformation in Chile and Alaska was limited by accessible exposure, the coseismic vertical movements do not appear to have been dominated by development of local structures such as supracrustal folds or faults.

From historic data therefore it is evident that regional

vertical deformation of areas greater than 10^5 km^2 is associated with subduction-style great earthquakes. However, localized folding occurred during at least one of the above great earthquakes and may be more prevalent than recognized. Superimposed on the regional uplift during the 1964 Alaska earthquake was the growth of a localized anticlinal fold that pierces above sea level to form Middleton Island [Plafker, 1969], an island whose 30-km length is similar to the subaerially exposed axial length of folds at Cape Arago [Plafker, 1969]. The island consists of five uplifted wave-cut platforms of mid to late Holocene age. These five platforms record periodic abrupt emergence of this island, and a sixth uplifted platform was generated in 1964 when the island was again coseismically uplifted, this time by 3.3 m [Plafker, 1969]. The Middleton Island anticline therefore grew coseismically during the same 1964 event that elsewhere in the Alaskan forearc resulted in more regional vertical uplift or subsidence. It is likely that local growth of folds during the 1964 Alaska earthquake was more common than was documented because most folding probably occurred below sea level. From the Alaskan deformation data we reason that localized folds of the scale observed near Cape Arago can be generated by great earthquakes that deform a much larger region of the forearc.

SUMMARY

Late Quaternary strain in the Cape Arago region appears to be accommodated mostly by contraction on local folds with half wavelengths of 6–7 km and axial lengths of greater than 20 km. These folds produce both landward and seaward tilts to the wave-cut platforms rather than a uniform landward tilt to platforms such as is observed on the convergent margin in southwest Japan. The observed strain in south coastal Oregon therefore lacks in a simple sense the evidence for regional vertical uplift and subsidence associated with historic, large-magnitude subduction-related earthquakes elsewhere [Plafker, 1972].

Localized folding can occur during great earthquakes, as exemplified by the 1964 coseismic growth of the Middleton Island (Alaska) anticline, even though the historic record indicates that the most notable strain pattern during great earthquakes is regional vertical movement. Therefore, though the late Quaternary folds at Cape Arago need not develop during great subduction-related earthquakes, the folds do not preclude the possibility of great earthquakes whose deformation would include the Cape Arago portion of the Cascadia subduction zone.

Acknowledgments. Field work was supported by U.S. Geological Survey Earthquake Hazards Reduction Program, contract 14-08-0001-G1387. A. R. Nelson provided funding for a ^{14}C age determination. Discussion with D. R. Muhs improved the manuscript. We thank D. C. Engebretson, D. Merritts, D. R. Muhs, A. R. Nelson, J. L. Talbot, and R. S. Yeats for reviews.

REFERENCES

- Adams, J., Active deformation of the Pacific Northwest continental margin, *Tectonics*, 3, 449–472, 1984.
- Armentrout, J. M., Field trip road log for the Cenozoic stratigraphy of Coos Bay and Cape Blanco, southwestern Oregon, *Geologic Field Trips in Western Oregon and Southwestern Washington*, edited by K. Oles, J. Johnson, A. Niem, and W. Niem, *Bull. Oreg. Dep. Geol. Miner. Ind.*, 101, 177–180, 1980.
- Atwater, B. F., Evidence for great Holocene earthquakes along the outer coast of Washington State, *Science*, 236, 942–944, 1987.
- Baldwin, E. M., Some revisions of the late Cenozoic stratigraphy of the southern Oregon coast, *J. Geol.*, 52, 35–46, 1945.
- Baldwin, E. M., Some revisions of the geology of Coos Bay area, Oregon, *Ore. Bin*, 28, 189–204, 1966.
- Beaulieu, J. D., and P. W. Hughes, Environmental geology of western Coos and Douglas counties, Oregon, *Bull. Oreg. Dep. Geol. Miner. Ind.*, 87, 148 pp., 1975.
- Bender, M. L., R. G. Fairbanks, F. W. Taylor, R. K. Matthews, J. G. Goddard, and W. S. Broecker, Uranium-series dating of the Pleistocene reef tracts of Barbados, West Indies, *Geol. Soc. Am. Bull., Part 1*, 90, 577–594, 1979.
- Bloom, A. L., W. S. Broecker, J. M. A. Chappell, R. K. Matthews, and K. J. Mesolella, Quaternary sea level fluctuations on a tectonic coast: New $^{230}\text{Th}/^{234}\text{U}$ dates from the Huon Peninsula, New Guinea, *Quat. Res. N. Y.*, 4, 185–205, 1974.
- Bradley, W. C., and G. B. Griggs, Form, genesis, and deformation of central California wave-cut platforms, *Geol. Soc. Am. Bull.*, 87, 433–449, 1976.
- Chappell, J., and N. J. Shackleton, Oxygen isotopes and sea level, *Nature*, 324, 137–140, 1986.
- Clarke, S. H., M. E. Field, and C. A. Hirozawa, Reconnaissance geology and geologic hazards of the offshore Coos Bay basin, Oregon, *U.S. Geol. Surv. Bull.*, 1645, 41 pp., 1985.
- Currie, J. B., H. W. Patnode, and R. P. Trump, Development of folds in sedimentary strata, *Geol. Soc. Am. Bull.*, 73, 655–674, 1962.
- Ehlen, J., Geology of state parks near Cape Arago, Coos County, Oregon, *Ore. Bin*, 29, 63–83, 1967.
- Griggs, A. B., Chromite-bearing sands of the southern part of the coast of Oregon, *U.S. Geol. Surv. Bull.*, 945-E, 113–150, 1945.
- Harmon, R. S., R. M. Mitterer, N. Kriausakul, L. S. Land, H. P. Schwarcz, P. Garrett, G. J. Larson, H. L. Vacher, and M. Rowe, U-series and amino-acid racemization geochronology of Bermuda—Implications for eustatic sea-level fluctuation over the past 250,000 years, *Palaeogeogr. Palaeoclimatol. Palaeoecol.*, 44, 41–70, 1983.
- Heaton, T. H., and S. H. Hartzell, Earthquake hazards on the Cascadia subduction zone, *Science*, 236, 162–168, 1987.
- Heaton, T. H., and H. Kanamori, Seismic potential associated with subduction in the northwestern United States, *Bull. Seismol. Soc. Am.*, 74, 933–941, 1984.
- Janda, R. J., Age and correlation of marine terraces near Cape Blanco, Oregon, *Geol. Soc. Am. Abst. Programs*, 3, 29–30, 1969.
- Kelsey, H. M., Late Quaternary deformation of marine terraces on the Cascadia subduction zone near Cape Blanco, Oregon, *Tectonics*, in press, 1990.
- Kennedy, G. L., K. R. Lajoie, and J. F. Wehmiller, Aminostratigraphy and faunal correlations of late Quaternary marine terraces, Pacific coast, USA, *Nature*, 299, 545–547, 1982.
- King, G. C. P., and C. Vita-Finzi, Active folding in the Algerian earthquake of 10 October 1980, *Nature*, 292, 22–26, 1981.
- Ku, T.-L., M. A. Kimmel, W. H. Easton, and T. J. O'Neil, Eustatic sea level 120,000 years ago on Oahu, Hawaii, *Science*, 183, 959–962, 1974.
- Kulm, L. D., and G. A. Fowler, Oregon continental margin structure and stratigraphy: A test of the imbricate thrust model, in *The Geology of Continental Margins*, edited by C. A. Burk and C. L. Drake, pp. 261–284, Springer-Verlag, New York, 1974.
- Lajoie, K. R., Coastal tectonics, in *Active Tectonics*, pp. 95–124, National Academy Press, Washington, D. C., 1986.
- Lund, E. H., Landforms along the coast of southern Coos County, Oregon, *Ore. Bin*, 35, 189–210, 1973.
- Machida, H., Pleistocene sea level of south Kanto, Japan, analyzed by tephrochronology, *Bull. R. Soc. N. Z.*, 13, 215–222, 1975.
- McInnelly, G. W., H. M. Kelsey, and A. R. Nelson, Late Pleistocene and Holocene tectonic deformation of the Whisky Run wave-cut platform in the Cape Arago-Coos Bay area, coastal Oregon, *Geol. Soc. Am. Abstr. Prog.*, 21, 115, 1989.
- Mesolella, K. J., R. K. Matthews, W. S. Broecker, and D. L. Thurber, The astronomical theory of climatic change: Barbados data, *J. Geol.*, 77, 250–274, 1969.
- Muhs, D. R., and C. A. Bush, Uranium-series age determinations of Quaternary eolianites and implications for sea-level history, New

21

- Providence Islands Bahamas, *Geol. Soc. Am. Abstr. Prog.*, 19, 780, 1987.
- Muhs, D. R., G. L. Kennedy, and T. K. Rockwell, Uranium-series ages of corals from marine terraces, Pacific coast of North America: Implications for the timing and magnitude of late Pleistocene sea level changes, in *Programs and Abstracts of 10th Biennial Meeting*, p. 140, Illinois State Water Survey, Urbana, 1988.
- Muhs, D. R., H. M. Kelsey, G. H. Miller, G. L. Kennedy, J. F. Whelan, and G. W. McInelly, Age estimates and uplift rates for late Pleistocene marine terraces: Southern Oregon portion of the Cascadia forearc, *J. Geophys. Res.*, this issue.
- Nelson, A. R., Apparent gradual rise in relative sea level on the south-central Oregon coast during the late Holocene—Implications for the Great Cascadia earthquake hypothesis, *Eos Trans. AGU*, 68, 1240, 1987.
- Nelson, A. R., S. F. Personius, and S. Rhea, Earthquake recurrence and Quaternary deformation in the Cascadia subduction zone, coastal Oregon, *U.S. Geol. Surv. Open File Rep.*, 88-673, 492-497, 1988.
- Newton, V. C., Jr., L. P. Kulm, R. W. Couch, D. Braman, G. S. Pitts, R. O. Van Atta, and D. R. McKeel, Prospects for oil and gas in the Coos Basin, western Coos, Douglas, and Lane counties, Oregon, *Oil Gas Invest.* 6, 74 pp., Oreg. Dep. of Geol. and Miner. Ind., Portland, 1980.
- Ota, Y., Marine terraces as reference surfaces in late Quaternary tectonic studies: Examples from the Pacific rim, *Bull. R. Soc. N. Z.*, 24, 357-375, 1986.
- Peterson, C. D., and M. E. Darienzo, Episodic, abrupt tectonic subsidence recorded in late Holocene deposits of the South Slough syncline: An on-land expression of shelf fold belt deformation from the southern Cascadia margin, *Geol. Soc. Am. Abstr. Programs*, 21, 129, 1989.
- Peterson, C. D., G. W. Gleeson, and N. Wetzel, Stratigraphic development, mineral sources, and preservation of marine placers from Pleistocene terraces in southern Oregon, USA, *Sediment. Geol.*, 53, 203-229, 1987.
- Peterson, C. L., L. D. Kulm, and J. J. Gray, Geologic map of the ocean floor off Oregon and the adjacent continental margin, scale 1:500,000, *Oreg. Dep. Geol. Miner. Ind., GMS-42*, 1986.
- Plafker, G., Tectonics of the March 27, 1964 Alaskan earthquake, *U.S. Geol. Surv. Prof. Pap.*, 543-I, 74 pp., 1969.
- Plafker, G., Alaskan earthquake of 1964 and Chilean earthquake of 1960: Implications for arc tectonics, *J. Geophys. Res.*, 77, 901-925, 1972.
- Rockwell, T. K., E. A. Keller, and G. R. Dembroff, Quaternary rate of folding of the Ventura Avenue anticline, western Transverse Ranges, southern California, *Geol. Soc. Am. Bull.*, 100, 850-858, 1988.
- Shackelton, N. J., and N. D. Opdyke, Oxygen isotope and palaeomagnetic stratigraphy of equatorial Pacific core V28-238: Oxygen isotope temperatures and ice volumes on a 10^5 year and 10^6 year scale, *Quat. Res.*, N. Y., 3, 39-55, 1973.
- Spence, W., Stress origins and earthquake potentials in Cascadia, *J. Geophys. Res.*, 94, 3076-3088, 1989.
- Stein, R. S., G. C. P. King, Seismic potential revealed by surface folding: 1983 Coalinga, California, earthquake, *Science*, 224, 869-872, 1984.
- Uyeda, S., and H. Kanamori, Back arc opening and the mode of subduction, *J. Geophys. Res.*, 84, 1049-1061, 1979.
- Weast, R. C., (Ed.), *CRC Handbook of Physics and Chemistry*, 49th ed., pp. A-166 and A-167, CRC Press, Boca Raton, Flor., 1979.
- West, D. O., and D. R. McCrumb, Coastline uplift in Oregon and Washington and the nature of Cascadia subduction-zone tectonics, *Geology*, 16, 169-172, 1988.
- Yeats, R. S., M. N. Clark, E. A. Keller, and T. K. Rockwell, Active fault hazard in southern California: ground rupture versus seismic shaking, *Geol. Soc. Am. Bull., Part 1*, 92, 189-196, 1981.
- Yonekura, N., Late Quaternary vertical crustal movements in and around the Pacific as deduced from former shoreline data, in *Geodynamics of the Western Pacific-Indonesian Region, Geodyn. Ser.*, vol. 11, edited by T. W. C. Hilde and S. Uyeda, pp. 41-50, AGU, Washington, D. C., 1983.
- H. M. Kelsey, Department of Geology, Western Washington University, Bellingham, WA 98225.
- G. W. McInelly, Geo Engineers, 2405 140 Avenue NE, Suite 105, Bellevue, WA 98005.

(Received July 14, 1989;
revised November 20, 1989;
accepted December 27, 1989.)

by Paul D. Komar, College of Oceanography, Oregon State University, Corvallis, Oregon

Early explorers of the Oregon coast (Figure 1) were impressed by the tremendous variety of its scenery. Today, visitors can still appreciate those same qualities. The low rolling mountains of the Coast Range serve as a backdrop for most of the length of its ocean shore. In the south, the Klamath Mountains extend to the coast, and the edge of the land is characterized by high cliffs being slowly cut away by ocean waves. The most resistant rocks persist as sea stacks scattered in the offshore. Sand and gravel are able to accumulate only in sheltered areas where they form small pocket beaches within the otherwise rocky landscape.

tween the headlands. Portions of these beaches form the ocean shores of sand spits such as Siletz, Netarts, Nehalem, and Bayocean. Landward from the spits are bays or estuaries of rivers that drain the Coast Range.

The first western explorers and settlers were attracted to the Oregon coast by the potential richness of its natural resources. Earliest were the traders who obtained pelts of ocean otter and beaver from the Indians. Later came prospectors who sought gold in the beach sands and coastal mountains but in many cases were content to settle down and "mine" the fertile farm lands found along the river margins. Others turned to fishing, supporting themselves by harvesting the abundant Dungeness crab, salmon, and other fish in the coastal waters. Also important to the early economy of the coast were the vast tracts of cedar and sitka spruce, a significance that continues to the present.

In contrast, today the most important "commodity" for the Northwest coast economy is the vacation visitor. Vacationers arrive in thousands during the summer months, but in spite of their numbers it is still possible to leave coastal Highway 101 and find the seclusion of a lonely beach or the stillness of a trail through the forest.

OREGON COASTAL LANDFORMS

cliffs and headlands
sandy shorelines

0 50
kilometers

N

Cape Perpetua
Heceta Head
Sluslaw River
Dunes
Umpqua River
Oregon
Coos Bay
Cape Arago
Coquille River
Coquille Point
Cape Blanco
Rogue River
Cape Sebastian

CALIFORNIA

WASHINGTON

Columbia River
Nehalem R.
Nehalem Spit
jetties
former breach with dike
Cape Meares
Netarts Spit and Bay
Cape Lookout
Cape Kiwanda
Neslucce Spit
Cascade Head
Siletz Spit
Cape Foulweather
Yaquina Head
Yaquina River
Alsea River
Cape Perpetua

Clatsop Plains
Tillamook Head
Cape Falcon
Nehalem Spit
Boyceon Spit
Cape Meares
Netarts Spit
Cape Lookout
Cape Kiwanda
Neslucce Spit
Cascade Head
Siletz Spit
Cape Foulweather
Yaquina Head
Cape Perpetua

10 km
1 km

Newport
jetties
marine
mixed marine-fluvialite
Yaquina R. fluvialite

Figure 1. Coastal landforms of Oregon, consisting of stretches of rocky shorelines and headlands, separating pockets of sandy beaches. From Komar (1985).

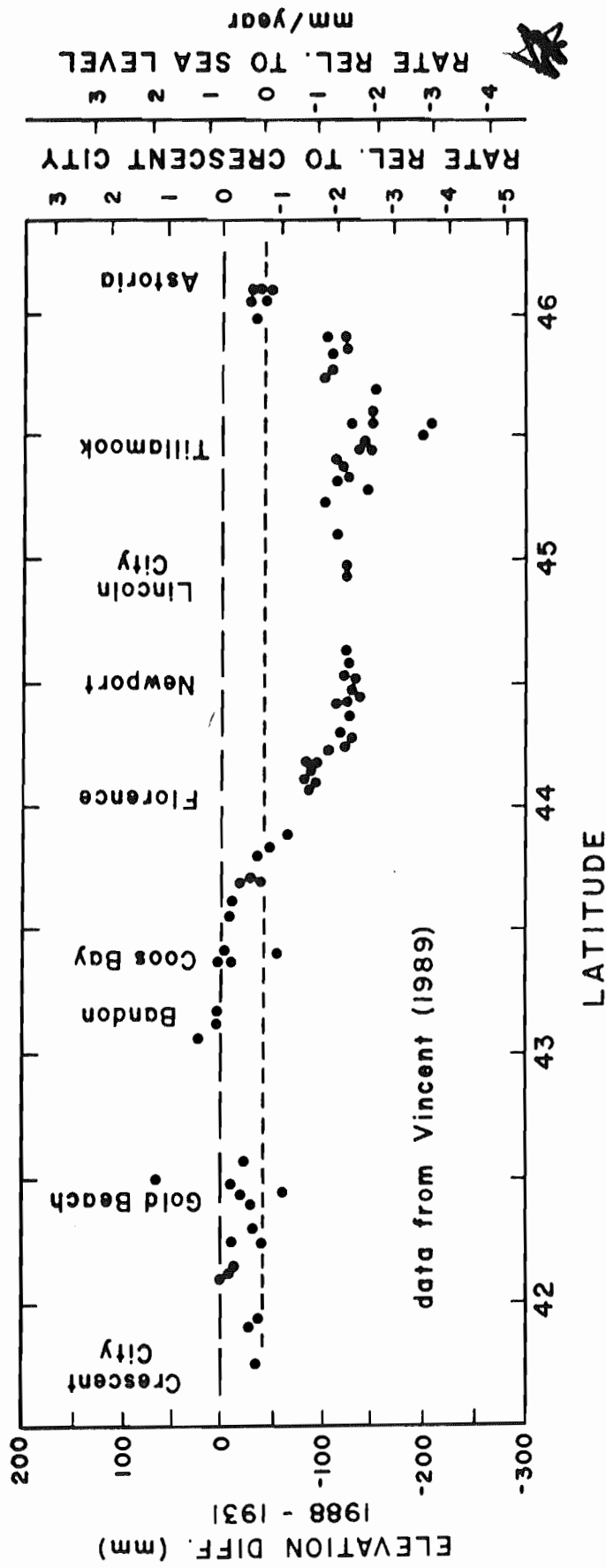


Figure 3. Elevation changes and the relationship to sea-level rise along the length of the Oregon coast from Crescent City in California north to Astoria on the Columbia River, based on repeated geodetic surveys along the coast. After Vincent (1989).

ernmost portion of the coast toward Astoria and the Columbia River. The first scale on the right of Figure 3 indicates the equivalent rates, the elevation changes divided by the lapsed time between surveys, 1988-1931 = 57 years. The differential rates are significant, for example amounting to 2-3 mm/year when comparing Astoria and the south coast with the Newport and Lincoln City areas.

It is possible to use the tide gauge data

coasts of the United States (Figure 2). The global rise in sea level has been estimated by various workers to be on the order of 1-3 mm/year (4-12 in. per century). The large range is due to the difficulty of separating that worldwide component from local tectonic and isostatic effects included in records from tide gauges. Assuming that the eustatic rise in sea level is on the order of 2 mm/year

in
fro
eve
for
duc
the
of
rel
the
dro
wh
sid
is a
upl
gau
tim
day
upl
acc
futu
atur
1.5
sear
turn
acce
glac

River, part of which moves southward until it is blocked by Tillamook Head. However, the bulk of sand derived from the Columbia River moves northward along the coast of Washington. The quantities of this northward sand transport can be only roughly estimated, but the primary evidence for this sand supply is that many of the beaches along the southern half of the Washington coast are growing (Phipps and Smith, 1978). The highest rates of beach growth tend to be in the south, closest to the Columbia River, decreasing to the north until, beyond Copalis Head, net erosion prevails.

On many coastlines, sand spits grow in the direction of the net littoral drift. The Long Beach Peninsula extends northward from the Columbia River and likely reflects the net sand movement along the Washington coast. It is unclear whether this northward growth has continued within historic times, since there have been many cycles of growth and erosion at the tip of the Peninsula. There are several sand spits along the northern coast of Oregon, some pointing north, while others point to the south (Figure 1). Those spits are located within the beach cells where zero net littoral drift prevails, and their directions do not provide testimony as to net longshore sand movements.

In view of the pocket-beach nature of the Oregon coast, the question arises as to the sources of beach sand contained within those littoral cells. These sources are reflected in the small quantities of heavy minerals contained within the beach sand. On the Oregon coast, the beach sand generally consists of grains of quartz and feldspar minerals. Those particles are transparent or a light tan, and this is what governs the color of most beaches. However, the sands also contain small fractions of heavy minerals that are black, pink, various shades of green, and other colors. These grains are readily apparent as specks in a handful of beach sand and are sometimes concentrated by the waves into black-sand placer deposits on the beaches. Of importance is that these heavy minerals are indicative of the rocks they came from and in many cases can be traced back to specific rocks and therefore geographical sources. That is the case for the heavy minerals in the sands of the Oregon coast. Most distinctive are the minerals derived from the Klamath Mountains: a variety of ancient metamorphosed rocks is found in those mountains of southern Oregon and northern California. As shown in the diagram of Figure 14, sands derived from the Klamath Mountains contain such minerals as glaucophane, staurolite, epidote, zircon, hornblende, hypersthene, and the distinctive pink garnet that, in particular, can often be seen concentrated on the beach. In contrast, the rivers that drain the Coast Range transport sand containing almost exclusively two heavy minerals: dark-green augite and a small amount of brown hornblende (Figure

14). Augite comes from volcanic rocks and is contributed to the rivers by erosion of the ancient sea-floor rocks uplifted into the Coast Range. With the sand of the Columbia River comes a diversity of heavy minerals because the river drains a vast area that contains many types of rocks (Figure 14).

The presence of sand derived from the Klamath Mountains in beaches along almost the entire length of the Oregon coast is at first surprising—in view of the many headlands that prevent any longshore sand transport for that distance. However, thousands of years ago, during the maximum development of glaciers, the sea level was considerably lower, the shoreline was then on what is now the continental shelf, many miles to the west of its present position, and the beaches were backed by a smooth coastal plain. At that time, sand derived from rivers draining the Klamath Mountains could move freely northward as littoral drift without being blocked by headlands. Studies of heavy minerals contained within continental-shelf sands demonstrate that this was indeed the case (Scheidegger and others, 1971): the metamorphic minerals from the Klamaths can be found in the shelf sands nearly as far north as the Columbia River. As the Klamath-derived sand moved north, additional sand was contributed to the beaches by rivers draining the Coast Range, so there is progressively more augite and a smaller proportion of metamorphic minerals from the Klamaths in these beach sands. The Columbia River was a large source of sediment, but most of that sand

moved to the north and dominates the mineralogy of ancient beach sands found on the Washington continental shelf. Some Columbia River sand did move south along the Oregon beaches during lowered sea levels and mixed with the sand from the Klamath Mountains and the Coast Range.

Therefore, the absence of headlands during lowered sea levels permitted an along-coast mixing of sands derived from multiple sources, principally from the Klamath Mountain metamorphics, the Coast-Range volcanics, and the Columbia River sands. Varying with the location along this former shoreline of the Oregon coast, the beach consisted of various proportions of mineral grains from those sources. Although a portion of the beach sand was left behind during the rapid rise in sea level and now can be found on the continental shelf, some of it migrated landward with the transgressing shoreline. The beaches would have been low in relief so that storm waves were able to wash over them, transporting sand from the ocean shores to the landward sides of the beaches and thereby producing the migration. Additional sand was contributed by the various river sources and from sediments eroded from the coastal plain.

About 5,000-7,000 years ago, the rate of rise in sea level decreased as the water approached its present level. Just about at that time, the beaches of Oregon came under the influence of headlands that segmented the formerly continuous shoreline. At some stage several thousand years ago, the headlands extended into sufficiently deep water to hinder further along-coast transport of the beach sands. This is shown by a study of the mineralogy of sand found on the present-day beaches (Clemens and Komar, 1988a,b). The pattern of along-coast mixing of sand from the various sources, established during lowered sea levels, is still partly preserved within the series of pocket beaches now separated by headlands. Therefore, one can still find minerals derived from the Klamath Mountains in virtually all of the beaches along the Oregon coast, even though it is certain that the sand can no longer pass around the many headlands that separate those beaches from the Klamath Mountains. In most cases, the Klamath-derived sand could have reached the modern beach only by along-coast mixing during lowered sea levels and subsequent on-shore transport with the rise of the sea. However, there has been some modification of the beach-sand mineralogy from that along-coast mixing pattern, as local sources have contributed sand to the beaches during the last few thousand years. Such beach-sand sources include eroding sea-cliffs and some sand from the rivers and streams entering the isolated pocket beaches.

There can be distinct changes in beach-sand mineralogies on opposite sides of headlands, that is, within adjacent but isolated

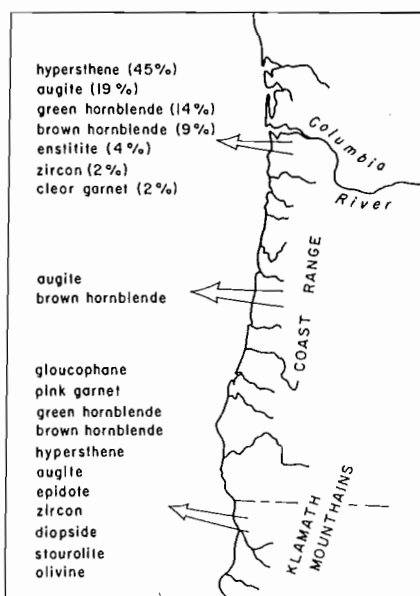


Figure 14. Principal sources of sand to Northwest beaches are the Columbia River and rivers draining the Coast Range and the Klamath Mountains. Each source supplies different suites of heavy minerals to beach and estuarine sands. From Clemens and Komar (1988b).

OTHER FACTORS

1. rain wash on cliff face
2. ground-water flow and pore pressures
3. vegetation cover
4. burrowing by rodents, etc.
5. people
 - walking on cliff and talus
 - carving graffiti on cliff face
 - watering lawns
 - culverts, etc.
 - protective structures (sea walls, etc.)

OCEAN FACTORS

1. waves
 - heights and periods (energy or energy flux)
 - approach angle (longshore currents and littoral drift)
 - set-up and run-up
2. cell circulation with rip currents
3. tidal variations
4. storm surge
5. sea level (seasonal and long-term net changes)

CLIFF FACTORS

1. composition
 - "hardness" (e.g., compressive strength)
 - talus production
 - source of beach sediments
2. layering (bedding), joints, and fractures
3. inclination of rock layers
4. height and slope of cliff face

BEACH FACTORS

1. volume of beach sediments (buffering ability)
2. composition and grain size
 - control on beach morphology
 - sand "blasting"
3. presence of drift logs

Figure 29. Schematic diagram illustrating the many factors and processes in

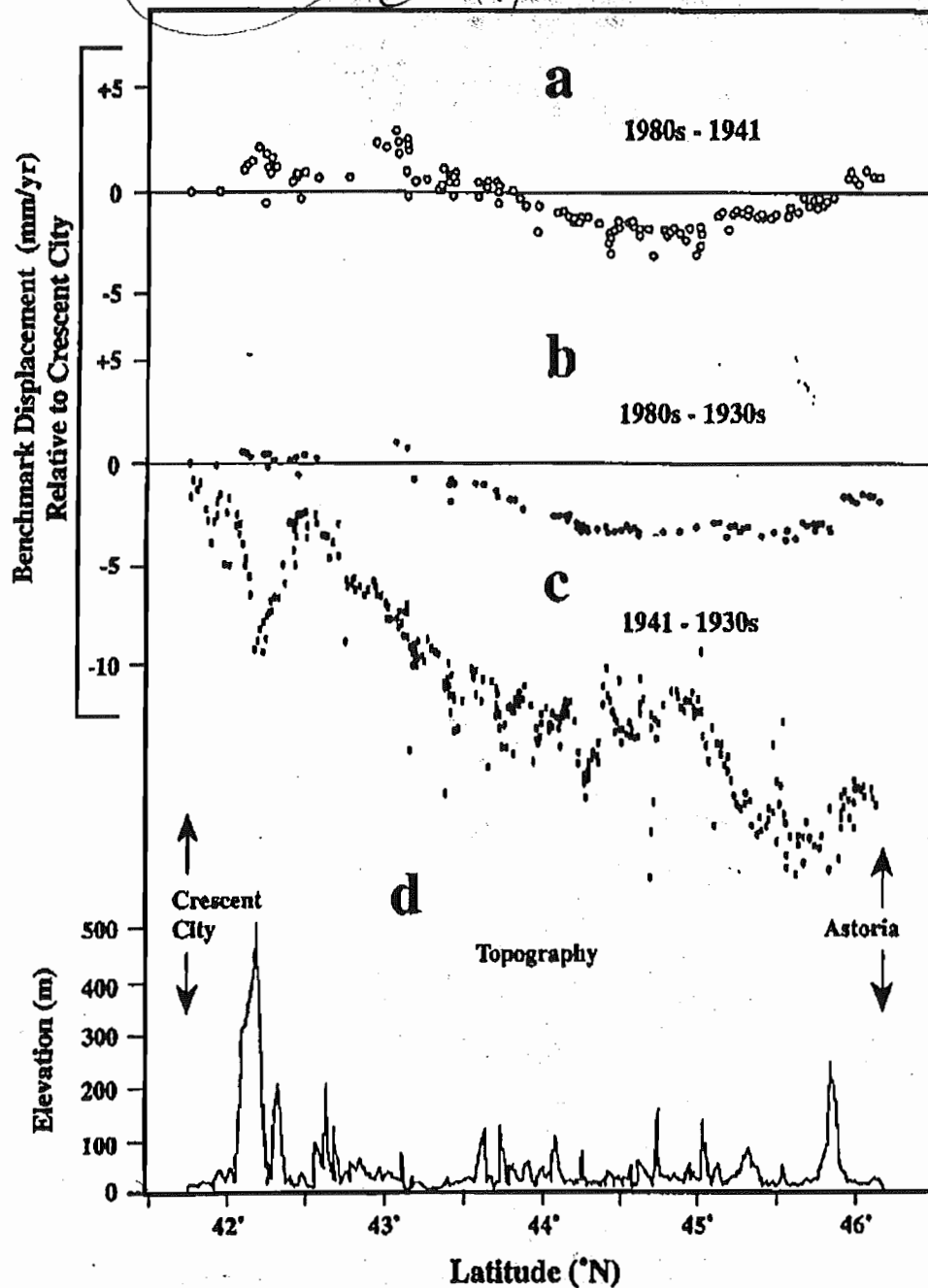


Figure 10. Uplift rates relative to Crescent City calculated from repeated first-order leveling along the Cascadia coast. Rates are calculated by differencing the heights determined by three epochs of leveling. Note similarity in the shape of the 1980s-1930s and 1980s-1941 profiles. The 1941-1930s profile probably contains minor systematic error that is amplified by plotting as rate of change because of the short time interval between surveys. Also note that several sharp cusps in the data correlate with peaks in topography, suggestive of local errors.

level route reaches an elevation of 500 m, and the other is at Tillamook Head (45.9°N) where the level route reaches an elevation of 250 m. Both locales show a relatively sharp change of inferred rate associated with relatively high local relief. Also, both anomalies are about the same wavelength as their corresponding local topographic highs, suggesting that these signals might be related to topography. The 1941 coastal survey is possibly questionable, a conclusion support-

ed below by consideration of loop misclosure. Topography does not, however, appear related to some of the other short wavelength anomalies nor to the longer wavelength tilt signals along the coast (Figure 10).

Loop Closure

Loop closure analysis is done to determine the accuracy of leveling data. Elevation differences between beginning and

1923 north	-99.00	626	-3.96	-0.16
54 south				
30s Sly E-W				
1980s inland	43.0	626	1.72	0.07
<i>Loop V</i>				
1919, 1920,	-85.00	798	-3.40	-0.11
1930s from	15.76	798	0.63	0.02
y to				

b for loop locations and locales.

Its, based on three surveys,
 It with time suggesting a
 atic error. Third, the tilts
 Newport-to-Albany line are
 atic error there unlikely.
 he Portland-to-Albany leg
 s not surveyed in 1941) and
 close to acceptable values.
 errors during that epoch.
 suspected systematic error
 o-Portland segment. This
 toria-to-Portland line is
 e Newport-to-Albany line
 land valley profile in this
 sure around the loop is

ng data set are very poor.
 op V have a very large
 nch mark F56 at Grants
 et for two reasons. First,
 by tide gauges are quite
 influence of errors on the
 ss time between surveys
 ns. Figure 10c illustrates
 e between surveys, as in
 usable results from this
 at with independent tidal

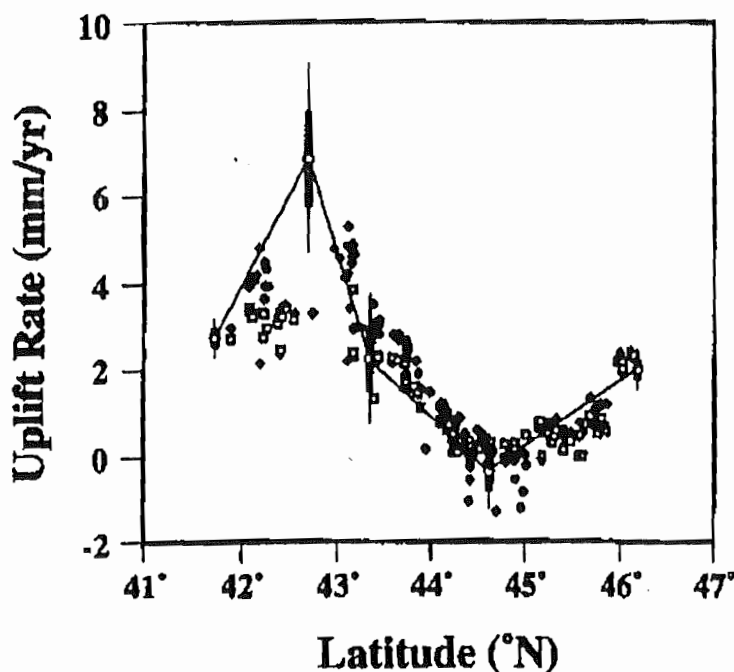


Figure 12. The Crescent City-to-Astoria uplift rate profiles derived from releveling (Figures 10a and 10b) are arbitrarily referenced to the tidally indicated uplift rate at each end of the Crescent City-to-Astoria portion of the uplift rate profile (Figure 9) determined from tidal data. Shapes of uplift rate profiles from releveling compare quite well to the uplift profile from tidal data.

MITCHELL ET AL.: CASCADIA PRESENT-DAY VERTICAL DEFORMATION

agment (Rainier-to-Portland, Portland-to-Al-
some later relevelings have different starting
ints) is attached to east-west lines, and then a
is drawn through the entire profile. The
ts of the various north-south and east-west
sonably consistent, suggesting very crude rate
the network of leveling lines. For example,
a low on the coastal profile (Figure 13c), as is
inland profile (Figure 13b); the flat slope in
ween them (Figure 14c) is therefore consistent.

of Regional Uplift Rates

the uplift rate data in map view, we use the
through the tidally adjusted uplift rate profiles
ata (Figures 12 through 14) and pick off integer
are plotted and hand-contoured to produce a
f uplift rates (Figure 15). To complete the map
state, inland from the region of rapid uplift, we
ier uplift rate contouring [Ando and Balazs,
et al., 1989], first correcting for different rates
e used in those studies. We extend the map
Mendocino, beyond the tide gauges which
train the north-south coastal uplift rate profile
auges. Cape Mendocino is no farther from tide
me portions of the inland valley north-south
file but lacks the constraint of fitting to tidally
eling results from more than one direction.
nations of leveling epochs near Cape Mendo-
lightly varying results, just as along the coast to
e adjustment of a freely floating end is not great
example), but the internal detail of the uplift
the Cape Mendocino vicinity is of interest.

ring approach is fairly crude and locally
we do not believe the data justify more detailed
d the overall regional pattern is well-resolved.
eling data are not confirmed by independent
al Positioning System (GPS) observations of
nch marks and level line junctions have been
d will be analyzed to determine vertical posi-
comparison (M. Murray, personal communi-
Nonetheless, comparable uplift rate patterns
the independent data sets of tidal records and
ng the coast constitute a test of consistency
There is, however, distortion of the uplift rate
ography-related error where the inland N-S
cross the Siskiyou Mountains in the vicinity of
rapid present-day uplift and several connecting

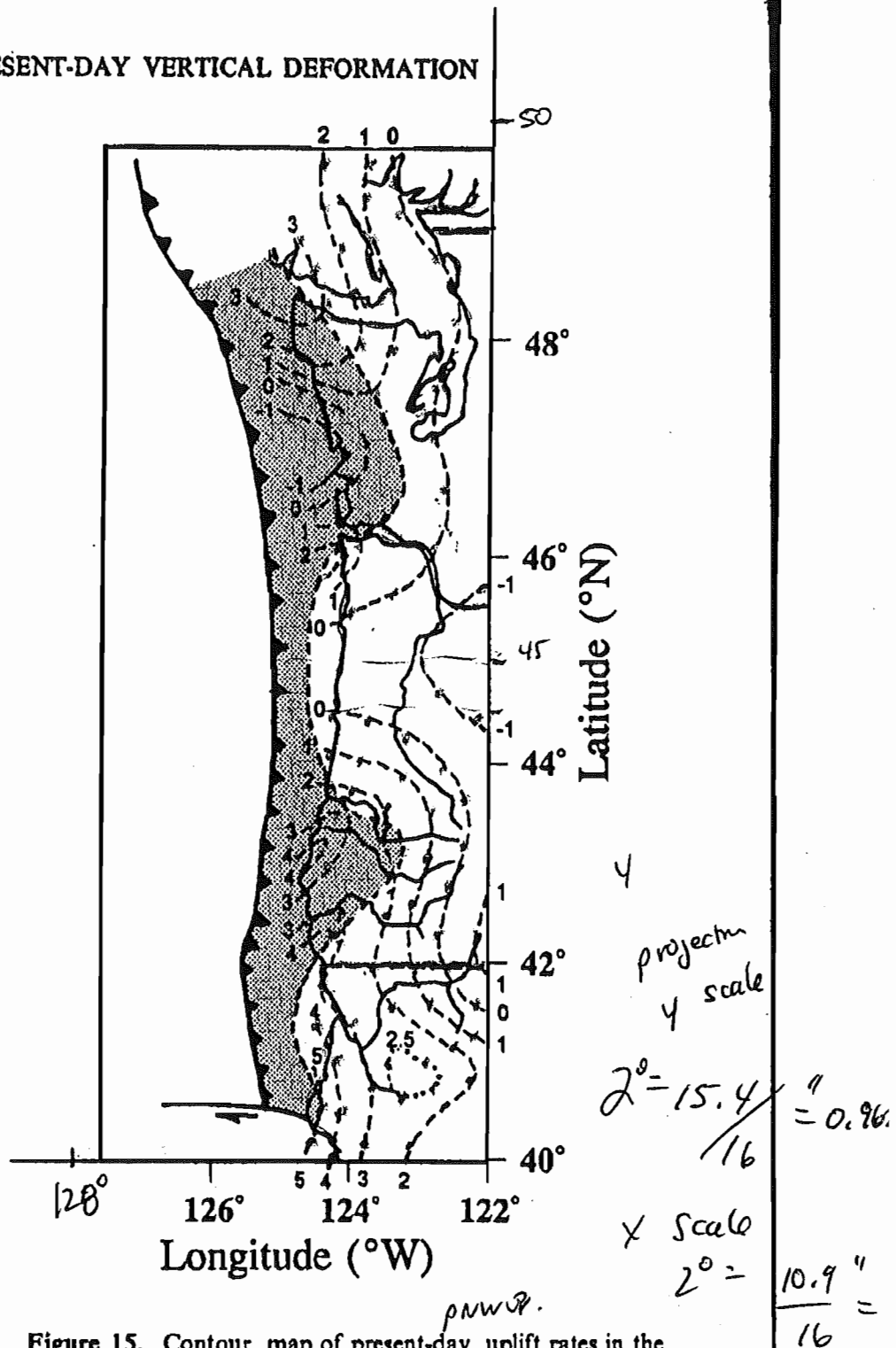


Figure 15. Contour map of present-day uplift rates in the Pacific Northwest, west of the Cascade Range and south of Canada. Contours are generated from tidal records and leveling profiles, with much of Washington state recontoured from Ando and Balazs [1979] and Holdahl et al. [1989], as discussed in the text. The stippled area is an interpretation of the region of elastic strain accumulation, assuming that the most rapid uplift at the surface approximately overlies the downdip edge of that portion of the subduction interface [Savage, 1983].

Grays Harbor/Willapa Bay. In southwestern Oregon, an axis of rapid uplift extends northeasterly from the Cape Blanco region (42.2-43.2°N). The overall shape of the uplift rate

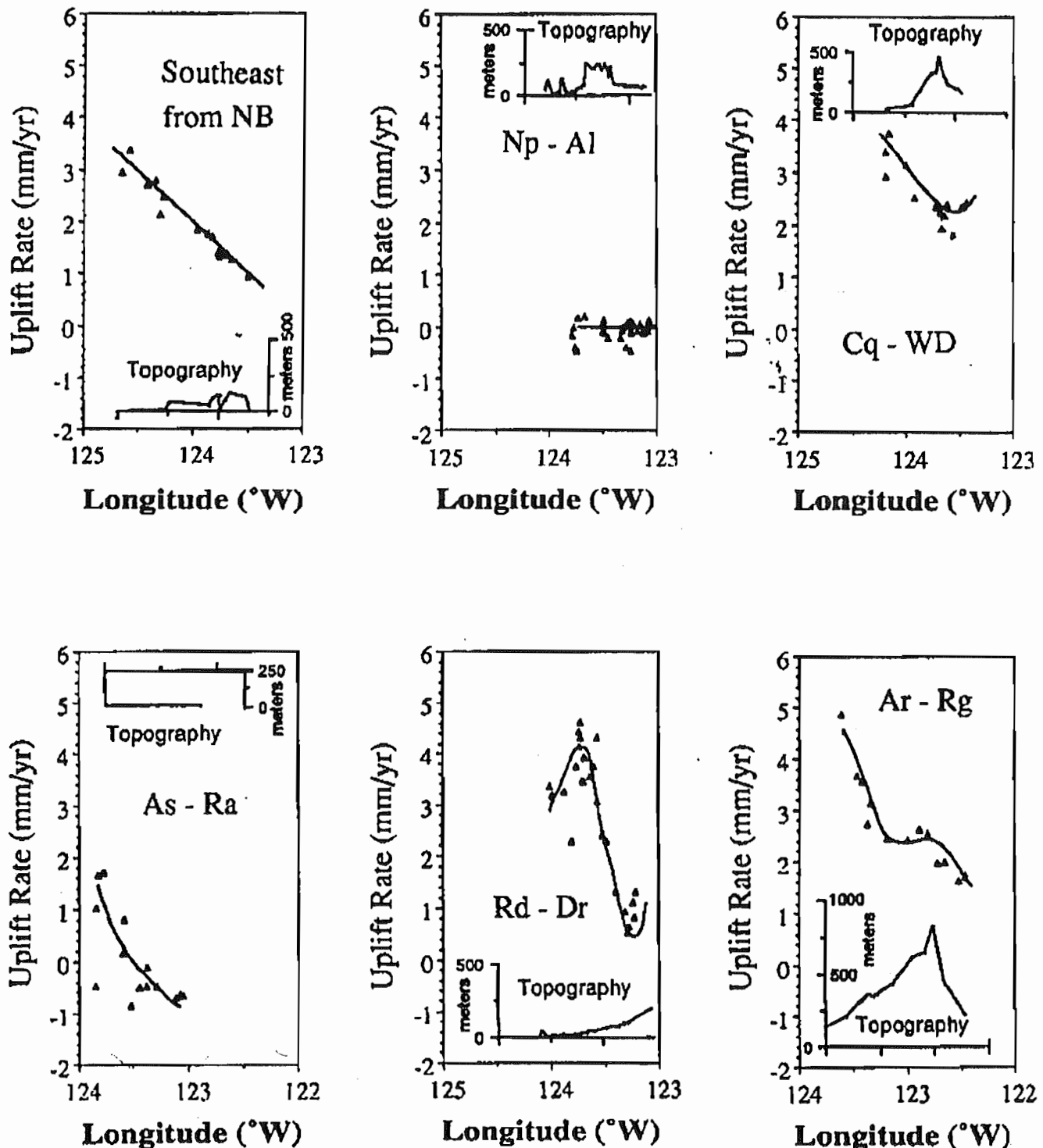


Figure 14. East-west uplift rate profiles connect the tidally adjusted north-south coastal profile (Figure 13a) to the north-south inland valley profile (Figure 13b). Refer to Figure 1b for locations. Notice that most of the east-west profiles tilt to the east, though at different rates. An exception is the Newport-to-Albany profile, which is essentially flat. *Reillinger and Adams* [1982] report similar tilts, but the longer time intervals available due to releveling in the late 1980s allow the tilts to exceed their random error envelopes.

ties to tide gauges at Crescent City and Astoria arbitrarily force the ends to match, the internal shapes of the releveling profiles and tidal profile are entirely independent. There is

Astoria-to-Rainier profile to the Astoria tide gauge, the Newport-to-Albany profile to the South Beach/Newport tide gauges. The Reedsport-to-Drain, Coquille-to-Winston/Dil-

30

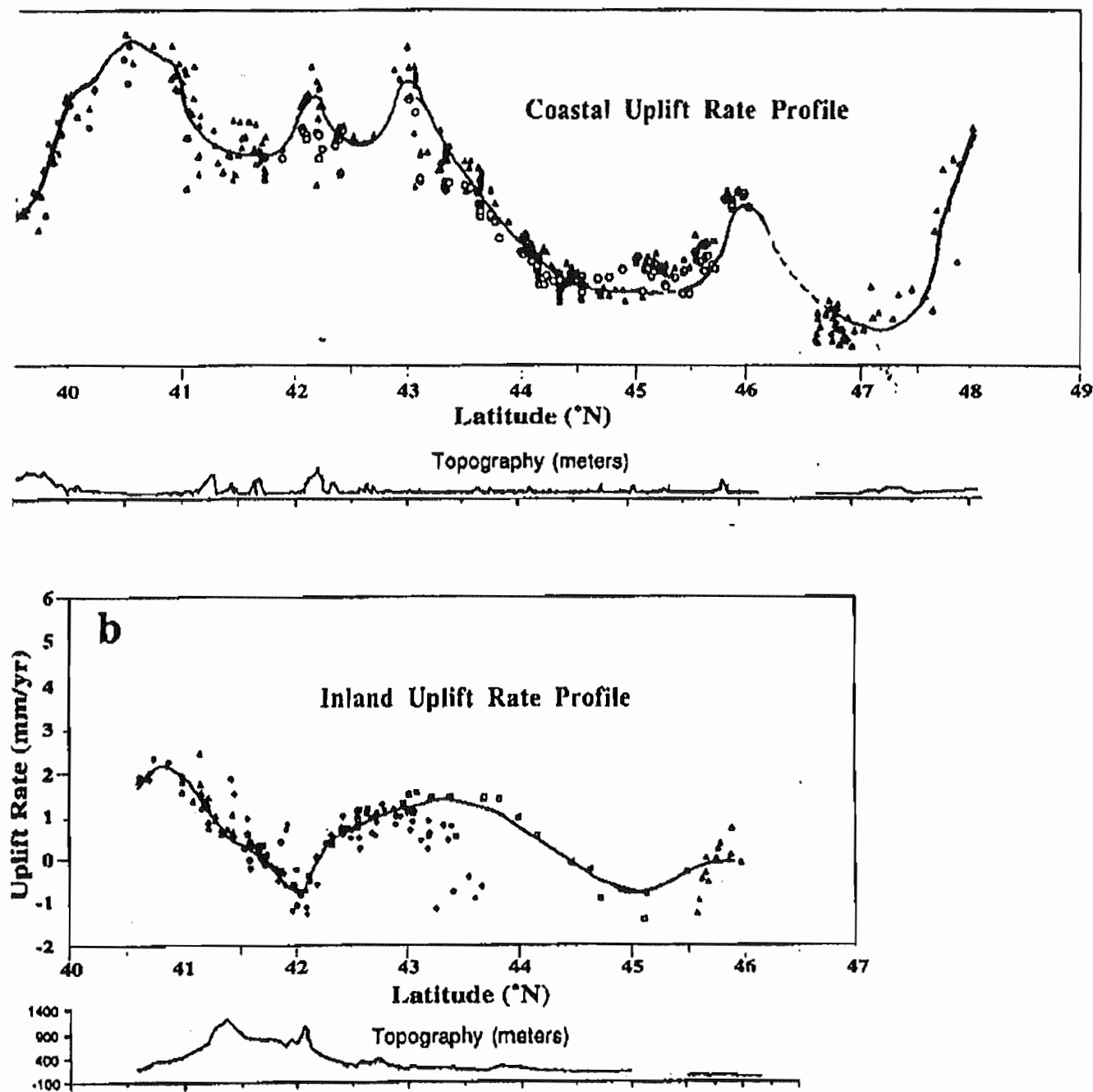


Figure 13. Detailed north-south uplift rate profiles from leveling: (a) along the coast and (b) through the north-south inland valleys. The shapes are similar, though the inland profile is more subdued and appears to be shifted slightly to the north, relative to the coastal profile. The coastal profile is in several pieces, which are tied to absolute rates indicated by tidal data (Table 2 and Figure 9) at Crescent City, Astoria, Toke Point, and Neah. The absolute rate of the inland valley profile is determined by adjusting it in segments to the east-west profiles in Figure 14. Small regions of subsidence, near Redding and south of Portland may be due to leveling lines crossing sediment filled basins, rather than tectonic motion.

12). Second, as *Wellman* [1972] points out, between independent data sets, such as leveling records as a specific example, are better and more useful internal tests for systematic and random

are defined. At the Astoria end, we get an uplift rate that is too rapid using the 1980s-1941 (Figure 10a) and too slow using the 1980s-1930s data (Figure 10b), compared to the tidally indicated difference in uplift rate, which is 0.9 ± 0.3

1994

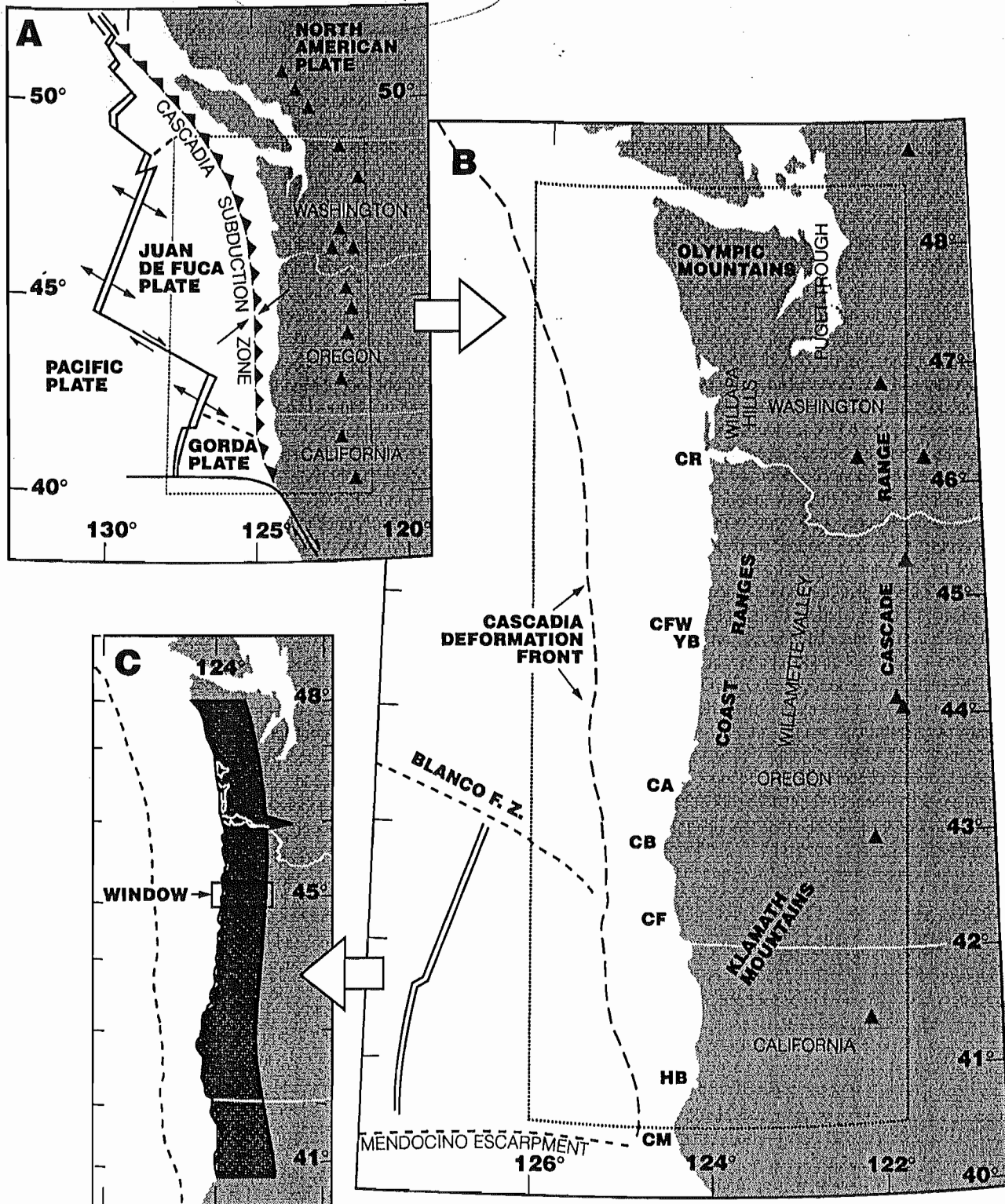


Figure 1. (a) Location map of the Pacific Northwest in the context of plate tectonics; triangles are Cascade volcanoes. (b) Location map of the coastal ranges situated on the leading edge of the North American plate between the Mendocino escarpment and the Canadian border. Triangles denote selected Cascade volcanoes. CR, mouth of the Columbia River; CFW, Cape Foulweather; YB, Yaquina Bay; CA, Cape Arago; CB, Cape Blanco; CF, Cape Ferrel; HB, Humboldt Bay; CM, Cape Mendocino. (c) Shading shows the area of the Coast Ranges, 65 arc min of longitude wide, for which the digital elevation model ETOPO-5 was employed to compute average topography. The box depicts the size of the computational window (65 arc min x 15 arc min) that was employed for each individual calculation of average topography. See text for further explanation.

32

sea level is an expression of Earth's geoidal surface. The geodetically derived uplift is in reference to present sea level and the shore platform uplift is in reference to the appropriate late Pliocene eustatic sea level high stand (see below). Because rock uplift relative to the geoid is equal to surface uplift minus exhumation [England and Molnar, 1990] and because there has been negligible erosion of either the shore platforms or the highway benchmarks, the coastal uplift rates that we discuss are both uplift rates of rock relative to the geoid as well as surface uplift rates. Subsequent use of the term "uplift rate" should thus be unambiguous. Using uplift rate data integrated over the last 45 years and that integrated over the last 80,000-125,000 years, we can compare interseismic uplift with long-term uplift at the coast along the Cascadia margin.

Average Topography Along the Crest of the Coast Ranges

We calculated average topography for the Coast Ranges (Figure 2) using the public domain 5 arc min digital elevation model ETOPO-5 [National Geophysical Data Center, 1988]. Using ETOPO-5, we calculated a running average for the topography of the Coast Ranges in a north-south trending swath extending from the coast inland for 65 arc min of longitude (Figure 1c). The swath extends between latitudes 41° and 47° N along the trend of the Coast Ranges, for a total length of 778 km. The average width of the swath is 86.6 km (90.9 km at latitude 41° and 82.2 km at latitude 47°). Each individual calculation of average topography at 5-arc min latitudinal intervals is the running average of the average altitude at 39 different grid points, 13 grid points from each of

three adjacent lines of latitude (computational window (Figure 1c) is 65 arc min of longitude \times 15 arc min of latitude on a 5 arc min grid), with 13 out of 39 of the grid points changing for each calculation. Thus each calculation of average topography represents an area of about 2400 km² (27.8 km \times 86.6 km).

Because we will subsequently compare uplift rates at the coast to trends in average topography for the Coast Ranges as a whole, we determined whether north-south trends in average topography for the coastal (western) side of the Coast Ranges are similar in form to trends of average topography for the Coast Ranges as a whole. Using the same computational technique but applied to narrower widths, we determined average topography for a 25-arc-min-wide swath on the west side of the Coast Ranges, and we also computed average topography for a nonoverlapping 25-arc-min-wide swath on the eastern side of the Coast Ranges. Comparing the western profile to the profile for the Coast Ranges as a whole (Figure 2), the profiles show that first, the highest average topography is between 41° and 45° , corresponding to the Klamath Mountains; second, average topography fluctuates around 200 m between 43.5° and 46° ; and third, a spike in average topography occurs at 47.5° - 48° , corresponding to the Olympic Mountains. The two profiles differ considerably along two segments where coastal plains or embayments are unusually wide, extending as much as 20 km inland. These segments include the southern Oregon coastal plain (Cape Blanco to Coos Bay; latitudes 43° - 43.3°) and the embayments of southern Washington (Columbia River, Willapa Bay, Grays Harbor; latitudes 46° - 47°). With the exception of these coastal lowlands, the western portion of the Coast Ranges has latitudinal trends in elevation similar to that of the Coast Range as a whole (Figure 2), albeit the average elevations

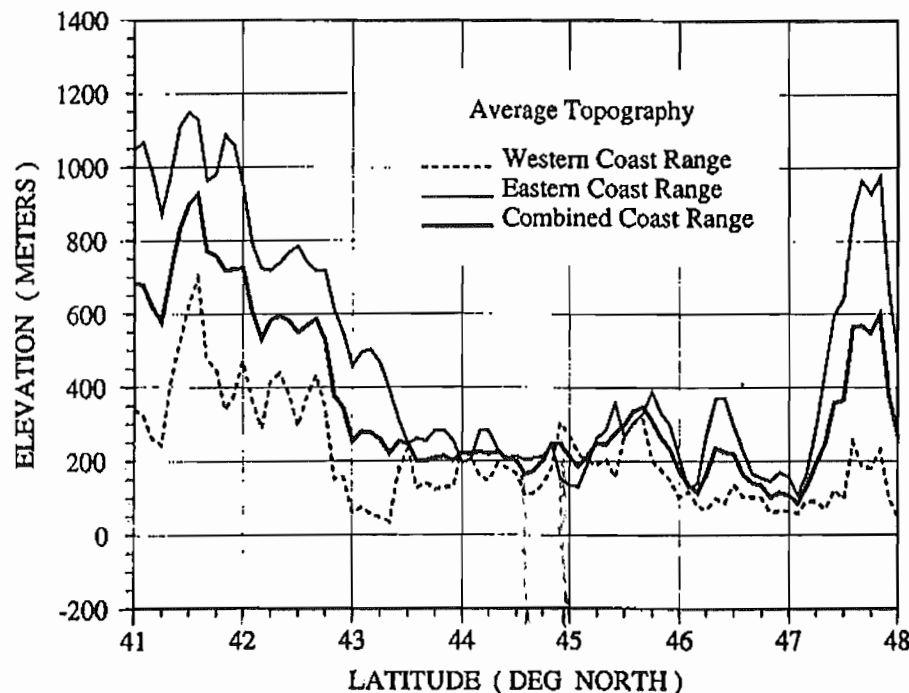


Figure 2. Latitudinal variation in average topography for the 25-arc-min-wide western portion of the Coast Ranges, for the 25-arc-min-wide eastern portion of the Coast Ranges and for the entire 65-arc-min-wide Coast Ranges. All longitudinal distances are measured eastward (inland) from the coast. The eastern and western data sets do not use overlapping data. General topographic trends are similar for the eastern, western, and combined data sets.

along the coast are lower because Coast Range drainages transport sediment to the west.

The error limit for the latitudinal variation in average topography of the Coast Ranges (Figure 3) is the standard error of the mean. Because of the running average, sequential standard errors are correlated, but every third standard error is independent. We also show an envelope curve depicting the upper bound of elevations used in the calculation at each latitude ("maximum elevation" in Figure 3). The maximum elevation is the average elevation of the crest of the Coast Ranges computed as a three-point running average. The maximum elevation profile shows the magnitude of surface uplift, or uplift of rocks minus exhumation, along the Coast Range crest.

Overlying Topography Versus Age of Subducted Juan de Fuca Plate

Subsidence, or change in elevation, of the ocean floor as it moves away from the spreading ridge is expressed by

$$e(t) = ct^{1/2}$$

[Parsons and Sclater, 1977], where $e(t)$ is the vertical distance in meters that the ocean floor has subsided in moving away from the spreading ridge and t is the age of the plate in millions of years. Constant c , the linear slope of the change-in-elevation versus $t^{1/2}$ relation, is 350 [Parsons and Sclater, 1977]. The use of this subsidence model, in conjunction with an approximate age distribution of the Juan de Fuca and Gorda

plates presently subducting at the Cascadia margin, yields latitudinal estimates of the relative elevation of the subducting plate at a position beneath the crest of the Coast Ranges (Figure 3).

The lithospheric subsidence model predicts that rapid density changes occur within the oceanic plate in close proximity to ridges. However, thick accumulations of young sediments along the Cascadia margin and a lack of seismicity near the trench axis preclude direct measurement of depths to the top of the subducting Juan de Fuca plate beneath the Coast Range. We acknowledge problems inherent in estimating slab morphology near subduction zones using the simple age-depth relationship cited above and emphasize that our interpretation focuses on the relative subsidence of the slab due to changes in slab age along the margin. When oceanic plates are loaded by subduction under continental crust, the differential subsidence would be enhanced over that caused by an increase in age of the plate alone. This enhancement is because a less dense, younger slab will subside less than an adjacent older, denser slab, if both are loaded by the same overlying continental plate. Thus the differential elevation of two adjacent subsiding slabs, as computed by the Parsons-Sclater relation in the case of no loading, is a minimum estimate for the amount of differential subsidence that must occur if both slabs are subsequently loaded by an overriding plate.

Approximations for the age of the subducting plates, needed to calculate relative subsidence, are made difficult by a complex pattern of spreading along the Juan de Fuca and Gorda ridges. These complications include propagating rifts, changes in relative motion poles, deformation within the

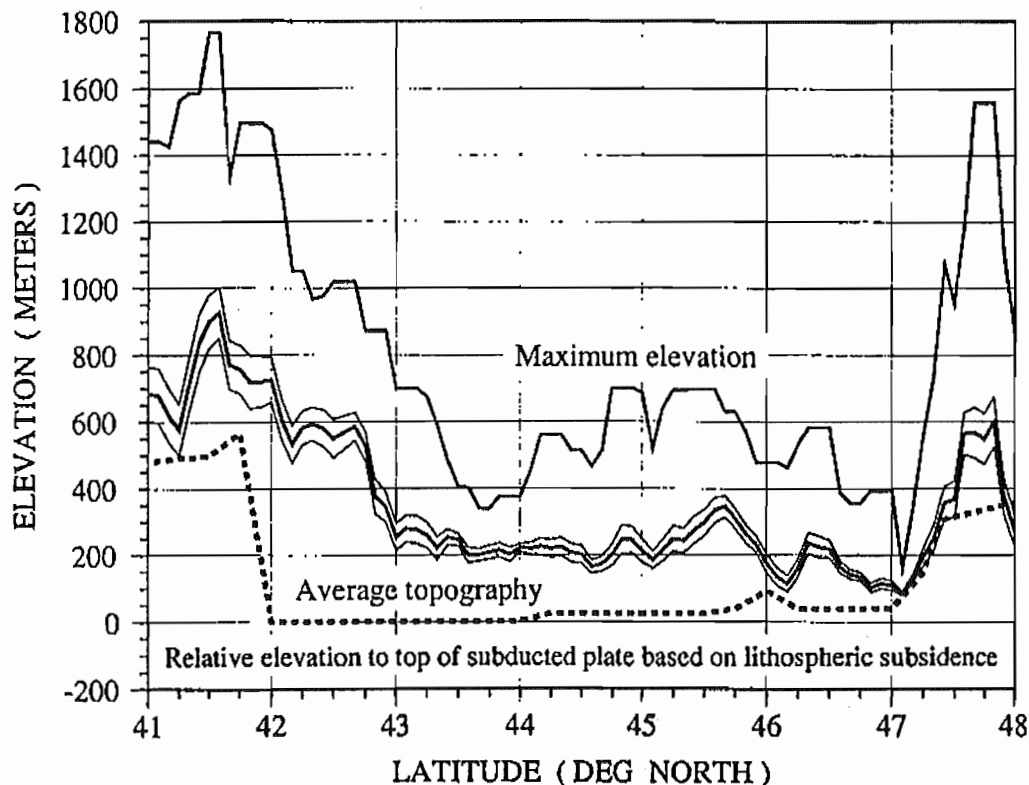


Figure 3. Latitudinal variation in average topography and age of subducted slab along the crest of the Coast Ranges. Top curve, maximum average elevation used in each topographic calculation; middle curves, average topography bounded by the standard error of the mean; bottom dashed line, relative elevation of the top of the subducted slab beneath the crest of the Coast Ranges.

Gorda plate, and an uncertain history for the development of the Blanco Fracture Zone [Wilson, 1986, 1990; Embley and Wilson, 1992]. Age estimates (Table 1) were determined by reflecting recognizable magnetic isochrons from the Pacific plate onto the Juan de Fuca and Gorda plates using the magnetic isochron map of Atwater and Severinghaus [1989]. A similar result is obtained through an eastward extrapolation of the isochron patterns observed immediately to the west of the Cascadia deformation front.

The age of the slab beneath the crest of the Coast Ranges is uniform except for markedly younger slab at the southern end beneath the Klamath Mountains, which form the Coast Ranges in southernmost Oregon and northernmost California (Figure 3). Younger slab also underlies the Olympic Mountains at the north end of the Coast Range. The age discontinuity in the subducted slab beneath the Klamath Mountains is due to subduction of the Blanco Fracture Zone (Figure 1b), which juxtaposes young crust to the south against older crust to the north (Table 1). The younger slab beneath the Olympic Mountains reflects subduction of progressively younger plate to the north as the Pacific-Juan de Fuca spreading center becomes closer to the leading edge of the North American plate (Figure 1b) (Table 1).

The most abrupt latitudinal change in average topography occurs above the subducted Blanco Fracture Zone (Figure 3).

Table 1. Age of the Subducted Juan de Fuca Plate as Projected through the Overlying Pacific Plate to the Crest of the Coast Ranges

Latitude* °N	Chron †	Age, Ma
48.0	5/5A	11.0
47.4	5A	12.0
47.25	5B	15.3
47.0	5D	17.86
46.75	5D	17.86
46.5	5D	17.86
46.25	5D	17.86
	<i>Pseudo Fault</i>	
46.0	5C	16.60
45.75	5D	17.86
45.5	5D	17.86
45.25	5D	17.86
45.0	5D	17.86
44.75	5D	17.86
44.50	5D/5E	18.2
44.25	5D/5E	18.2
44.0	5E	18.8
43.75	5E	18.8
43.5	5E	18.8
43.25	5E	18.8
43.0	5E	18.8
42.75	5E	18.8
42.5	5E	18.8
42.25	5E	18.8
42.0	5E	18.8
	<i>Blanco Fracture Zone</i>	
41.75	4	7.41
41.5	5E/4	8.5

*Latitude position is along crest of Coast Ranges

† Chron on the Juan de Fuca plate determined from reflection of chrons from Pacific plate to Juan de Fuca plate across the spreading center.

The top of the relatively young, more buoyant subducted crust south of the Blanco Fracture Zone has an elevation that is about 500 m higher relative to the top of the slab north of the Blanco Fracture Zone. The north facing scarp in the downgoing slab, with relatively higher slab to the south, is presently directly below the zone of maximum change in average topography along the Coast Range crest (Figure 3). This altitudinal change marks the topographic division between the Klamath Mountains to the south and the elevationally lower Oregon Coast Ranges to the north. Similarly, the topographically higher Olympic Mountains, at the northern end of the Coast Ranges in Washington, are underlain by relatively young subducted plate that is, in relative elevation, about 300 m higher than older subducted plate further south.

Geodetic Uplift Rates

Differences in the relative heights of bench marks reoccupied by successive first-order leveling surveys provide a data set of geodetically derived uplift rates along the coast for the past ~45 years, from 1941 to the period 1987-1988 (Figure 4) [Mitchell *et al.*, 1991, 1992, this issue]. The trends in relative bench mark elevation changes between leveling surveys (Figure 4) are probably real and of tectonic origin because analysis of tidal records along the same segment of coast yields the same magnitudes and trends in uplift. The tidal gage records and the leveling survey records are two independent data sets; differencing the tidal records and differencing the leveling records yield similar relative differences in uplift rate between coastal localities [Mitchell *et al.*, this issue].

The geodetically derived uplift rates are referenced to a contemporary sea level rise of 1.8 mm/yr [Douglas, 1991], with no correction for post glacial rebound. In magnitude and variability, the uplift rates are several times larger than the predicted magnitude of present-day post glacial rebound, and the regional variation of uplift rate is of a much shorter wavelength than that predicted for present-day post glacial rebound [Mitchell *et al.*, this issue]. These geodetically derived uplift rates are uplift rates of rock relative to the geoid and thus are directly comparable to the shore platform uplift rates, described below.

Uplift Rates of Shore Platforms

Uplift rates are calculated for uplifted shore platforms in the latitude range 42° to 45°N. The magnitude of uplift, relative to present sea level, was determined for the junction of the paleo-sea cliff and the platform (the shoreline angle). Uncertainties in calculation of the magnitude of uplift of the shoreline angle are (1) the altitude of the shoreline angle at the time of its formation relative to altitude of the eustatic sea level high stand that eroded the shoreline angle (according to Wright [1970] and Trenhaile [1980], the two elevations are the same, ± 2 m); (2) altitude of paleo-sea level high stand, this altitude being a function of the age of the high stand and the sea level model employed (see below); (3) present-day altitude of shoreline angle, where the error in assigned altitude is a function of surveying accuracy; we used 7.5 arc min topographic maps for assigning altitude, where the error is ± 6 m, or one half the contour interval; and (4) original seaward tilt of the platform; this uncertainty only applies in cases of

35

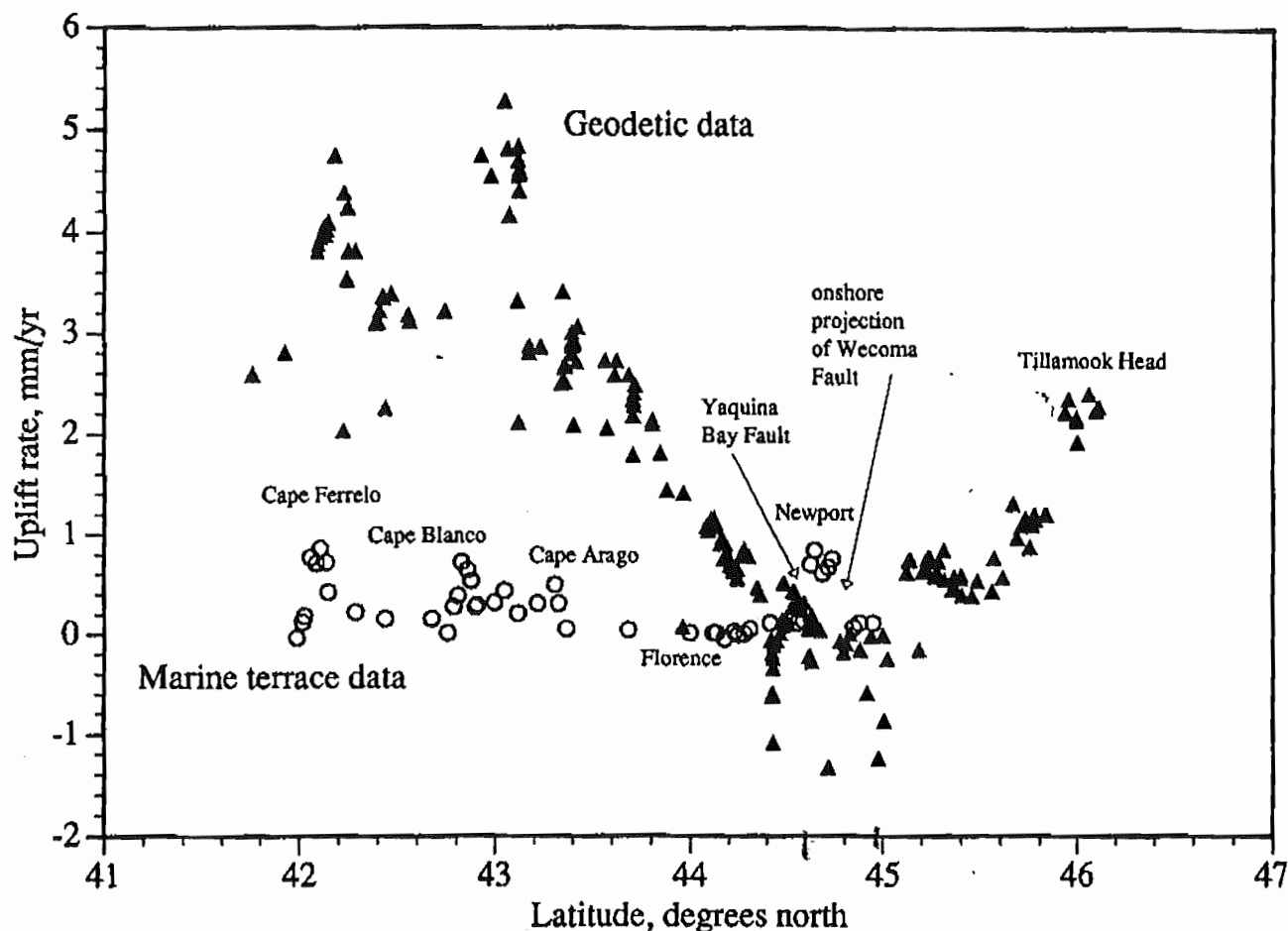


Figure 4. Latitudinal variation in uplift rates derived from resurveyed bench marks between 1941 and the 1987-1988 period, and from sea cliff/platform junctions of 80-125 ka shore platforms. Triangles, resurveyed bench marks; circles, shore platform data.

poor exposure where platform altitude is measured at a point seaward of the shoreline angle, necessitating calculation of shoreline angle elevation using the original slope of the platform [Bradley and Griggs, 1976].

Uplift rates can only be determined at localities where the shoreline angle elevation can be located on a terrace of a known age. The ages of the late Quaternary eustatic sea level high stands are well established at 80, 105, and 125 ka [Mesolella et al., 1969; Bloom et al., 1974; Chappell and Shackleton, 1986]. The 80 ka and 105 ka wave-cut platforms were identified based on terrace correlation, using soil development [Bockheim et al., 1992] and altitudinal surveys, to terraces of known age in the Cape Blanco [Kelsey, 1990] and Cape Arago [McInelly and Kelsey, 1990] areas. Marine terrace sediments of known age have age assignments based on a radiometric age from U-series dating of coral and amino-acid racemization-ratio correlation ages using molluscs [Muhs et al., 1990]. In central coastal Oregon, 125 ka platform ages were assigned [Ticknor, 1993] either based on terrace sequence (the terrace in question being the next one altitudinally above the 105 ka terrace) or based on correlation with a 125 ka age-assigned wave-cut platform near Yaquina Bay, Oregon [Kennedy et al., 1982].

We used paleo-sea level high stand elevations as determined from the coastal California sea level high stand elevation

model [Muhs et al., 1992], rather than the New Guinea sea level high stand model [Bloom et al., 1974; Chappell and Shackleton, 1986]. If the New Guinea model is more appropriate for the west coast of North America, uplift rates would be systematically higher for surveyed points on the 80 ka and 105 ka platforms but not for points on the 125 ka platform. The maximum increase in uplift rates would be about 0.1 mm/yr. Given all the above uncertainties in the magnitude of uplift of a shoreline angle formed at 80, 105, or 125 ka, the maximum error in the uplift rate calculation is about ± 0.2 mm/yr.

Shore platform uplift rates are for the most part <0.25 mm/yr and have a range of -0.04 to 0.87 mm/yr (Figure 4). Abrupt changes in shore platform uplift rate, in some cases by almost an order of magnitude, occur at several localities along the Cascadia margin. All abrupt changes in uplift rate can be related to a distinct structure, a fault or a fold, that displaces the shore platform. Uplift rates abruptly change across structures near Cape Ferrelo (CF, Figure 1b and Figure 4) [Kelsey and Bockheim, 1994], Cape Blanco (CB, Figure 1b and Figure 4) [Kelsey, 1990], Cape Arago (CA, Figure 1b and Figure 4) [McInelly and Kelsey, 1990] and Newport/Yaquina Bay (YB, Figure 1b and Figure 4) [Ticknor, 1993].

The platform offsets near Newport (Figure 4) are part of a regionally extensive upper plate fault zone at this latitude,

Quaternary upper plate deformation in coastal Oregon

Harvey M. Kelsey

Robert L. Ticknor

James G. Bockheim

Clifton E. Mitchell

Department of Geology, Humboldt State University, Arcata, California 95521

74 Russell Avenue, Watertown, Massachusetts 02172

Department of Soil Science, University of Wisconsin, Madison, Wisconsin 53706

Science Department, Lane Community College, Eugene, Oregon 97403-0640

ABSTRACT

The leading edge of the North American plate along the Cascadia subduction zone is deforming and rotating clockwise as a consequence of both underthrusting of the Gorda-Juan de Fuca plate and collision of the North American plate with the Pacific plate. The details of late Quaternary (≤ 125 ka) upper-plate deformation resulting from these plate interactions are largely obscured because the most recent deformation overprints earlier deformation in the Tertiary rocks of the Coast Range. However, by mapping uplifted wave-cut platforms formed during times of high sea level in the past ≈ 500 000 yr, we identify faults and folds active in the late Quaternary in central coastal Oregon. Through along-coast correlation of these platforms using elevation and soil development, we infer that several major faults have vertically offset platforms at rates as high as 0.6 m/k.y. for the past 125 k.y. We regionally extend our analysis by incorporating all known faults and folds in southern and central coastal Oregon that deform wave-cut platforms. Most platforms along the southern and central Oregon coast have been uplifted at rates of 0.1–0.3 m/k.y. since the late Pleistocene; however, platform uplift rates approach 1 m/k.y. in the vicinity of faults. The trend and distribution of these upper-plate coastal faults are consistent with their interpreted role as left-lateral, strike-slip, block-bounding structures accommodating clockwise rotation. We speculate that these upper-plate faults have a component of dip slip because of their association, in many instances, with localized uplift. If these faults bound rotating blocks, the dip-slip component of displacement may be either contractional or extensional, depending on the orientation of the fault relative to the north-south trend of the plate margin.

INTRODUCTION

Studies in Holocene tidal-wetland deposits along the Cascadia subduction zone in northern California, Oregon, Washington, and British Columbia have shown that the Cascadia margin has generated plate-boundary earthquakes of magnitude 8 or larger (Atwater, 1987, 1992; Darienzo and Peterson, 1990; Clarke and Carver, 1992; Clague and Bobrowsky, 1994; Darienzo et al., 1994; Atwater et al., 1995). Among the uncertainties concerning the nature of the plate boundary are the times and maximum size of plate-boundary earthquakes and the tectonic role of folds and faults in the upper plate. This paper addresses the second question by capitalizing on a unique late Pleistocene datum—the wave-cut platform—that records uplift, folding, and faulting of the upper plate in the past 100 000 yr. Wave-cut platforms provide a catalog of the location and movement history of upper-plate structures, thereby contributing to the development and assessment of kinematic models of upper-plate deformation.

In the first part of this report we describe geologic structures that have been active in the Holocene and/or late Quaternary within the upper plate in the onshore region of coastal central Oregon (Fig. 1). Onshore upper-plate structures active in the late Quaternary have been recognized elsewhere in coastal Oregon (Adams, 1984; Kelsey, 1990; Muhs et al., 1990; McInelly and Kelsey, 1990; Kelsey and Bockheim, 1994), but we focus on the central Oregon coast because these structures have not been described. In the latter part of the paper, we will address all active upper-plate structures in coastal Oregon, where we define “active” structures as those that deform surfaces cut in the past 125 k.y. or sediments deposited in the past 125 k.y. In our analysis of upper-plate deformation, we primarily consider the data set consisting of elevations of late Pleistocene (≤ 125 ka) wave-cut platforms and secondarily

a data set consisting of level-line surveys over an ≈ 45 yr period along western Oregon highways. We also draw from several other published data sets that document differential vertical displacement in the upper plate during the Quaternary.

This study attempts to demonstrate the youthfulness of several upper-plate structures, to constrain their style of deformation, and to relate this deformation to plate tectonics of the Cascadia margin. We hypothesize that upper-plate structures in central coastal Oregon are active, that they deform as part of the broad deformation zone that bounds the western margin of the North American plate, and that these structures are compatible with a prevailing upper-plate deformation model of dextral shear and clockwise rotation. We test these hypotheses through the following approaches. Upper-plate structures are recognized on the basis of deformation of marine terraces and geodetic leveling. Age assignments for marine terraces are determined through analyses of the degree of soil development on marine terraces and correlation of these soils to those on marine terraces elsewhere in coastal Oregon that have numerical ages. Fault style and fault-slip rate are constrained by mapping of fault trends and by evaluating magnitude of fault offset of marine platforms. Using all upper-plate active structures in coastal Oregon as a data base, we evaluate whether a model of dextral shear and clockwise rotation of the upper plate is compatible with late Pleistocene faulting and folding along the Oregon coast of the Cascadia margin.

UPPER PLATE GEOLOGY IN CENTRAL COASTAL OREGON

Regional Bedrock Geology of the Oregon Coast Range

The Oregon Coast Range consists of a tectonically elevated belt of crust lying 150–200 km

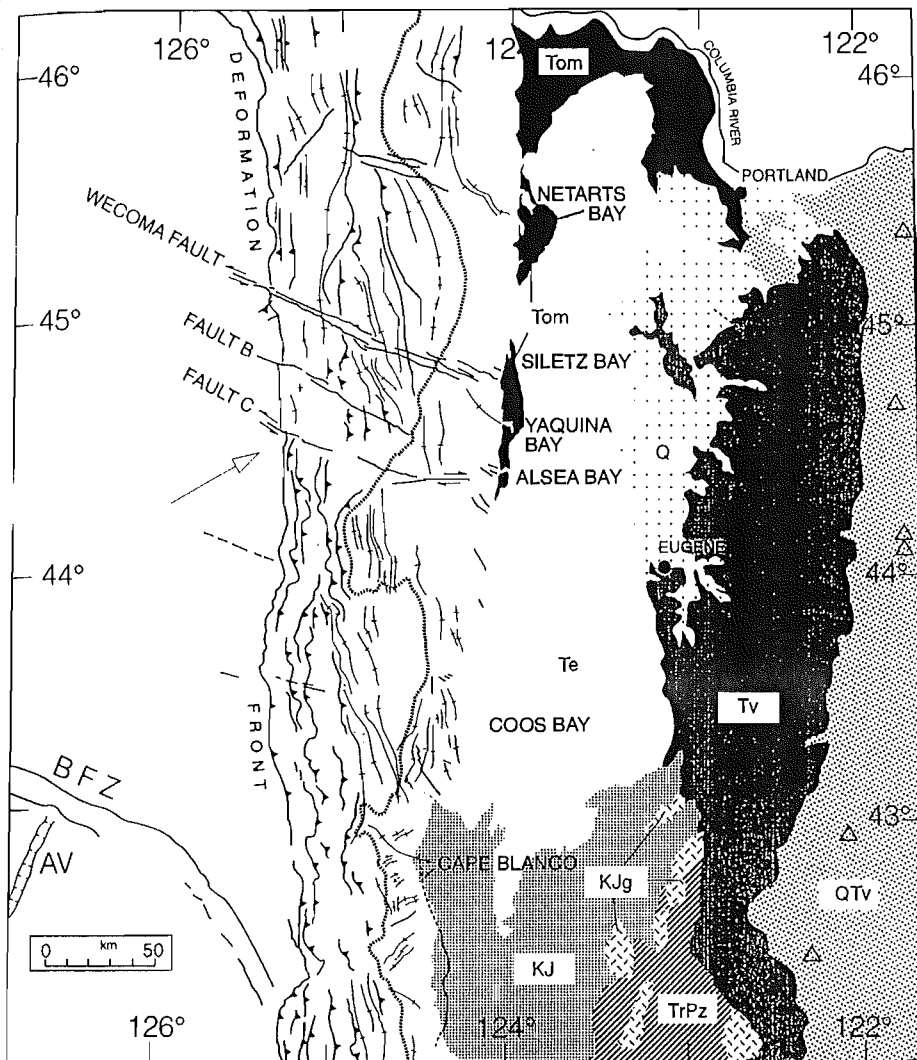


Figure 2. Tectonic map for continental shelf and rise of offshore Oregon and generalized geologic map for western Oregon west of the Cascade Mountains. Offshore data from Goldfinger et al. (1992b); onshore data from Walker and MacLeod (1991). All structures displace Pleistocene or younger sediments. This paper focuses on the late Quaternary deformation along the Oregon coast in the vicinity of Alsea, Yaquina, and Siletz Bays. Sites along the Oregon coast where late Holocene coseismic subsidence has been reported include, from north to south, Netarts Bay (Darioenzo and Peterson, 1990), Siletz and Yaquina Bays (Darioenzo et al., 1994), Coos Bay (Nelson, 1992), and the Sixes River at Cape Blanco (Kelsey et al., 1993). Bold dashed line is edge of continental shelf; bold solid line is steeply dipping fault; bold solid line with teeth is thrust fault with teeth on upper plate; thin solid lines with short cross bars are fold axes. AV is axial valley of the spreading ridge separating the Pacific plate to the west from the Gorda plate to the east. BFZ is Blanco fracture zone. The Juan de Fuca plate is bounded by the BFZ on the south and the deformation front on the east. The North American plate occurs east of the deformation front. The young (ca. 19 Ma) Juan de Fuca plate is obliquely subducting under the North American plate at ≈ 40 mm/yr (Riddiough, 1984). Explanation of geologic symbols: Q, Quaternary sedimentary fill in the Willamette valley; QTv, Quaternary and Tertiary volcanic rocks and volcanoclastic sediments of the Cascade Mountains; Tv, Tertiary volcanic rocks east of the Willamette valley and the Coast Range; Tom, Tertiary Oligocene and Miocene sedimentary and volcanic rocks of the Coast Range; Te, Tertiary Eocene volcanic and sedimentary rocks of the Coast Range; KJ, Cretaceous and Jurassic rocks of the Klamath Mountains; KJg, intrusive igneous rocks of the Klamath Mountains; TrPz, Triassic and Paleozoic rocks of the Klamath Mountains. Triangles denote volcanoes of the Cascade Range.

level highstands (Bloom et al., 1974) can serve as reference horizons from which to estimate late Quaternary deformation (Adams, 1984; Lajoie, 1986; Merritts and Bull, 1989; Kelsey, 1990; McInelly and Kelsey, 1990; Clarke and Carver, 1992). Such platforms are preserved along the central Oregon coast in the form of uplifted marine terraces. Each terrace is underlain by a thin (2–40 m) veneer of mostly marine sediment that covers the wave-cut platform.

We identified a set of six marine terraces on the central Oregon coast (Ticknor, 1993) (Fig. 3 and Table 1). Terraces are preserved discontinuously, range in elevation from sea level to 153 m and extend as much as 3 km inland. The younger and better preserved terraces typically form narrow strips ranging from <100 to ≈ 800 m in width. In the vicinity of Yaquina and Alsea Bays, the terraces are widest, attaining widths up to 2000 m.

Marine terraces were differentiated by terrace elevation, wave-cut platform elevation, terrace back-edge relief, and cover-bed stratigraphy (Table 1), as well as by degree of soil development. Platform elevations were measured wherever possible. Measurement sites were located on 1:24 000 maps using aerial photographs. Elevations were read off the maps with an accuracy of one-half the contour interval, which is ± 6 m. Altimeter surveys (error ± 3.3 m) were employed for the lowest wave-cut platforms, wherever ties to permanent benchmarks could be established.

Sediments that underlie the terraces are typically high-energy nearshore marine deposits capped by beach sand. Vegetated relict sand dunes commonly cover part of the beach deposits. These deposits are most prevalent in the vicinity of Alsea Bay, where hummocky dunal topography is characteristic of the surfaces of the lower terraces.

Previously reported ages for uplifted marine terraces in central coastal Oregon are limited to the vicinity of Yaquina Bay. Kennedy (1978) and Kennedy et al. (1982) assigned an age of 125 ka (oxygen isotope stage 5e) to cover sediments above the wave-cut platform at Hinton Point (also named Idaho Point) on the south side of Yaquina Bay (Fig. 3). This age assignment is based on a warm-water affinity of the fossil mollusk shells, in conjunction with amino acid enantiomeric (D:L) ratios for fossil shells. In contrast, amino acid D:L ratios for shells collected from terrace sediments above a wave-cut platform at Yaquina Bay State Park, on the north side of Yaquina Bay, correlate with amino acid D/L ratios from southern Oregon, and suggest an age of 80–85 ka (oxygen isotope 5a) (Kennedy, 1978; Kennedy et al., 1982). The difference in D:L ratios between

The oldest and highest terraces, the Fern Ridge and Alder Grove terraces, are preserved only in the vicinity of Alsea Bay on hill tops and ridge crests (Fig. 3). The platforms of both these terraces are tilted to the south.

Yachats to Heceta Head. South of Yachats, a single marine terrace crops out as a low bench, informally referred to as the Yachats Bench (Fig. 3). Platform elevations along the Yachats Bench decrease to the south and range from 13 to 0 m. The platform becomes submerged just north of Heceta Head (Fig. 1). Cover sediments on the Yachats Bench consist of beach sand that is in almost all instances overlain by eolian sand, debris flows, or both.

Marine Terrace Soils

We defined a soil chronosequence (a sequence of soils that differ in certain properties primarily as a function of time) for central Oregon coastal marine terraces and then used the chronosequence as a tool to correlate marine terraces across the three coastal reaches and to correlate the terraces to flights of marine terraces at other localities on the Cascadia margin. These correlations are the basis for identifying long-term, permanent vertical deformation along the coast. Ticknor (1993) provided more thorough discussion of soil properties, laboratory analyses of particle size, and aspects of pedogenesis for the central Oregon coast. The parent material for all the soils is unconsolidated Pleistocene beach or dune sand. Some soils described on the Yachats bench developed on basalt-rich debris flow deposits that overlie beach sand.

Field-identifiable soil properties that are both time dependent and can be used to distinguish the terraces include the depth to the Cox horizon (oxidized parent material), the thickness of the clay-enriched (Bt) horizon, the estimated maximum percent clay, and maximum clay skins. From these properties, we assigned development stages for the soils (Table 2) (Kelsey and Bockheim, 1994).

Soils were examined at 56 sites (Fig. 5) on the 6 marine terraces within the study area. Soil pits were excavated for 14 sites to a depth of 2 m, with continued augering down to the Cox horizon. Soils at 42 other sites were described from samples obtained with a 7.5-cm-diameter bucket auger. Soil data are presented separately for the three subregions: Siletz Bay to Newport (Table 3), Newport to Yachats (Table 4) and Yachats to Heceta Head (Table 5).

Soil properties change as a function of time for the six terraces (Fig. 6; Tables 3 and 4). Significant aspects of the Figure 6 data are: the average depth to the C horizon steadily increases (Fig. 6A); the Bt horizon thickness increases al-

TABLE 2. DEVELOPMENT STAGES OF SOILS ON ELEVATED MARINE TERRACES ALONG THE CENTRAL AND SOUTHERN OREGON COAST

Development stage	Depth to Cox (m)	B horizon hue	Bt (cm) thickness	Maximum B horizon texture* (% clay) [†]	Maximum clay films [§]
1	0.8–1.4	7.5–10YR	0	sil, l, sl (<30)	1–3npfpo
2	1.0–1.4	7.5YR	<50	sicl, cl, scl (30–40)	2–3n-mkpfpo
3	1.0–1.7	7.5YR	<50	sicl, cl, scl (30–40)	2–3mkpfpo
4	1.4–1.8	5–7.5YR	50–100	sicl, sic, cl, c (35–42)	3–4mkpfpo
5	1.9–2.8	5–7.5YR	100–200	sic, c (40–58)	3–4mk-kpfpo
6	2.6–4.5	5YR	>200	sic, c (40–65)	3–4mk-kpfpo
7	3.2–>4.5	2.5YR	>200	sic, c (45–65)	3–4mk-kpfpo

*S, sand; l, loam; sl, sandy loam; sil, silt loam; sicl, silty clay loam; sic, silty clay; cl, clay loam; c, clay. Abbreviations follow Soil Survey Staff (1975).

[†]We estimated percent clay for each horizon at each soil locality during field work. We have confidence in our ability to estimate clay content in the field because we obtained a significant correlation ($R = 0.81$; $p \leq 0.01$) between percent clay measured in the field and percent clay measured in the laboratory (28 samples).

[§]Notations for clay films: number denotes extent of ped faces covered by film: 1, 5%–25%; 2, 25%–50%; 3, 50%–90%; 4, >90%; n, thin; mk, moderately thick; k, thick; pf, film on ped face; po, film lines the pores. Abbreviations follow Soil Survey Staff (1975).

most linearly for the first five terraces (Fig. 6B); the average estimated percent clay increases along with Bt thickness from ≈30% on the youngest two terraces to slightly >40% on the next three older terraces (Fig. 6C); and the development stage increases almost linearly from 1.8 on the youngest terrace to 6.0 on the next to oldest terrace (Fig. 6D). It is also clear from Figure 6 that soils on the two oldest terraces cannot be distinguished from each other. Distinctions between these two terraces, however, were not critical for the platform correlations.

In the vicinity of Alsea Bay, development stages for soils on terrace sediments were conspicuously lower than the surrounding regions. Thirteen soil sites, which were notably underdeveloped, are not included in Table 4 or in Figures 5 and 6, and were not used for relative dating. Soils at these sites have developed on extensive sand dune deposits. Prolonged eolian activity on terrace surfaces in proximity to Alsea Bay is the likely explanation for the poorly developed soils.

In summary, the lowermost four marine terraces can be distinguished from one another on the basis of field-identifiable soil properties. The soils on Fern Ridge and Alder Grove terraces, in contrast, are old enough for the soils to have developed to such an extreme that distinguishing between the two is difficult (terrace 5 versus terrace 6 in Table 4). However, their relative ages are established based on elevation of the respective terraces.

Correlation of Marine Terraces on Either Side of Yaquina Bay Using Soils: The Yaquina Bay Fault

Matching of marine terraces across Yaquina Bay is necessary for evaluation of the hypothesis that a fault underlies the bay. A sequence of three terraces is preserved in the first 10 km north of the bay and a sequence of five terraces is preserved in the first 10 km south of the bay (Figs. 3 and 7A). We compared soil descriptions for the lowest three terraces 10 km south of the bay with the lowest three terraces 10 km north of the bay to evaluate the possible matches (Fig. 7B and Table 6). The best match based on soil properties (Fig. 7C and Table 6) indicates that the highest terrace north of Yaquina Bay can reasonably be matched with either the second- or third-highest terrace south of the bay. However, the only set of terrace matches entirely consistent with the soil data is the one that matches the highest (third) terrace north of the bay to the second-highest terrace south of the bay (Fig. 7D).

Matching of wave-cut platforms across Yaquina Bay shows that correlative platforms occur at different elevations on opposite sides of the bay, and the preferred match of terraces can only be accommodated if a fault beneath Yaquina Bay displaces the platforms up to the north (Figs. 7D and 8). A fault with the same sense of displacement, situated underneath

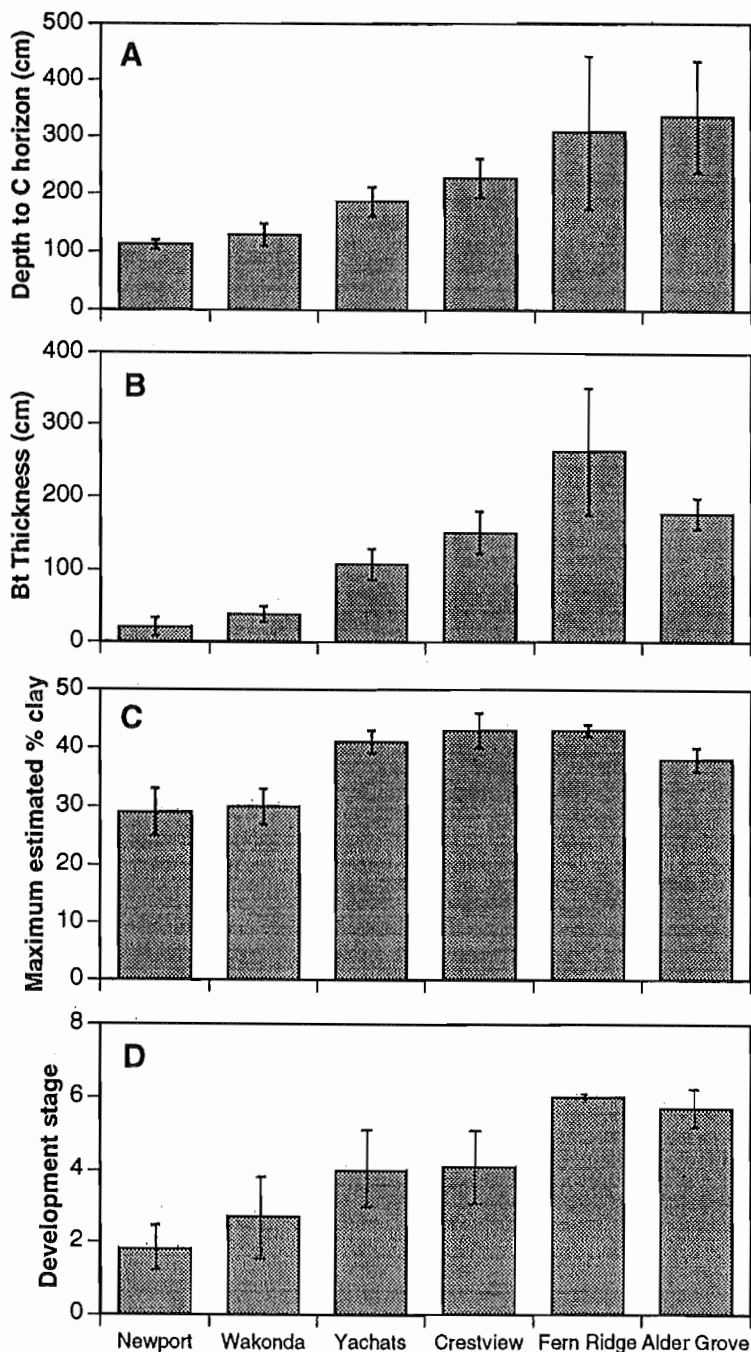


Figure 6. Charts showing average soil properties used as relative age indicators for soils developed on the six marine terraces. (A) Depth to C horizon. (B) Bt horizon thickness. (C) Estimated maximum percent clay in the Bt horizon. (D) Development stage (see Table 2). Vertical lines represent the standard error for the averages.

nated by deformation of the Crestview wave-cut platform, which is the only extensively preserved platform on the downthrown side of the Waldport fault zone. Shore-parallel profiles of platform elevation (Fig. 8) show that, in the vicinity of Alsea Bay, there is a crustal downwarp on the downthrown block of the Waldport

fault defined by an uplift minimum for the Crestview platform (no. 4 platform; Fig. 8). The Alsea Bay downwarp (ABD; Fig. 8) is ≈ 4 km in wavelength, and the amplitude of the downwarp, considering the ± 6 m elevation measurement error, is 14–37 m. Because the location of the downwarp is just east of the

Waldport fault (Fig. 8), we infer that the Alsea Bay downwarp is a product of displacement on the Waldport fault zone. The inference that the 14–37 m amplitude downwarp is associated with the fault zone is consistent with the time of formation of the surface (the Crestview platform was cut ca. 200 ka) and the minimum rate of vertical offset of the Waldport fault (0.1–0.15 m/k.y.) during the late Pleistocene.

In conclusion, both of the major embayments, Yaquina Bay and Alsea Bay, appear to be structurally controlled by faults that have been active in the late Quaternary. Alsea Bay appears to straddle a region of downwarping on the downthrown side of the Waldport fault zone and Yaquina Bay rests on the downthrown block of the Yaquina Bay fault (Fig. 9).

South of Alsea Bay, uplift rates decrease to the south. For the 12 km coastal reach south of Yachats (Yachats bench) (Figs. 3 and 8), there has been little vertical displacement of the Yachats platform in the past 125 k.y. (data for lat 44.23°N to 44.28°N in Table 8). Thus, the Yachats bench is one of the few coastal segments along the Oregon and northern California portion of the Cascadia margin that records negligible net vertical crustal displacement since the last interglacial (125 ka). At Searose Beach at the southern end of the study area (Fig. 1), uplift rates reach a minimum of 0.00 to 0.04 m/k.y., calculated for the 125 ka platform (lat 44.23°N in Table 8).

DEFORMATION SINCE THE LATE PLEISTOCENE IN CENTRAL COASTAL OREGON

Deformation since the formation of the wave-cut platforms (since the late Pleistocene) is the result of many hundreds of cycles of interseismic and coseismic deformation. However, the paleoseismicity of upper-plate faults cannot be addressed through marine terrace studies. Although we know that these faults offset datums that are on the order of 100 ka in age and that the faults have a vertical component of slip rate of 0.1–0.6 m/k.y., no earthquakes have occurred on these faults since ca. 1870, and we do not know if these faults have the capability of rupturing independently of ruptures on the underlying megathrust or if these upper-plate faults could play a role in segmenting ruptures on the subduction zone.

Differences in the relative heights of benchmarks reoccupied by successive first-order leveling surveys provide a data set of historic, geodetically derived uplift rates along the coast for the past ≈ 45 yr, from 1941 to the releveled epoch 1987–1988 (Fig. 10) (Mitchell et al., 1994). Although the data are noisy because of

Figure 9. (A) Summary tectonic map of the Oregon coast and offshore area (sources are Walker and MacLeod, 1991; Goldfinger et al., 1992b) showing more detailed tectonic maps for the following four coastal regions: (B) central Oregon coast; (C) Coos Bay–Cape Arago region (McInelly and Kelsey, 1990); (D) Cape Blanco region (Kelsey, 1990); and (E) southernmost coastal Oregon (Kelsey and Bockheim, 1994). All onshore structures have been active in the past 125 k.y. Bold lines are faults, and thin lines are synclines and anticlines.

ern continental margin, relative to stable North America, as a consequence of dextral shear and clockwise rotation.

Faults and folds that deform late Pleistocene wave-cut surfaces have been identified along three other segments of the Oregon coast, in addition to the central Oregon coast: Cape Arago–Coos Bay (McInelly and Kelsey, 1990); Cape Blanco (Kelsey, 1990); and Cape Ferrel–Brookings (Kelsey and Bockheim, 1994)

(Fig. 9, C, D, and E). Adjacent to the faults and folds, uplift rates are higher (≈ 0.4 – 1.0 m/k.y.) relative to the background rate of 0.0 – 0.2 m/k.y. (Kelsey and Bockheim, 1994).

The pattern of uplift and fault deformation in central coastal Oregon is the same as in the other coastal segments; wave-cut platforms between Yachats and Siletz Bay underwent a slow, long-term permanent uplift that averaged 0.1 – 0.3 m/k.y. in the late Pleistocene, with the exception of

the fault-bounded block extending from Yaquina Bay to Cape Foulweather, where uplift rates approached 1 m/k.y. (Table 8). The Yaquina Bay fault bounds this block to the south and the Cape Foulweather fault bounds it to the north (Fig. 8). The zone of coastal faulting associated with this block is ≈ 20 km to the east of the eastern end of an east-southeast–trending fault zone, described by Goldfinger et al. (1992a, 1992b), that extends from the Cascadia deformation front across the continental slope and shelf to the coast (Fig. 9). The on-land faults and the faults on the shelf and slope project toward each other, but there are no data to suggest that they connect.

Within the 2- to 10-km-wide zone of marine terrace deformation in coastal Oregon, fold axes are variable in trend and the faults are diverse in trend and style from one coastal segment to the next, as well as within a single seg-

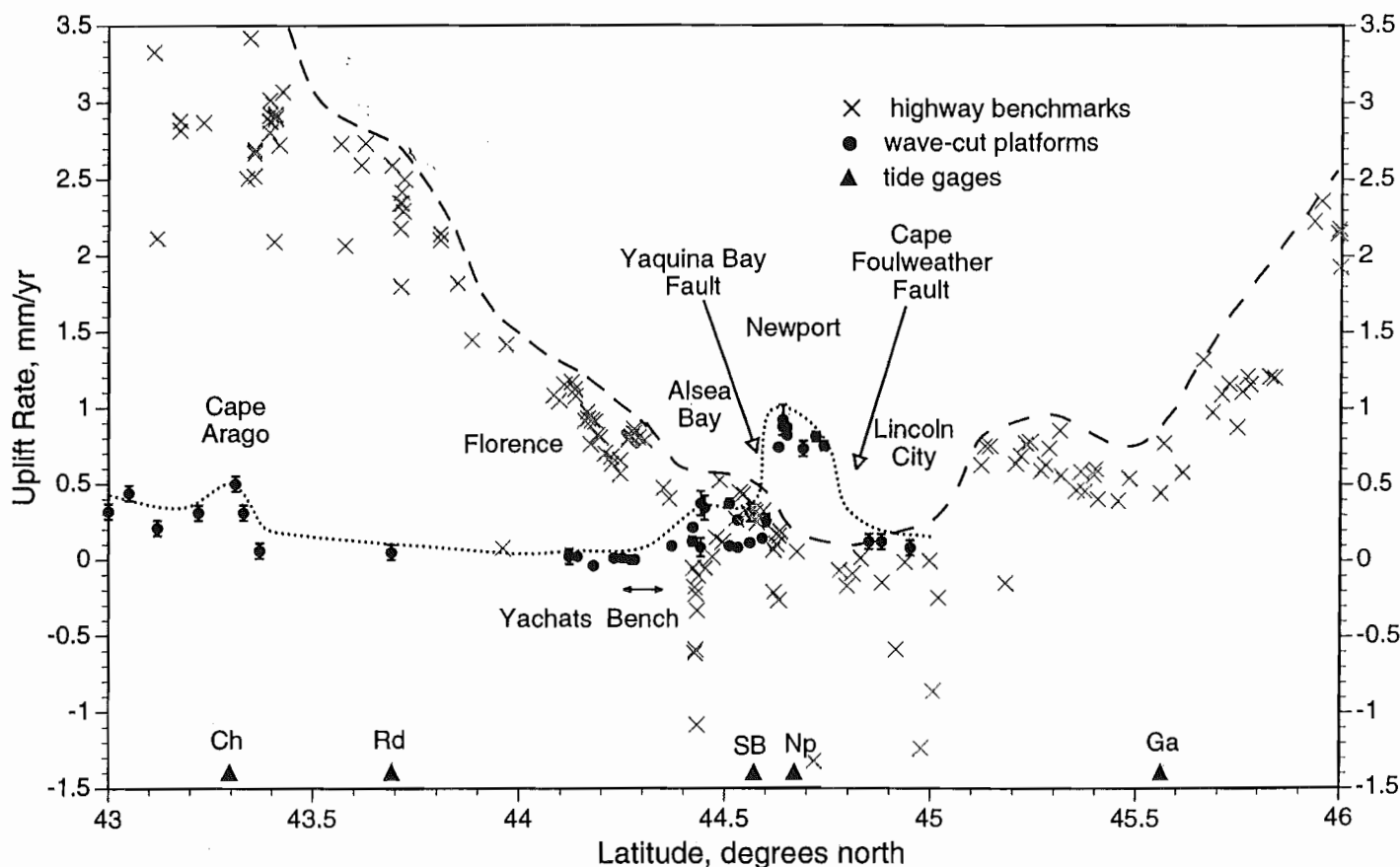


Figure 10. Along-coast variation in average uplift rates since 125 ka (solid dot symbol, derived from elevations and assigned ages for wave-cut platforms) versus uplift rates for 1941–1987 (\times symbol, derived from leveling of highway benchmarks; Mitchell et al., 1994) for the central Oregon coast. Dotted line tracks the variation in average platform uplift rates. Dashed line delineates the upper limit for benchmark uplift rates. Triangles show locations of the tide gages that provide an independent check on the historic uplift rates from leveling. Some benchmarks yield uplift rates significantly below the upper limit, probably because of local subsidence, or settling, of individual benchmarks. Vertical bars represent range of platform uplift rates determined for the shoreline angle of the 80, 105, and 125 ka platforms using the minimum and maximum platform gradients from Bradley and Griggs (1976) and North American sea-level model (Muhs, 1992; Muhs et al., 1992) (see Table 8).

41

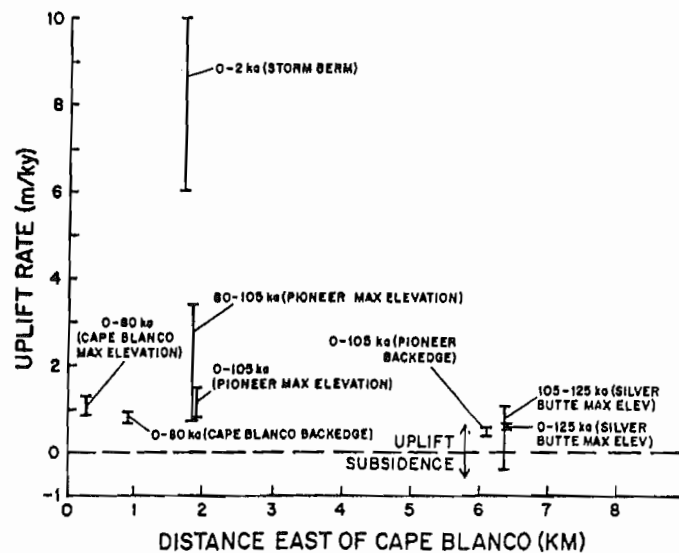


Fig. 12. Temporal and spatial variations in uplift rate for the three youngest wave-cut platforms near Cape Blanco, the Cape Blanco (80 ka), Pioneer (105 ka) and Silver Butte (125 ka) platforms. Uplift rate data are for points along the Cape Blanco anticline axis, except for the storm berm data, which are projected onto the axis from a point 1.3 km to the south. Uplift rates are from Tables 2 and 3, with the exception of the rate for 0-2 ka (see text).

of several coseismic uplift events at the apex of a fold growing in the accretionary margin in the late Holocene. The storm berm provides no data from which to infer the uplift mechanism. However, coseismic deformation of such a local structure as the Cape Blanco anticline is conceivable because only 55 km to the north in the Cape Arago-South Slough region, coseismic uplift and subsidence both have probably occurred during Holocene tightening of another fold, the South Slough syncline (Figure 1) [Nelson, 1987; Nelson et al., 1988; McInelly and Kelsey, 1990]. Nelson [1987] and Peterson and Darienzo [1989] describe stratigraphic evidence for as many as 7 or 8 abruptly buried salt marsh surfaces along the axial trace of the syncline. These abrupt subsidence events have all occurred during the late Holocene time span of the storm berm, and coseismic deformation of the synclinal fold is the most reasonable explanation for the buried surfaces.

Work elsewhere along the coast of Cascadia, including to the north of Cape Blanco at Netarts Bay in northwest Oregon [Darienzo and Peterson, 1990] and at

Willapa Bay in southwest Washington (Figure 1) [Atwater, 1987, 1988] and to the south of Cape Blanco at Humboldt Bay (Figure 1) [Carver and Burke, 1989] suggests at least four earthquakes on the Cascadia subduction zone during the time interval since the storm berm was deposited. The earthquake events that may have uplifted the berm would not necessarily be coincident in time with the earthquake events to the north and the south, but major earthquakes along the Cascadia zone are sufficiently frequent to accommodate several coseismic uplift events of the Cape Blanco anticline in the last two thousand years.

Cape Blanco Deformation in the Context of Observed Regional Strain and Inferred Regional Stress

The deformation observed in the marine terraces at Cape Blanco probably is an on-land expression of the north-northwest-trending fold belt on the continental shelf of the Cascadia margin (Figure 13) [Kulm and Fowler, 1974; Clarke et al., 1985; Peterson et al., 1986]. Structural

EPISODIC TECTONIC SUBSIDENCE OF LATE HOLOCENE SALT MARSHES, NORTHERN OREGON CENTRAL CASCADIA MARGIN

Mark E. Darienzo and Curt D. Peterson

Geology Department, Portland State University,
Oregon

Abstract. Salt marsh subsurface deposits (0-4 m depth) in Netarts Bay, a small coastal lagoon of northern Oregon, record six events of marsh burial in the last several thousand years. Five of the buried marsh surfaces show sharp, nonerosional upper contacts with either anomalous sand layers (tsunami deposits) or tidal flat mud deposits. These sequences indicate episodic, abrupt subsidence of the marsh surfaces to low intertidal levels. In contrast, lower marsh contacts with underlying intertidal muds are gradational, indicating gradual uplift and development of the marsh. Three independent measures of deposit elevation relative to mean tidal level (percent organics, diatom assemblages, and percent eolian sand) have been used to estimate vertical displacements of marsh surfaces. Abrupt subsidence displacements of 1-1.5 m alternate with gradual uplift displacements of the order of 0.5-1.0 m. The vertical tectonic movements are interpreted to reflect coseismic strain release (abrupt subsidence) following interseismic strain accumulation (gradual uplift), associated with interplate coupling between the Juan de Fuca Plate and the North American plate in the Cascadia subduction zone. Recurrence intervals between subsidence events range from possibly less than 300 years to at least 1000 years, with the last dated event likely occurring 300-400 radiocarbon years before present (RCYBP). Significant ^{14}C age overlaps of at least four subsidence events recorded at Netarts and reported for southern Washington and other northern

Oregon bays (at 300-500, 1000-1300, 1400-1800, and 3000-3300 RCYBP) suggest the potential for event synchronicity over at least 200 km of the central part of the Cascadia subduction zone. Additional work is needed to test the synchronicity of these episodic events of coseismic subsidence.

INTRODUCTION

The Oregon continental margin extends along 450 km of the central part of the Cascadia subduction zone. However, this segment, along with the Northern California, Washington, and British Columbia segments, has not experienced a substantial subduction zone earthquake in historical time (Figure 1). The absence of large thrust earthquakes has been attributed to terminated subduction or to aseismic subduction associated with a shallow angle of subduction, excessive sediment lubrication or malleability of the young, subducting Juan de Fuca plate [Ando and Balazs, 1979; Acharya, 1981]. However, the historical record (<200 years) might be too short to rule out coseismic subduction processes [Heaton and Kanamori, 1984; Heaton and Hartzell, 1986]. Studies of relative plate motion and of recent oceanic plate seismicity indicate an oblique subduction and north-south compression of the southern Juan de Fuca plate, in accord with the northward migration of the Mendocino triple junction [Riddihough, 1984; Kelsey and Carver, 1988; Spence, 1989]. Yet Pliocene-Pleistocene imbricate thrusts and shelf fold and fault belts that dominantly trend north-south off the Oregon coast demonstrate a significant component of east-west convergent strain [Kulm and Fowler, 1974; Clarke et al., 1985]. Recent studies of deep, small-scale seismicity along the northern Cascadia

Copyright 1990
by the American Geophysical Union.

Paper number 89TC01268.
0278-7407/90/89TC-01268 \$10.00

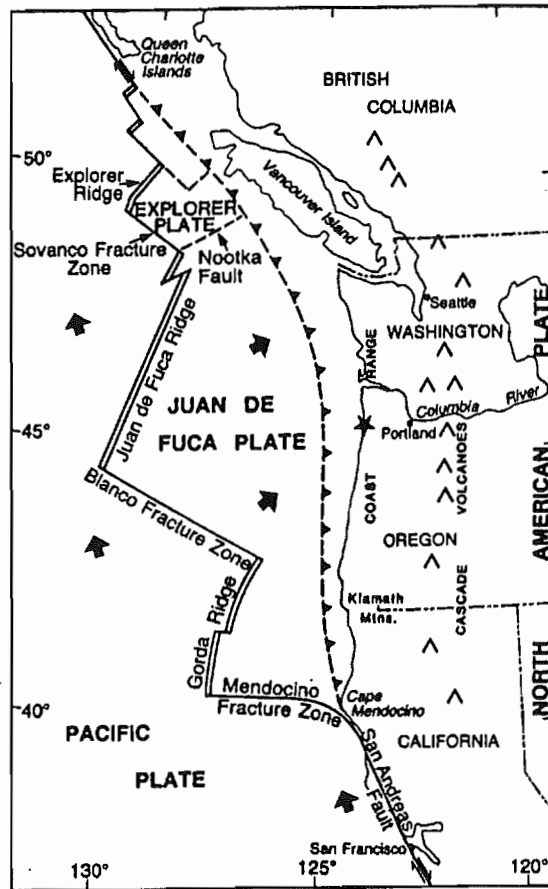


Fig. 1. Tectonic map of the Cascadia Margin. Star marks the study site. The approximate location of the trench axis, marking the boundary between the North American plate and the subducting Juan de Fuca Plate, is shown by a thrust boundary (dashed line).

margin, north of 46° latitude, indicate tensional forces associated with trench normal subduction of the northern Juan de Fuca plate [Taber and Smith, 1985; Weaver and Baker, 1988].

One test of active subduction tectonics in the Cascadia margin would be the evidence of cyclic uplift and abrupt subsidence of coastal areas. Such vertical tectonics are forced by the alternation of interseismic coupling (strain accumulation) and coseismic shear dislocation (strain release) of the subducting oceanic plate and overlying continental plate [Fitch and Scholtz, 1971]. When the subducting plate and overlying continental plate are coupled, the leading edge of the continental plate is dragged downward, producing an associated uplift on the opposite (landward) side of a flexure hinge line (Figure 2). When interseismic stresses overcome the frictional coupling, the coseismic strain release results in abrupt tectonic uplift (seaward of the hinge line) and corresponding abrupt subsidence (landward of

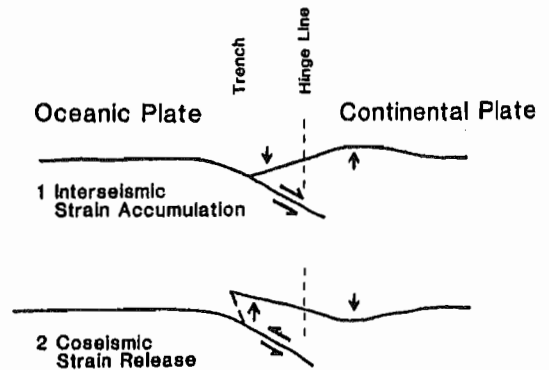


Fig. 2. Diagram of vertical coastal tectonics associated with (1) coupled strain accumulation and (2) coseismic shear dislocation between a subducting oceanic plate and an overriding continental plate [after Ando and Balazs, 1979].

the hinge line). Significantly, such abrupt vertical displacements of the sea floor produce large tsunamis [Heaton and Hartzell, 1986]. The alternation of coastal uplift and abrupt coastal subsidence together with tsunami deposition provides a potentially unique record of interplate paleoseismicity in strongly coupled subduction zones.

Such events of abrupt coastal subsidence (1-3 m) on the landward side of trench parallel hinge lines were observed in association with the 1946 Nankaido earthquake [Fitch and Scholz, 1971], the 1960 Chile earthquake [Plafker and Savage, 1970] and the 1964 Alaska earthquake [Savage and Hastie, 1966; Plafker, 1972; Ovenshine et al., 1976]. Multiple events of abrupt submergence of late Holocene wetland surfaces have also recently been reported for the coast of southwest Washington [Atwater, 1987] and for northwestern Oregon (W. Grant, personal communication, 1988). These records of relative sea level change are interpreted as positive evidence for active subduction tectonics (including coseismic subsidence) along the central Cascadia margin. Similar field evidence of abrupt changes in relative sea level have been reported for Netarts Bay in northern Oregon [Peterson et al., 1988].

In this paper we describe in detail the stratigraphy and tectonic implications of buried marsh deposits from Netarts Bay, a coastal lagoon in northern Oregon (Figure 3). The small marsh of Netarts Bay was chosen for a detailed study of late Holocene records of relative sea level change on the basis of its protection from ocean storm waves and its negligible fluvial influence. These conditions are important to insure as complete and uncomplicated a record of relative sea level change as possible. In addition, its central position in the Cascadia margin (45° N) allows for the comparison of neotectonic processes in northwestern Oregon with reported marsh burial events in larger estuaries of southwestern Washington

Magnitude and frequency of subduction-zone earthquakes along the northern Oregon coast in the past 3,000 years

by Mark E. Darienzo and Curt D. Peterson, Department of Geology, Portland State University, P.O. Box 751, Portland, Oregon 97207

ABSTRACT

Similarities in number, depth, sequence stratigraphy, and radiocarbon ages characterize buried peats of seven estuaries along 175 km of the northern Oregon coast. We use these peats to infer the extent of earthquake-induced subsidence, earthquake magnitudes, and average recurrence intervals for late Holocene earthquakes at the Cascadia Subduction Zone. Synchronicity of earthquake-induced subsidence from Alsea Bay to the Necanicum River over a coastal distance of 175 km is inferred most confidently for the most recent (first) event and the third through sixth events. In contrast, earthquake-induced subsidence for the second event was lacking in at least three of the seven estuaries. However, tsunamis generated by the second event deposited sands in the unsubsided estuaries. Therefore, the second event is also considered synchronous between Alsea and Necanicum. A segment boundary between Yaquina and Netarts is inferred for the second event.

From these findings of synchronicity, we estimated the length of rupture for the late Holocene earthquakes. The corresponding magnitudes are at least 8.0, based on a rupture length of 175 km, a rupture width of at least 60 km, an average recurrence interval of 400 years, an average convergence rate of 4 cm/yr, and a shear modulus of 3×10^{11} dynes/cm². Using a range of convergence rates (3.5–4.5 cm/yr) and average recurrence intervals (300–500 years), rupture lengths (105–175 km), and rupture widths (60–90 km), calculated magnitudes for five of the last six earthquakes are greater than 8.0 for the central 175 km of the Cascadia Subduction Zone.

Average recurrence intervals between earthquakes for the estuaries on the northern Oregon coast range between 200 and 600 years. The wide range is due to the uncertainties associated with radiocarbon ages. Although more accurate recurrence intervals are desirable, these average recurrence intervals provide a useful estimate for assisting coastal communities with their disaster planning and for determining probabilities for future subduction-zone earthquakes off the northern Oregon coast.

INTRODUCTION

In the past ten years, several geophysicists have called attention to the potential for great earthquakes (greater than magnitude 8) related to the Pacific Northwest subduction-zone known as the Cascadia Subduction Zone (Heaton and Hartzell, 1987; Savage and Lisowski, 1991; Hyndman and Wang, 1993) (Figure 1). Although there have been large (up to magnitude 7.5) earthquakes in the region during historic times (last 150 years), there is no historical record of Pacific Northwest subduction-zone earthquakes, which are often greater than magnitude 8—with the possible exception of the 1992 Cape Mendocino earthquake (G. Carver, personal communication, 1994). However, evidence for subduction-zone earthquakes in the late Holocene has been found in the deposits of coastal wetlands of estuaries in British Columbia, Washington, Oregon, and northern California (Atwater, 1987, 1992; Darienzo and Peterson, 1990; Peterson and Darienzo, 1991; Clarke and Carver, 1992; Nelson, 1992a; Clague and Bobrowsky, 1994; Darienzo and others, 1994).

Now that subduction-zone earthquakes have been recognized in the stratigraphic record, questions arise as to what are the magnitudes of these Holocene earthquakes and the frequency with which they occur. Knowledge of the magnitudes and frequency is necessary to calculate the probability of the next earthquake and to help communities with disaster planning and the building of new and upgrading of existing structures.

In this study, we compare the stratigraphy and associated radiocarbon ages of seven estuaries along the northern Oregon coast: at Alsea Bay, Yaquina Bay, Siletz Bay, Nestucca Bay, Netarts Bay, Ecola Creek, and Necanicum River—an along-coast distance of 175 km (Figure 1). We selected these estuaries because we have made detailed studies of marsh stratigraphy at each of them. Results have been published for Alsea by Peterson and Darienzo (1991); for Netarts by Darienzo and Peterson (1990) and Darienzo (1991); for Yaquina, Siletz, Nestucca, and Necanicum by Darienzo (1991), Darienzo and others (1993), and Darienzo and others (1994); and for Ecola by Gallaway and others (1992). Stratigraphic patterns and radiocarbon ages were used to calculate possible ranges for paleo-magnitudes and average recurrence intervals. These results can potentially be compared with similar patterns and ages of paleoseismic events recorded in estuaries of other segments of the Cascadia Subduction Zone.

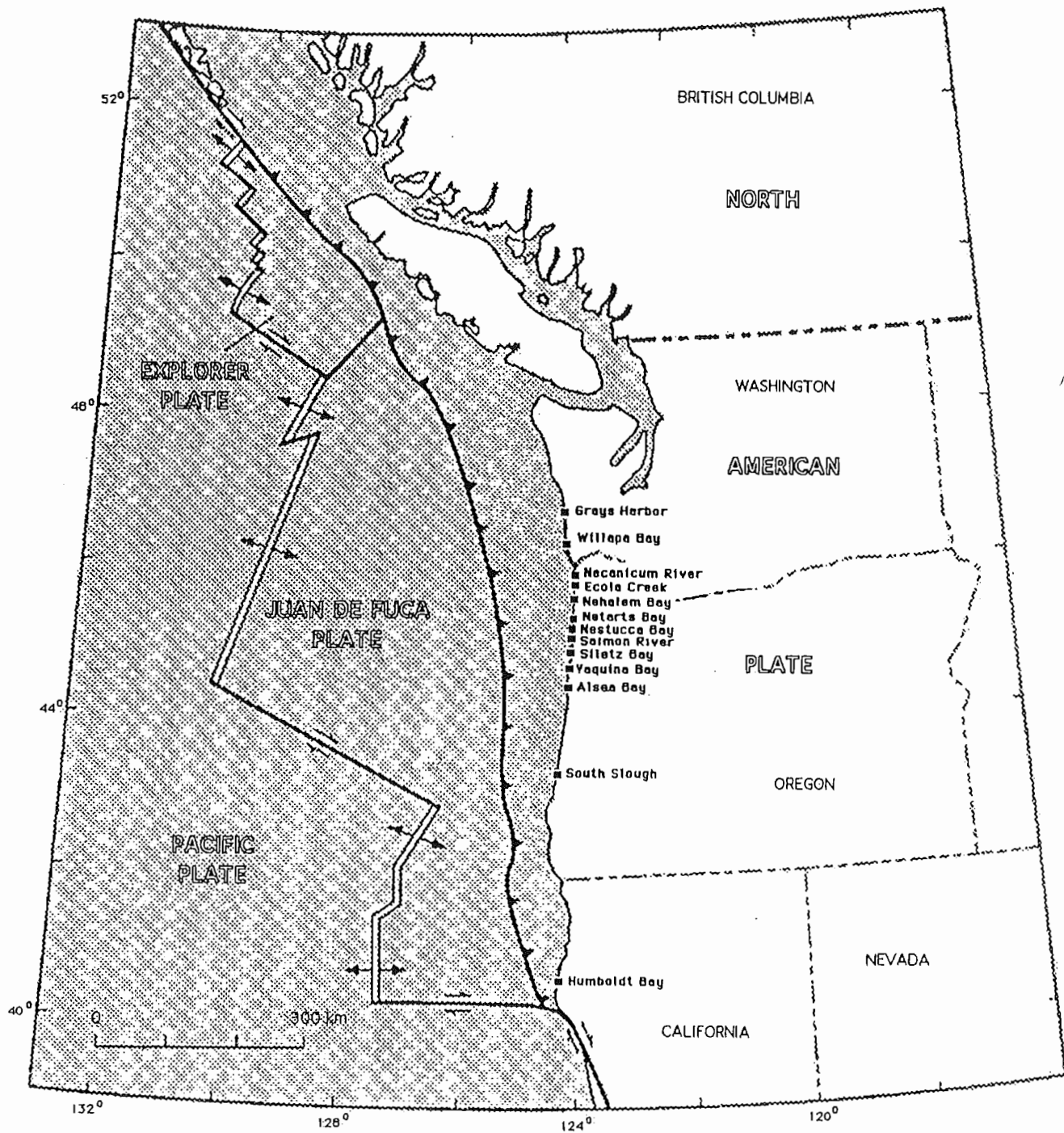
ESTIMATION OF MAGNITUDE

Establishment of event synchronicity

We used the late Holocene stratigraphic records in individual estuaries to assess the synchronicity of the paleoearthquakes among the estuaries along the northern Oregon coast. In this study, we examined and compared the following stratigraphic patterns in the paleoseismic record: the number and stratigraphic location of inferred tsunami deposits and the number, age, and stratigraphic position (depth) of earthquake-buried peats recorded within a specific period of time. If the events are synchronous, the magnitudes of the Holocene earthquakes can be estimated for rupture segments of at least the length of the northern Oregon coast. Synchronicity of coseismic events between estuaries provides information on the length of earthquake rupture along the coast. Therefore, the rupture length, as determined by synchronicity of events, would be a key parameter in paleomagnitude determinations. Formulas that use rupture length (coastline distance of event synchronicity) and estimates of rupture width and seismic slip could then be used to describe paleoearthquakes (Kanamori, 1977; Abe, 1981, 1984; Rogers, 1988; Byrne and others, 1990; Geomatrix, 1993).

A possible alternative to synchronicity of events along the northern Oregon coast is segmentation. In other words, ruptures occur along smaller segments of the locked subduction zone at different times, producing earthquakes of lesser coastline extent and magnitude. For example, a pair of earthquakes off Japan in the Nankai Trough resulted from rupture of adjacent segments in 1944 and 1946, while the 1707 Nankai Trough earthquake resulted from rupture of both segments simultaneously (Ando, 1975). The use of prehistoric dating, no matter how sensitive the dating technique, could not conclusively prove earthquake synchronicity because of the range of possible ages associated with conventional radiocarbon (± 100 yrs), high-precision radiocarbon (± 10 years), or dendrochronology (± 10 years) (Yamaguchi and others, 1989). However, synchronicity of the 300-yr-B.P. (before present) paleoseismic event between widely separated estuaries is suggested by similarities between high-precision radiocarbon ages and tree-ring ages of buried trees in coastal wetlands of Washington, Oregon, and northern California (Yamaguchi and others, 1989; Atwater and others, 1991; Carver and others, 1992; Nelson and Atwater, 1993). Further evidence for synchronicity has come from similarities in stratigraphic patterns of marsh deposits. For example, Atwater (1992) inferred correlations largely on the basis of appear-

45




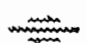

-  Seaward edge of plate boundary--Barbs show direction of dip
-  High-angle fault--Arrows show strike slip
-  Spreading ridge

Figure 1. Cascadia Subduction Zone and northern Oregon estuaries. Distance between the Necanicum and Alsea estuaries is approximately 175 km.

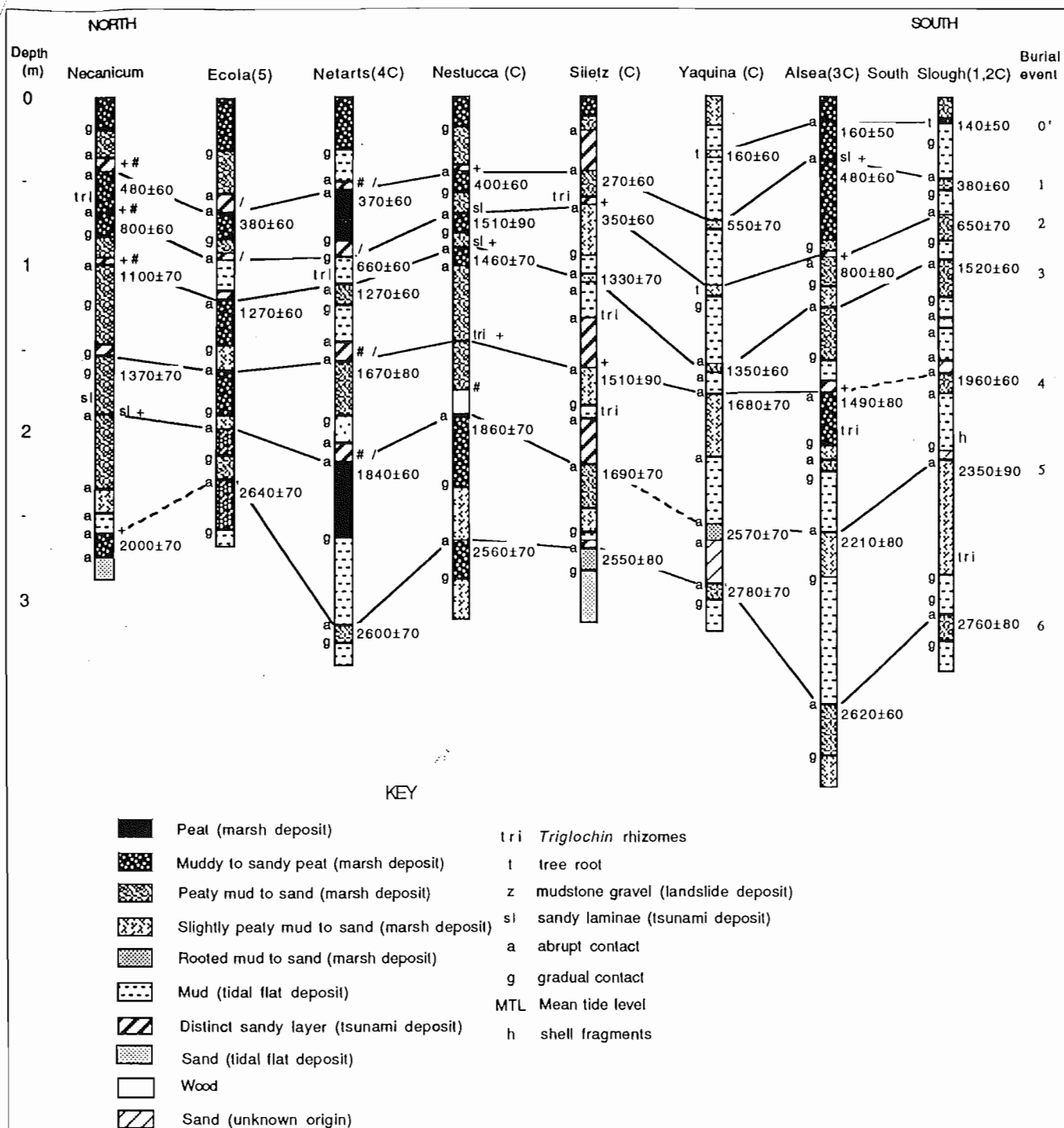


Figure 2. Representative stratigraphic columns with evidence for subduction-zone earthquakes and radiocarbon ages for all estuaries studied along the northern Oregon coast as well as South Slough, an estuary at Coos Bay on the south-central Oregon coast. Necanicum, Nestucca, Yaquina, and South Slough stratigraphic columns are composites. "#" indicates an increase or first appearance of brackish or marine diatoms from the buried peat to overlying sediments; "+" indicates an increase or first appearance of beach sand from the peat to overlying sediments; "/" indicates >50 percent beach sand in a probable tsunami deposit above the peat. Unnumbered stratigraphic columns are from Darienzo (1991) and Darienzo and others (1994). Columns numbered 1–5 are from (1) Nelson (1992b), (2) Peterson and Darienzo (1989), (3) Peterson and Darienzo (1991), (4) Darienzo and Peterson (1990), and (5) Gallaway and others (1993). "C" indicates that column is a composite of two or more sites.

Table 1. Radiocarbon ages of materials (peats unless otherwise noted) from estuaries along the northern Oregon coast that have produced evidence for Holocene subduction-zone earthquakes

Estuary (sources)	Site, location	Depth in cm (burial event no.)	Age in radiocarbon yrs B.P.	Age range in yrs B.P. 2 error multiplier (Cal. age range at 2 σ)	Laboratory no. (Beta)
Necanicum (Darienzo and others, 1994)	Neawanna 2, UTM428900, 5092300, zone 10, N	48 (1)	480 \pm 60	240-720 (300-680)	42112
		70 (2)	800 \pm 60	560-1,040	42113
		111 (3)	1,100 \pm 70	820-1,380	42088
		158 (4)	1,370 \pm 70	1,090-1,650	44595
		268 (6)	2,000 \pm 70	1,720-2,280 (1,610-2,340)	42114
	Neawanna 5, UTM 428900, 5092600, zone 10, N	78 (2) 167 (6)	680 \pm 80 2,200 \pm 90	360-1,000 1,840-2,560	43127 42115
Ecola (Gallaway and others, 1992)	115-R, UTM 426000, 5083300, zone 10, N	70 (1)	380 \pm 60	140-620 (0-590)	56402
		120 (3)	1,270 \pm 60	1,030-1,510	56401
		230 (6)	2,640 \pm 70	2,360-2,920 (2360-3050)	56404
Netarts (Darienzo and Peterson, 1990; Darienzo, 1991)	5, UTM 424400, 5024200, zone 10, N	55 (1)	370 \pm 60	130-610 (0-578)	24933
		111 (3)	1,270 \pm 60	1,030-1,510	24934
		157 (4)	1,670 \pm 80	1,350-1,990	24520
		220 (5)	1,840 \pm 60	1,600-2,080 (1490-2030)	24521
		316 (6)	2,600 \pm 70	2,320-2,880 (2360-3050)	41668
	Oyster farm, UTM 426800, 5029900, zone 10, N	97 (2)	660 \pm 60	420-900	41638
Nestucca (Darienzo and others, 1994)	Nestucca Duck, UTM 425500, 5004200, zone 10, N	80 (1)	400 \pm 60	160-640 (0-620)	43123
		70 (2)	1,510 \pm 90	1,150-1,870	42000
		90 (3)	1,460 \pm 70	1,180-1,740	42084
		190 (5)	1,860 \pm 70	1,580-2,140 (1,460-2,110)	41637
	Little Nestucca 5, UTM 426800, 5000500, zone 10, N	266 (6)	2,560 \pm 70	2,280-2,840 (2,320-2,920)	41671
Siletz (Darienzo and others, 1994)	Salishan House, UTM 418700, 4971500, zone 10, N	47 (1)	270 \pm 60	30-510 (0-520)	42089
		67 (2)	350 \pm 60	110-590	42090
		163 (4)	1,510 \pm 90	1,150-1,870	42001
		220 (5)	1,690 \pm 70	1,410-1,970 (1,310-1,900)	42091
		273 (6)	2,550 \pm 80	2,230-2,870 (2,200-2,970)	42002
	Millport Slough 1, UTM 421500, 4970800, zone 10, N	48 (1) 135 (3) 159 (4) 210 (5)	480 \pm 60 1,330 \pm 70 1,630 \pm 70 1,850 \pm 70	240-720 (300-680) 1,050-1,610 1,350-1,910 1,570-2,130 (1,440-2,100)	42085 43126 43125 42086
Yaquina (Darienzo and others, 1994)	Hatfield, UTM 417400, 4940200, zone 10, N	30 (0')	160 \pm 60	0-400	41991
	Outcrop B, UTM 428300, 4938400, zone 10, N	77 (1)	550 \pm 70	270-830 (310-720)	38862 (wood)
	Slack 1, UTM 427800, 4938000, zone 10, N	62 (3)	1,350 \pm 60	1,110-1,590	42092
		81 (4)	1,680 \pm 70	1,400-1,960	42093
		160 (5) 196 (6)	2,570 \pm 60 2,780 \pm 70	2,330-2,810 (2,340-2,890) 2,500-3,060 (2,530-3,260)	42094 42095
Alsea (Peterson and Darienzo, 1991)	Outcrop, UTM 419500, 4918700, zone 10, N	50 (1)	480 \pm 60	240-720 (300-680)	39181 (wood)
	AB 8, UTM 419000, 4918800, zone 10, N	87 (2)	800 \pm 80	480-1,120	27184
		177 (4)	1,490 \pm 80	1,170-1,810	26791
		242 (5)	2,210 \pm 80	1,890-2,540 (1,830-2,710)	27185
		327 (6)	2,620 \pm 60	2,380-2,860 (2,370-2,960)	26792
South Slough	Winchester 12, UTM 3931000, 4792400, zone 10, N (Nelson, 1992b)	47 (1)	380 \pm 60	140-620 (0-590)	26289
		15 (0')	140 \pm 50	0-340 (0-450)	41639 (wood)
		72 (2)	650 \pm 70	370-930	27675
		98 (3)	1,520 \pm 60	1,280-1,760	34280
		167 (4)	1,960 \pm 60	1,720-2,200	27744
	Day Creek, UTM 393800, 4796500, zone 10, N (Peterson and Darienzo, 1989)	220 (5) 310 (6)	2,350 \pm 90 2,760 \pm 80	1,990-2,710 (1,920-2,800) 2,440-3,080 (2,440-3,300)	27743 34278

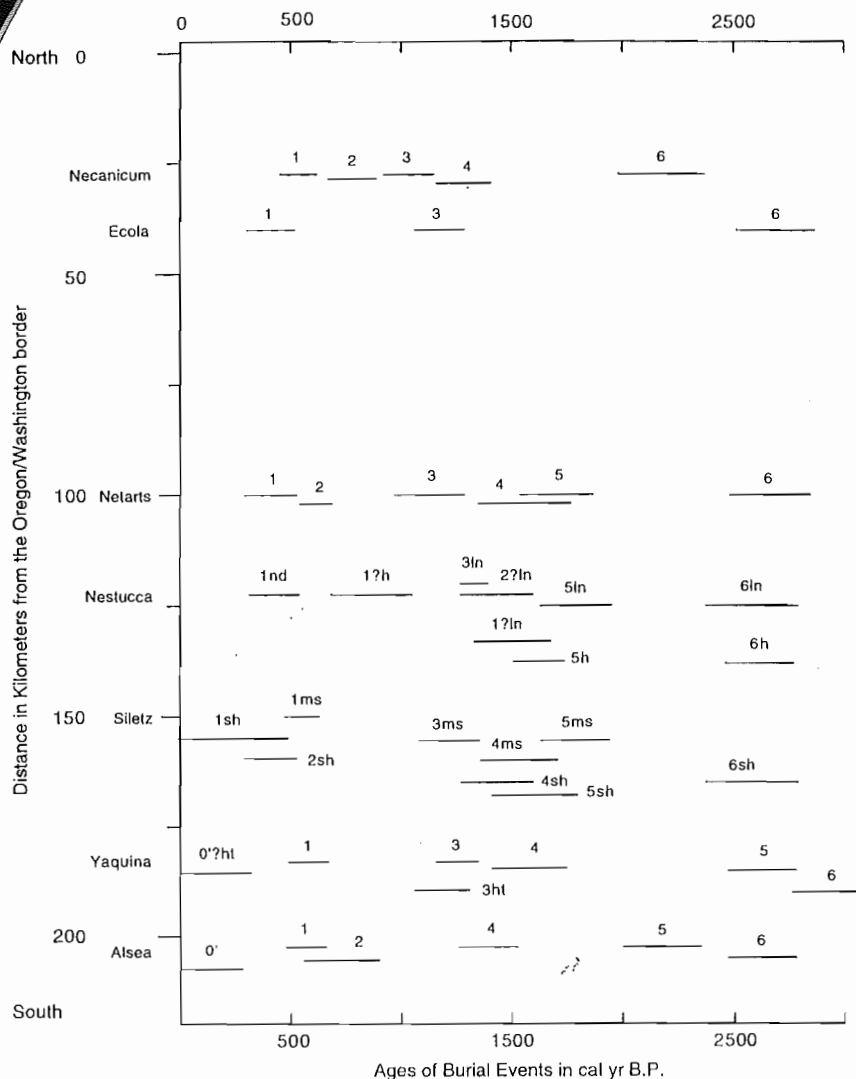


Figure 4. Ranges of calibrated radiocarbon ages with two deviations (2σ) of the last six earthquake events for all estuaries. Numbers designate events. Question marks indicate event designation uncertainties. Lower-case initials designate specific sites within the estuary where materials were radiocarbon dated (nd = Nestucca duck; ln = Little Nestucca; h = Hurliman; sh = Salishan House; ms = Millport Slough; ht = Hatfield). See Darienzo and others (1994) for stratigraphy of the Nestucca and Siletz cores.

dence in Netarts, Ecola, and possibly Necanicum; (2) tsunami sand and subsidence in Alsea, Nestucca, and Yaquina; and (3) tsunami sand at several sites and possible evidence of subsidence at a few sites in Siletz Bay (Figure 2) (Darienzo and others, 1994; Peterson and Darienzo, 1994; Peterson and Priest, in preparation). Age control for the second event is weak. The ages of the buried peats for the second event overlap at 2σ for Necanicum, Netarts, and Alsea (Figure 4). However, the age from Nestucca is much older than these, and it is not clear if this event, documented at four estuaries in northern Oregon, affected Nestucca Bay. The age of the second buried peat at Nestucca might be suspect and require additional dating to solve this problem (Darienzo and others, 1994).

In contrast to Nestucca, the age of the second peat from Siletz is younger and does not overlap at 2σ with the peats from Necanicum, Netarts, and Alsea. The young age is perhaps due to root contamination from above. The second buried peat at Ecola and Yaquina was not dated. The sands without accompanying subsidence stratigraphy that record the second event at the three northernmost estuaries

suggest deposition by a tsunami generated by an offshore subduction-zone earthquake off an adjacent segment of the Oregon coast to the south. The lack of evidence for this second event along the Washington coast further supports a segment rupture limited to the southern Oregon coast (Atwater, 1992). Possible segment boundaries are located either between the Netarts and Nestucca bays or between Siletz and Yaquina (Figure 1). Supporting a segment boundary between Netarts and Nestucca is the fact that there is evidence of subsidence for the second earthquake burial event at Nestucca but no such evidence at Netarts. Support for a segment boundary between Yaquina and Siletz includes evidence of subsidence at Yaquina, weak subsidence evidence at Siletz, and a possible segment boundary at this same location for the fifth earthquake burial event. Further work is necessary to accurately locate the boundary. Nevertheless, all estuaries were affected by this second paleoearthquake either directly, by subsidence and a tsunami, or indirectly, by a tsunami only. Therefore, the record of the second event could be considered synchronous among the estuaries on the northern Oregon coast.

The **third burial event** is recognized in all estuaries, and the ages of the buried peats at nearly all estuaries overlap at 2σ (Alsea was not dated) (Figure 4). The exception is the age of the third buried peat at Nestucca, which overlaps all estuaries except Necanicum. A distinct sandy layer is present over the third buried peat at four of the seven northern estuaries but absent at Alsea, Siletz, and Netarts (Figure 2). The Hatfield site in the lower reaches of Yaquina Bay had tsunami sand deposited over what is considered the third buried peat, based on radiocarbon age (Figure 4). However, the third buried peat at other sites in Yaquina Bay is not capped by tsunami sands (Peterson and Priest, in preparation). The tsunami sand in the lower reaches of Yaquina Bay is not shown in Figure 2, because the representative stratigraphy for Yaquina in Figure 2 is from the upper reaches of the estuary (Darienzo and others, 1994). Based on ages, evidence of subsidence, and one-to-one correspondence of tsunami sand from the Hatfield site with subsidence, this third event possibly occurred synchronously from the Necanicum River to Alsea Bay.

The **fourth burial event** is recognized in all seven estuaries. At five of the estuaries, the ages of the event overlap at 2σ (no age from Ecola or Nestucca). Tsunami sands overlie peats in four out of seven estuaries but are absent at core sites in Ecola and Nestucca. Based on ages, evidence of subsidence, and one-to-one correspondence of tsunamis with subsidence, this fourth event possibly occurred synchronously from the Necanicum River to Alsea Bay (Figures 2 and 4) (Darienzo and others, 1994; Peterson and Priest, in preparation).

The **fifth burial event** is recognized in all estuaries. Only three of the seven estuaries were observed to record tsunami sands above buried peats (Figure 2), and the age ranges for the fifth event overlap in only three out of the five estuaries dated (Figure 4). The ages of the event at Alsea and Yaquina, the two southernmost estuaries, are greater than at the other dated estuaries. This suggests a separate event (or more) for them and a segment boundary between Yaquina and Siletz. Or, buried peats with similar ages have not been identified in adjacent estuaries because of nondeposition or erosion. Ages of

49

Episodically buried forests in the Oregon surf zone

by Roger Hart, *College of Oceanic and Atmospheric Sciences, Oregon State University, Hatfield Marine Science Center, Newport, Oregon 97365;* and Curt Peterson, *Department of Geology, Portland State University, Portland, Oregon 97207*

ABSTRACT

Severe winter storms, especially in ENSO¹ years, expose rooted tree stumps in the surf zone of the central Oregon coast. Root mats up to 6 m in diameter are anchored in the Tertiary rocks of the late Holocene wave-cut platform. We studied more than 275 stumps at 14 localities between Neskowin and Coos Bay. Forest soil preserved beneath some roots can be traced landward, where it overlies creek mouth marsh and paleo-sand dune deposits. The stump fields and the forest soil are remnants of a continuous forest or series of forests that extended farther seaward than present-day temperate coniferous rain forest. Litter in the soil indicates that the forest soil was rapidly buried. Ages of the rooted stumps range from $1,970 \pm 50$ to $4,340 \pm 70$ radiocarbon years before the present (RCYBP).

Eustatic change of sea level and migration of sand barriers are considered as explanations for preservation of rooted stumps at some sites. However, large-diameter stumps rooted on continuously active late Holocene wave-cut platforms depleted of littoral sand are indicators of tectonic movements on the central Oregon coast. A necessary history requires six stages: (1) wave cutting of platform at sea level, (2) tectonic uplift of the platform, (3) growth of the forest on the wave-cut platform, (4) rapid burial and preservation of the forest, (5) inundation of the forest at sea level, and (6) renewed erosion of the beach platform. These results corroborate salt-marsh evidence of late Holocene vertical tectonic displacements associated with local or regional earthquake sources along the Oregon coast. Further radiocarbon dating of annular rings in the rooted stumps and preserved litter in the soil can potentially constrain the nature, age, and extent of the tectonic displacements.

INTRODUCTION

For several decades, scientists have reported tree stumps rooted on the wave-cut platforms of the surf zone along Oregon beaches (Kelley and others, 1978; Peterson and others, 1993; oral communications from R. Bayer, Yaquina Birders and Naturalists, 1985; E. Zoebel, Department of Botany, Oregon State University,

1995; and R. Loeffel, Fisheries Manager, retired, 1996). However, no systematic study of these rooted stumps has been published. The stumps stand upright, with broad root mats spread parallel to the wave-cut platform (cover photo). They have been observed in place for over ten years, even during periods when the surrounding sand has been stripped from the beach. Although some stumps may be rooted in submerged late Pleistocene stream channels, most are rooted in the Tertiary bedrock of the late Holocene wave-cut platforms. Similar roots associated with currently living trees are found only inland from the surf zone. The live trees that left the stumps on the beach must have grown on the wave-cut platform after regression of the surf zone. Following at least several hundred years of growth, transgression of the surf zone must have invaded the tree growing zone. These observations led to early concepts of late Holocene seismic activity along the central Oregon coast (Darienzo and Peterson, 1990).

We report on a study of 1.9- to 4.4-ka (kilo-annum = 10^3 years) trees rooted on the wave-cut platforms of the central Oregon coast, lat 43.23° – 45.00° N. (Figure 1). We document the association of forest soils, debris flows, and liquefaction features with the buried stumps. In the discussion, we evaluate three mechanisms for regression and transgression of the surf zone: (1) growth and removal of sand barriers, (2) eustatic change of sea level, and (3) vertical tectonic displacement of the Cascadia margin. We use observed stratigraphic relations to rule out mechanisms 1 and 2 at most localities.

BACKGROUND

The beaches of the central Oregon coast occupy late Holocene wave-cut platforms, at least several hundred meters in width, that are carved in late Pleistocene marine terrace deposits or in Tertiary sedimentary rocks. South of Newport, the surf zone may have reoccupied late Pleistocene platforms (Ticknor, 1993). North of Newport the youngest apparent Pleistocene platform is elevated as much as 30 m above present sea level.

In general, elevated wave-cut platforms underlie a series of inland marine terraces composed mainly of Pleistocene beach and dune sand (Kelsey and others, 1994; Ticknor, 1993).

Ticknor (1993) used the uplifted platforms to calculate average vertical displacement rates for the past 105 ka and found 0.85 ± 0.06 mm/year north of Newport and -0.01 ± 0.03 /year for the area around Yachats.

¹ El Niño Southern Oscillation. El Niño refers to the equatorial Pacific warm water anomaly. The Southern Oscillation traditionally refers to associated variations in atmospheric circulation in the south Pacific. Recently, teleconnection links to enhancement of the Aleutian low-pressure system off the Oregon coast have been documented and are thought to cause an increase in storminess and associated coastal erosion.

Rooted Stumps on Beaches of the Central Oregon Coast

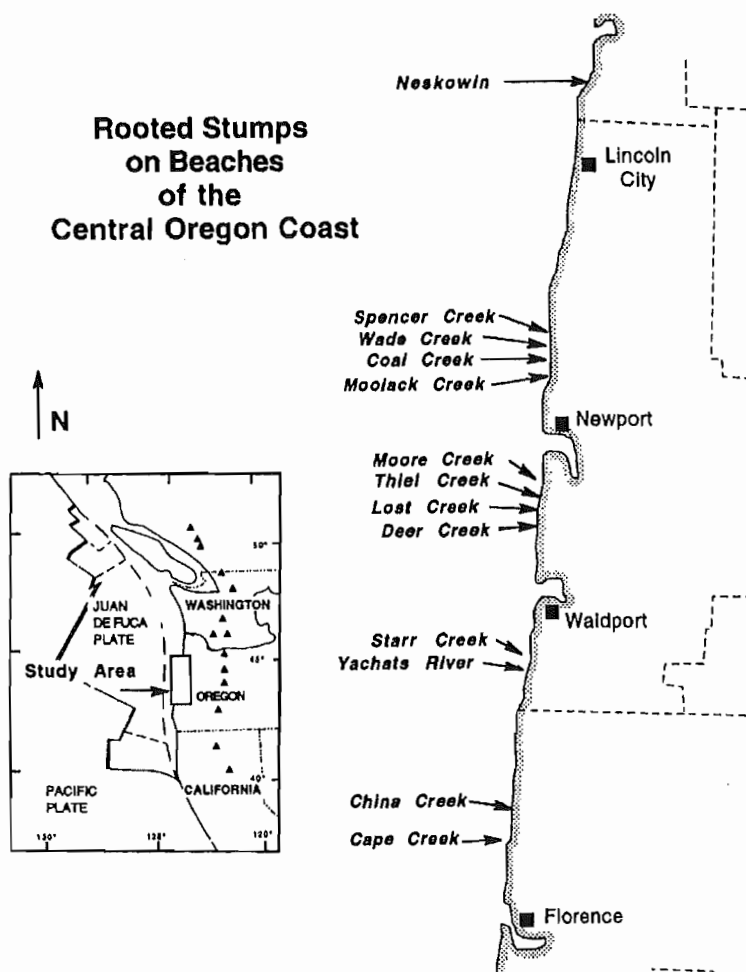


Figure 1. Location of the study area where rooted stumps have been mapped. The stump field at Sunset Bay discussed in the text and referred to in Table 1 is south of the enlarged area.

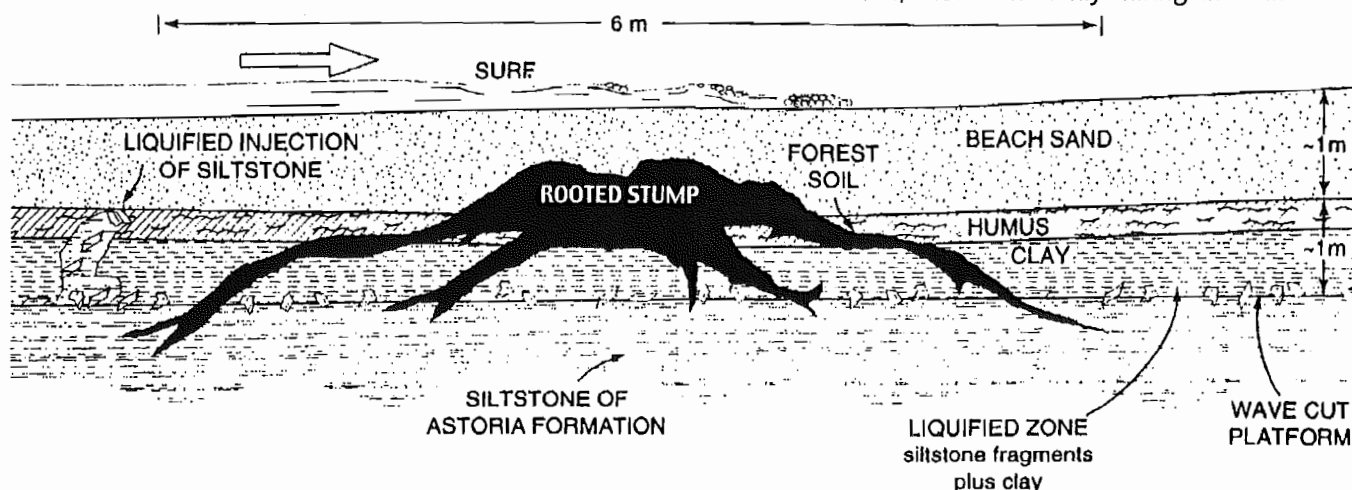


Figure 2. Diagrammatic figure of the principal features of the buried stumps beneath beach sand. The roots extend into the Tertiary siltstone on which the platform was cut. Some of the stumps have erosional remnants of forest soil with fresh litter, humus, and gray clay directly on the wave-cut platform. The inferred liquefied injection of siltstone fragments into the soil was probably coseismic but not necessarily synchronous with burial of the rooted stump.

Mitchell and others (1994) calculated present-day vertical displacement rates from repeated leveling surveys and tide gauge records. Their results indicate that, at the present time, the area around Newport is stationary or subsiding, whereas the area around Yachats is being uplifted.

The wave-cut platforms in the vicinity of Newport terminate landward in wave-cut cliffs; whereas, the wave-cut platforms north and south of Yachats most frequently terminate landward in Holocene foredunes.

RESULTS

More than 288 rooted stumps were mapped at 14 localities between Coos Bay and Neskowin, a distance of 206 km (Figure 1). Additional rooted stumps and soil profiles were studied and sampled at seven localities in creek mouths and backshore deposits. We collected 26 wood samples and 59 soil samples from beaches, creek mouths, and soil run-ups and examined them under the microscope. Over 60 km of beaches, marine cliffs, and creek mouths were photographed and mapped on either U.S. Geological Survey 1:24,000-scale (7½-minute series) topographic maps or on 1:4,800-scale aerial orthophoto maps used by Priest and others (1994). Details of the mapping and sampling are given in Table 1.

Rooted stumps

Normally, 1–5 m of beach sand covers the stumps in the surf zone (Figure 2), but they are exposed during periods of extreme beach sand erosion, most commonly during the winters of

Table 1. *Rooted stumps and forest soil localities, continued*

Locality	Access	Stump field	Soil	Samples
19 Ten Mile Creek	Rooted stump, forest soil, and marsh soil at top of beach 75 m S. of beach access from Stonefield Beach State Wayside.	1 rooted stump at the top of the beach.	Creek mouth marsh soil and forest soil at top of beach. Forest soil runs up marine cliffs S. Separated from modern soil by dune sands and shell midden 390 m S. of beach access.	3 sections measured. Wood sample TMC-1.
20 China Creek	Access beach from Muriel O. Ponsler Memorial Wayside. 3 rooted stumps on beach 50 m N. of access. Extensive stump field and forest soil horizon on beach S. across China Creek continues 1.2 km S.	3 rooted stumps in beach high-water zone exposed 6/96, 50 m N. of wayside. First noted 1982/83 by E. Zoebel. 5 rooted stumps exposed in higher high-water zone of beach S. of China Creek. 1 stump continuously exposed in bank at top of beach 500 m S. of Creek (Figure 4).	Forest soil on beach with litter S. of China Creek runs up to bank at top of beach and underlies dune field continuously 0.9 km to S. (Figures 5 and 8). Exposed 3/25/95–8/4/95. Extensive fire-scorched layers.	Wood samples from rooted stumps CCs-1, to -5. Cones of <i>Tsuga heterophylla</i> from beach S. of China Creek. Soil samples CC-1, CC-2, and CC-5. 3 sections measured.
21 Blowout Creek	Forest soil in bed of Blowout Creek 200 m S. of picnic area beach access at Carl G. Washburne Memorial State Park.	1 rooted stump in marine cliff 12 m S. of Blowout Creek.	Forest soil runs up from Blowout Creek and continues 2.1 km to Heceta Head. Runs up 12 m over large dune form (Figure 7). Litter exposed south of dune form.	Litter sample BC-1. Wood sample BC-1 from stump rooted in soil runoff.
22 Cape Creek	1 rooted stump on top of beach near picnic area of Devil's Elbow State Park.	1 rooted stump.	None observed.	Wood sample CaC-1.
23 Sunset Bay	18 rooted stumps and buried soil horizons on beach and in bed of Big Creek at Sunset Bay State Park.	18 stumps from Big Creek to fault line on N. end of beach. Intermittently exposed since 1983 ENSO.	Laminated soil of uncertain origin underlies beach sand.	Wood samples SSB-1 to -6; soil samples SSB-1 to -17.

(Continued from page 136)

clay underlying a horizon of forest soil. The clay layer, 1–3 m thick, is characterized by rooted stumps, layers of peat, marsh grass fragments, and clasts of siltstone. The forest soil, 0.5–2 m thick, is characterized by humus, litter, and rooted stumps. At some sites, two or more forest soil layers are divided by layers of beach sand and/or cobbles. The bottom forest layer is thickest and contains cones, bark, and needles. The top forest layer is sandy and contains a zone of fire-scorched material with red iron oxide minerals and possible charcoal.

Soil horizons stratigraphically equivalent to the surf zone soil ascend creek mouth valley walls and cross-cut Pleistocene sand-dune deposits of the marine terraces at seven localities (Figures 5, 6, 7; Table 1). The ascending forest horizons are characterized by Podzol profiles similar to the present day profile formed on top of Holocene dune deposits (Corliss, 1973). The top layer of undecomposed forest litter, shredded bark, cones, and twigs in a matrix of sandy loam varies in thickness from 2 in. to 20 in. This layer grades down into the humus layer which is 10–54 in. thick. The humus is friable with a few firm aggregates, slightly sticky, and nonplastic. Woody debris is locally abundant, and in places 10-cm-thick mats of bark and shredded bark are present. The gray leached zone, which varies from 0.1 to 1 m in thickness, is underlain by an orange-red B horizon 0.5–2 m thick and with well-developed laminae of sesquiox-

ides. The forest soil horizons terminate abruptly upward and are capped by Holocene debris flows, backshore beach sands, or dune sands that separate them from the present-day soil horizon.

Debris flows up to 5 m thick cover creek mouth and ascending forest horizons at nine sites (Table 1). The debris flows contain fragments of the underlying forest soil, angular dune-paleosol fragments, semiangular siltstone fragments, and woody debris mixed in with gravel and mud. The high abundance of angular and unconsolidated fragments suggests that the flows did not travel long distances. At Coal Creek, a debris flow covers a rooted stump at the backshore edge of the beach, which suggests a possible coincidence between platform subsidence and the debris flow. The debris flows probably extended onto the wave-cut platform.

DISCUSSION

The location and abundance of the tree stumps and associated soil indicate that they are erosion remnants of extensive forests that grew on Holocene wave-cut platforms. Several questions are raised by the data: (1) what caused regression of the surf zone off the late-Holocene wave-cut platform? (2) what caused inundation and burial of the established forests? and (3) what was the extent and timing of the burial events? In this section, we discuss each of these questions in turn.

(Continued on page 141)

52

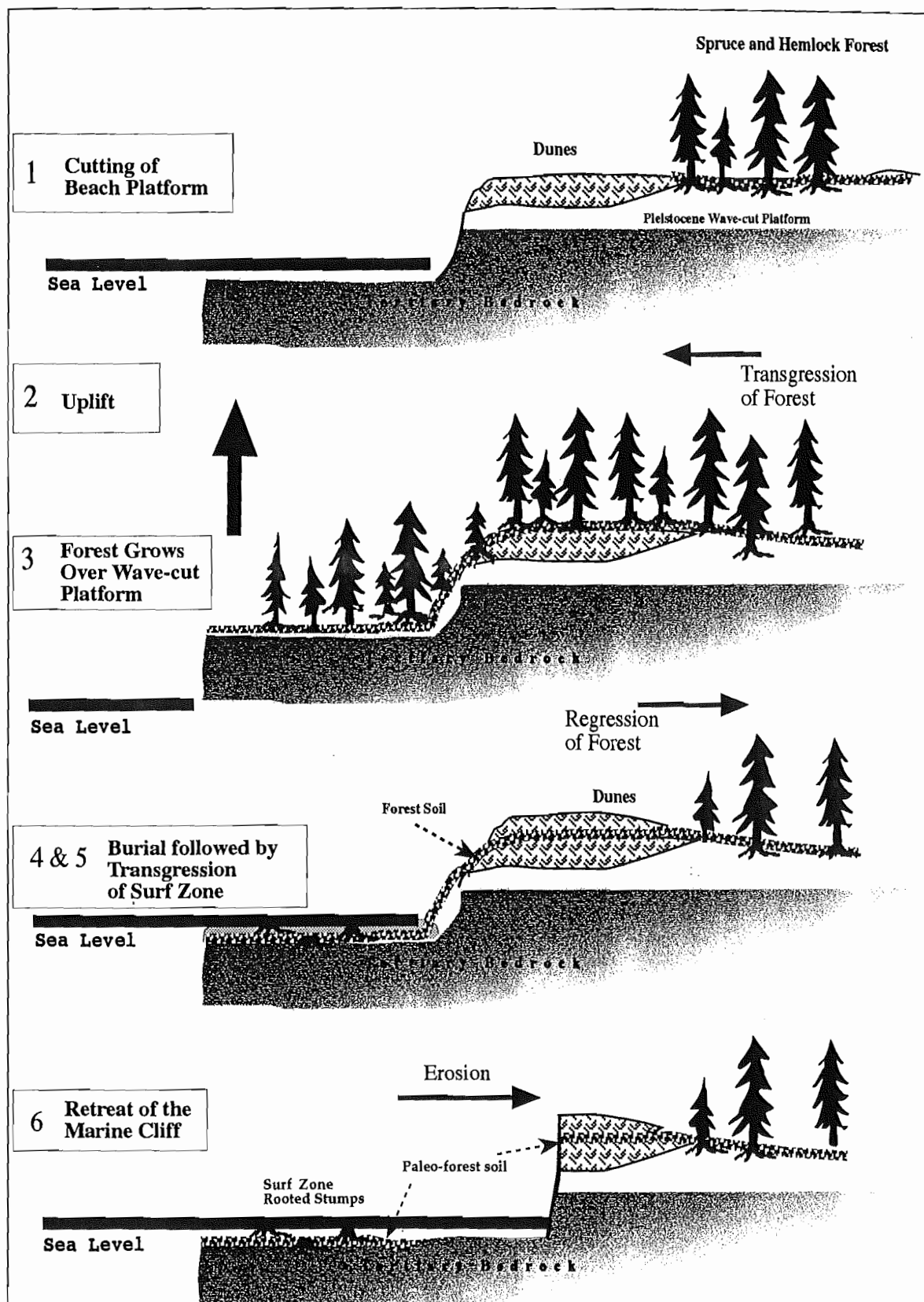


Figure 9. The six stages necessary to explain the occurrence of rooted stumps in the Oregon surf zone. Regression of the surf zone off the platform was probably the result of vertical tectonic displacement. Burial is inferred from the presence of nondecomposed forest litter. Transgression of the surf zone was not necessarily synchronous with burial and could have been the result of eustatic sea level rise, removal of sand barriers, or vertical tectonic displacement or any combination of the three.

Continued from page 141)

Forest soil at Deer Creek appears buried in beach sand. Trees growing near beaches can be buried in wet, salty sand if there is a rapid seaward growth of the beach. Growth of the beach can be caused by an abrupt increase of littoral sand supply induced by shifting nearshore currents or by an increase in sediment supply to the littoral cell (Peterson and others, 1990). Sudden vertical tectonic displacement could also induce burial of trees in beach sand if the displacement is great enough.

The ascending forest soil horizons are covered by dune sand at China Creek and Blowout Creek. Rapid migration of dunes over the trees as a result of an abrupt increase in littoral sand supply is a possible agent for burial and protection of the forest. Vertical tectonic displacement could also induce migration of dunes over forests by introducing the forest to areas of active dune formation at lower elevations.

Debris flows cover forest soil at nine localities north of Thiel Creek. A nearly continuous apron 15 mi wide may have covered the beaches between Spencer Creek and Lost Creek and could have buried the forest on the beach platform. Although it is nearly impossible to determine whether or not debris flows are coseismic, debris flows are commonly associated with earthquakes. For example, over 10,000 debris flows occurred during the 1976 Guatemalan earthquake (M_s 7.5) (Harp and others, 1981).

Additional work is needed to verify whether deposits currently covering the forest soils reflect the initial burial of the forests.

Inundation of the forest

Inundation of the forest in the surf zone was not necessarily synchronous with burial. Preservation of litter by burial in beach sand or in a peat bog would have required a synchronous drop to sea level. However, burial by debris flows or eolian dunes could have taken place above sea level before inundation. At any rate, the forest was inundated by a transgressing surf zone that could have been the result of eustatic rise of sea level and/or removal of sand barriers and/or tectonic subsidence.

In this paper we do not attempt to discriminate between the possible mechanism of inundation. Possibly all are involved. For example, even though eustatic rise of sea level was a factor, it was less than 1 mm per year at 1.9–4.4 ka (Berger, 1983). Some parts of the coastline were tectonically uplifted faster than this. Others were probably tectonically submerging.

Sequence of events

Although we cannot assume the same sequence of events for all sites, we propose a six-step sequence (Figure 9) as the most likely one for the majority of sites of rooted stumps and associated forest soil. First, the

wave-cut platform was cut at sea level prior to growth of the trees. Second, sea level regressed off the platform due to tectonic uplift. In the third stage, the forest grew over the platform. In the fourth stage, the forest was rapidly buried and the litter preserved. In the fifth stage, the forest was inundated by the surf zone. In the sixth and final stage, the forest soils and overlying deposits were eroded during the retreat of the marine cliffs.

CONCLUSIONS

The rooted stumps and forest soils on Oregon's beaches are remnants of forests similar to present-day coastal temperate rain forest that grew on the Holocene wave-cut platform and adjacent creeks, dune fields, and marine terraces. The paleo-forest soils exposed in the surf zone, in creek mouths, and on valley walls are probably contemporaneous with rooted stumps in the surf zone, but this cannot be established without further mapping, coring, and radiocarbon dating. The abrupt upward termination of the forest soil and the preservation of undecomposed litter indicates rapid burial by debris flows, dunes, or beach sands. The burial may have been coseismic and synchronous with inundation, but this cannot be established with the data set on hand. The preliminary ages of the stumps, 1.9–4.4 ka, show that the growth and burial of some of the trees took place after the time of major eustatic sea level rise in early mid-Holocene time. The rapid colonization and deterioration of the stumps and exposed soils in the surf zone indicate that these forest remnants were exposed only during short-lived erosion events or have not been previously exposed. The full cycle of platform cutting, uplift, forest growth, burial, inundation, and renewed platform cutting may have taken place over a period upward of 1,000 years. Additional platform-forest site coring/mapping and radiocarbon dating are necessary to test the extent, duration, and possible cyclicity of these processes. For example, do other forest remnants exist landward under Holocene dune fields or offshore on the inner shelf?

ACKNOWLEDGMENTS

Radiocarbon dating was supported by the Portland State University Department of Geology. This work was partially supported by grant No. NA36RG0451 from the National Oceanic and Atmospheric Administration to the Oregon State University Sea Grant College and by appropriations made by the Oregon State Legislature. The views expressed herein are those of the authors and do not necessarily reflect the views of NOAA or any of its subagencies. Author Hart is grateful to Ian Hart, Cathy Heflin, and Bob Shivers for their assistance in the field and to Cathy Heflin for her assistance in preparation of the manuscript and figures. The field work and manuscript benefited from discussions with Alan Niem and Paul Komar.

54

FIELD TRIP ROAD LOG FOR THE
CENOZOIC STRATIGRAPHY OF COOS BAY AND CAPE BLANCO,
SOUTHWESTERN OREGON

John M. Armentrout
1107 Wiltshire Drive
Carrollton, Texas 75006

INTRODUCTION

This two-day field trip is concerned with the Cenozoic stratigraphy of the southwestern Oregon Coast at Coos Bay and Cape Blanco (Fig. 2). The log is presented as two separate mileage sequences. Twelve rock units of early Eocene to Pleistocene age will be examined (Fig. 3).

The reader is referred to Baldwin (1966, 1974) and Baldwin and others (1973) for a description of the Cenozoic formations of Coos Bay and to Beaulieu (1971), Roth (1979), and Addicott (in preparation) for Cape Blanco. The molluscan paleontology of Coos Bay is discussed by Dall (1909), Turner (1938), Weaver (1945), and Armentrout (1967). Foraminiferal paleontology of Coos Bay is reviewed by Bird (1967), Rooth (1974), and Tipton (1975). The molluscan paleontology of Cape Blanco has recently been restudied by Addicott (in preparation) and Roth (1979). Foraminiferal paleontology of Cape Blanco is being restudied and initial results are presented in this paper.

CAUTION: Several of the stops are intertidal areas along sea cliffs. Participants are urged to be aware of the time of high and low tides. Caution is urged as onshore winds can significantly alter the timing and amplitude of the tide and the size of individual waves. The stop sequence should be adjusted to fit the tide and weather situations at the time of the field excursion. Many of the stops are at sea cliff view points. These areas are underlain by Pleistocene terrace sands and are often undercut. Approach all bluffs with great caution.

Overnight accommodations are available at Coos Bay, Bandon, and Port Orford. Campgrounds at Sunset Bay, Bullard's Beach near Bandon, and Cape Blanco are operated by the State of Oregon. Contact the State Parks and Recreation Section, 525 Trade Street, S.E., Salem, Oregon 97310, for information on the seasonal schedule and availability of camp sites.

ACKNOWLEDGEMENTS

The author is indebted to those Pacific Northwest geologists who shared their ideas and field data, in particular: Ewart Baldwin, University of Oregon; Ken Bird, Warren Addicott, Kristin McDougall, and Richard Janda, U.S. Geological Survey; Barry Roth, California Academy of Sciences; and Bruce Welton, Los Angeles County Museum of Natural History. Time has not permitted review of this guide by the above geologists: all interpretations as presented are the responsibility of the author.

55



Figure 1. Aerial View of Cape Arago Area. a) Assembly area - Stop 1: Flagpole View Point. b) Middle Cove. c) South Cove overlook - Stop 2. d) North Cove overlook - Stop 3. e) Channel-fill sequence of figure 11. f) Sea Lion View Point - Stop 4. g) Shore Acres State Park - Stop 5. h) Sunset Bay State Park - Stop 6. i) Gregory Point. j) Mouth of Coos Bay. Photograph courtesy of Oregon State Highway Division.

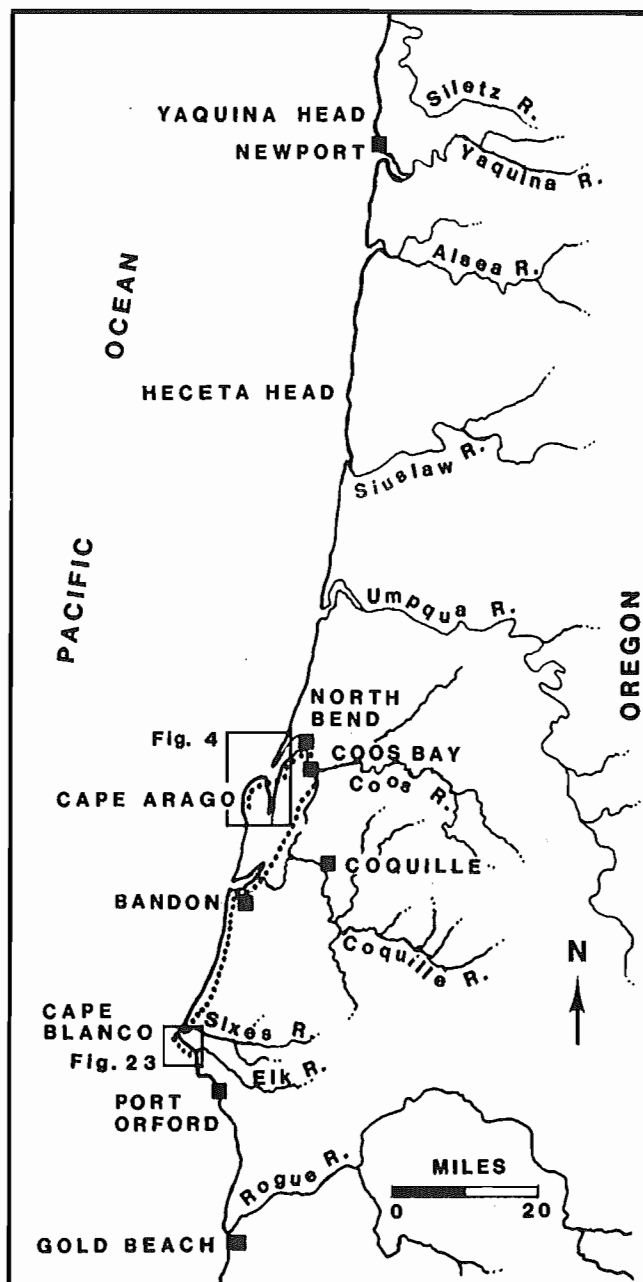


Figure 2. Index map to the field trip area.

SERIES		WEST COAST FORAM. STAGES	ORE./WASH. MOLLUSCAN STAGES	COOS BAY SECTION	CAPE BLANCO SECTION
NEOGENE	QUAT.	UNNAMED	UNNAMED	TERRACES	TERRACES
	PLEISTO.				ELK RIVER BEDS
		QUINAULT. ASSEM.	MOCLIPSAN		PORT ORFORD FM.
	MIOCENE	UNDIFF. ASSEM. MONTESANO FM.	GRAYSAN		
			-?-?-?-?- WISHKAHAN	EMPIRE FORMATION	EMPIRE FORMATION (RESTRICTED)
	MIDDLE	LUISIAN RELIZIAN	-?-?-?-?- NEWPORTIAN		
	EARLY	SAUCESIAN	PILLARIAN	MIOCENE BEDS	SANDSTONES OF FLORAS LAKE
	OLIGOCENE		JUANIAN		
		ZEMORRIAN	MATLOCKIAN		
	LATE	REFUGIAN	GALVINIAN	TUNNEL PT. FM.	
PALEOGENE	EOCENE		UNDIFF. ASSEM. COWLITZ & COALEDO FMS.	BASTENDORFF FORMATION	
		NARIZIAN		COALEDO FORMATION	
	EARLY	ULATISIAN	UNDIFF. ASSEM UMPQUA & TYEE FMS.	?-?-?-? ELKTON SILTSTONE	
	LATE	PENUTIAN			ROSEBURG FM. ?-?-?-?-?
		?	?		

Figure 3. Correlation of provincial time scale, biochronologies and formations at Coos Bay and Cape Blanco. Usage of Foraminiferal Stages follows W. W. Rau (pers. commun., 1979); molluscan stages follows Armentrout (1975) and Addicott (1976).

COOS BAY SEGMENT

The Coos Bay field trip segment consists of a one-day excursion of 9.8 miles with 13 stops (Figs. 1, 4, and 11).

The Cenozoic geology of Coos Bay consists of Paleocene to Pleistocene continental margin marine rocks which were folded into the Coos synclinorium during Oligocene and early Miocene time (Baldwin and others, 1973). Subsequent Neogene deposition in the area was confined to the axis of this synclinorium, along the South Slough Syncline (Figs. 4 and 5). The Coos Bay Cenozoic section measures more than 12,000 feet thick (Fig. 6). Paleocene units crop out in the Coast Range around the perimeter of the Coos synclinorium but will not be visited on the field trip. The Seven Cenozoic units that will be visited are separated into four unconformity bound sequences of rocks: (1) Eocene to lower Oligocene (Elkton Siltstone, Coaledo Formation, Bastendorff Formation, and Tunnel Point Formation); (2) upper lower to middle Miocene (Miocene Beds); (3) upper Miocene (Empire Formation); and (4) Pleistocene (terrace deposits).

MILEAGE DESCRIPTION

Cumulative (Interval)

Drive to Cape Arago State Park from either North Bend or Coos Bay. The route is well marked. Cumulative mileage will be started at Stop 4.

0.0 Begin interval mileage at the entrance to Cape Arago State Park. Drive counterclockwise around the park road.

(0.5)

0.0 STOP 1: FLAG-POLE AREA: Cape Arago State Park. Park along the roadway and walk out to the stone observation area at the western edge of the Cape overlooking Middle Cove on the south (Fig. 1-a).

Cape Arago consists of Eocene sedimentary rocks folded into a north-trending anticline which is now truncated by a coastal terrace. The anticline extends from North Cove to South Cove, and is cut by a normal fault with downdropped strata on the west. A secondary fault trends through Middle Cove and may intersect the primary fault in North Cove. Resistant sandstone of the downfaulted middle Eocene Coaledo Formation form the seaward face of Cape Arago. North Cove and South Cove are eroded into the early Eocene Elkton Siltstone Member of the Tyee Formation (Beaulieu, 1971). The Elkton Siltstone is discordantly overlain by the Coaledo Formation (Dott and Bird, 1979). The Elkton Siltstone is abundantly microfossiliferous (Bird, 1967; Dott and Bird, 1979). Sandstone of the Coaledo Formation contains megafossils, particularly at Middle Cove where sand dollars are moderately abundant along with numerous mollusks (Turner, 1938). Shale interbeds of the Coaledo Formation are microfossiliferous (Rooth, 1974).

Return to the roadway and proceed eastward.

(0.4)

0.0 STOP 2: SOUTH COVE OVERLOOK: Park along the road and walk southwest on the terrace surface to the bluff overlooking South Cove.

South from Cape Arago the coastline follows the cliff area of the Seven Devils area southward along Sacchi Beach, Agate Beach, and Merchant's Beach to Five Mile Point. Beyond Five Mile Point is the long sandy area near Whisky Run and Bullard's Beach and finally the rocky headland of Coquille Point at Bandon. On a very clear day Cape Blanco can also be seen far to the south.

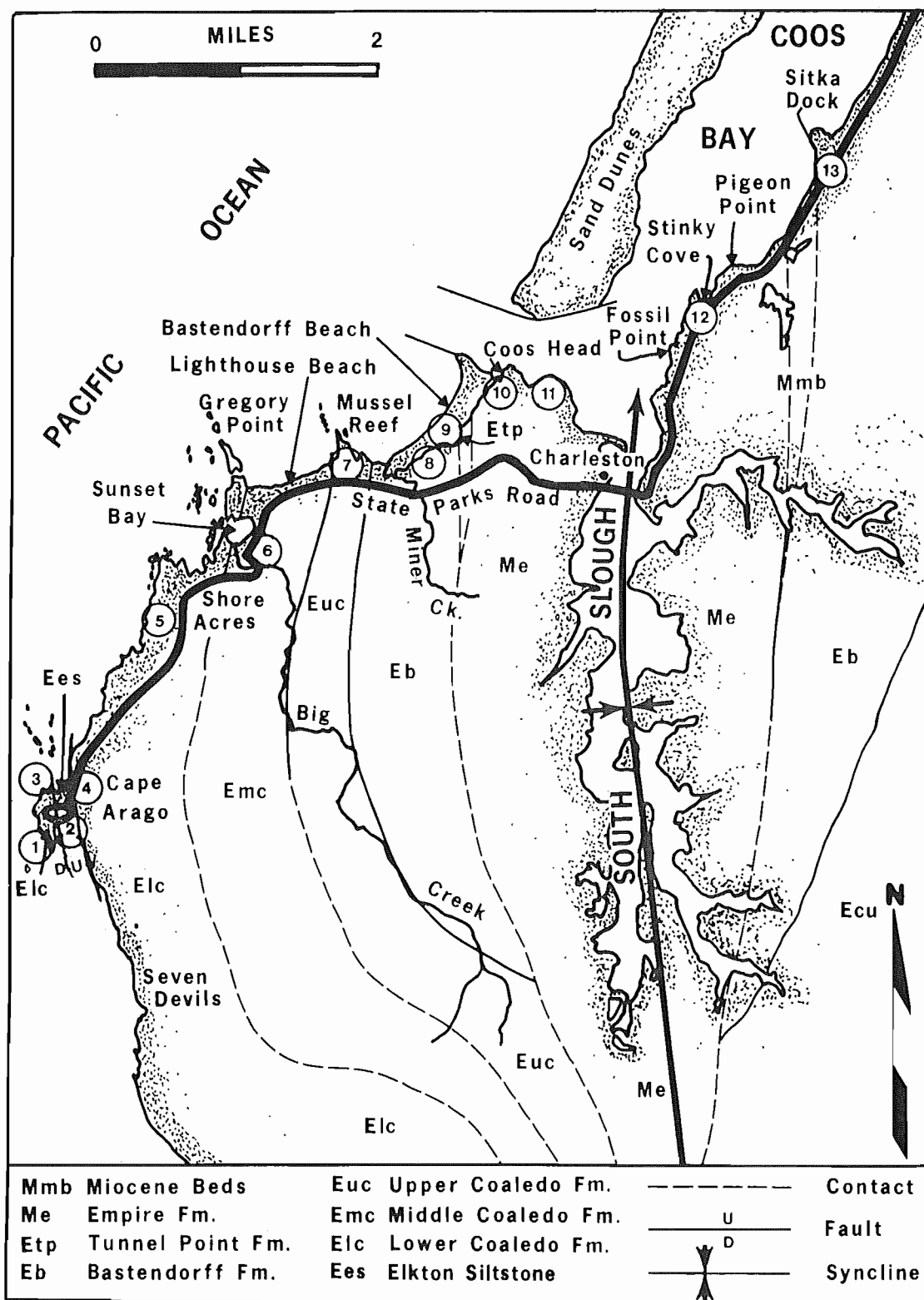


Figure 4. Geologic map for Coos Bay area (modified from Baldwin and others, 1973). Circled numbers indicate field trip stops.

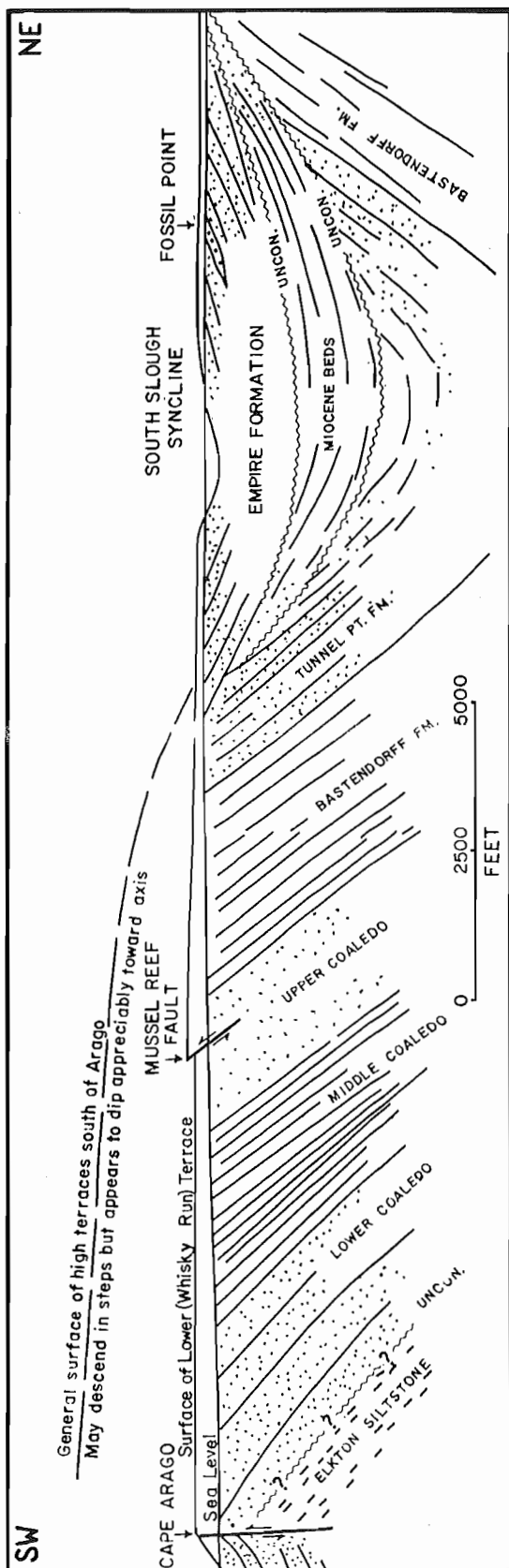


Figure 5. Geologic cross section of South Slough Syncline (modified from Baldwin 1966).

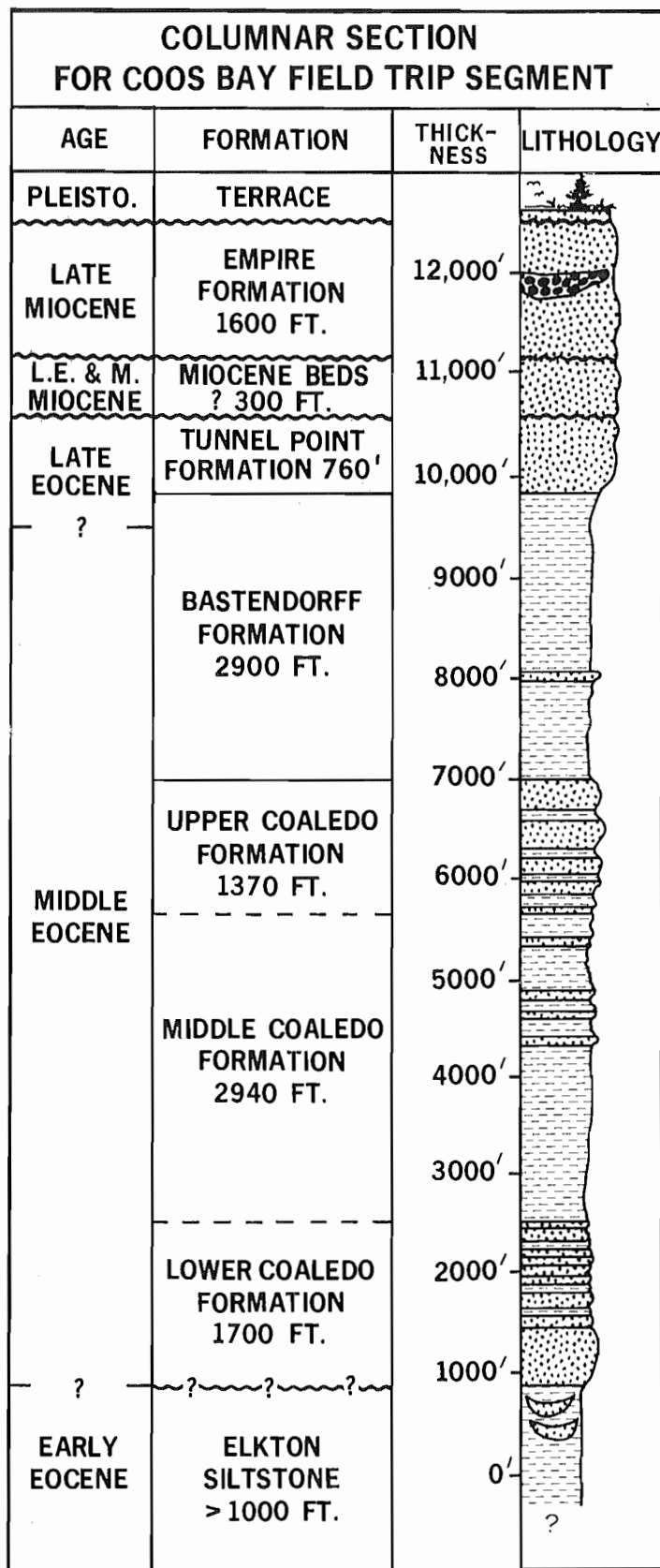
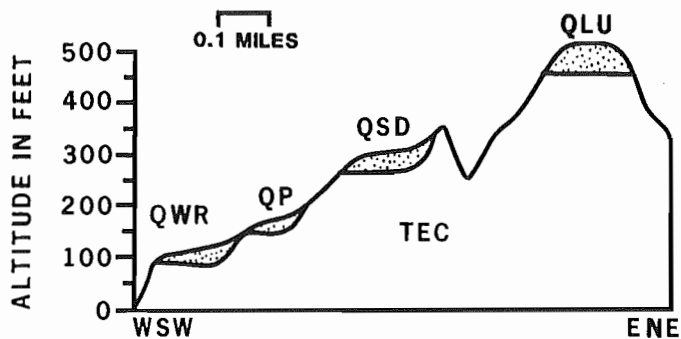


Figure 6. Stratigraphic column for Coos Bay Cenozoic formations.



QWR WHISKY RUN TERRACE
 QP PIONEER TERRACE
 QSD SEVEN DEVILS TERRACE
 QLU LOWER UNNAMED TERRACE
 TEC EOCENE COALEDO FORMATION

Figure 7. Coastal Terrace Sequence: STOP 2. Griggs (1945) has mapped five coastal terraces in the vicinity of Cape Arago. This diagram shows the relative relationship of the four lower and more visible terraces which can be seen from STOP 2. The cross section is drawn trending east-northeast.

A sequence of five coastal terraces can be seen from this vantage point (Fig. 7). Griggs (1945) mapped, named, and cursorily described these terraces. Baldwin (1945, 1966) and Armentrout (1967) have made observations at selected key localities. Cape Arago is capped with 10 to 40 feet of colluvium and marine sands and gravels of the Whisky Run terrace. At Cape Arago the paleoshoreline of the Whisky Run terrace is at an altitude of about 95 feet. Southward along the Seven Devils area the prominent bench of the Seven Devils terrace occurs at an altitude of about 300 feet. Farther south, the Pioneer terrace is well developed at about 150 feet above the valley at Two Mile Creek which is just north of Five Mile Point. The Whisky Run terrace at 100 feet elevation forms the flat surface of Five Mile Point. The break between the Pioneer and Whisky Run terraces is visible in the coastal bluffs between Five Mile Point and Two Mile Creek. Two prominent high terraces at altitudes of 730 and 500 feet were unnamed by Griggs (1945), and are difficult to identify at Cape Arago.

Large channels filled with lenticular sequences of massive sandstone and mudstone can be seen in the eastern cliffs of South Cove (Figs. 8-9). These rocks of the Elkton Siltstone are transitional stratigraphically from thick-bedded, mid-fan sandy turbidites of the underlying Tyee Formation to the overlying coal-bearing deltaic Coaledo Formation (Dott and Bird, 1979). Foraminifers suggest a shoaling sequence from upper bathyal Tyee faunas to inner neritic, upper Elkton faunas. Channel fills are either laminated mudstone-siltstone identical with the channelized deposits or massive to faintly parallel-laminated and rarely graded light-colored sandstones.

Dott and Bird (1979) interpret the Elkton Siltstone at Cape Arago as shelf and slope deposits cut by an array of sea gullies which range in size up to 300 feet wide and 75 feet deep. These gullies may have acted as conduits of sand from a sandy littoral and deltaic zone (Coaledo Formation-like facies) across a narrow shelf and slope feeding deeper marine turbidity currents and other gravity flows (Tyee Formation-like facies), which built subsea fans (Dott and Bird, 1979).

Return to roadway and proceed north and west back through the main entrance of Cape Arago State Park, stopping at the drinking fountain at the north end of the main parking area.

(0.3)

62

- 0.0 STOP 3: NORTH COVE OVERLOOK: Walk along the paved trail to the north end of the picnic area. (Fig 1-d). From vantage points along this trail the geology of North Cove can be seen.

The geology of North Cove is similar to that of South Cove. The eastern cliffs of the Cove are Elkton Siltstone while the seastacks farthest to the west are Coaledo Formation sandstone. The traverse along the North Cove beach is passable even at normal high tide. The trail from the Cape Arago-North Cove picnic area descends to the beach. A major Elkton Siltstone channel crops out at the eastern margin of North Cove (Figs. 1-e and 10). The channel axis has been reoccupied by a modern stream which cascades down a prominent rib of sandstone. The sandstone rib stands in marked relief compared to exposures of the same sandstone on either side of the waterfall. The constantly wet sandstone may be more erosionally resistant than alternately wet and dry cliff faces to either side (Ehlen, 1967). The major "waterfall" channel is only one of several Elkton Siltstone channels which occur along the cliffs to the north of the waterfall. Sedimentary structures in the Elkton Siltstone are exposed on the wave-cut terrace just north of the lobate beach north of the waterfall. Primary sedimentary structures include flame structures, rill-type solemarks, load features, groove and flute casts, interclast conglomerates, climbing ripple laminations, flaser bedding, cross-trough stratification, laminated mudstone and sandstone, and clastic dikes. Paleocurrents are to the northwest. Northward, past the area of Sea Lion View Point (STOP 4), the Elkton Siltstone is overlain by massive tan conglomeratic sandstones of the Coaledo Formation.

Return to the North Cove parking area and leave Cape Arago State Park on State Parks Road.

- (0.4)
0.0 STOP 4: SEA LION VIEW POINT: From this view point (Fig. 1-f) one can see the seastacks of North Cove and Simpson's Reef. Shell Island is the largest sea stack of the North Cove group.

Simpson's Reef, the farthest offshore and most elongate reef, dips landward. Most of the North Cove sea stacks dip seaward. These structural attitudes define Simpson's Reef Syncline (Ehlen, 1967).

- 0.0 START CUMULATIVE MILEAGE. Continue north on State Parks Road. Road cuts along this area are in alluvium and colluvium on the back of Whisky Run terrace.

- (1.0)
1.0 Shore Acres State Park: turn left into the park. Proceed to and park in the main viewpoint parking area. Walk out to the view area at the sea cliff.

- (0.2)
1.2 STOP 5: SHORE ACRES STATE PARK: Shore Acres (Fig. 1-g) was developed as an estate by the Louis Simpson family, prominent in lumbering and ship-building in the Coos Bay area. The manor house burned in the late 1930's and the estate (including the land of Cape Arago State Park) was donated by the Simpson family to the State of Oregon in 1942.

Shore Acres is underlain by the lower sandstone member of the Coaledo Formation. These strata dip eastward at about 40° and are part of the east limb of the Cape Arago Anticline (Ehlen, 1967). Numerous down to the south normal faults trend northwest. The five coves in the park area are eroded along zones of weakness associated with faults. The lower sandstone member of the Coaledo Formation is about 1,300 feet thick in the coastal section (Ryberg, 1978) and thickens to 1,800 feet to the southeast (Allen and Baldwin, 1944) where the outcrop area of the Coaledo Formation wraps around the south end of the South Slough Syncline. The lower sandstone member is predominantly fine- to medium-grained, cross-bedded and

laminated sandstones with minor interbeds of siltstone and mudstone. At Shore Acres the sandstones stand out as erosionally resistant, concretionary ribs where the interbedded fine-grained rocks have been differentially eroded. Large iron-cemented concretions are characteristic features of the lower Coaledo Formation. Fossils are abundant in some intervals of the lower Coaledo. Ophiuroids (brittle stars) are moderately common within one bed which crops out in both the northern and southern coves at Shore Acres State Park.

Shore Acres State Park is developed upon the Whisky Run terrace (Fig. 7). Four to nine feet of littoral sand rest upon this terrace platform. Whisky Run terrace sands can best be viewed from the north end of the viewpoint area.

Proceed back to State Parks Road.

- (0.4)
1.6 Turn left toward Sunset Bay State Park.
- (0.4)
2.0 View at 11:00 o'clock of Gregory Point and Cape Arago Lighthouse (Fig. 1-i and 11-b). Gregory Point is underlain by lower Coaledo Formation sandstone. These sandstones dip northeastward and strike increasingly more westward around the northern end of the Cape Arago Anticline (Ehlen, 1967).
- (0.5)
2.5 Bridge across Big Creek. Big Creek heads in shales of the Bastendorff Formation to the east and cuts through the upper and middle Coaledo Formation.
- (0.2)
2.7 STOP 6: SUNSET BAY STATE PARK: Park in the beach parking area. Traverses along either the north or south margins of Sunset Bay afford access to outcrops of lower Coaledo sandstone and middle Coaledo siltstone and mudstone. Access is best at low tide when outcrops of the surf-cut terrace are exposed over large areas along the north side of the cove. Trails along the north bluff of the bay provide excellent views of the faulting of the wave-cut terrace (beware of undercutting of the trails along the bluff).

Sunset Bay is an arcuate bay formed along a complex set of northwest-trending faults transverse to the strike of bedding (Fig. 11-a). Sunset Bay is offset 450 feet in a right lateral sense, between the north side and south side of the bay. Whether this displacement is along a single fault, or a series of smaller faults such as those exposed along the bay margins, is unknown. Orientation of drag folds suggests that the fault motion was oblique slip (Ehlen, 1967) (Fig. 12).

Ryberg (1978) identified several lithofacies in coarsening upward sequences within the lower Coaledo Formation. Outcrops exposing these coarsening upward sequences occur along the shores of Sunset Bay. The top of each sequence is generally identified by dark-brown, concretionary, coarse pebbly sandstone which forms erosionally resistant ribs. The typical sequence from bottom to top includes interdistributary siltstone and fine-grained sandstone, overlain by coarser distributary channel (and possibly fluvial) sandstone with interbedded lagoon or swamp coal and carbonaceous siltstone. These coarsening upward sequences are interpreted by Ryberg (1978) as representative of the outbuilding of individual distributary channels during progradation of a delta. This agrees with Dott's (1966) deltaic model for the Coaledo Formation.

Sedimentary structures are well developed and beautifully exposed in outcrops along the north side of Sunset Bay and on the cliffs and terraces beyond the southwest edge of the bay entrance. Primary sedimentary structures include tabular, trough, wedge and hummocky cross-stratification, ripple cross-stratification, and rare flute and groove sole marks. Secondary

64



Figure 12. Coaledo Formation: STOP 6. View of drag-folds along faults in the Coaledo Formation. Photo taken at low tide from bluffs above the north side of Sunset Bay.

structures resulting from gravity deformation of the sediments include contorted bedding and flare, and ball and pillow structures. Clastic dikes and isolated sandstone "load-balls" represent liquification structures. Bioturbation includes both vertical and horizontal burrows.

The lower Coaledo is abundantly fossiliferous (Turner, 1938; Rooth, 1974). Mollusks and Foraminifera dominate the fauna but echinoids, shark teeth, and rare crustacean fossils also occur. The mollusks suggest deposition in middle to lower neritic depths (Rooth, 1974).

Paleocurrents are predominantly to the northwest and mineralogic studies suggest a mixed andesitic (e.g., Cascade-like) and metaplutonic (e.g., Klamath Mountains-like) provenance (Dott, 1966; Ryberg, 1978). This fits well with Dott's (1966) paleogeographic reconstruction for middle Eocene time which consists of a broad coastal plain prograding westward across a narrow shelf and slope. The coastal plain was flanked by highlands on the southeast. The highland included both volcanic and metaplutonic terrains.

Outcrops of the middle member of the Coaledo Formation in Sunset Bay consist of interbedded laminated siltstone and mudstone with minor amounts of sandstone. Ryberg (1978) considered this lithofacies to represent intertidal flat and delta front deposits. The abundant molluscan (Turner, 1938) and foraminiferal faunas (Detling, 1946; Cushman and others, 1947; Rooth, 1974) represent deepening conditions from outer neritic just above the lower Coaledo sandstones to upper bathyal conditions above. The best outcrops and a complete section of the middle Coaledo siltstones and mudstones occurs along Lighthouse Beach at STOP 7.

The steeply dipping beds of the Coaledo Formation are truncated by the Pleistocene Whisky Run terrace. The Whisky Run terrace platform and presumably the shoreline angle are at an altitude of about 50 feet at the rear of the north side of Sunset Bay. The terrace platform along the south side of the bay is at 70 feet. The terrace has probably been offset by movement along a fault hidden beneath the water of Sunset Bay.

Tree stumps with root spreads up to 35 feet are exposed along Big Creek and in the intertidal zone of Sunset Bay beach. One set of root systems occurs in association with peat toward the north end of the beach. The trees could have been growing on the Holocene flood plain of Big Creek and drowned as the sea carved out the Sunset Bay amphitheater long after sea level attained its present position. Previously unpublished carbon

14 data on one root from along Big Creek yields an estimated age of about 1,200 years B.P. (Southern Methodist University Radiocarbon Laboratory Sample 593-B8/12-Count 1439: 10/11/78; Armentrout, unpub. data).

Return to the parking area and proceed north on State Parks Road. The road climbs from the Big Creek Holocene flood plain to the top of the Pleistocene Whisky Run terrace.

- (0.4)
3.1 Road to the left provides access to the Cape Arago Lighthouse on Gregory Point. Steeply dipping beds of the lower Coaledo sandstone underlie the point.
- (0.6)
3.7 STOP 7: YOAKAM POINT - MUSSEL REEF: Park along State Parks Road and walk northwest along a dirt road; about 150 feet from the main road, bear right (north) at the Y-junction, and continue to the sea cliff overlook area.

STOP 7A: Looking westward from Yoakam Point the three members of the Coaledo Formation can be observed. The lower sandstone member underlies Gregory Point to the west (Fig. 11-b). The middle mudstone and siltstone member has been eroded back forming Lighthouse Beach (Fig. 11-c). Yoakam Point and its seaward extension, Mussel Reef, consists of the upper sandstone member of the Coaledo Formation (Fig. 11-d). The cove immediately east of Yoakam Point is eroded in a siltstone of the upper sandstone member of the Coaledo Formation. The small point at the east side of this cove is the uppermost Coaledo Formation sandstone.

The platform of the Gregory Point-Yoakam Point area is formed by the Whisky Run terrace and is veneered by about 11 feet of littoral sand. At Yoakam Point the terrace is faulted with the eastern block offset about 10 feet above the western block. The fault trends north-northwest, parallel to the strike of the underlying Coaledo Formation and appears to be a high-angle reverse fault (Baldwin, 1966) (Fig. 5). The fault is best observed from the beach where the offset of a coal seam delineates the fault motion.

Griggs (1945) has mapped the eastward continuation of the Whisky Run terrace at the back of Bastendorff Beach where it forms the platform as far northeast as Tunnel Point (Fig. 11-g). The Pioneer terrace surface forms the platform at Coos Head, the northernmost point at the mouth of Coos Bay (Griggs, 1945) (Fig. 11-h).

Descend to Lighthouse Beach along the trail just south of Yoakam Point and walk to Gregory Point. Stop 7B consists of a traverse from Gregory Point to Yoakam Point.

STOP 7B: Gregory Point is formed of uppermost lower Coaledo sandstone interpreted to be deltaic distributary channel deposits (Ryberg, 1978). The sandstone is conformably overlain by middle Coaledo siltstone, mudstone and thinly bedded sandstone interpreted by Ryberg (1978) as intertidal flat to delta front deposits. Thick channelized massive sandstone occurs at several intervals within the finer grained sequence and is interpreted as prodelta front slump deposits (proximal turbidite or grainflow gravitite). A white tuff 3- to 6-feet-thick occurs just above the middle part of the middle Coaledo member at Lighthouse Beach.

At several points along Lighthouse Beach the truncated ends of middle Coaledo sandstone beds at the abrasion surface of Whisky Run terrace are bored by rock-boring clams. These features will be examined in detail at STOP 11.

The middle Coaledo Formation mudstone and siltstone is gradational with the overlying upper Coaledo sandstone. Upper Coaledo sandstone units are very similar to those of the lower Coaledo, representing fluvial and

6413



Figure 21. Aerial View of Cape Blanco Traverse. a) Jurassic Otter Point Formation. b) Late Miocene Empire Formation. c) Cape Blanco Coast Guard facility. d) Eocene Shales - Stop 4. e) Miocene Sandstones - Stop 6. f) Fin Rock Miocene Sandstones - Stop 7. g) Terrace Fossil Beds - Stop 3. h) View Point - Stop 2. i) Cape Blanco State Park Campground. j) Goldwasher's Gully - Stop 11. k) Cliff at Stop 12. l) Cliffs at Stops 13-15. m) Mouth of Elk River. n) Port Orford. o) Humbug Mountain. Photograph courtesy of Oregon State Highway Division.

64C

FLUVIAL FIELD TRIP EQUATION LIST

p. 58-59 NOTES

FROUDE NO. - DESCRIBES FLOW TYPE

$$Fr = \frac{V}{\sqrt{dg}}$$

V = velocity m/sec
d = depth in
g = gravity acc. = 9.8 m/sec²

F < 1 = TRANQUIL FLOW

F = 1 = CRITICAL FLOW

F > 1 = SUPERCRITICAL FLOW

MANNING'S EQUATION - TO CALCULATE STREAM VELOCITY

$$V = \frac{R^{2/3} S^{1/2}}{n}$$

V = VELOCITY m/sec

R = HYDRAULIC RADIUS = $\frac{A}{P}$ — A = CHANNEL AREA m²
P = WETTED PERIMETER m

S = SLOPE

n = ROUGHNESS

$T_c = \gamma R S$ = CRITICAL STREAM FORCE FOR EROSION

γ = SPECIFIC WT. of H₂O = 9800 N/m³

R = HYDRAULIC RADIUS = $\frac{A}{P}$

S = SLOPE

STREAM POWER = KINETIC ENERGY AVAILABLE FOR WORK

TOTAL POWER $\Sigma = \gamma Q S$ (WATTS)

UNIT POWER $w = \frac{\gamma Q S}{W}$ (WATTS/m)

γ = SP. WT. H₂O = 9800 N/m³

Q = DISCHARGE = m³/sec

S = SLOPE

W = WIDTH m

CONTINUITY EQUATION

$$Q = VA$$

Q = DISCHARGE m³/sec

V = VELOCITY m/sec

A = AREA OF CHANNEL m²

WATER BUDGET

$$P = R + I + S$$

P = Total Precipitation

R = Surface Runoff

I = Soil ~~Infiltration~~ ^{Interception}

S = Soil / Groundwater Storage

PERMANENCE INTERVAL

$$RI = \frac{\text{Total No. of Years Rainfall}}{\text{No. Observations in Time Period}}$$

No. Observations in Time Period

FLUID MECHANICS

Force of water

$$F_p = F_g (\sin \theta)$$

F_p = force parallel to channel

F_g = force of gravity

θ = angle of channel slope

Momentum

$$M = (\text{mass})(\text{velocity})$$

Friction No.

$$Fr = \frac{u}{\sqrt{gd}}$$

u = velocity m/s

g = force of gravity $\frac{m}{s^2}$

d = depth of flow m

Reynolds No.

$$Re = \frac{\rho du}{\nu}$$

ρ = fluid density

ν = viscosity

d = depth

u = velocity

Re = Reynolds No.

Porosity & Permeability

$$P\% = \frac{V_T - V_S}{V_T} \times 100\%$$

V_T

V_T = total vol.

V_S = vol. solid

Darcy's Law

$$Q = \frac{K A (P_2 - P_1)}{\mu L}$$

Q = Discharge (L^3/t)

K = permeability

A = x-sectional area

L = length

$P_2 - P_1$ = head

μ = viscosity

River Morphometry

= Sinusoid

$$S = \frac{\text{Stream length}}{\text{valley length}}$$

= Station Stream order

= Drainage frequency $f = \frac{No.}{A}$

= Bifurcation Ratio

$$R_b = \frac{No}{No + 1}$$

= Length Ratio

$$R_L = \frac{L_{Avg}}{L_{Avg} + 1}$$

= Drainage Density

$$D = \frac{L_{Total}}{A}$$

= Extension Ratio

$$T = N/P$$

Stream Flow CONTINUITY EQUATION

$$Q = VA = Vwd$$

Q = Discharge (L^3/t)

V = Velocity (L/t)

A = x-sectional area

w = channel width

d = channel depth

$$P = 2d + w$$

P = wetted perimeter

Hydraulic Radius

$$R = \frac{A}{P} = \frac{m^2}{m}$$

MANNING'S EQUATION METRIC UNITS

$$V = \frac{R^{0.66} S^{0.5}}{n}$$

V = mean velocity m/s

n = coefficient of roughness

R = hydraulic radius m

S = Slope (gradient)

HYPSOMETRIC ANALYSIS

$$X = \frac{a}{A} = \frac{\text{area above datum}}{\text{Total Basin Area}}$$

$$Y = \frac{h}{H} = \frac{\text{Ht. above datum}}{\text{Total Basin Elev.}}$$

hypsometric curve

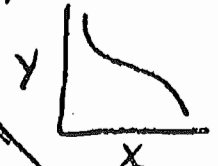


TABLE 1 - ROUGHNESSES

A. ~~Values of~~ Values of Roughness, n

River Description	Roughness, n
Ordinary rivers:	
clean, straight channel, no riffles or pools	0.030
straight, weedy, boulders	0.035
clean winding channel, pools and riffles	0.040
weedy, winding, deep pools	0.070
Alluvial channels:	
vegetated, no brush, grassy	0.030-.035
vegetated, brushy	0.050-.10
no vegetation	
ripples, dunes	0.017-.035
plane bed	0.011-.015
antidunes	0.012-.020
Mountain streams: rocky beds	
no vegetation, steep banks	
bed of gravel, cobbles,	0.040
bed of cobbles and boulders	0.050

Compiled and adapted from Chow (1959 and 1964)

p. 59 NOTES

B.

~~Table 1~~ Manning roughness coefficients (n) for different boundary types.

Boundary	Manning n (ft ^{1/3})
Very smooth surfaces such as glass, plastic, or brass	0.010
Very smooth concrete and planed timber	0.011
Smooth concrete	0.012
Ordinary concrete lining	0.013
Good wood	0.014
Vitrified clay	0.015
Shot concrete, untroweled, and earth channels in best condition	0.017
Straight unlined earth canals in good condition	0.020
Rivers and earth canals in fair condition; some growth	0.025
Winding natural streams and canals in poor condition; considerable moss growth	0.035
Mountain streams with rocky beds and rivers with variable sections and some vegetation along banks	0.041-0.050

Source: *Handbook of Applied Hydrology*, ed. by Ven T. Chow, copyright 1964 McGraw-Hill Publishing Co., Inc.

HYDROLOGY SURFACE WATER EQUATION LIST

(1) CONTINUITY EQUATION FOR RIVER DISCHARGE

$$Q = AV = wdV = wd \frac{L}{t} = \frac{Vol}{t}$$

Where Q = DISCHARGE (L^3/t)

A = channel cross-sectional area (L^2)

V = Velocity (L/t)

w = channel width (L)

d = channel depth (d)

Vol = VOLUME (L^3)

t = time (time units)

(2) WATERSHED DRAINAGE DENSITY

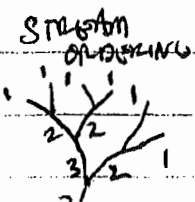
$$D_d = \frac{\sum L}{A_d}$$

Where $\sum L$ = sum of total stream lengths (L)

A_d = drainage area (L^2)

D_d = DRAINAGE DENSITY
($L/L^2 = m/Km^2$)

(3) STRAIVE MAGNITUDE FOR WATERSHEDS



M = \sum Frequency of first order streams

68

58

(4) RATIONAL RUNOFF METHOD (for watersheds)

$$Q_p = CIA \quad \text{where}$$

Q_p = PEAK RUNOFF DISCHARGE (L^3/t)

C = RATIONAL RUNOFF COEFFICIENT (dimensionless)

I = RAINFALL INTENSITY (L/t)

A_d = DRAINAGE AREA (L^2)

VALUES OF "C"

PAVEMENT $C = 0.70 - 0.95$

SANDY SOILS $C = 0.20 - 0.40$

CLAYEY SOILS / COLLUVIUM $C = 0.40 - 0.50$

NOTE: WHERE SOILS ARE 100% SATURATED, $C \rightarrow 1.0$,
SO IN THIS CASE $Q_p = IA$

(5) FLOOD RECURRENT INTERVAL

$$R.I. = \frac{n+1}{m} \quad \text{where } n = \text{TOTAL NO. OF EVENTS OR YEARS}$$

m = RANK OF EVENT,
WITH 1 = LARGEST

$$P = \frac{1}{R.I.}$$

P = PROBABILITY OF GIVEN
MAGNITUDE OF FLOOD

(6) PEAK DISCHARGE

Q_p = MAXIMUM DISCHARGE ON RECORD
(L^3/t)

$Q_{p \text{ DAILY}}$ = MAX. DAILY DISCHARGE

$Q_{p \text{ ANNUAL}}$ = MAX YEARLY Q

(7) EMPIRICAL HYDROLOGIC RELATIONS FOR
SELECT REGIONAL WATERSHEDS

(A) $Q_{\max} = 38 M^{0.89} D^{-0.50}$ FOR APPALACHIAN
PLATEAU REGION

Where Q_{\max} = maximum DISCHARGE (L^3/t)
 M = SILLVE MAGNITUDE (DIMENSIONLESS)
 D = DRAINAGE DENSITY (L/L^2)

(B) $Q_{2.33} = 34.5 A^{0.93}$ (VERMONT
WATERSHED)

$Q_{2.33}$ = DISCHARGE WITH A 2.33 yr
RETURN PERIOD

A = DRAINAGE AREA

(8) GENERALIZED RELATIONSHIP

$Q_x = a A^b$ b range: 0.5-0.9

where x = RETURN PERIOD, Q = DISCHARGE,
 A = DRAINAGE AREA, a = COEFFICIENT, b = EXPONENT.

(8) TIME FOR HYDRAULIC CONCENTRATION OF DRAINAGE BASIN

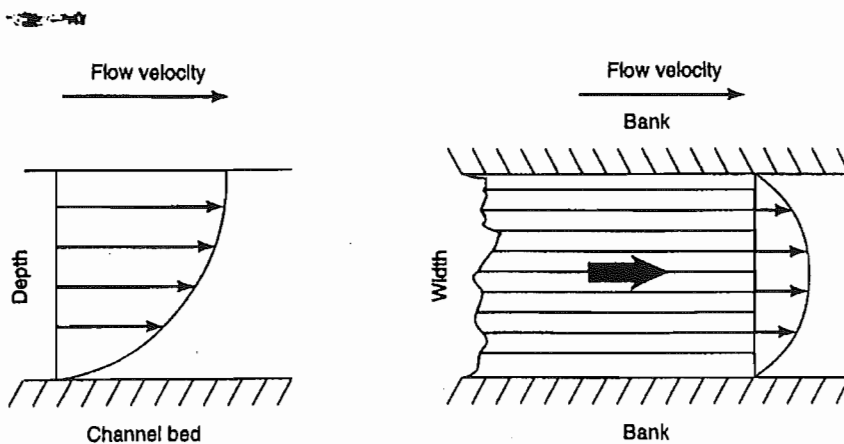
↓
 DEFINED: TIME REQUIRED DURING A STORM, FOR OVERLAND AND CHANNEL FLOW TO TRAVEL FROM THE MOST DISTANT DRAINAGE DIVIDE TO THE OUTLET OF THE BASIN

$$t_c = \frac{L^{1.15}}{7700 H^{0.38}} \quad (\text{EMPIRICAL EQUATION})$$

t_c = TIME OF CONCENTRATION (HOURS)

L = LENGTH FROM DIVIDE TO BASIN OUTLET (ft)

H = BASIN RICHNESS BETWEEN DIVIDE AND OUTLET (ft)

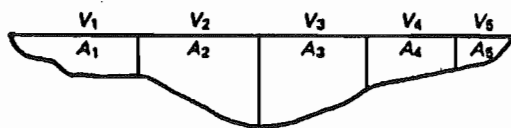


(A)

(B)

FIGURE 6.1

Diagram showing the changes in flow velocity with (A) flow depth and (B) flow width. Resistance to flow along the bed and banks allows the greatest velocities to occur toward the center of the channel near the water surface.



subareas of velocity domains.

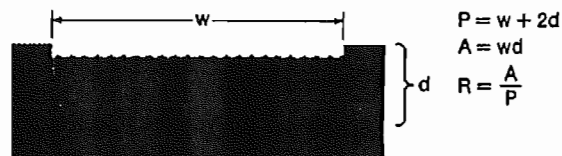


FIGURE 6.2

Cross-sectional measurements of a stream channel: w = width, d = depth, A = area, R = hydraulic radius, P = distance along wetted perimeter.

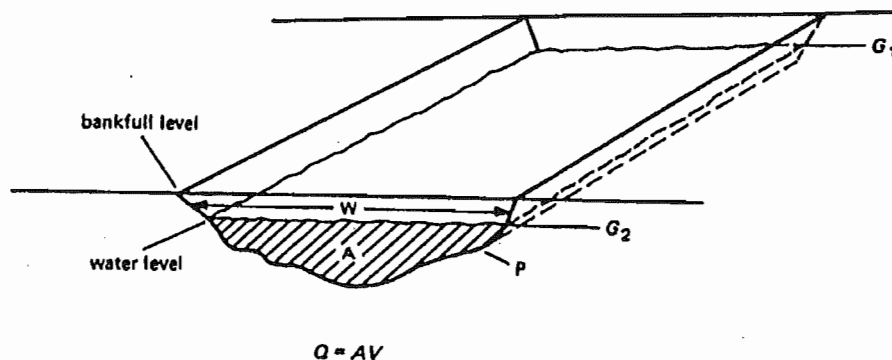


Figure 9.2. Nomenclature of channel morphology.

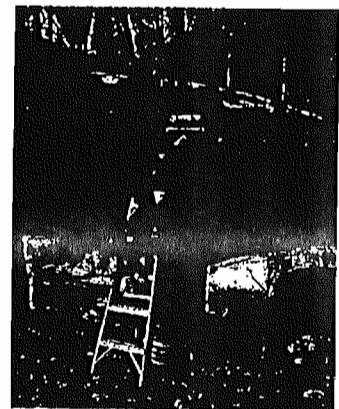
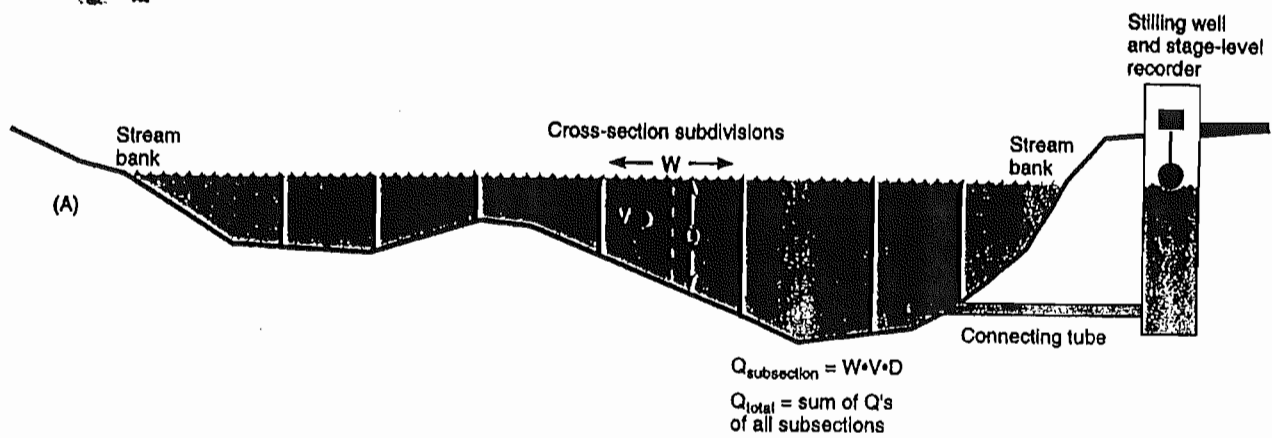
elevation
 $G_1 - G_2$ = fall

distance from
 G_1 to G_2 = length

Fall/length = gradient

$$\frac{A}{P} = R$$

p. 58-59 NOTES



(D)

p. 59 notes

FIGURE 5.33

Rating curve for low flow, Rock Creek near Red Lodge, Mont.

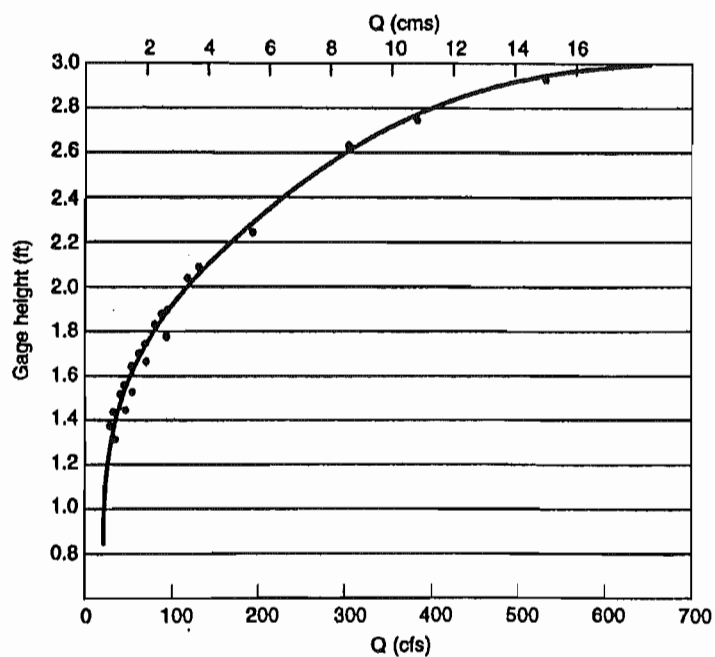


TABLE 6.1 Flow Characterization in Open Channels.

Type of flow	Flow character
Spatial variations in velocity	Velocity is constant along the channel
Uniform flow	
Nonuniform (varied)	Velocity changes with distance along the channel
Temporal variations in velocity	
Steady flow	Velocity does not change in magnitude or direction with time
Unsteady flow	Velocity fluctuates in magnitude or direction with time
Degree of particle mixing	
Laminar flow	Fluid elements move along specific paths with no significant mixing among the adjacent layers; $Re < 500$
Turbulent flow	Fluid elements do not flow along parallel paths, but repeatedly move between adjacent layers; involve large-scale transfer of momentum across layer boundaries; $Re > 2000$

another (Leopold et al. 1964). The intensity of the resistance is related to the *molecular viscosity* of the fluid, where viscosity is governed by internal characteristics of the fluid such as temperature and the concentration of suspended sediment.

In **turbulent flow**, the water does not move in parallel layers; its velocity fluctuates continuously in all directions within the fluid. Water repeatedly interchanges between neighboring zones of flow, and shear stress is transmitted across layer boundaries in another form of viscosity, called *eddy viscosity*. Eddy viscosity greatly increases the flow resistance and thus the dissipation of energy. Because turbulence is generated along the channel boundaries, most resistance in this type of flow results from external factors such as the channel configuration and the size of the bed material.

As depth and velocity increase, the conditions at which laminar flow changes to turbulent can be predicted by a dimensionless parameter called the **Reynolds number (Re)**:

$$Re = VR\rho/\mu$$

where V is the mean velocity, R the hydraulic radius, ρ the density, and μ the molecular viscosity. The hydraulic radius is determined by the relationship

$$R = A/P$$

where A is the cross-sectional area of the channel and P is the wetted perimeter (fig. 6.1). In wide, shallow channels the hydraulic radius closely approximates the mean depth.

Because the factor μ/ρ defines the fluid property called *kinematic viscosity* (ν), the Reynolds number represents a ratio between driving and resisting forces:

$$Re = VR\rho/\mu = VR/\nu = \frac{\text{driving forces}}{\text{resisting forces}}$$

In normal situations true laminar flow occurs where Re values are less than 500, and well-defined turbulent flow when Re is greater than about 2000.

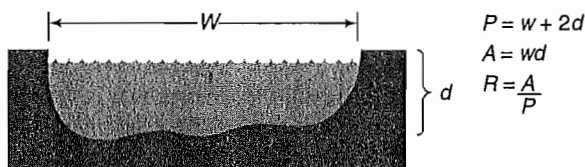
Another dimensionless number used to describe the conditions of flow is the **Froude number (Fr)**:

$$Fr = V/\sqrt{dg}$$

where d is depth and g is gravity. The Froude number is important because it can be used to distinguish subtypes of turbulent flow called *tranquil flow* ($Fr < 1$), *critical flow* ($Fr = 1$), and *rapid flow* ($Fr > 1$). The energy that is expended by these flow types differs considerably. In addition, within sand bed channels, tranquil, critical, and rapid flow have been related to the development of distinct sedimentary bedforms (fig. 6.2), which also exert an important influence on the resistance to flow in open channels (as will be discussed in more detail in the next section).

Flow within natural channels is invariably turbulent, although a very thin layer of quasi-laminar flow may be present along the channel boundaries. Most of the turbulence is generated along the water and sediment interface, causing an increase in resistance and a decrease in velocity toward the channel perimeter (fig. 6.3). Thus, across a channel the highest velocities occur near the center of the flow. The location of highest velocities may vary significantly, however, as a function of channel alignment and cross-sectional shape (fig. 6.3B), becoming more asymmetrical in meander bends (Knighton 1998).

In rivers formed in sand or finer-grained sediments with smooth channel beds, the vertical velocity profile is typically characterized by two zones of flow in addition to the laminar sublayer (fig. 6.3A). The lower zone encompasses about 20 percent of the total flow depth, and exhibits a quasi-logarithmic decrease in velocity toward the channel floor. The overlying upper zone is less affected by flow resistance along the channel bed, and vertical velocity profiles are more nearly parabolic in

**Figure 6.1**

Cross-sectional measurements of a stream channel: w = width, d = depth, A = area, R = hydraulic radius, P = distance along wetted perimeter.

74

25

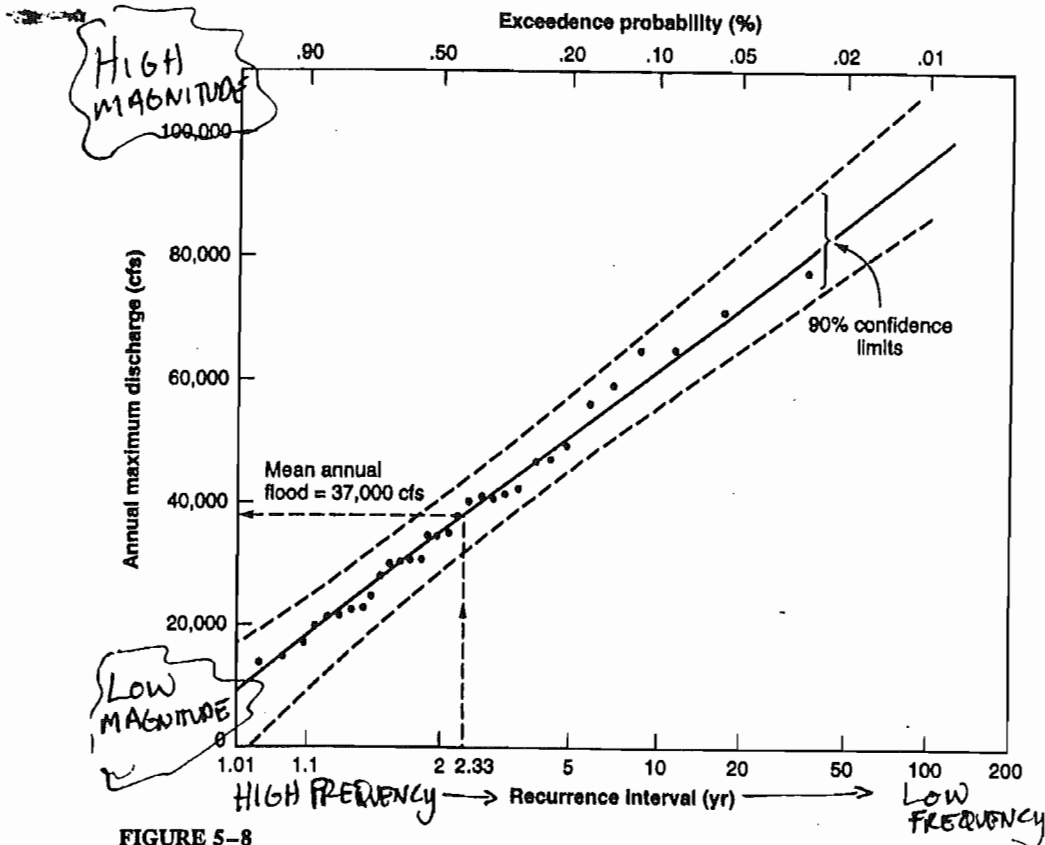


FIGURE 5-8

Flood frequency curve for annual floods on the Skykomish River, Washington. Dashed lines are 90-percent confidence limits. (Data from U.S. Geological Survey; plot from Dunne and Leopold, 1978)

p. 59
NOTES

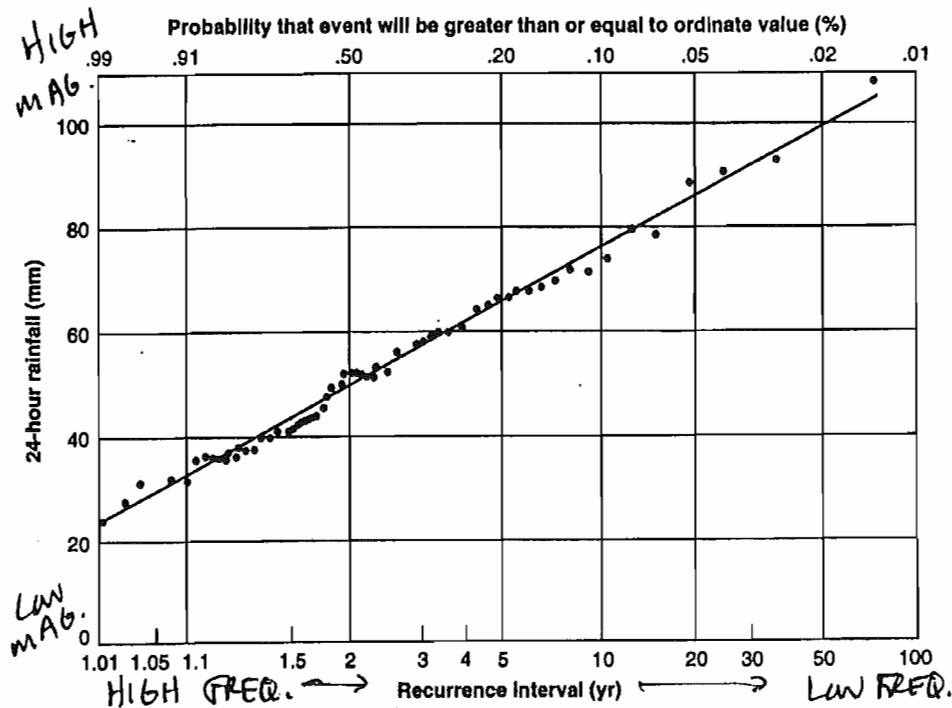
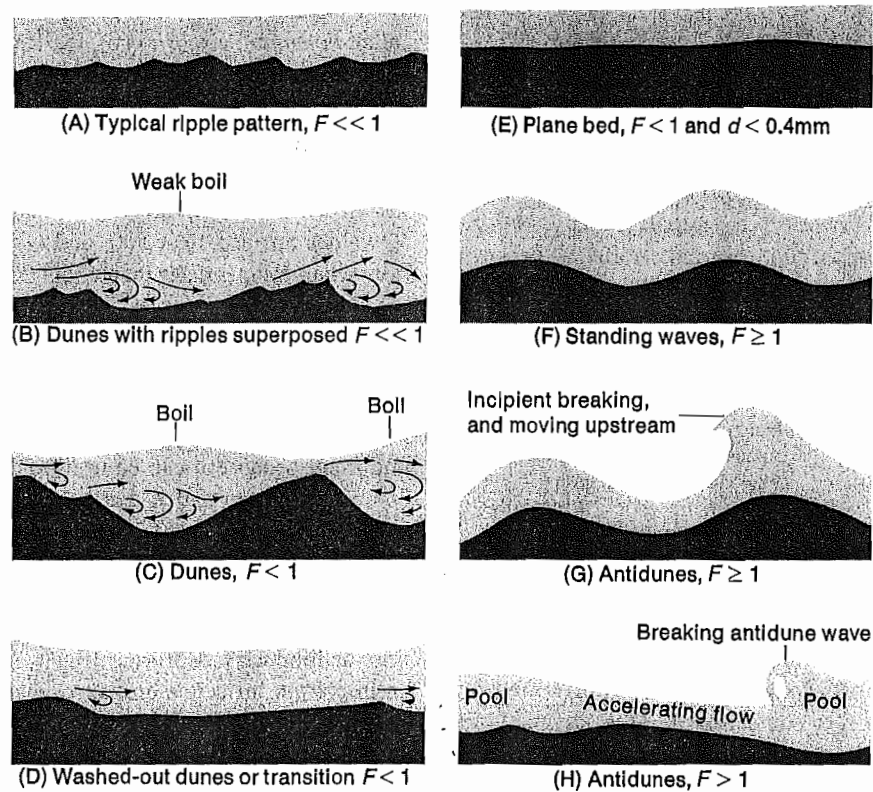


FIGURE 5-1

Recurrence interval of 24-hour precipitation, Buffalo, New York, 1891-1961. (From Dunne and Leopold, 1978)

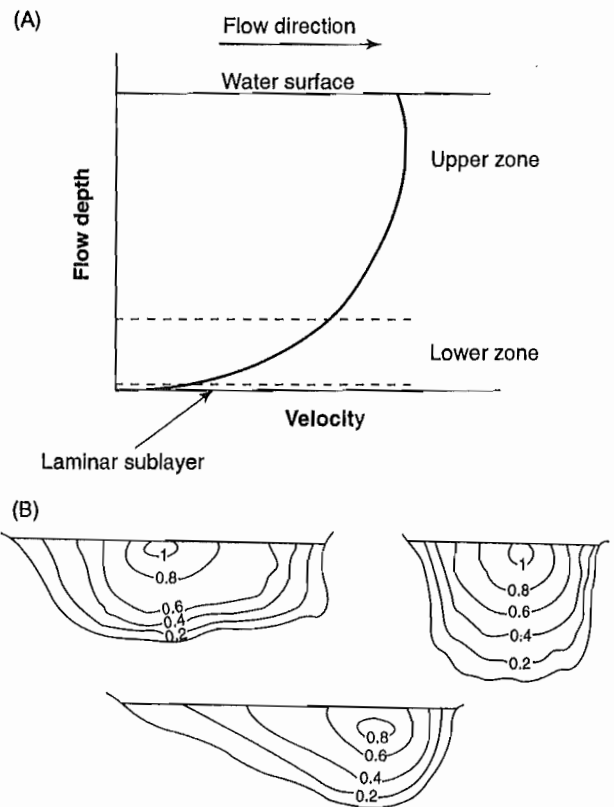
25

25

**Figure 6.2**

Bed forms in alluvial channels and their relation to flow conditions. F = Froude number, d = depth.

(Simmons and Richardson 1963)

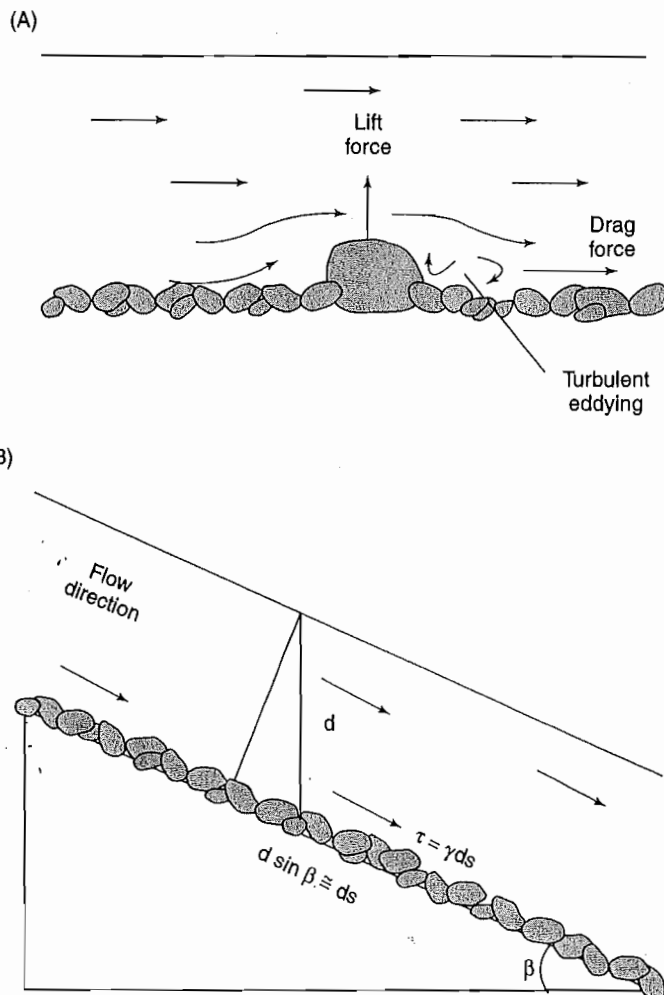
**Figure 6.3**

Variations in flow velocity as a function of water depth. The lower zone exhibits a quasi-logarithmic form induced by resistance along the channel bed. The upper zone is less affected by the bed roughness, and is more nearly parabolic in shape. The laminar sublayer may be absent or discontinuous in coarse-grained channels. (B) Typical variations in velocity across the channel. Isovets (lines of equal velocity) are in m/s.

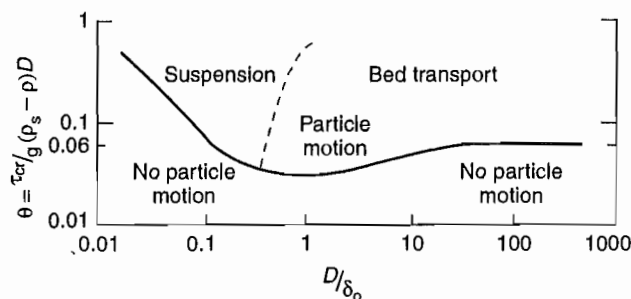
(Modified from Wolman 1955)

76

45

**Figure 6.8**

(A) Orientation of lift and drag forces acting on submerged channel bed sediment. Lift forces are due to variations in flow velocity over the top and bottom of the particle. Turbulent eddying may also create upward directed forces that act on the particles. (B) Component of flow weight exerted as shear stress on the channel bottom. The critical shear stress is equal to the depth-slope product (dS) multiplied by the specific weight of the water γ and β is the angle of slope.

**Figure 6.9**

Shield curve for the entrainment of bed particles where D is grain diameter, τ_{cr} is critical shear stress, ρ_s is sediment density, ρ is fluid density, and δ_o is thickness of laminar sublayer.

The Shields diagram illustrates that within hydraulically smooth channels characterized by silt and clay, dimensionless shear stress (θ) varies with grain Reynolds numbers (D/δ_o), reaching a minimum at a value of D/δ_o of approximately 0.03 (fig. 6.9). Dimensionless shear stress increases for smaller values of D/δ_o (fig. 6.9). Given that grain Reynolds number is related to particle

size, it follows that more shear stress is required to entrain fine-grained sediments that reside below the surface of the laminar sublayer and that are not subjected to the effects of turbulent flow. Cohesion, generally associated with smaller particles, may also play a role in increasing the shear stress required for entrainment. For hydraulically rough channel beds (in which the particles are relatively large in comparison to the thickness of the laminar sublayer), motion is initiated predominantly by turbulent action (Morisawa 1985), and θ obtains a constant value of approximately 0.06 (although constant values as low as 0.03 have been reported in some studies).

Knighton (1998) notes that a disadvantage of critical shear stress formulas is that they ignore the effects of lift that may promote particle entrainment. Lift is primarily generated by differences in the velocity of the flow over the top and bottom of an individual particle, a process that creates a vertical pressure gradient leading to the upward motion of the grain (fig. 6.8). Lift may also be created by turbulent eddying generated downstream of the particle that produces locally upward directed flow. The use of critical shear stress in competence studies has been criticized for other reasons as well (Yang 1973), but the simple reality that depth and

b. Grain-Size / Hydraulic Equations - What equations can one plug into?

$T_c = 166 d$	
$D = 0.0001 A^{1.21} S^{-0.57}$	(Knox, 1987)
$V = 0.065 d^{0.5}$	(Williams, 1983)
$V_c = 0.18 d^{0.44}$	(Koster, 1978)
$V_c = 0.18 d^{0.49}$	(Costa, 1983)
$Q_{1.5} = 0.011 L_m^{1.54}$	(Williams, 1983)
$\lambda_m = 166 Q_m^{0.46}$	(Carlston, 1965)
$T = 0.030 d^{1.49}$	(Williams, 1983)
$T = 0.17 d$	(Williams, 1983)
$\omega = 0.079 d^{1.29}$	(Williams, 1983)

Symbols (Williams, 1984)

A = intermediate axis of largest clasts, mm
 d = particle diameter, mm
 D = competent flow depth, m
 λ_m = meander wavelength, m
 $Q_{1.5}$ = discharge of 1.5 yr flood, m³/s
 Q_m = mean annual discharge, m³/s
 S = energy slope (approx. = topo. gradient), m/m
 V = mean flow velocity, m/s
 V_c = threshold (critical) flow velocity, m/s
 T_c = threshold (critical) tractive force, N/m
 T = bed shear stress, N/m
 ω = stream power/m of width, watts/m²

Table 1. Equations to yield entrainment threshold a -axis for boulders [from Hopkins, 1844]

boulder cross section parallel to flow	equation from Hopkins [@]	equation reduced ^{\$} solved for v
<i>terms</i>		
a = streamwise axis of the boulder		
a' = (spheroidal case) the average radius calculated as $= \sqrt{(0.5(a^2+c^2))}$ see note below		
b = axis transverse or perpendicular to flow (all results are independent of this axis)		
c = vertical axis		
v = mean fluid velocity at threshold		
μ = coefficient of friction, $1 = \tan 45^\circ$		
g = acceleration due to gravity		
f = internal angle of the boulder		
g = specific gravity of boulder - Hopkins used 2.5 when missing from equation below		
g' = specific gravity of water (or the fluid in question), taken as 1		
$n = c/a$, except for the spheroidal case when $n = (a/(a-c))$, where $a > c$		
(note: Hopkins uses a and b for the two axes of the spheroid in cross section, but to allow for the b axis transverse to flow we have changed his b to c for consistency with the above.		
<i>triangle</i>	$a = (1-(\mu/\sqrt{3}))(v^2/g)$	$v = 4.82\sqrt{a}$
for the equilateral - inside angle $f = 60$		
when f represents the internal angle of the boulder, then he shows that for sliding to take place that it is required that $\tan f > \mu$. He shows that no triangular section boulder can roll continuously.		
<i>cube</i>	$a = (0.667n)(v^2/g)$	$v = 3.84\sqrt{a}$ - sliding [also found in analysis of Graf, 1979]
where $n = c/a$, and $n = 1$ represents a cubical section.		
For $c=na$ the boulder rolls for $m > 1/n$, and when $c=a$ it rolls if $m > 1$.		
for rolling		
	$a = (0.667/\mu)(v^2/g)$	$v = 0.78\sqrt{a}$ - rolling
<i>pentagon</i>	$a = 0.568(v^2/g)$	$v = 4.24\sqrt{a}$
almost identical equations for either sliding and rolling		
<i>hexagon</i>	$a = 0.57(v^2/g)$	$v = 4.24\sqrt{a}$
almost identical equations for either sliding and rolling		
<i>spheroids*</i>	$a = (n/6)(v^2/g)$ rolling	$v = 4.43\sqrt{a'}$ taking $n = 3$

[@]

we have organised the terms from Hopkins [1844] in a more consistent manner

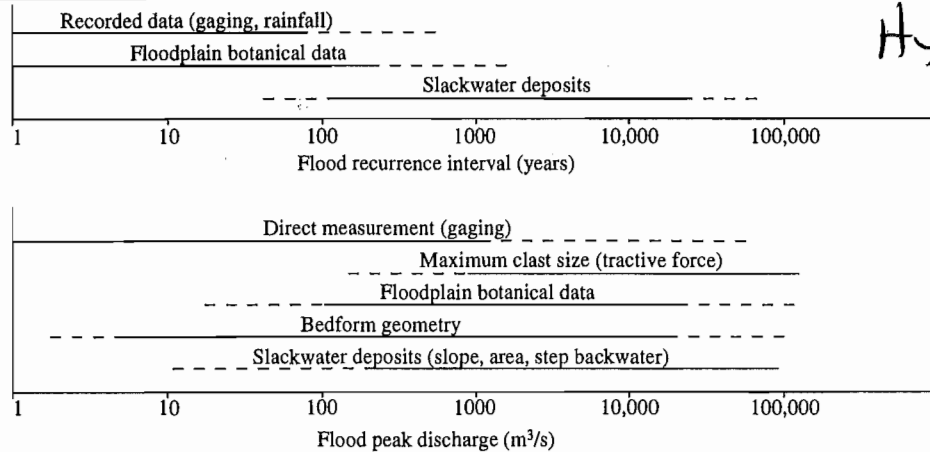
^{\$}we have taken g as 9.81 m s^{-2} and submerged specific gravity as 1.6 t m^3 rather than 1.5.^{*}for spheroids it is assumed that the a axis is not equal to the b axis, and the ratio $n = (a/(a-c))$ acts as an index of shape relative to a sphere.

same 'immovability'. For example, a boulder with a density of 2 g/cm^3 and length of 1 m, has the same I_n value as a boulder with a density of 3 g/cm^3 and 0.5 m length. Interestingly, Butcher and Atkinson dismissed the importance of the coefficient of friction for sliding. They argued instead, that boulders are either stationary, or in unsteady motion owing to turbulence so that true sliding does not effectively occur.

For experimental verification of the theory, different sized boulders with the characteristic length measured in cm and with densities in the range 1.5 g/cm^3 to 4.0 g/cm^3 such that $I_{0.5}$, I_1 etc., were employed in flow models at three different scales to represent entrainment conditions on a full-scale concrete apron. Model results were consistent, demonstrating for example that for the field conditions the full scale value of I needed to be greater than 2, when units

PALEOFLOOD

TABLE 5.6 Common Methods for Estimating Paleofloods.



Hydrology

curves used in highway design. Successful techniques used in the Wyoming study included study of terraces, slackwater deposits, debris lines, dendrogeomorphology, and soils. Table 5.6 provides a summary of common paleoflood techniques and the range of applications.

A tremendous explosion in research related to paleohydrology has occurred since Schumm's (1965) seminal paper focusing attention on the prospects for Quaternary paleohydrologic studies (see, for example, entire books dealing with paleohydrologic studies such as Gregory 1983; Starkel et al. 1991). Paleohydraulic flood reconstructions have been used to gain perspective on the magnitude of some of the most catastrophic flows experienced in the Quaternary record such as the great Missoula floods responsible for carving the Channeled Scablands of eastern Washington (Baker 1973; Baker and Nummedal 1978; O'Connor and Baker 1992) and similar glacial lake-related floods in Siberia (Baker et al. 1993). Similar techniques have been used to detail the hydrology of Pleistocene lakes and breakout floods associated with the midcontinent portion of the Laurentide ice sheet (Kehew and Lord 1986; Lord and Kehew 1987).

Paleohydrological techniques also promise to play a major role in assessing the impact of human modifications on global climate, by facilitating the reconstruction of Holocene hydrologic regimes. Recent research has focused on fluvial responses to climatic change. This work is being done in arid bedrock channels (O'Connor et al. 1994) as well as in alluvial channels in semiarid regions (McQueen et al. 1993) and humid climates (Knox 1993; Patton 1988; Martin 1992). Paleoflood studies have been able to elucidate connections between climate and hydrology (Hirschboeck 1987) as well as the spatial variations in flooding between small basins (Martinez-Goytre et al. 1994). Ely (1997) found significant correlations in the frequency of Holocene paleofloods with climate fluctuations in the American southwest. Knox (1993;

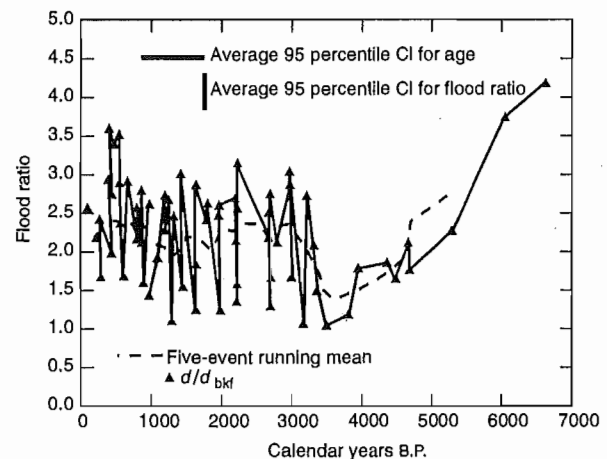


Figure 5.39

Holocene flood variations in the upper Mississippi River basin in response to small variations in climate.

(From Knox 1993)

Knox and Kundzewicz 1997) presented a detailed reconstruction of paleofloods for the upper Mississippi River showing distinctive hydrologic variations during the Holocene. His data indicate that a drier and warmer climate prevailed from 5000 to 3300 B.P. Since then it has been cooler and wetter with more frequent large floods, perhaps similar to the devastating high water experienced in the summer of 1993 (fig. 5.39). Regional and even global correlations are now beginning to appear in paleoflood syntheses (Ely and Baker 1990; O'Connor et al. 1994; Smith 1992; Baker et al. 1995; Gregory et al. 1995; Kale et al. 1997) indicating that these methods may be able to function as useful tools for reconstructing hydroclimatic variations during the Holocene. The apparent correlation of regional paleoflood events with climatic variations should be anticipated because of the

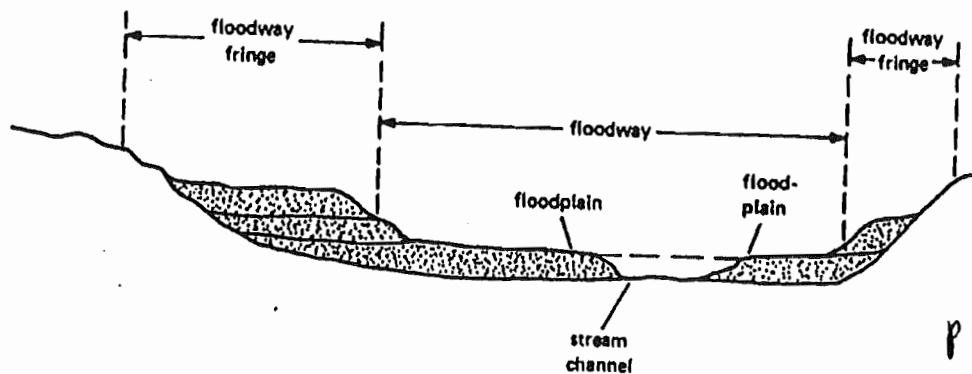


Figure 11.1. View across a river. The floodway is the area along the river which is frequently flooded, an area over which the flood discharge moves with great velocity. The floodway fringe includes areas which are further from the actual channel and which are infrequently flooded by rare events. The floodway fringe is that area flooded by the "100-year" flood.

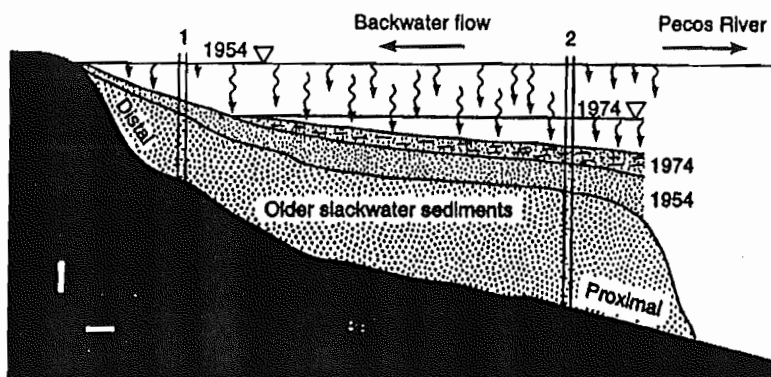


FIGURE 5.37

Schematic of on- and off-lap sequences and peak flood stage in a tributary valley for the 1954 and 1974 floods on the Pecos River, Texas. Sections in the proximal region (area 2) contain both floods, while distal regions (area 1) farther up the tributary record only the larger 1954 flood. Paleostage reconstructions are based on the elevation of the most distal sediments of each flood unit.

(Kochel et al, 1982)

81

81

STREAM CLASSIFICATION

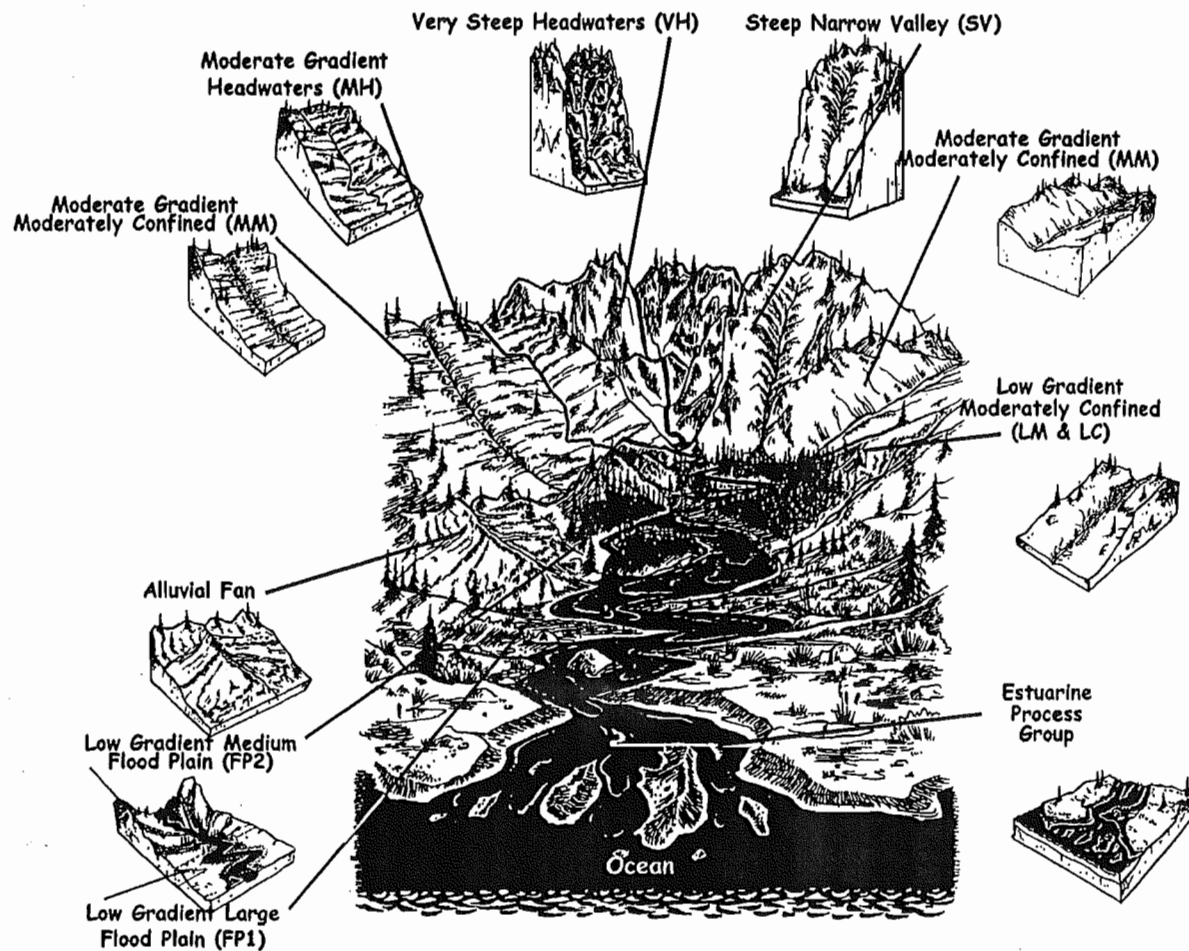


Figure 5. Typical distribution of CHTs in a mountainous watershed.

provides a framework and mechanism for evaluating (1) basin-wide stream channel conditions, (2) the influences of land management activities on specific stream reaches, and (3) potential restoration opportunities.

The Historical Conditions Assessment component provides a methodology for obtaining and interpreting historical material to identify where potential impacts may have occurred, and to

See Historical Conditions and Channel Modification components to map human impacts to the stream channels.

describe what the watershed may have looked like before human activities. The Channel Modification Assessment component systematically determines how the channels in the watershed have been modified by various human uses. Often, it is hard to separate impacts resulting from current, ongoing land and water management activities from

historical or *legacy activities*. For that reason, knowledge of past use can provide a context to help us understand the current condition of a watershed.

p. 64 NOTES

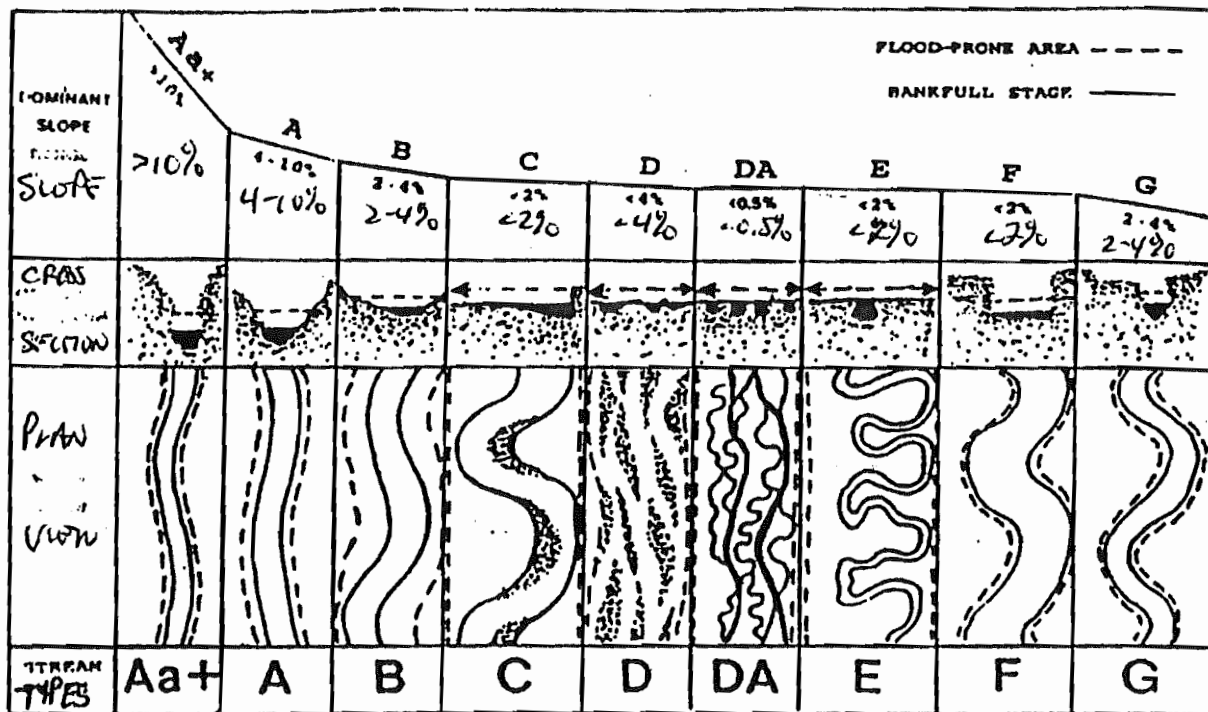


Fig. 2. Longitudinal, cross-sectional and plan views of major stream types.

Rosen, 1994

Table 2
Summary of delineative criteria for broad-level classification

Stream type	General description	Entrenchment ratio	W/D ratio	Sinuosity	Slope	Landform soils features
Aa +	Very steep, deeply entrenched, debris transport streams.	< 1.4	< 12	1.0 to 1.1	> 0.10	Very high relief. Erosional, bedrock or depositional features; debris flow potential. Deeply entrenched streams. Vertical steps with deep scour pools; waterfalls.
A	Steep, entrenched, cascading, step pool streams. High energy/debris transport associated with depositional soils. Very stable if bedrock or boulder dominated channel.	< 1.4	< 12	1.0 to 1.2	0.04 to 0.10	High relief. Erosional or depositional and bedrock forms. Entrenched and confined streams with cascading reaches. Frequently spaced, deep pools in associated step-pool bed morphology.
B	Moderately entrenched, moderate gradient, riffle dominated channel, with infrequently spaced pools. Very stable plan and profile. Stable banks.	1.4 to 2.2	> 12	> 1.2	0.02 to 0.039	Moderate relief, colluvial deposition and or residual soils. Moderate entrenchment and W/D ratio. Narrow, gently sloping valleys. Rapids predominate with occasional pools.
C	Low gradient, meandering, point-bar, riffle-pool, alluvial channels with broad, well defined floodplains	> 2.2	> 12	> 1.4	< 0.02	Broad valleys with terraces, in association with floodplains, alluvial soils. Slightly entrenched with well-defined meandering channel. Riffle-pool bed morphology.
D	Braided channel with longitudinal and transverse bars. Very wide channel with eroding banks.	n/a	> 40	n/a	< 0.04	Broad valleys with alluvial and colluvial fans. Glacial debris and depositional features. Active lateral adjustment, with abundance of sediment supply.
DA	Anastomosing (multiple channels) narrow and deep with expansive well vegetated floodplain and associated wetlands. Very gentle relief with highly variable sinuosities. Stable streambanks.	> 4.0	< 40	variable	< 0.005	Broad, low-gradient valleys with fine alluvium and/or lacustrine soils. Anastomosed (multiple channel) geologic control creating fine deposition with well-vegetated bars that are laterally stable with broad wetland floodplains.
E	Low gradient, meandering riffle pool stream with low width depth ratio and little deposition. Very efficient and stable. High meander width ratio.	> 2.2	< 12	> 1.5	< 0.02	Broad valley meadows. Alluvial materials with floodplain. Highly sinuous with stable, well vegetated banks. Riffle-pool morphology with very low width depth ratio.
F	Entrenched meandering riffle pool channel on low gradients with high width depth ratio.	< 1.4	> 12	> 1.4	< 0.02	Entrenched in highly weathered material. Gentle gradients, with a high W/D ratio. Meandering, laterally unstable with high bank-erosion rates. Riffle-pool morphology.
G	Entrenched "gully" step pool and low width depth ratio on moderate gradients.	< 1.4	< 12	> 1.2	0.02 to 0.039	Gully, step-pool morphology with moderate slopes and low W/D ratio. Narrow valleys, or deeply incised in alluvial or colluvial materials; i.e., fans or deltas. Unstable, with grade control problems and high bank erosion rates.

92

TABLE 1. DIAGNOSTIC FEATURES OF EACH CHANNEL TYPE

	Dune ripple	Pool riffle	Plane bed	Step pool	Cascade	Bedrock	Colluvial
Typical bed material	Sand	Gravel	Gravel-cobble	Cobble-boulder	Boulder	Rock	Variable
Bedform pattern	Multilayered	Laterally oscillatory	Featureless	Vertically oscillatory	Random	Irregular	Variable
Dominant roughness elements	Sinuosity, bedforms (dunes, ripples, bars) grains, banks	Bedforms (bars, pools), grains, sinuosity, banks	Grains, banks	Bedforms (steps, pools), grains, banks	Grains, banks	Boundaries (bed and banks)	Grains
Dominant sediment sources	Fluvial, bank failure	Fluvial, bank failure	Fluvial, bank failure, debris flows	Fluvial, hillslope, debris flows	Fluvial, hillslope, debris flows	Fluvial, hillslope, debris flows	Hillslope, debris flows
Sediment storage elements	Overbank, bedforms	Overbank, bedforms	Overbank	Bedforms	Lee and stoss sides of flow obstructions	Pockets	Bed
Typical confinement	Unconfined	Unconfined	Variable	Confined	Confined	Confined	Confined
Typical pool spacing (channel widths)	5 to 7	5 to 7	None	1 to 4	<1	Variable	Unknown

We recognize three primary channel-reach substrates: bedrock, alluvium, and colluvium. Bedrock reaches lack a contiguous alluvial bed and reflect high transport capacities relative to sediment supply; they are typically confined by valley walls and have steep slopes. In contrast, alluvial channels exhibit a wide variety of morphologies and roughness configurations that vary with slope and position within the channel network, and may be either confined, with little to no associated flood plain, or unconfined, with a well-established flood plain. We recognize five distinct alluvial reach morphologies: cascade, step pool, plane bed, pool riffle, and dune ripple. Colluvial channels form an additional reach type that we recognize separately from alluvial channels, despite the common presence of a thin alluvial substrate. Colluvial channels typically are small headwater streams that flow over a colluvial valley fill and exhibit weak or ephemeral fluvial transport. Each of these channel types is distinguished by a distinctive channel-bed morphology, allowing rapid visual classification. Diagnostic features of each channel type are summarized in Table 1 and discussed below.

Cascade Channels

The term "cascade" connotes tumbling flow, although its specific morphologic definition varies and often is applied to both channel units and reaches (e.g., Bisson et al., 1982; Grant et al., 1990). Our delineation of cascade channels focuses on streams in which energy dissipation is dominated by continuous tumbling and jet-and-wake flow over and around individual large clasts (e.g., Peterson and Mohanty, 1960) (Fig. 1A). Cascade channels generally occur on steep slopes, are narrowly confined by valley walls, and are characterized by longitudinally and laterally disorganized bed material typically consisting of cobbles and boulders (Fig. 2A). Small, partially channel-spanning pools spaced less than a channel width apart are common in cascade channels. Tumbling flow over individual grain steps and turbulence associated with jet-and-wake flow around grains dissipates much of the mechanical energy of the flow (Fig. 3A).

Large particle size relative to flow depth makes the largest bed-forming material of cascade reaches effectively immobile during typical flows. Studies of steep-gradient channels report that large bed-forming grains typically become mobile only during infrequent (i.e., 50–100 yr) hydrologic events (Grant et al., 1990; Kondolf et al., 1991; Whittaker, 1987b). Mobilization of these larger clasts is accompanied by high sediment transport rates due to the release of finer sediment trapped under and around large grains (Sawada et al., 1983; Warburton, 1992). During lesser floods, gravel stored in low energy sites is mobilized and travels as bedload over larger bed-forming clasts (Griffiths, 1980; Schmidt and Ergenzinger, 1992). Gravel and finer material

are locally stored on stoss and lee sides of flow obstructions (i.e., large grains and large woody debris) due to physical impoundment and generation of velocity shadows. One tracer study (Kondolf et al., 1991) showed that material in such depositional sites was completely mobilized during a seven-year recurrence-interval event, whereas no tracer movement was observed during flows of less than the annual recurrence interval.

These observations suggest that there are two thresholds for sediment transport in cascade channels. During moderate recurrence-interval flows, bedload material is rapidly and efficiently transported over the more stable bed-forming clasts, which have a higher mobility threshold corresponding to more infrequent events. The lack of significant in-channel storage (Kondolf et al., 1991) and the rapid scour of depositional sites during moderately frequent high flows suggest that sediment transport is effectively supply limited in cascade channels. Bedload transport studies demonstrate that steep channels in mountain drainage basins are typically supply limited, receiving seasonal or stochastic sediment inputs (Nanson, 1974; Griffiths, 1980; Ashida et al., 1981; Whittaker, 1987). Because of this high transport capacity relative to sediment supply, cascade channels function primarily as sediment transport zones that rapidly deliver sediment to lower-gradient channels.

Step-Pool Channels

Step-pool channels are characterized by longitudinal steps formed by large clasts organized into discrete channel-spanning accumulations that separate pools containing finer material (Figs. 1B and 2B) (Ashida et al., 1976, 1981; Griffiths, 1980; Whittaker and Jaeggi, 1982; Whittaker and Davies, 1982; Whittaker, 1987a, 1987b; Chin, 1989; Grant et al., 1990). Primary flow and channel bed oscillations in step-pool reaches are vertical, rather than lateral, as in pool-riffle channels (Fig. 3B). The stepped morphology of the bed results in alternating critical to supercritical flow over steps and subcritical flow in pools (Bowman, 1977; Chin, 1989). Step-pool channels exhibit a pool spacing of roughly one to four channel widths (Bowman, 1977; Whittaker, 1987b; Chin, 1989; Grant et al., 1990), significantly less than the five to seven channel widths that typify self-formed pool-riffle channels (Leopold et al., 1964; Keller and Melhorn, 1978). Steps provide much of the elevation drop and roughness in step-pool channels (Ashida et al., 1976; Whittaker and Jaeggi, 1982; Whittaker, 1987a, 1987b; Chin, 1989). Step-pool morphology generally is associated with steep gradients, small width to depth ratios, and pronounced confinement by valley walls. Although step-forming clast sizes typically are comparable to annual high flow depths, a stepped longitudinal profile also may develop in steep sand-bedded channels (G. E. Grant, 1996, personal commun.).

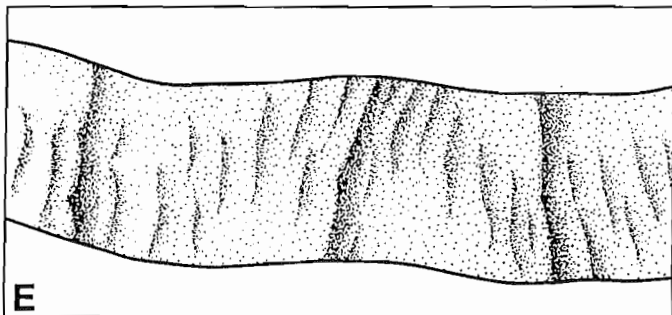
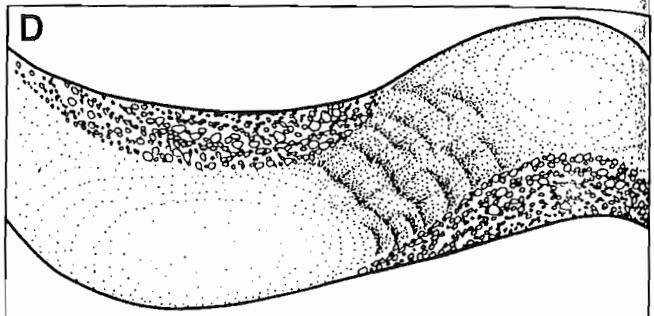
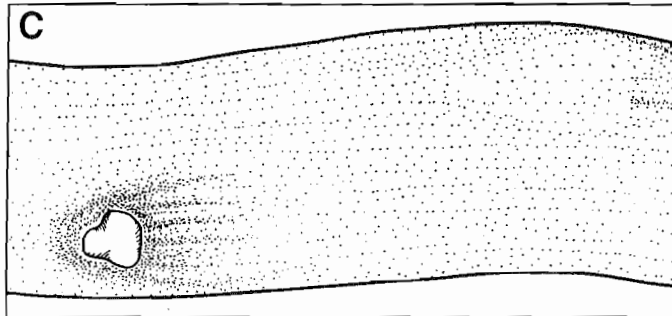
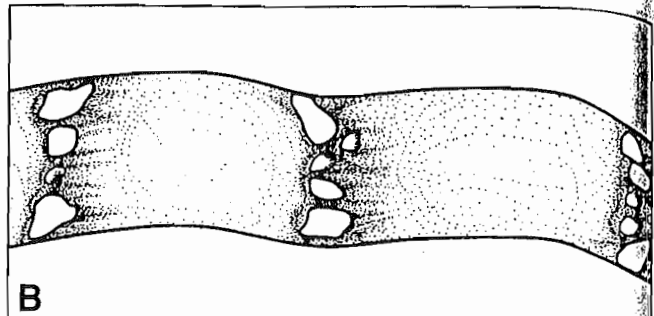
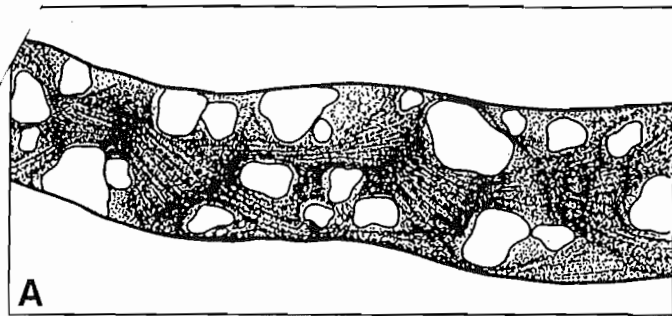


Figure 2. Schematic planform illustration of alluvial channel morphologies at low flow: (A) cascade channel showing nearly continuous, highly turbulent flow around large grains; (B) step-pool channel showing sequential highly turbulent flow over steps and more tranquil flow through intervening pools; (C) plane-bed channel showing single boulder protruding through otherwise uniform flow; (D) pool-riffle channel showing exposed bars, highly turbulent flow through riffles, and more tranquil flow through pools; and (E) dune-ripple channel showing dune and ripple forms as viewed through the flow.

density and organization of large clasts. Step-pool channels are defined by discrete channel-spanning steps less than a channel width in length that separate pools spaced every one to four channel widths. Cascade channels are defined by ubiquitous tumbling and jet-and-wake flow over a series of individual large clasts that together exceed a channel width in length, with small, irregularly placed pools spaced less than a channel width apart. The regular sequence of pools and steps in step-pool channels probably represents the emergence of a fluvially organized morphology in alluvial channels. In contrast, the disorganized large clasts of cascade channels may include lag deposits forced by nonfluvial processes (e.g., debris flows, glaciers, and rock falls).

Plane-Bed Channels

The term "plane bed" has been applied to both planar bed phases observed to form in sand-bed channels (Simons et al., 1965) and planar gravel and cobble-bed channels (Florsheim, 1985) like the coarse-grained, threshold canals described by Lane and Carlson (1953). Our use of the term refers to the latter and encompasses glide (run), riffle, and rapid morphologies described in the fisheries literature (e.g., Bisson et al., 1982). Plane-bed channels lack discrete bars, a condition that is associated with low width to depth ratios (Sukegawa, 1973; Ikeda, 1975, 1977) and large values of relative

roughness (ratio of 90th percentile grain size to bankfull flow depth). Church and Jones (1982) considered bar formation unlikely at relative roughnesses of 0.3 to 1.0. Plane-bed reaches occur at moderate to high slopes in relatively straight channels that may be either unconfined or confined by valley walls. They typically are composed of sand to small boulder grain sizes, but are dominantly gravel to cobble bedded.

Plane-bed channels differ morphologically from both step-pool and pool-riffle channels in that they lack rhythmic bedforms and are characterized by long stretches of relatively featureless bed (Figs. 1C and 2C). The absence of tumbling flow and smaller relative roughness distinguish plane-bed reaches from cascade and step-pool channels (Fig. 3C). Plane-bed channels lack sufficient lateral flow convergence to develop pool-riffle morphology due to lower width to depth ratios and greater relative roughness, which may decompose lateral flow into smaller circulation cells. However, introduction of flow obstructions may force local pool and bar formation.

Plane-bed channels typically exhibit armored bed surfaces calculated to have a near-bankfull threshold for mobility, although elevated sediment loading can cause textural fining and a lower calculated mobility threshold (Buffington, 1995). Plane-bed channels with armored bed surfaces indicate a transport capacity greater than sediment supply (i.e., supply-limited conditions), whereas unarmored surfaces indicate a balance between transport capacity and sediment supply (Dietrich et al., 1989). Nevertheless, beyond

Figure 3. Schematic planform illustration of alluvial channel morphologies at low flow: (A) cascade channel; (B) step-pool channel; (C) plane-bed channel; (D) pool-riffle channel; and (E) dune-ripple channel.

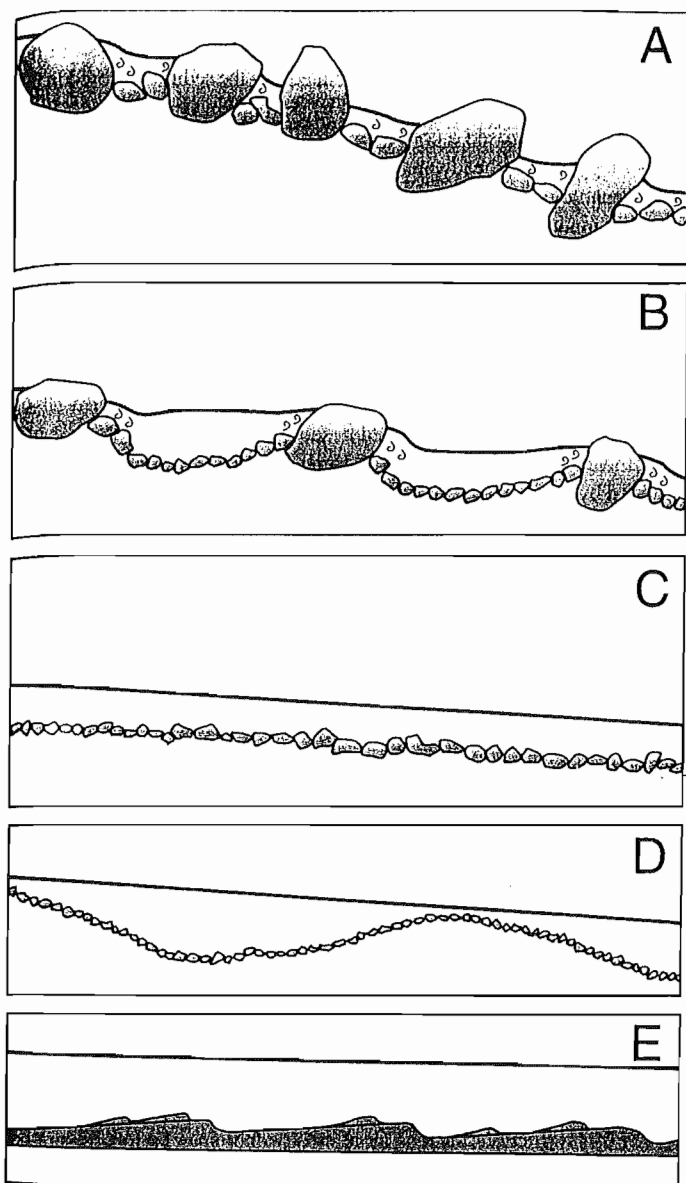


Figure 3. Schematic longitudinal profiles of alluvial channel morphologies at low flow: (A) cascade; (B) step pool; (C) plane bed; (D) pool riffle; and (E) dune ripple.

the threshold for significant bed-surface mobility, many armored gravel-bedded channels exhibit a general correspondence between bedload transport rate and discharge (e.g., Milhous, 1973; Jackson and Beschta, 1982; Sidle, 1988), implying transport-limited conditions. The above observations suggest that plane-bed channels are transitional between supply- and transport-limited morphologies.

Pool-Riffle Channels

Pool-riffle channels have an undulating bed that defines a sequence of bars, pools, and riffles (Leopold et al., 1964) (Fig. 1D). This lateral bedform oscillation distinguishes pool-riffle channels from the other channel types discussed above (Fig. 2D). Pools are topographic depressions within the channel and bars are corresponding high points (Fig. 3D); these bedforms

are thus defined relative to each other (O'Neill and Abrahams, 1984). Pools are rhythmically spaced about every five to seven channel widths in self-formed, pool-riffle channels (Leopold et al., 1964; Keller and Mellhorn, 1978), but channels with a high loading of large woody debris exhibit smaller pool spacing (Montgomery et al., 1995). Pool-riffle channels occur at moderate to low gradients and are generally unconfined, and have well-established flood plains. Substrate size in pool-riffle streams varies from sand to cobble, but typically is gravel sized.

Bar and pool topography generated by local flow convergence and divergence may be either freely formed by cross-stream flow and sediment transport, or forced by channel bends and obstructions (e.g., Lisle, 1986). Free-formed pool-riffle sequences initially result from internal flow perturbation that causes flow convergence and scour on alternating banks of the channel; concordant downstream flow divergence results in local sediment accumulation in discrete bars. Topographically driven convective accelerations reinforce convergent and divergent flow patterns, and thus pool-riffle morphogenesis (Dietrich and Smith, 1983; Dietrich and Whiting, 1989; Nelson and Smith, 1989). Alluvial bar development requires a sufficiently large width to depth ratio and small grain sizes that are easily mobilized and stacked by the flow (Church and Jones, 1982). Bar formation in natural channels appears to be limited to gradients ≤ 0.02 (Ikeda, 1977; Florsheim, 1985), although flume studies indicate that alternate bars may form at steeper gradients (Bathurst et al., 1983; Lisle et al., 1991). Bedform and grain roughness provide the primary flow resistance in free-formed pool-riffle channels.

Pool-riffle channels have heterogeneous beds that exhibit a variety of sorting and packing, commonly with a coarse surface layer and a finer subsurface (Leopold et al., 1964; Milhous, 1973). Armored gravel-bed channels typically exhibit a near-bankfull threshold for general and significant bed-surface mobility (e.g., Parker et al., 1982; Jackson and Beschta, 1982; Andrews, 1984; Carling, 1988; Buffington, 1995). Movement of surface grains releases fine sediment trapped by larger grains and exposes finer subsurface sediment to the flow, contributing to a steep rise in bedload transport with increasing shear stress (Milhous, 1973; Jackson and Beschta, 1982; Emmett, 1984). Bed movement is sporadic and discontinuous, depending on grain protrusion (Fenton and Abbott, 1977; Kirchner et al., 1990), friction angle (Kirchner et al., 1990; Buffington et al., 1992), imbrication (Komar and Li, 1986), degree of burial (Hammond et al., 1984; Buffington et al., 1992), and turbulent high-velocity sweeps of the channel bed. Very rarely is the whole bed in motion, and material eroded from one riffle commonly is deposited on a proximal downstream riffle.

Pool-riffle channels, like plane-bed channels, exhibit a mixture of supply- and transport-limited characteristics depending on the degree of bed-surface armoring and consequent mobility thresholds. Unarmored pool-riffle channels indicate a balance between transport capacity and sediment supply, while armored surfaces represent supply-limited conditions (e.g., Dietrich et al., 1989). Nevertheless, during armor-breaching events, bedload transport rates are generally correlated with discharge, demonstrating that sediment transport is not limited by supply once the bed is mobilized. Considerable fluctuations in observed transport rates, however, reflect a stochastic component of grain mobility caused by grain interactions, turbulent sweeps, and transient grain entrapment by bedforms (Jackson and Beschta, 1982; Sidle, 1988). Magnitudes of bedload transport also may vary for similar discharge events, depending on the chronology of antecedent transport events (Milhous, 1973; Reid et al., 1985; Sidle, 1988). Although both pool-riffle and plane-bed channels display a mix of supply- and transport-limited characteristics, the presence of depositional barforms in pool-riffle channels suggests that they are generally more transport limited than plane-bed channels. The transport-limited character of both of these morphologies, however, contrasts with the more supply-limited character of step-pool and cascade channels.

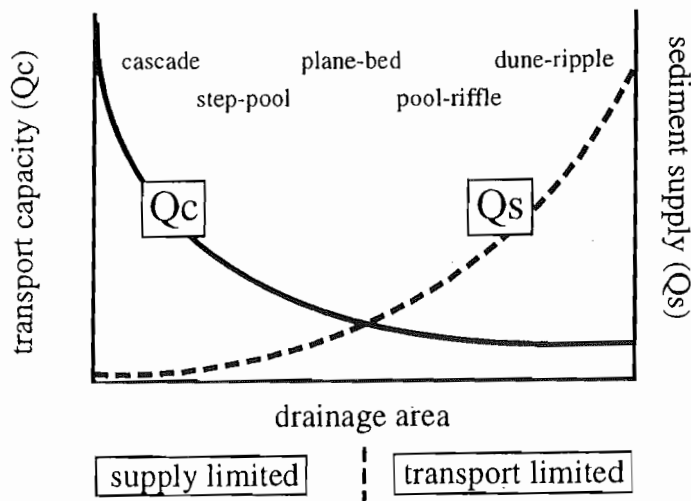


Figure 10. Schematic illustration of generalized relative trends in sediment supply (Q_s) and transport capacity (Q_c) in mountain drainage basins.

indicated by the accumulation of colluvium within valley bottoms. In contrast, the lack of an alluvial bed indicates that bedrock channels are supply limited ($q_r \gg 1$). For a given drainage area (and thus Q_s), bedrock reaches have greater slopes and shear stresses (Figs. 5 and 9), implying that they have higher transport capacities and thus greater q_r values than other channel types. Alluvial channels, however, probably represent a broad range of q_r : steep alluvial channels (cascade and step-pool) have higher shear stresses (Fig. 9) and thus higher Q_c and q_r values for a given drainage area and sediment supply; the lower-gradient plane-bed and pool-riffle channels are transitional between $q_r > 1$ and $q_r \approx 1$, depending on the degree of armoring (e.g., Dietrich et al., 1989) and the frequency of bed-surface mobility; and the live-bed mobility of dune-ripple channels indicates that $q_r \leq 1$. The variety of alluvial channel morphologies probably reflects a broad spectrum of q_r expressed through fining and organization of the bedload (Fig. 11), which leads to formation of distinct alluvial bed morphologies that represent the stable bed form for the imposed q_r . This hypothesized relation between q_r and stable channel morphologies in mountain drainage basins provides a genetic framework for explaining reach-level morphologies that elaborates on Lindley's (1919) regime concept. An alluvial channel with $q_r > 1$ will become stable when the bed morphology and consequent hydraulic roughness

produce an effective transport capacity that matches the sediment supply ($Q_c' \approx Q_s$).

Different channel types are stabilized by different roughness configurations that provide resistance to flow. In steep channels energy is dissipated primarily by hydraulic jumps and jet-and-wake turbulence. This style of energy dissipation is pervasive in cascade channels and periodic in step-pool channels. Skin friction and local turbulence associated with moderate particle sizes are sufficient to stabilize the bed for lower shear stresses characteristic of plane-bed channels. In pool-riffle channels, skin friction and bedform drag dominate energy dissipation. Particle roughness in dune-ripple channels is small due to the low relative roughness, and bedforms govern hydraulic resistance. The importance of bank roughness varies with channel type, depending on the width to depth ratio and vegetative influence, but in steep channels bank resistance is less important compared to energy dissipation caused by tumbling flow. These different roughness configurations represent a range in q_r values that varies from high in cascade reaches to low in dune-ripple channels.

Our hypothesis that different channel types represent stable roughness configurations for different q_r values implies that there should be an association of channel type and roughness. Even though the general correlation of morphology and slope (Fig. 6) implies discrete roughness characteristics among channel types, different channel morphologies occurring on the same slope should exhibit distinct roughness. Photographs and descriptions of channel morphology from previous studies in which roughness was determined from measured velocities (Barnes, 1967; Marcus et al., 1992) and a low direct assessment of the roughness associated with different channel types. For similar slopes, plane-bed channels exhibit greater roughness than pool-riffle channels, and step-pool channels, in turn, appear to have greater roughness than plane-bed channels with comparable gradients (Fig. 12). Moreover, intermediate morphology reaches plot between their defining channel types. These systematic trends in roughness for a given slope strongly support the hypothesis that reach-level channel morphology reflects a dynamic adjustment of the bed surface to the imposed shear stress and sediment supply (i.e., the specific q_r value).

CHANNEL DISTURBANCE AND RESPONSE POTENTIAL

Natural and anthropogenic disturbances that change hydrology, sediment supply, riparian vegetation, or large woody debris loading can alter channel processes and morphology. The effect that watershed disturbance has on a particular channel reach depends on hillslope and channel coupling, the sequence of upstream channel types, and site-specific channel morphology. In particular, the variety and magnitude of possible morphologic responses to

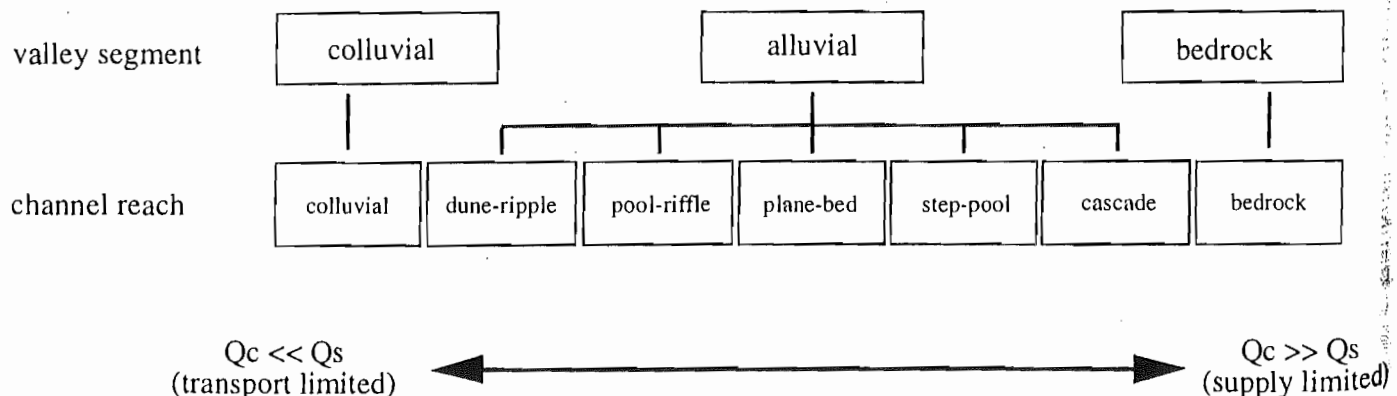


Figure 11. Schematic illustration of the transport capacities relative to sediment supply for reach-level channel types.

Figure 12. Photographs of channel types and descriptions of channel morphology from previous studies in which roughness was determined from measured velocities (Barnes, 1967; Marcus et al., 1992) and a low direct assessment of the roughness associated with different channel types. For similar slopes, plane-bed channels exhibit greater roughness than pool-riffle channels, and step-pool channels, in turn, appear to have greater roughness than plane-bed channels with comparable gradients (Fig. 12). Moreover, intermediate morphology reaches plot between their defining channel types. These systematic trends in roughness for a given slope strongly support the hypothesis that reach-level channel morphology reflects a dynamic adjustment of the bed surface to the imposed shear stress and sediment supply (i.e., the specific q_r value).

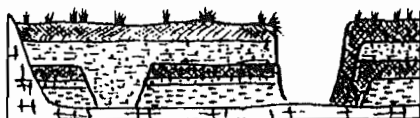
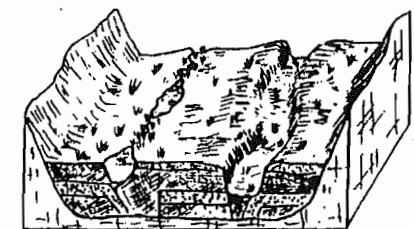
Figure 12. Photographs of channel types and descriptions of channel morphology from previous studies in which roughness was determined from measured velocities (Barnes, 1967; Marcus et al., 1992) and a low direct assessment of the roughness associated with different channel types. For similar slopes, plane-bed channels exhibit greater roughness than pool-riffle channels, and step-pool channels, in turn, appear to have greater roughness than plane-bed channels with comparable gradients (Fig. 12). Moreover, intermediate morphology reaches plot between their defining channel types. These systematic trends in roughness for a given slope strongly support the hypothesis that reach-level channel morphology reflects a dynamic adjustment of the bed surface to the imposed shear stress and sediment supply (i.e., the specific q_r value).

Figure 12. Photographs of channel types and descriptions of channel morphology from previous studies in which roughness was determined from measured velocities (Barnes, 1967; Marcus et al., 1992) and a low direct assessment of the roughness associated with different channel types. For similar slopes, plane-bed channels exhibit greater roughness than pool-riffle channels, and step-pool channels, in turn, appear to have greater roughness than plane-bed channels with comparable gradients (Fig. 12). Moreover, intermediate morphology reaches plot between their defining channel types. These systematic trends in roughness for a given slope strongly support the hypothesis that reach-level channel morphology reflects a dynamic adjustment of the bed surface to the imposed shear stress and sediment supply (i.e., the specific q_r value).

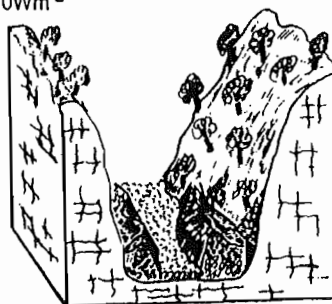
Figure 12. Photographs of channel types and descriptions of channel morphology from previous studies in which roughness was determined from measured velocities (Barnes, 1967; Marcus et al., 1992) and a low direct assessment of the roughness associated with different channel types. For similar slopes, plane-bed channels exhibit greater roughness than pool-riffle channels, and step-pool channels, in turn, appear to have greater roughness than plane-bed channels with comparable gradients (Fig. 12). Moreover, intermediate morphology reaches plot between their defining channel types. These systematic trends in roughness for a given slope strongly support the hypothesis that reach-level channel morphology reflects a dynamic adjustment of the bed surface to the imposed shear stress and sediment supply (i.e., the specific q_r value).

Fluvial LAND FORMS

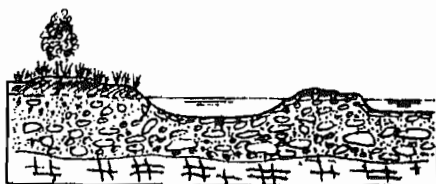
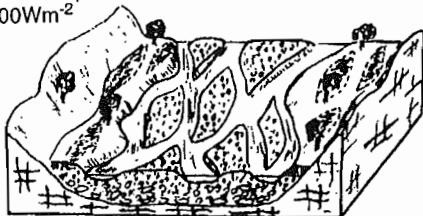
(A) Cut and fill floodplain
 $\omega = \sim 300 \text{Wm}^{-2}$



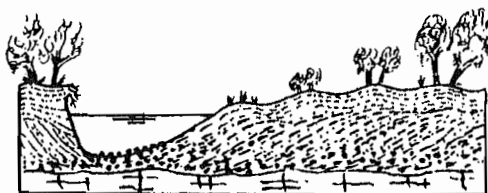
Confined coarse-textured
floodplain
 $\omega = > 1000 \text{Wm}^{-2}$



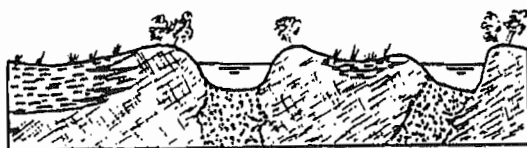
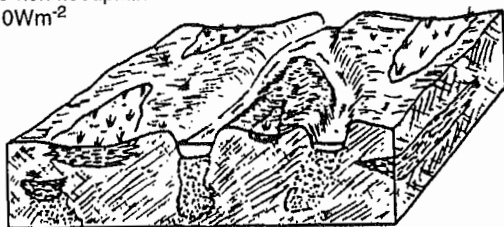
(B) Braided river floodplain
 $\omega = 50-300 \text{Wm}^{-2}$



Lateral migration, scrolled floodplain
 $\omega = 10-60 \text{Wm}^{-2}$



(C) Anastomosing river,
organic-rich floodplain
 $\omega = < 10 \text{Wm}^{-2}$



Anastomosing river,
inorganic floodplain
 $\omega = < 10 \text{Wm}^{-2}$

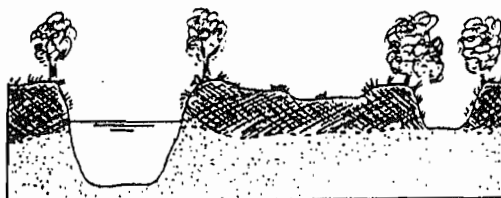
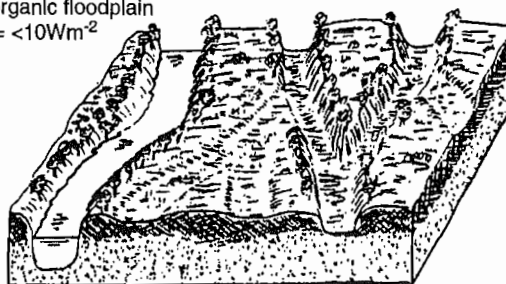


Figure 7.1

Examples of floodplain types in the classification of genetic floodplains. (A) High energy, noncohesive; (B) Medium energy, noncohesive; (C) High energy, noncohesive. (After Nanson and Croke 1992.)

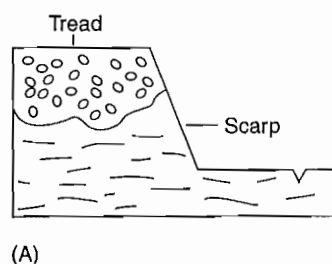
(Figures 1-3 from pp. 471, 474, 478 by Nanson and Croke in GEOMORPHOLOGY, Vol. 4, pp. 459-486. Copyright © 1992. Reprinted by permission of Elsevier Science.)

by simultaneous processes of lateral migration and overbank flooding. The deposits of lateral accretion are spread in a rather even sheet across the valley bottom, whereas overbank deposits accumulate over the entire floodplain surface away from the channel. The floodplain acts as a storage area for sediment that cannot be transported directly from the basin when it is eroded. In arid climates, floodplain development is more complex and may not manifest a process-form equilibrium between river flow and the feature. In many cases overbank flows are rare or absent. Braided rivers tend to shift laterally without the undercut banks and point bar phenomena so common in humid-climate meandering patterns. Abandoned channels and islands occupy much of the valley bottom, and these are also subject to periodic shifts of position.

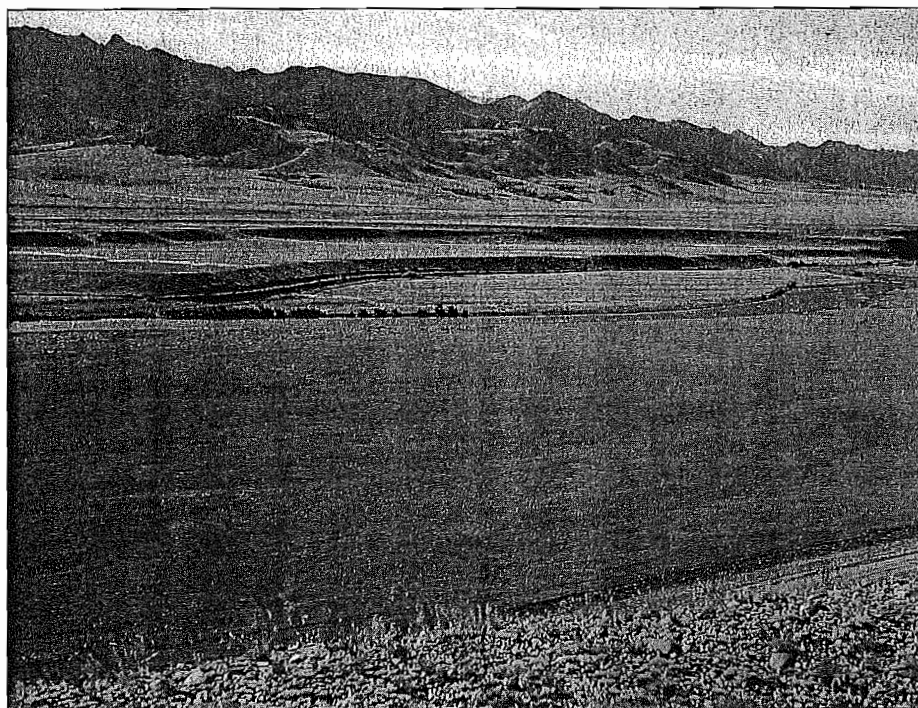
Floodplains are usually considered to be associated with stable rivers, but there is no overriding reason why they cannot be present when a channel is undergoing long-term aggradation or degradation. In fact, the observed frequency of overbank flooding can continue during valley filling if the channel floor and the floodplain surface are raised at the same rate. Once the thickness of the valley deposits exceeds the limits of a reasonable scouring depth, however, the sediment below that depth can no longer be considered part of the active floodplain. In a degrading channel, the floodplain becomes a terrace when channel incision prevents the river from inundating the surface on a regular and frequent basis.

FLUVIAL TERRACES

Terraces are abandoned floodplains that were formed when the river flowed at a higher level than at present. Topographically, a terrace consists of two parts: a **tread**, which is the flat surface representing the level of the former floodplain, and the **scarp**, which is the steep slope connecting the tread to any surface standing lower in the valley (fig. 7.10). The surface of a terrace is no longer inundated as frequently as a normal, active floodplain. It is important to remember, however, that floodplain surfaces elevated by vertical accretion also have a low frequency of inundation. Thus, it may be problematic to define a floodplain (and by contrast, a terrace) on the basis of the recurrence interval of overbank flow. Most geomorphologists would recognize a surface constructed by continuous vertical accretion as a floodplain; that is, the surface and the river are still hydrologically related even though overbank flow rarely occurs. For our purposes then, the distinguishing factor in terrace formation is that the river channel floor associated with the abandoned floodplain surface (tread) must have previously been at a higher level. In fact, the presence of a terrace demands an episode of downcutting (channel entrenchment), and indicates that some significant change must have occurred between the conditions that prevailed during development of the tread and those that produced the scarp. Usually the downcutting phase begins as a response to climatic or tectonic changes, but these are not always necessary. The tread surface normally is under-



(A)



(B)

Figure 7.10

(A) Parts of a fluvial terrace.

(B) Terraces along the Madison River upstream from Ennis, Mont.

lain by alluvium of variable thickness, but these deposits are not a true part of the terrace. To avoid confusion, it is better to limit the term to the topographic form and refer to the deposits as fill, alluvium, gravel, and so on.

Types and Classification

In general, terraces are broadly categorized as erosional or depositional. **Erosional terraces** are those in which the tread has been formed primarily by lateral erosion. If the lateral erosion truncates bedrock, the terms *bench*, *strath*, or *rock-cut terrace* are commonly used. If the erosion crosses unconsolidated debris, the terms *fill-cut* or *fillstrath* may be used. **Depositional terraces**, the second major grouping, are terraces where the tread represents the surface of a valley fill. Figure 7.11 illustrates both types.

Erosional terraces, especially rock-cut types, are identifiable by the following, rather distinct, properties (Mackin 1937): (1) they are capped by a uniformly thin layer of alluvium in which the total thickness is controlled by the scouring depth of the river involved, and (2) the surface cut on the bedrock or older alluvium is a flat mirror image of the surface on top of the capping alluvium. In contrast, the alluvium beneath the tread of depositional terraces varies in thickness and commonly exceeds any reasonable scouring depth of the associated river. Although the tread surface may be flat, the surface beneath the fill can be very irregular.

The classification of terraces as erosional or depositional is clearly a genetic distinction, and must be supported by evidence of the formative processes. Bull (1990) refines this approach by suggesting that major erosional terraces (straths) are the fundamental tectonic stream-terrace landform; that is, major straths are tectonically controlled. In contrast, terrace treads resulting from significant depositional events are the fundamental climatic stream-terrace landform; they are related to climatically controlled aggradation.

Another classification scheme is based on the topographic relationship between terrace levels within a given valley, as illustrated in figure 7.12. In this method, terrace treads that stand at the same elevation on both sides of the valley are called **paired (matched) terraces** and presumably are the same age. If the levels are staggered across the valley, they are said to be **unpaired (unmatched) terraces**. Most investigators interpret unpaired terraces as erosional types formed by a stream simultaneously cutting laterally and downcutting very slowly. Levels across the valley, therefore, are not exactly equivalent in age but differ by the amount of time needed for the river to traverse the valley bottom.

The Origin of Terraces

Depositional Terraces The development of a depositional terrace always requires a period of valley filling and subsequent entrenchment into or adjacent to the fill. This cyclic pattern is necessary because the alluvium at the tread surface takes its form from purely depositional processes. The tread, in fact, represents the highest level attained by the valley floor as it rose during aggradation. The initial entrenchment that forms the terrace scarp is primarily vertical, and so the tread surface is virtually unaffected by subsequent lateral erosion at a lower level (see fig. 7.11).

Valley filling occurs when, over an extended period, the amount of sediment produced in a basin exceeds the amount that the river system can carry away. Prolonged aggradation is usually triggered by (1) glacial outwash, (2) climate change, or (3) changes in base level, slope, or load caused by rising sea level, rising local or regional base level, or an influx of coarse load because of uplift in source areas. Where tectonics are ruled out, the balance between load and discharge is determined primarily by climatic processes, although it may be driven by glaciation and may be complexly interrelated with sea level changes. Although entrenchment has been considered

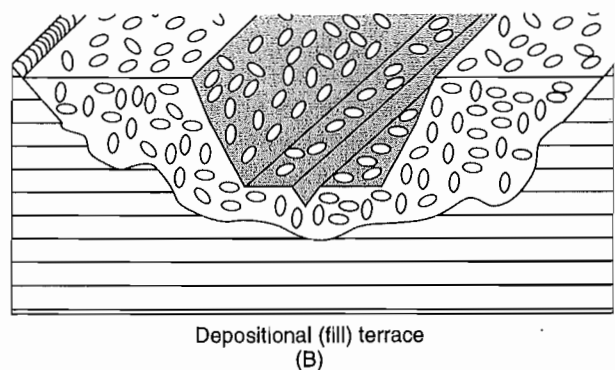
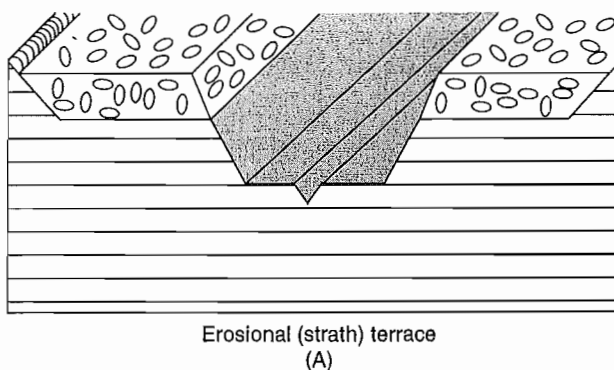


Figure 7.11

(A) Erosional (strath) terrace. Thin alluvial cover with truncation of underlying bedrock along smooth, even surface.

(B) Depositional (fill) terrace. Terrace scarp underlain by alluvium that is highest level of fill deposited in valley. Note thickness of alluvium and irregular bedrock surface beneath the fill.

100

92

RIVER INCISION, EROSION, KNICKPOINTS

HANCOCK, ANDERSON, AND WHIPPLE

39

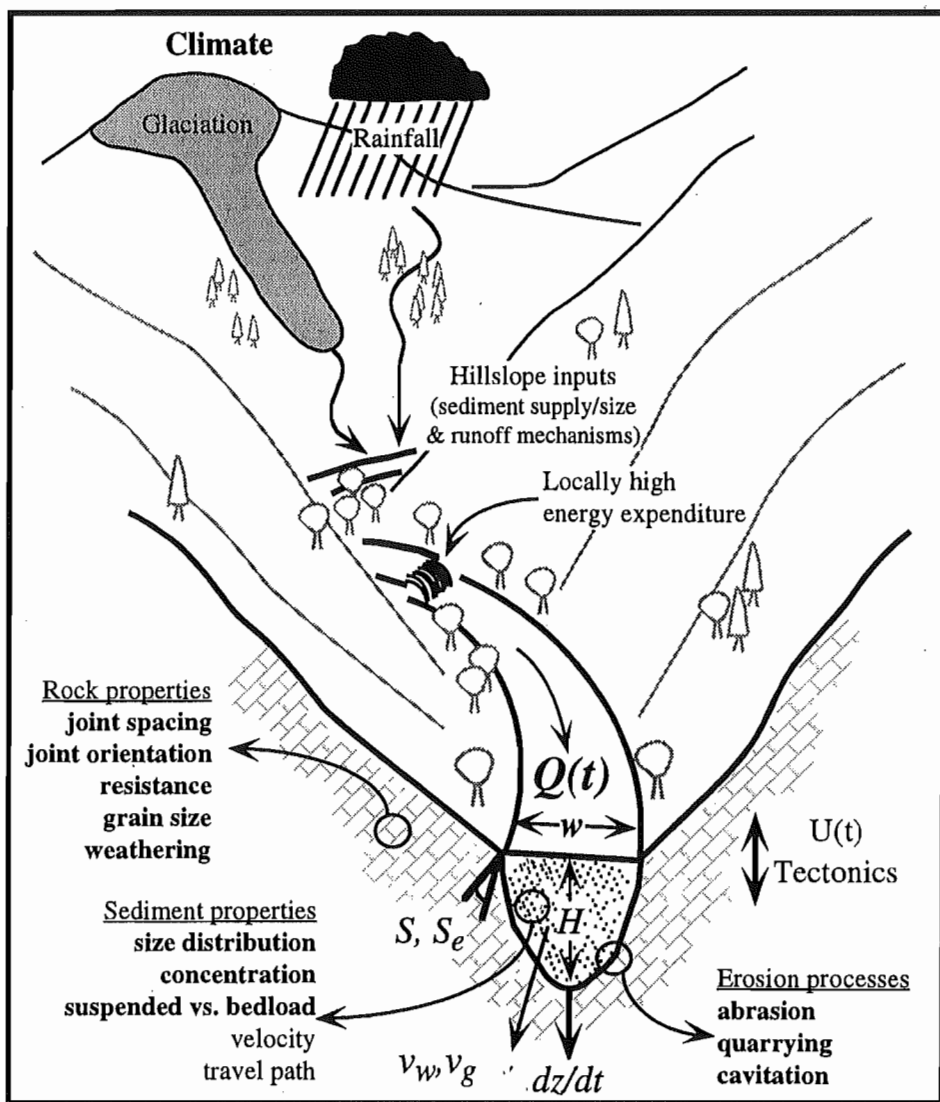


Figure 1. A schematic of a bedrock channel system, showing important variables that act to set the erosion rate, dz/dt , of the channel and terms used in the text. Channel variables are: $Q(t)$: discharge as a function of time; w : channel width; H : flow depth; v_w : water velocity; v_g : sediment velocity; A_D : drainage area; and S and S_e : channel and energy slope, respectively. Variables that are at least partially subsumed within the parameter, K , found in all reach-scale erosion rules, are shown in bold.

2.1. Abrasion

2.1.1. *Theory.* Rock erosion by abrasion is accomplished by removal of material from a rock surface through forcible impact by entrained sediment. The rate at which material is removed depends upon the kinetic energy flux to the surface, delivered by impacting grains, and the "susceptibility" of the rock surface to abrasion [e.g., Anderson, 1986; Foley, 1980a]. The impacts produce fractures within minerals, dislodge individual grains, or break off flakes from the rock surface. Experimental studies

of abrasion by aeolian sediment transport reveal that the mass of material removed is roughly proportional to the kinetic energy delivered by the impact [e.g., Greeley and Iversen, 1985; Suzuki and Takahashi, 1981]. At the grain scale, the grain velocity, v_g , diameter, D , and density, ρ_g , set its kinetic energy, and the delivery of this kinetic energy increases as grain impact angle, α , relative to the bed, increases toward vertical (90 degrees). The "susceptibility", S_a , relates kinetic energy delivery to mass of rock material removed, and is dependent primarily on the density, hardness, and fracture-mechanical properties of the

101

98

Table 1. Published long-term average rates of bedrock channel incision (after Schumm and Chorley, 1983, Table 3-5, and Wohl et al., 1994b, Table 1).

Rate (cm/kyr)	Lithology	Location	Drainage Area (km ²)	Climate, tectonics	Time range of incision	Source
9	granite, andesite	Sierra Nevada, California, USA	35 000	arid, uplift	Pliocene- Quaternary	Huber, 1981
30	sedimentary	Colorado, USA	11 800	semiarid, uplift	Miocene- Quaternary	Larson et al., 1975
7	metamorphic	Colorado, USA	----	semiarid, uplift	Pliocene- Quaternary	Scott, 1975
45-130	sedimentary	Nahal Zin, Israel	1 540	hyperarid, uplift	Quaternary	Goldberg, 1976 Schwarcz et al., 1979 Yair et al., 1982
10	sedimentary	Nahal Paran, Israel	3 600	hyperarid, uplift	Quaternary	Wohl et al., 1994b
30	basalt, limestone	Utah, USA	9 900	semiarid, uplift	Quaternary	Hamblin et al., 1981
9.5 23-25	sedimentary basalt	Arizona, USA Jalisco, w. Mexico	68 500 ----	semiarid, uplift arid, uplift	Quaternary Pliocene- Quaternary	Rice, 1980 Righter, 1997
15 25-47	suggested average rate of bedrock channel incision in the sedimentary	Utah, USA	115 000	middle latitudes semiarid, uplift	Quaternary	Pitty, 1971 Harden and Coleman, 1989
1 000	igneous and metamorphic	Pakistan	260 000	semiarid, uplift	Quaternary	Leland et al., 1995
70-180	sedimentary	n. California, USA	655	Mediterranean, uplift	Holocene	Merritts et al., 1994
<25	sedimentary, intrusive igneous	Central California, USA	10-20	Mediterranean, uplift	Quaternary	Rosenbloom and Anderson, 1994
0.5-8	basalt	Kauai, USA	0.1-90	seasonal tropical to semiarid, uplift	Pliocene- Quaternary	Seidl et al., 1994
*40-100	basalt	Kauai, USA	0.1-90	seasonal tropical to semiarid, uplift	Pliocene- Quaternary	Seidl et al., 1997
50-690	sedimentary	Montana, USA	1 420	humid temperate, uplift	Quaternary	Foley, 1980b
≤1000	mudstone	s. Japan	0.15-0.4	humid temperate, uplift	Quaternary	Mizutani, 1996
5.7	limestone	New Guinea	0.02	humid tropical, uplift	Quaternary	Chappell, 1974
*≤1.57×10 ⁵	sedimentary	Ontario, Canada	686 000	humid temperate, passive	Quaternary	Tinkler et al., 1994
0.5-3	basalt, metamorphic	southeastern Australia	20-400	humid temperate, passive	Miocene- Quaternary	Young and McDougall, 1993
300	basalt, sedimentary	Svalbard, Norway	----	subpolar, passive	Quaternary	Büdel, 1982
2.7	Carbonates, Crystalline rocks	Virginia, USA	----	humid temperate, passive	Quaternary	Granger et al., 1997

* knickpoint migration upstream

102

89

Soil
BASICS

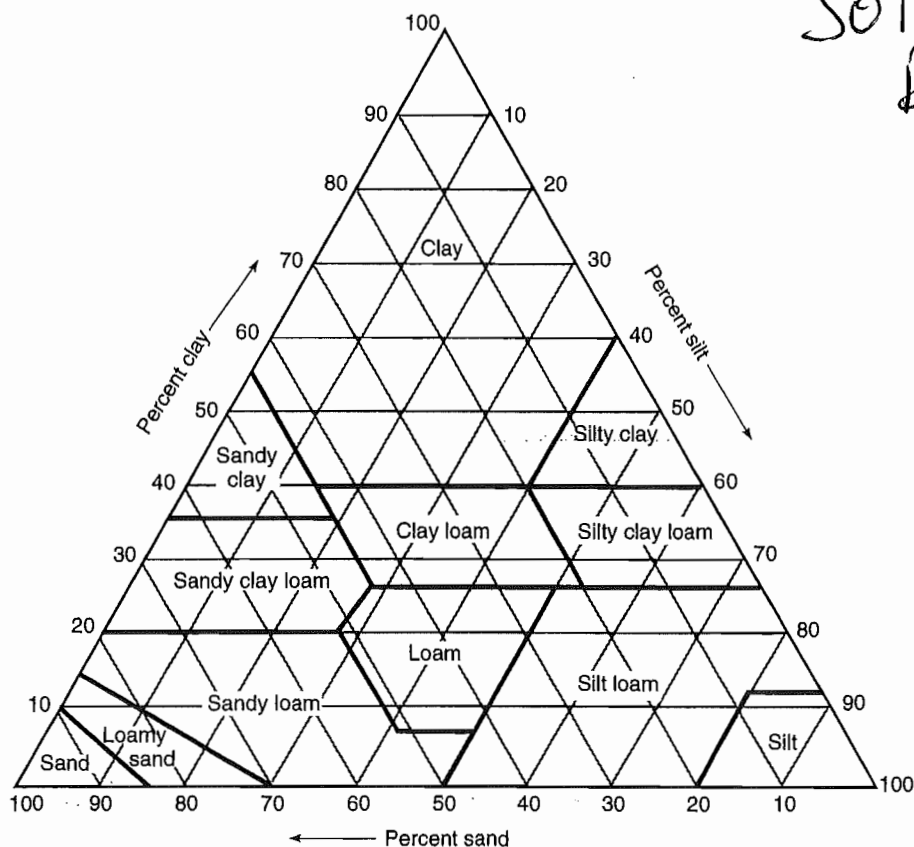


Figure 3.12

Percentages of clay (< 0.002 mm), silt (0.002–0.05 mm), and sand (0.05–2.0 mm) in basic soil textural classes as defined by the U.S. Department of Agriculture.

(Soil Survey Staff, 1951)

ganic content are typically black to dark brown, whereas the presence of ferric iron is indicated by yellow-brown to red colors. Light gray to white colors are associated with a concentration of SiO_2 or CaCO_3 . It should be recognized, however, that small amounts of a pigment can cause rather intense discoloration, and so color alone may be a poor index of the total quantity of the pigmenting substance. *Texture* is simply the relative proportions of different particle sizes in a soil horizon, and is somewhat analogous to the property of sorting as used by geologists. However, it is based only on the particles that are less than 2 mm in diameter (fig. 3.12). *Structure* in soils is a unique characteristic in that it designates the shape developed when individual particles cluster together into aggregates called *peds* (fig. 3.13). In clay-rich soils, the openings between peds may play an extremely important geomorphic role by providing the primary avenues for downward percolation through an otherwise impermeable soil. *Organic matter* in soils consists mainly of dead leaves, branches, and the like, called *litter*, and the amorphous residue, called *humus*, that develops when litter is decomposed. Litter may form at mean annual temperatures as low as freezing,

but its optimum production occurs at about 25° to 30° C and decreases rapidly above those levels. Microorganisms that convert litter to humus begin to function at temperatures slightly above freezing (5° C), but the optimum temperature for their life activities may be as high as 40° C (fig. 3.14). It is significant that at temperatures between 0° and 25° C, humus is produced in abundance, but above 25° C little if any humus is accumulated. Humus has an important effect on soil formation because it includes chelators that promote the leaching of iron and aluminum, and increases water absorption. In addition, the development of humus releases CO_2 in high concentrations, leading to unusual amounts of carbonic acid within the humic zone and an associated lowering of the pH.

The total quantity of water that can be held in a soil is the *available water capacity* (AWC). By combining this parameter with the bulk density (dry weight of soil/unit volume), an estimate of the depth of wetting can be made (see Birkeland 1999). Such information is significant in that it relates to many soil properties, especially those affected by the redistribution of material during the downward percolation of water.

105

102

4.1 SOIL COLOR¹

When we examine a soil, the first thing we are likely to notice is its color. In and of themselves, soil colors have little effect on the behavior and use of soils. An important exception to this statement is the fact that dark-colored surface soils absorb more solar energy than lighter-colored soils, and therefore may warm up faster.

The main reason for studying soil colors is that color provides valuable clues to the nature of other soil properties and conditions. Because of the importance of accurate color description in soil classification and interpretation, a standard system for color description has been developed using Munsell color charts (Figure 4.1). In this system, a small piece of soil is compared to standard color chips in a soil color book. Each color chip is described by the three components of color: the **hue**, the **chroma** (intensity or brightness), and the **value** (lightness or darkness).

Causes of Soil Colors

Soils display a wide range of reds, browns, yellows, and even greens (see Plate 13). Some soils are nearly black, others nearly white. Some soil colors are very bright, oth-

¹For an excellent collection of papers on the causes and measurement of soil colors, see Bigham and Ciolkosz (eds.), 1993.

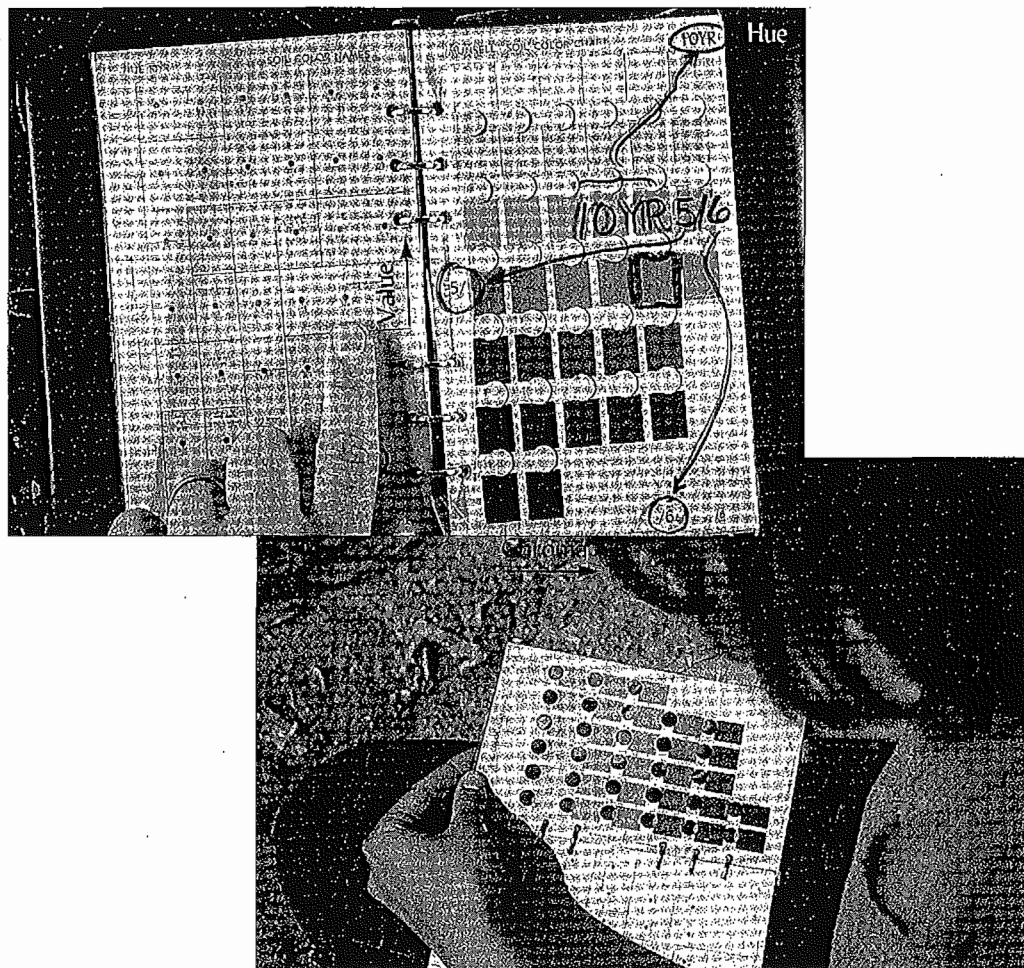


FIGURE 4.1 Determining soil color by comparison to color chips in a *Munsell Color Book*. Each page shows a different hue, ranging from 5R (red) to 5Y (yellow). On a single page, higher-value (lighter) colors are nearer the top and lower-value (darker) colors are near the bottom. Higher-chroma (brighter) colors are nearer the right-hand side and duller, grayish (low-chroma) colors are near the left-hand side. The complete Munsell color description of the soil pictured is 10YR 5/6 (yellowish brown), moist. (Photos by R. Weil)

105A

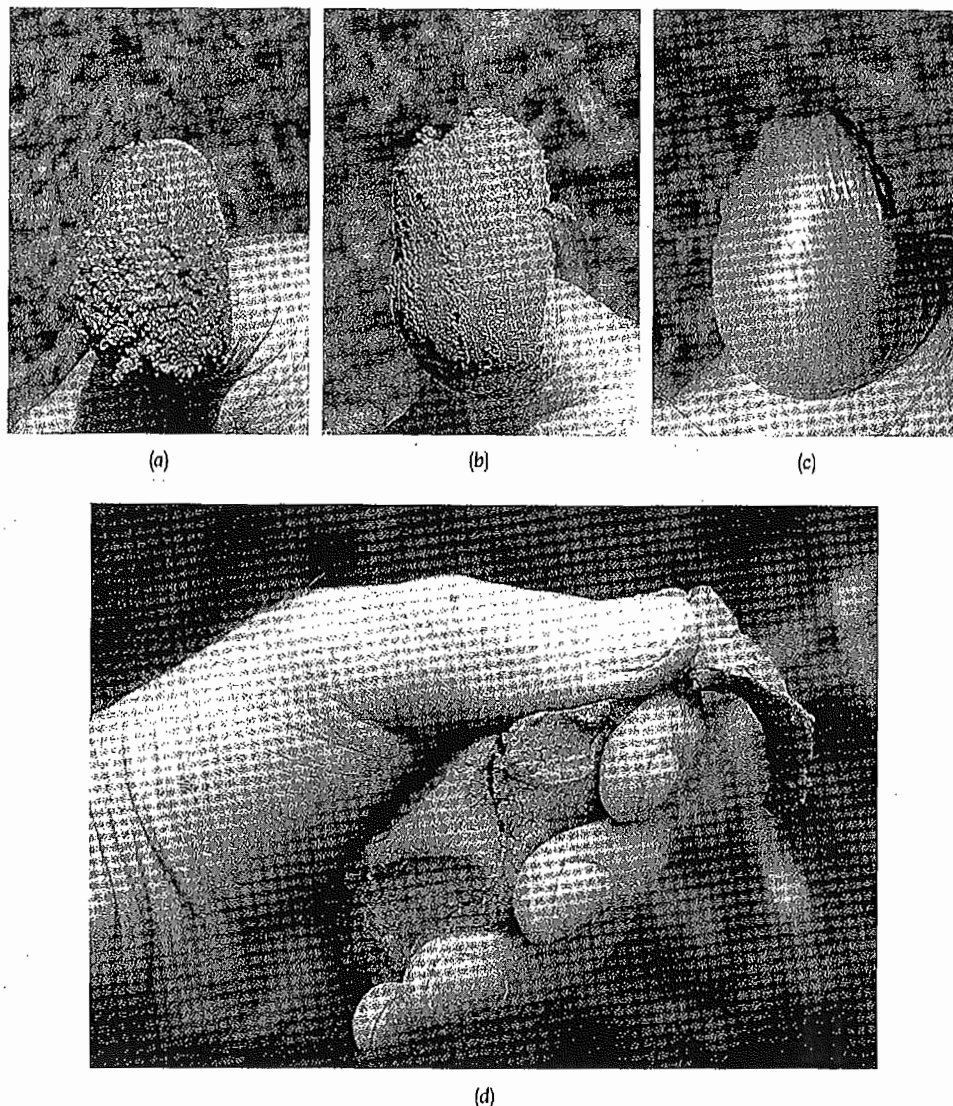


FIGURE 4.9 The "feel" method as used to distinguish between a sand (a), a silt loam (b), and a clay (c) soil. Moist samples are rubbed between the thumb and forefinger. Note the shiny appearance for the clay (c), the lack of cohesion in the sand (a), and the intermediate status of the silt loam. An estimate of percent clay is often a very useful first step in determining textural class by feel. Percent clay in a sample is best estimated by squeezing a ribbon of moist soil (d).

TABLE 4.4 Criteria Used with the Field Method of Determining Soil Texture Classes

Criterion	Sand	Sandy loam	Loam	Silt loam	Clay loam	Clay
1. Individual grains visible to eye	Yes	Yes	Some	Few	No	No
2. Stability of dry clods	Do not form	Do not form	Easily broken	Moderately easily broken	Hard and stable	Very hard and stable
3. Stability of wet clods	Unstable	Slightly stable	Moderately stable	Stable	Very stable	Very stable
4. Stability of "ribbon" when wet soil rubbed between thumb and fingers	Does not form	Does not form	Does not form	Broken appearance	Thin, will break	Very long, flexible

10513

the other
 properties
 y. These
 ing age,
 > subor-
 fferent
 ent ma-

 to read
 develop-
 urt with

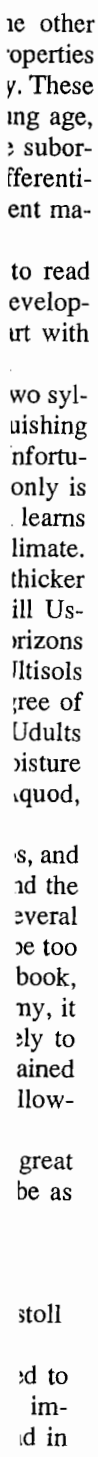
 wo syl-
 uishing
 nfortu-
 only is
 . learns
 limate.
 thicker
 ill Us-
 rizons
 lltisols
 gree of
 Uduits
 mixture
 quod,

 s, and
 ad the
 everal
 e too
 book,
 ny, it
 uly to
 ained
 llow-

 great
 be as

 stroll

 ed to
 im-
 d in



- the other
 properties
 y. These
 ing age,
 > subor-
 fferent
 ent ma-

 to read
 develop-
 urt with

 wo syl-
 uishing
 nfortu-
 only is
 . learns
 limate.
 thicker
 ill Us-
 rizons
 lltisols
 gree of
 Uduits
 mixture
 quod,

 s, and
 ad the
 everal
 e too
 book,
 ny, it
 uly to
 ained
 llow-

 great
 be as

 stroll

 ed to
 im-
 d in

the other
 properties
 y. These
 ing age,
 > subor-
 fferent
 ent ma-

 to read
 develop-
 urt with

 wo syl-
 uishing
 nfortu-
 only is
 . learns
 limate.
 thicker
 ill Us-
 rizons
 lltisols
 gree of
 Uduits
 mixture
 quod,

 s, and
 ad the
 everal
 e too
 book,
 ny, it
 uly to
 ained
 llow-

 great
 be as

 stroll

 ed to
 im-
 d in

the other
 properties
 y. These
 ing age,
 > subor-
 fferent
 ent ma-

 to read
 develop-
 urt with

 wo syl-
 uishing
 nfortu-
 only is
 . learns
 limate.
 thicker
 ill Us-
 rizons
 lltisols
 gree of
 Uduits
 mixture
 quod,

 s, and
 ad the
 everal
 e too
 book,
 ny, it
 uly to
 ained
 llow-

 great
 be as

 stroll

 ed to
 im-
 d in

Table 1.1 Soil-Horizon Nomenclature**Description of master horizon and subhorizons**

- O horizon—Surface accumulations of mainly organic material; may or may not be, or has been, saturated with water. Subdivided on the degree of decomposition as measured by the fiber content after the material is rubbed between the fingers.
- Oi horizon—Least decomposed organic materials; rubbed fiber content is greater than 40% by volume.
- Oe horizon—Intermediate degree of decomposition; rubbed fiber content is between 17 and 40% by volume.
- Oa horizon—Most decomposed organic materials; rubbed fiber content is less than 17% by volume.
- A horizon—Accumulation of humified organic matter mixed with mineral fraction; the latter is dominant. Occurs at the surface or below an O horizon; Ap is used for those horizons disturbed by cultivation.
- E horizon—Usually underlies an O or A horizon, and can be used for eluvial horizons within or between parts of the B horizon (e.g., common above fragipan, x). Characterized by less organic matter and/or fewer sesquioxides (compounds of iron and aluminum) and/or less clay than the underlying horizon. Many are marked by a concentration of sand and silt. Horizon is light colored due mainly to the color of the primary mineral grains because secondary coatings on the grains are absent; relative to the underlying horizon, color value will be higher or chroma will be lower.
- B horizon—Underlies an O, A, or E horizon, and shows little or no evidence of the original sediment or rock structure. Several kinds of B horizons are recognized, some based on the kinds of materials illuviated into them, others on residual concentrations of materials. Subdivisions are:
- Bh horizon—Illuvial accumulation of amorphous organic matter-sesquioxide complexes that either coat grains or form sufficient coatings and pore fillings to cement the horizon.
- Bhs horizon—Illuvial accumulation of amorphous organic matter-sesquioxide complexes, and sesquioxide component is significant; both color value and chroma are three or less.
- Bk horizon—Illuvial accumulation of alkaline earth carbonates, mainly calcium carbonate; the properties do not meet those for the K horizon.
- Bt horizon—Illuvial concentrations primarily of silt (Forman and Miller, 1984). Used when silt cap development reaches stages 5 and 6.
- Bo horizon—Residual concentration of sesquioxides, the more soluble materials having been removed.
- Bq horizon—Accumulation of secondary silica.
- Bs horizon—Illuvial accumulation of amorphous organic matter-sesquioxide complexes if both color value and chroma are greater than three.
- Bt horizon—Accumulation of silicate clay that has either formed in situ or is illuvial (clay translocated either within the horizon or into the horizon); hence it will have more clay than the assumed parent material and/or the overlying horizon. Illuvial clay can be recognized as grain coatings, bridges between grains, coatings on ped or grain surfaces or in pores, or thin, single or multiple near-horizontal discrete accumulation layers of pedogenic origin (clay bands or lamellae). In places, subsequent pedogenesis can destroy evidence of illuviation. Although Soil Survey Division Staff (1993) does not include this, clay accumulation that lacks evidence for illuviation is included (could have been formed in situ, for example).
- Bw horizon—Development of color (redder hue or higher chroma relative to C) or structure, or both, with little or no apparent illuvial accumulation of material.
- By horizon—Accumulation of secondary gypsum.
- Bz horizon—Accumulation of salts more soluble than gypsum.
- K horizon. A subsurface horizon so impregnated with carbonate that its morphology is determined by the carbonate (Gile and others, 1965). Authigenic carbonate coats or engulfs nearly all primary grains in a continuous medium. The uppermost part of a strongly developed horizon is laminated, brecciated, and/or pisolithic (Machette, 1985). The cemented horizon corresponds to some caliches and calcretes.
- C horizon—A subsurface horizon, excluding R, like or unlike material from which the soil formed, or is presumed to have formed. Lacks properties of A and B horizons, but includes materials in various stages of weathering.
- Cox and Cu horizons—In many unconsolidated deposits, the C horizon consists of oxidized material overlying seemingly unweathered C. The oxidized C does not meet the requirements of the Bw horizon. In stratigraphy, it is important to differentiate between these two kinds of C horizons. Here Cox is used for oxidized C horizons and Cu for unweathered C horizons. Cu is from the nomenclature of England and Wales (Hodson, 1976). Alternatively the Cox can be termed BC or CB.
- Cr horizon—In soils formed on bedrock, there commonly will be a zone of weathered rock between the soil and the underlying rock. If it can be shown that the weathered rock has formed in place, and has not been transported, it is designated Cr. Such material is the saprolite of geologists; in situ formation is demonstrated by preservation of original rock features, such as grain-to-grain texture, layering, or dikes. If such material has been moved, however, the original structural features of the rock are lost, and the transported material may be the C horizon for the overlying soil. Those Cr horizons with translocated clay, as shown by clay films, are termed Crt.
- R horizon—Consolidated bedrock underlying soil.

(continued)

107

107

tographs, so one can become familiar with the classification criteria. However, to avoid becoming overwhelmed, one should read Buol and others (1997). This readable text covers all the orders, chapter by chapter, and each is subdivided into the central concept and geographic distribution of the order, the setting, pedogenic processes, uses, and classification. The reader should be aware, however, that the classification has gone through many revisions, so consult Soil Conservation Service (1994) for the latest (watch for still more recent keys).

The new classification has much appeal for geomorphologists and ecologists, at least down to the suborder level. This is because soil profile development is included in the classification, as well as base saturation, amount of organic matter, and properties indicative of relative wetness and dryness. Most geomorphological soil studies deal with climatic and time factors, and the above properties will later be shown to be related to both.

Eleven orders are now recognized in the new classification; these are subdivided into 55 suborders, and the latter into over 200 great groups. One should be impressed with the magnitude of this task as it begins at the lowest level of classification, the approximately 12,000 soil series in the United States. The orders are basically differentiated by a particular horizon or horizon combinations that occur in the soil profile. These usually can be recognized in the field without recourse to laboratory analysis. One criticism of Soil Taxonomy, from a geomorphological point of view, is the overem-

phasis on classification at the order level by surface horizon (e.g., Mollisol). In contrast, horizons beneath the A horizon commonly are more important to geomorphologists. Classification into suborders requires an increasingly quantitative knowledge of soil properties and soil-moisture and soil-temperature regimes. However, it is often not necessary to take these measurements because, with experience, soil classification can be estimated from properties recognizable in the field (e.g., thin Av horizon with a calcic horizon at depth points toward aridic moisture regime).

To classify a soil at the order and suborder level, one must be able to identify the diagnostic horizons as well as the soil-moisture and -temperature regimes. The reader will find that some of these definitions are exceedingly complicated, but in time they will make some sense. Diagnostic horizons are so named because they are essential to classify the soil. Epipedons are the surface diagnostic horizons. The diagnostic horizons are somewhat similar to the field-designated soil horizons, although in places they can encompass several different field-designated soil horizons. In an extreme example of the latter, the mollic epipedon can include both the A and B horizons, as long as mollic properties are obtained. For some diagnostic horizons, the criteria are so complex that one has to read the defining criteria in detail using both the field and laboratory data (e.g., spodic horizon). Only the main discriminating criteria are given here (Table 2.1); Soil

Table 2.1 Common Diagnostic Horizons Used in Soil Taxonomy

Diagnostic Horizon	Defining Criteria	Probable Field Horizon Equivalent
Epipedons		
Mollic epipedon	Must be 10 cm thick if on bedrock, otherwise a minimum of 18 or 25 cm thick depending on subhorizon properties and thicknesses; color value darker than 3.5 (moist) and 5.5 (dry); chroma less than 3.5 (moist); organic carbon content at least 0.6%; structure developed and horizon not both massive and hard; base saturation $\geq 50\%$	A, A + E + B, A + B
Umbric epipedon	Meets all criteria for mollic epipedon, except base saturation $< 50\%$	A
Ochric epipedon	Epipedon that does not meet requirements of either mollic or umbric epipedons	A
Histic epipedon	Complex thickness requirements, but > 20 cm thick; $> 12\%$ organic carbon, with some adjustment for percent clay; saturated with water for 30 consecutive days or more per year, or artificially drained	O
Subsurface Horizons		
Albic horizon	Light colored with few to no coatings on grains—light color is that of grains; if color value (dry) is 7 or more, or color value (moist) is 6 or more,	E

(continued)

Table 2.1

Diagnosti

Argillic

Kandic

Natric

Spodic

Cambic

Oxic h

Calcic

Petroc

Gypsic

Petrog

Salic t

Durip

Fragip

Taken fr

108

Table 2.1 (continued)

Diagnostic Horizon	Defining Criteria	Probable Field Horizon Equivalent
Argillic horizon	chroma is 3 or less; if color value (dry) is 5 or 6, or color value (moist) is 4 or 5, chroma is closer to 2 than to 3 Complex thickness requirements, but at least 7.5 or 15 cm thick depending on texture and thickness of overlying horizons; must have these greater amounts of clay relative to overlying eluvial horizon(s) or underlying parent material: (a) if the latter horizons have <15% clay, argillic horizon must have a 3% absolute increase (10 vs. 13%); (b) if the latter horizons have 15 to 40% clay, the ratio of clay in argillic horizon relative to them must be 1.2 or more, and (c) if the latter horizons have >40% clay, the argillic horizon must have an 8% absolute increase (42 vs. 50%); in most cases, evidence for translocated clay should be present (clay as bridges between grains or clay films in pores or on ped faces)	Bt
Kandic horizon	Minimum thickness is either 15 or 30 cm; complex clay increase requirements relative to overlying eluvial horizon(s) or underlying parent material: if the latter horizons have <20% clay, the kandic horizon must have a 4% absolute increase; if the latter horizons have 20–40% clay, the kandic horizon must have at least 20% more clay; if the latter horizons have >40% clay, the kandic horizon must have at least 8% absolute increase; complex depth-texture relations; CEC <16 meq/100 g clay	Bt
Natric horizon	In addition to properties of argillic horizon: prismatic or columnar structure; 15% or more exchangeable sodium; exchangeable magnesium and sodium exceed exchangeable calcium and exchange acidity	Btn
Spodic horizon	Minimum thickness is 2.5 cm, and contains >85% spodic materials: the latter are amorphous materials composed of organic matter and Al, with or without Fe; usually beneath an albic or Ej horizon	Bh, Bs, Bhs
Cambic horizon	Base usually at least 25 cm deep; stronger chroma or redder hue relative to underlying horizon; soil structure or absence of rock or sediment structure; weatherable minerals present; carbonates removed if originally present; no cementation or brittle consistence	Bw
Oxic horizon	At least 30 cm thick; >15% clay and sandy loam or finer; cation exchange capacity ≤16 meq/100g soil; few weatherable minerals	Bo
Calcic horizon	At least 15 cm thick; 15% CaCO ₃ ; relative to underlying horizon, has at least 5% more CaCO ₃ , or at least 5% by volume secondary carbonate	Bk
Petrocalcic horizon	Horizon continuously cemented with CaCO ₃	Km
Gypsic horizon	At least 15 cm thick; at least 5% more gypsum than underlying horizon; product of thickness(cm) times content (%) is 150 or more	By
Petrogypsic horizon	Strongly cemented gypsic horizon, commonly with greater than 60% gypsum	Bym
Salic horizon	At least 15 cm thick; at least 2% salts more soluble than gypsum; product of thickness (cm) times content (%) is 60 or more	Bz
Duripan	Silica cementation is strong enough that fragments do not slack in water	Bqm
Fragipan	Horizon of high bulk density relative to overlying horizons; formed in loamy material; although seemingly cemented with a brittle appearance, slacks in water; slowly permeable to water, so usually mottled; very coarse prismatic structure, usually with some bleached faces	Bx, Cx

Taken from Soil Conservation Service (1994).

ntinued)

109

109

high K-feldspar content (ca. 70%) in the felsic rocks and high Ca-plagioclase (ca. 60%) in the basic rocks. Finally, the MgO and Fe oxides increase in the more mafic rocks because of the increase in mafic minerals (hornblende, pyroxenes, olivine). The ultrabasic rock dunite (mainly olivine) is included, as it is an extreme composition, and, as such, the direction of pedogenesis can be much different than in adjacent rocks of more average composition.

Average sedimentary rock compositions are quite variable (Table 7.2). Sandstone compositions reflect the source area rocks, and their high SiO₂ content is due to high quartz content. The cementing agent will vary, and common ones are carbonate and silica. Shale composition is dominated by that of the included clay minerals, with illite being common to many. Finally, limestone composition is dominantly that of CaO in CaCO₃ (CO₂ content usually not given). The few included mineral grains explain the rest of the chemistry.

Molar SiO₂/Al₂O₃ ratios (Table 7.2) give an idea of the changes that would have to take place during soil formation to produce the characteristic clay minerals from rocks of different composition (compare with Table 4.2).

■ Susceptibility of Rocks to Chemical Weathering

Rocks weather and erode at different rates, as can be seen in the variations in topographic relief that ac-

company variations in rock type. For rocks from widely spaced localities, however, factors other than rock type might influence the weathering variations observed. Nahon (1991) reviews data for several kinds of rocks in a variety of climatic settings. To compare rocks of differing lithology under similar conditions of weathering, however, it is best to study a sedimentary deposit, such as bouldery till or outwash, which includes a variety of rock types. Rocks from the same depth below the surface should have weathered under similar conditions.

Goldich's stability series for minerals (Table 7.1) can be used to predict igneous rock stability in the weathering environment. Rocks with a high content of more weatherable minerals should weather more rapidly than rocks with a high content of minerals resistant to weathering. To make a valid comparison, however, the rocks should be similar in crystallinity and grain size. For igneous rocks, therefore, resistance to weathering should be

rhyolite > granite > basalt > gabbro

Clay production should follow these trends, and it seems to (Barshad, 1958).

Grain size has an effect on the rate of weathering, for it is observed that coarser-grained igneous rocks commonly weather more rapidly than finer-grained rocks (Smith, 1962). This is readily seen in many tills in the Cordilleran Region. In the Sierra Nevada, for example, till of probable O-isotope stage 6 age has the

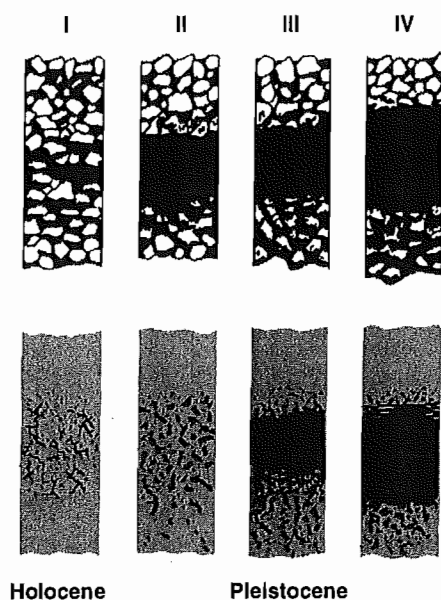
Table 7.2 Chemical Composition of Selected Igneous and Sedimentary Rocks

Oxide	Granite	Granodiorite	Diorite	Basalt	Ultrabasic rock	Average shale	Average sandstone	Average limestone
SiO ₂	71.3	66.1	57.5	49.2	38.3	63.3	78	5.2
TiO ₂	0.3	0.5	1	1.8	0.1	0.8		
Al ₂ O ₃	14.3	15.7	16.7	15.7	1.8	17.2	7.2	0.8
Fe ₂ O ₃	1.2	1.4	2.5	3.8	3.6	0.8	1.7	
FeO	1.6	2.7	4.9	7.1	9.4	5.5	1.5	0.5
MgO	0.7	1.7	3.7	6.7	37.9	3	1.2	8
CaO	1.8	3.8	6.6	9.5	1	3.5	3.2	43
Na ₂ O	3.7	3.8	3.5	2.9	0.2	1.5	1.2	0.1
K ₂ O	4.1	2.7	1.8	1.1	0.1	3.6	1.3	0.3
Molar SiO ₂ /Al ₂ O ₃	8.5	7.3	6	5.5	32	6.5	18.6	9

Data from Garrels and Mackenzie (1971, Table 9.1), Best (1982, Appendix D), and Boggs (1991, Table 7.7).

110

107



Stage	Gravelly sequence	Nongravelly sequence
I	Thin, partial or complete carbonate coatings.	Carbonate filaments and/or faint coatings on grains.
II	Carbonate coatings are thicker and there are some fillings in interstices.	Carbonate nodules separated by low-carbonate material.
III	Carbonate occurs essentially throughout the horizon, which is plugged in the last part of the stage.	
IV	Upper part of horizon nearly pure CaCO_3 exhibiting weakly platy structure; remainder of horizon plugged with carbonate.	
V	Laminar layering and strongly expressed platy structure; incipient brecciation and pisolith formation.	
VI	Brecciation and recementation of CaCO_3 layers are common.	

Figure 3.15

Schematic diagram of the stages of carbonate horizon formation in gravelly and nongravelly parent materials. Carbonate accumulations are indicated in black for clarity. Morphologic descriptions include stage additions by Machette (1985).

(Modified from Gile 1975)

with inconsistencies, Dokuchaiev's scheme had a great influence on American pedologists. His groups were defined in part by climate and vegetation, and until recently these genetic criteria were accepted as the basis of all soil classifications used in the United States. In fact, many Russian terms are still integrated in American soil nomenclature.

In the United States C. F. Marbut was the leading force in efforts to systematize soils. Marbut's classification, developed in the 1920s and 1930s, was based on characteristics that are present only in "mature" soils. The system, therefore, had no place for soils that were not fully developed. A more refined classification (Baldwin et al. 1938; Thorp and Smith 1949), designed to rectify many of the problems inherent in Marbut's system became the most extensively used soil classification in

the United States until a fundamentally new system was introduced. In 1960 the S.C.S. completely revised the descriptive nomenclature and the classification of soils (Soil Survey Staff 1960). This revision is not simply a formulation of new class names (although that occurred) but represents a fundamental departure from the philosophical basis of earlier classifications. Until the new system was devised, all classifications were essentially genetic in scope; that is, the major soil classes were based on climatic and vegetal factors. Although the subdivisions were linked to observable aspects of the profile, these were not explicitly defined, and soil scientists inescapably allowed their knowledge of climate and vegetation to influence decisions about placing a soil in a particular group. In many cases, pedologists were classifying the genetic factors and not the tangible resulting

5111

Available water capacity can be calculated if the moisture content at an upper limit (*field capacity*) and a lower limit (*permanent wilting point*) are known. Field capacity is determined by allowing a saturated sample to drain by gravity for at least 48 hours, by which time the remaining water content is held by adhesion to mineral and organic particles. After field capacity is reached, water can still be taken from the soil by plants until the tensional stresses holding the water in place become too great for the plants to break. At that point, the vegetation wilts. The water remaining in the soil is defined as the permanent wilting point. Both field capacity and permanent wilting point are expressed as a weight percentage according to the following equation:

$$P_w = \frac{W_s - W_d}{W_d} \times 100$$

where P_w is moisture percentage, W_s is total soil weight, and W_d is weight of soil after drying at 105°C. The available water capacity is simply the difference between the moisture content at field capacity and that at the permanent wilting point.

Soil Horizon Nomenclature and Description

Assuming that the vertical arrangement of the properties described above are distinct enough to identify a soil horizon, the pertinent consideration then becomes what nomenclature should be used to convey that information. In the United States, two systems of soil nomenclature are now in use. One is outlined in the *Soil Survey Manual* and is used in field descriptions of soil profiles (Soil Survey Division Staff 1993). The second is designed for the systematic classification of soils, and is based on the definition of diagnostic horizons, which, in many cases, can only be delineated following detailed laboratory analyses. The soil classification system used in the United States will be discussed in the next section. We will concentrate here on the nomenclature used to describe soils in the field.

Three kinds of symbols are used to denote horizons and layers in a soil profile. Capital letters, as shown in table 3.5, designate master horizons. Lowercase letters are used as suffixes to indicate specific characteristics of layers in the master horizon (table 3.6), and numbers are used as suffixes to connote vertical subdivision within a horizon or layer. In addition, numbers are prefixed to the master horizon designations to indicate a significant change in particle size or mineralogy within the soil. These signify a difference in the material from which the horizons have formed. In 1975 the Soil Conservation Service (S.C.S.) used Roman numerals as the prefix but have since changed to Arabic numerals (Soil Survey Division Staff 1993) (Note that the S.C.S. is now referred to as the National Resources Conservation Service). The number 1 is never used because it is implied to represent

TABLE 3.5 Nomenclature of Soil Horizons.

Horizon ^a	Characteristics
O	Upper layers dominated by organic material above mineral soil horizons. Must have > 30% organic content if mineral fraction contains > 50% clay minerals, or > 20% organics if no clay minerals.
A	Mineral horizons formed at the surface or below an O horizon. Contains humic organic material mixed with mineral fraction. Properties may result from cultivation or other similar disturbances.
E	Mineral horizons in which main characteristic is loss of silicate clay, iron, or aluminum, leaving a concentration of sand and silt particles of resistant minerals.
B	Dominated by obliteration of original rock structure and by illuvial concentration of various materials including clay minerals, carbonates, sesquioxides of iron and aluminum. Often has distinct color and soil structure.
C	Horizons, excluding hard bedrock, that are less affected by pedogenesis and lack properties of O, A, E, B horizons. Material may be either like or unlike that from which the solum presumably formed.
R	Hard bedrock underlying a soil.

Adapted from the Soil Survey Staff, 1960, 1975, 1981.

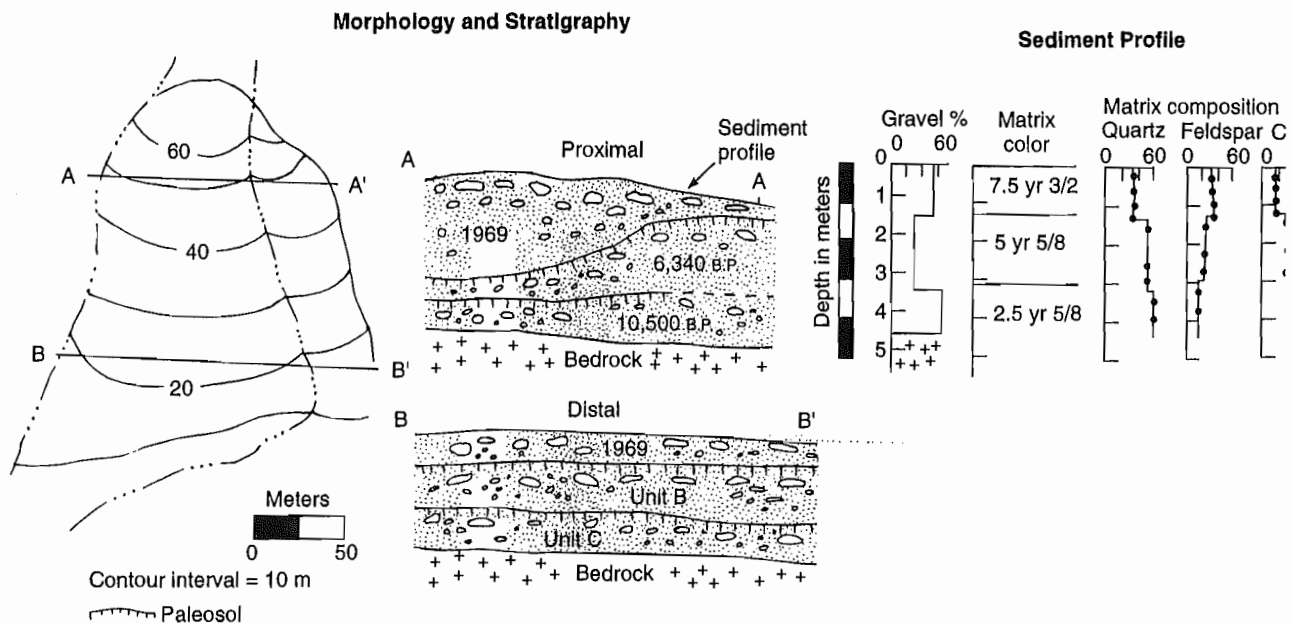
^aHorizons can be divided into subhorizons by adding Arabic numbers.

the material in the surface zones. Therefore, if no changes occur downward into the profile, prefix numbers are not needed.

The master horizons are designated by the capital letters O, A, E, B, C, and R (table 3.5). Horizons at the ground surface are called either O or A depending on the nature and amount of organic constituents they contain. The O horizon is dominated by undecomposed or partially decomposed materials, such as leaves, needles, lichens, or fungi. Mineral fragments represent only a small fraction (generally less than 50 percent) of the horizon by weight. In contrast, the A horizon is dominated by mineral grains and is normally considered to be the thin, dark-colored surface layer where decomposed organic matter is concentrated and where clays and mobile components are continuously leached downward, or *eluviated*. The E horizon underlies the O or A horizon. It is characterized by intense leaching that removes Fe⁺³ or organic coatings from the mineral grains, a process that usually imparts a bleached gray color to the horizon. The C and R horizons exist at the base of the profile. The C horizon is usually thought of as the underlying, unconsolidated parent materials that have been unmodified, or only very slightly modified, by soil-forming processes. The R horizon is simply consolidated bedrock beneath the soil.

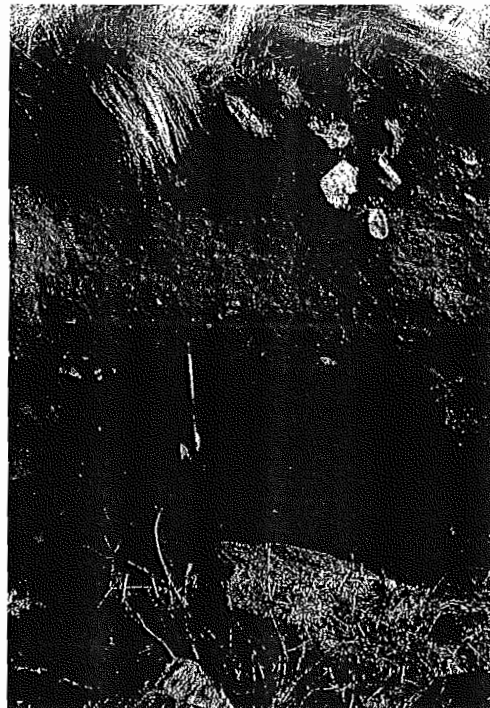
112

101



(A)

(B)

**Figure 4.47**

Stratified debris fan sediments in Nelson County, Va. (A) Radiocarbon-dated organic debris shows that events like the Camille flows have occurred there at least three times in the last 11,000 years. (B) Stratified floodplain sediments in Davis Creek, Va. The top layer above the glove was deposited by the Camille flood in 1969. The two lower units have paleosols developed on them and erosional upper boundaries.

(From R. C. Kochel, *Holocene Debris Flows in Central Virginia*, in "Debris Flows/Avalanches: Process, Recognition, Mitigation," *Reviews in Engineering Geology*, vol. 7, p. 148; 1987.)

(B): (R. Craig Kochel)

remote regions (Michaels 1985). As population continues to expand into more remote regions of the Appalachians, damage like that caused by the Camille storm in 1969 may become increasingly common. Detailed histories of debris flow frequency and magnitude have also been reconstructed by studying debris flow-induced damage in tree rings. Hupp (1984) used a dendrogeomorphic approach at Mount Shasta, California, to elucidate a 300-year record of debris flow activity. Bowers et al. (1997) were able to determine debris flow

history in the Grand Canyon using ecological aspects of plant colonization on debris flow surfaces.

Progress is being made in identifying threshold intensities required to destabilize slopes in selected regions of rainfall and snowmelt (Campbell 1975; Caine 1980; Church and Miles 1987; Wicczorek 1987; Takabatake et al. 1998). Recent studies have clarified the relationships between hillslope fires and subsequent debris flows (Parrett 1985) and identified a wide range of mechanisms that may ultimately produce debris flows

113

140

MASS WASTING BASICS

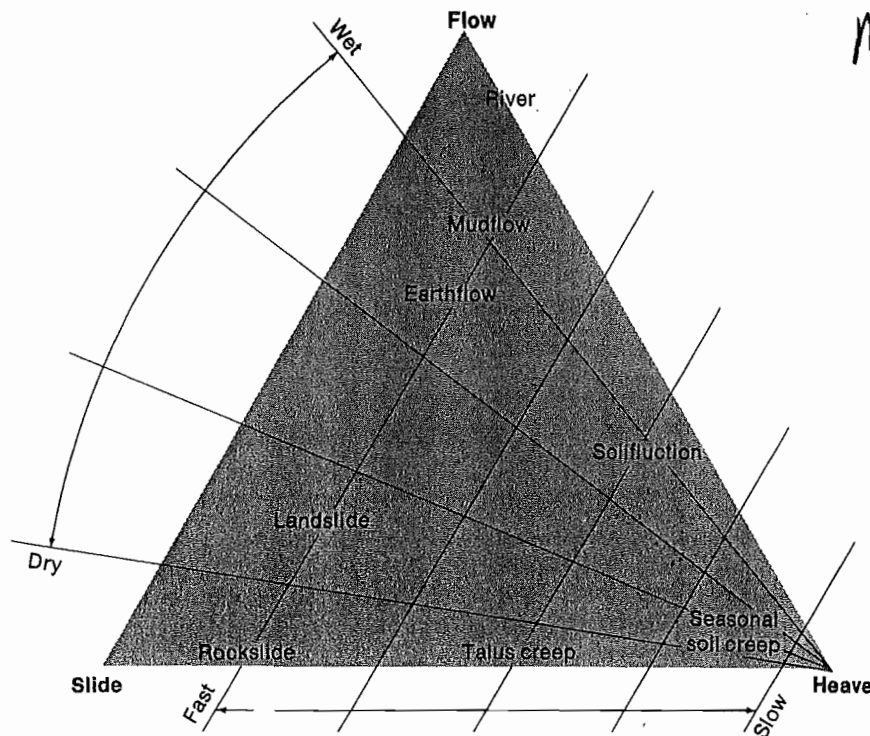


Figure 4.27

Classification of mass movement processes.

(From M. A. Carson and M. Kirkby, *Hillslope Form and Process*, copyright 1972 Cambridge University Press, Cambridge.)

TABLE 4.5 Factors that Influence Stress and Resistance in Slope Materials.

Factors that Increase Shear Stress

Removal of lateral support

Erosion (rivers, ice, waves)

Human activity (e.g., quarries, road cuts)

Addition of mass

Natural (e.g., rain, talus)

Human (e.g., fills, ore stockpiles, buildings)

Earthquakes

Regional tilting

Removal of underlying support

Natural (e.g., undercutting, solution, weathering)

Human activity (mining)

Lateral pressure

Natural (swelling, expansion by freezing, water addition)

Factors that Decrease Shear Strength

Weathering and other physicochemical reactions

Disintegration (lowers cohesion)

Hydration (lowers cohesion)

Base exchange

Solution

Drying

Pore water

Buoyancy

Capillary tension

Structural changes

Remolding

Fracturing

After Varnes (1958).

In most analyses the vertical height of the water table above the slide plane is expressed as a fraction of the soil thickness above the plane (m), where $m = 1.0$ if the water table is at the surface, and $m = 0$ if it is at or below the sliding plane. Thus, the pore pressure can be expressed as

$$\mu = \gamma_w m h \cos^2 \theta$$

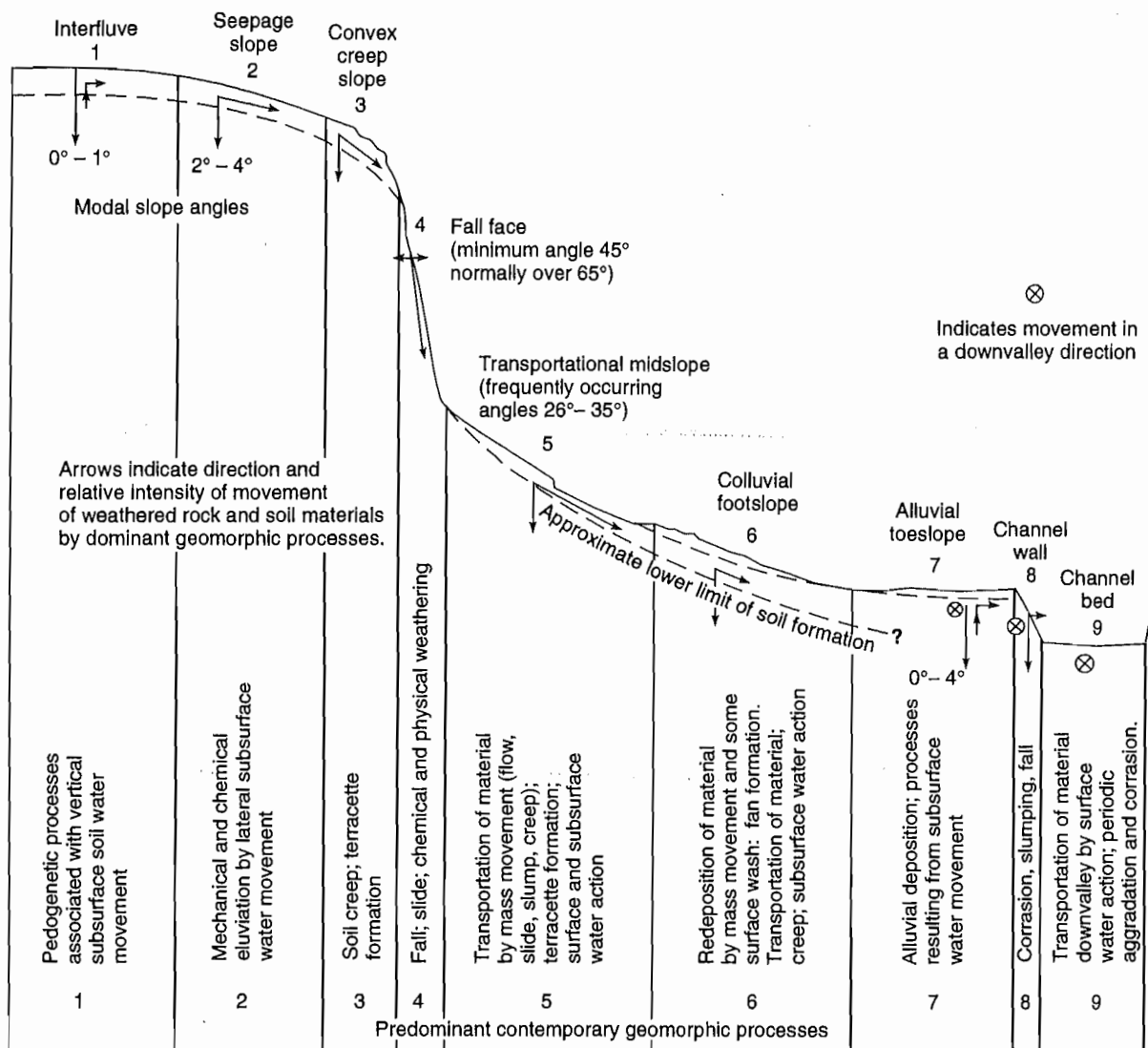
and

$$F = \frac{c + (\gamma - m\gamma_w) h \cos^2 \theta \tan \phi}{\gamma h \sin \theta \cos \theta}$$

The following hypothetical example will show how to determine whether the slope is stable or close to failure. If laboratory tests tell us that $\phi = 10^\circ$, $c = 45 \text{ lb/ft}^2$,

114

HP

**Figure 4.53**

Diagrammatic representation of the hypothetical nine-unit landsurface model.

(Redrawn from J. B. Dalrymple, et al., "A Hypothetical Nine-Unit Landsurface Model," *Zeitschrift für Geomorphologie* 12:60-76, 1968. Used by permission of Gebrüder Borntraeger Verlagsbuchhandlung, Stuttgart.)

mountainous terrain where erosion is rapid, and are normally characterized by thin, weakly developed rocky soils. The rate of physical weathering tends to be at a maximum when the thickness of the residuum (the soil and colluvium) is minimal (fig. 4.54). Chemical weathering, which proceeds most efficiently under a significant cover of residuum, will be slowed, however, when the residuum becomes so thick that it interrupts the movement of water to the bedrock weathering front (an example of negative feedback). Numerous examples of weathering-limited slopes can be seen on slick-rock slopes developed in sandstones of the Colorado Plateau (Oberlander 1977; Howard and Kochel 1988). In contrast, **transport-limited slopes** are formed where the rate of weathering is more rapid than erosion. Slopes

produced under this regime normally develop on any unconsolidated parent material regardless of environment, but they are typically dominant in humid-temperate zones where vegetation cover is continuous. These profiles are less affected by parent rock and more dependent on the type and rate of slope processes.

Selby (1982) has made a cogent argument that weathering-limited slopes are directly dependent on the relative resistance of the underlying parent rocks. As evidence, he has demonstrated a high correlation between rock mass strength (see table 4.4) and the angle developed on various slope segments (fig. 4.55). A line drawn around the data points shown in figure 4.55 creates what Selby calls the *strength equilibrium envelope*, and the slopes represented by points within that envelope are

115

112

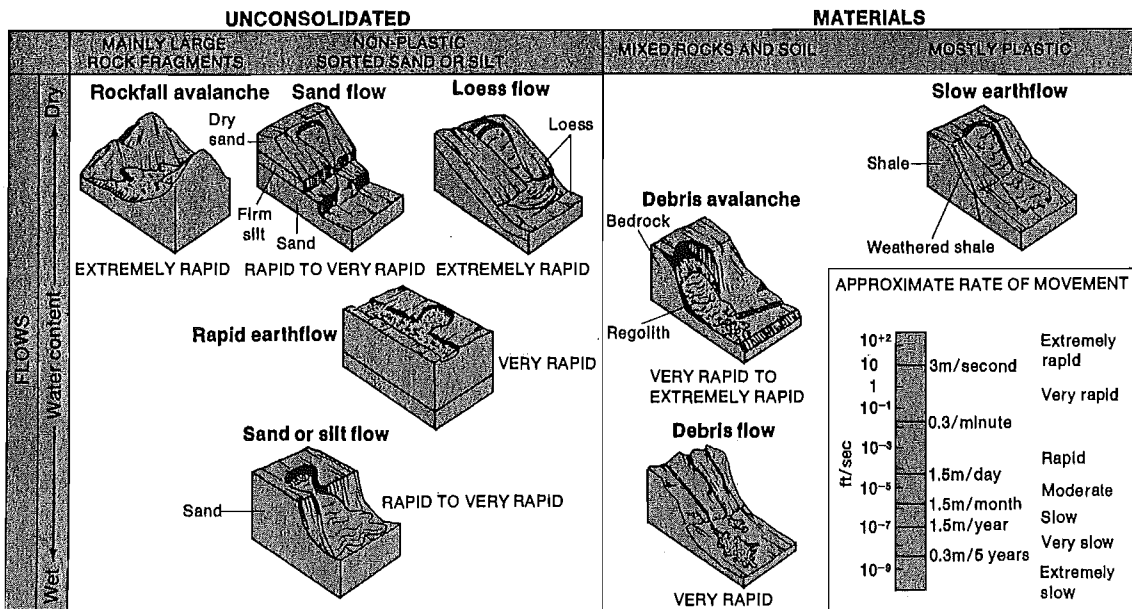
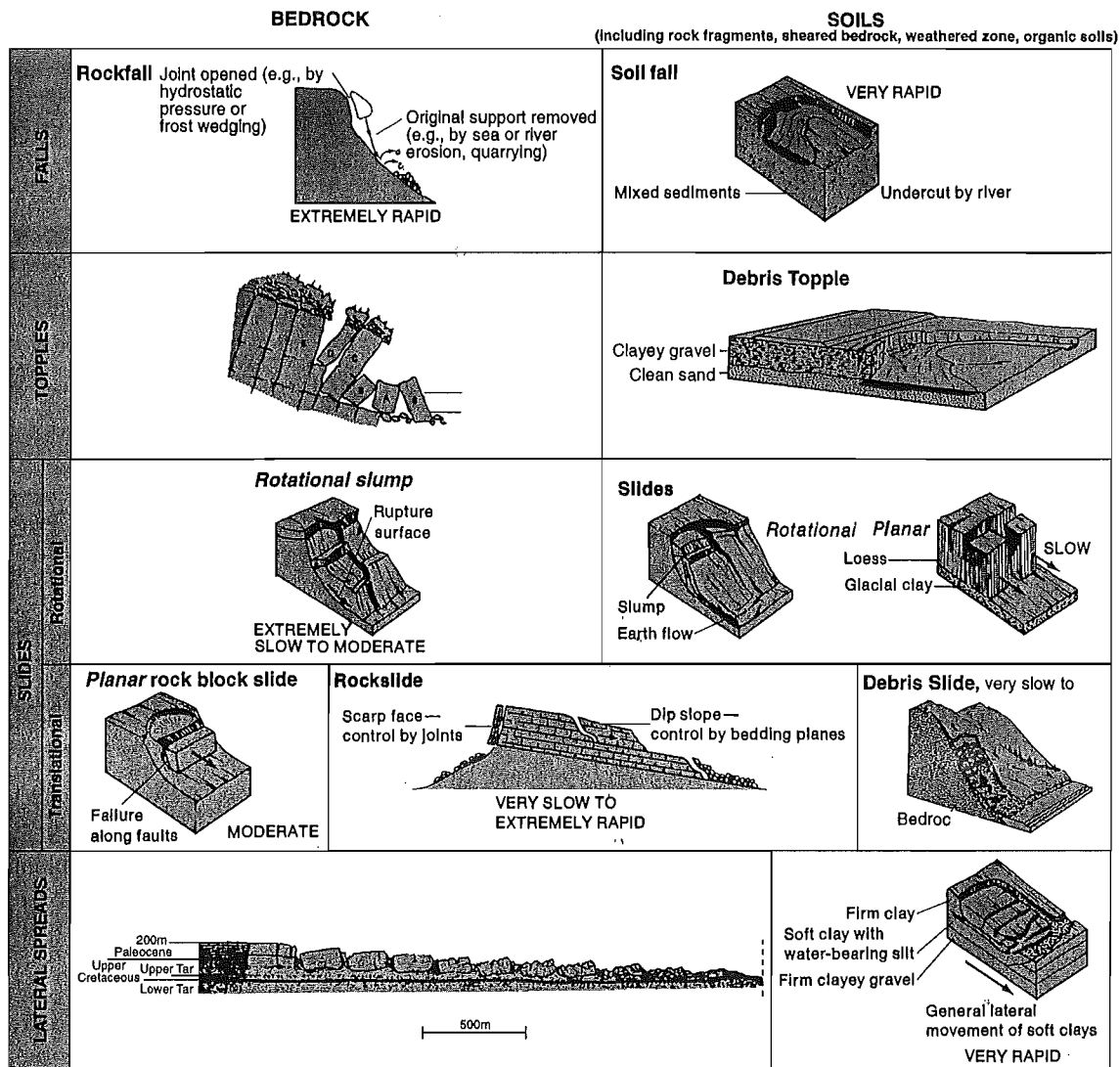


Figure 4.36

Classification of landslides.

(From D. J. Varnes, 1978, "Landslides: Analysis and Control," *TRB Special Report 176*, Transportation Research Board, National Research Council, Washington, D.C. Used by permission.)

SURFICIAL MAPPING methodology

A. Type I Criteria: Age, Origin, Landform, Material.

1. Age of Surficial Material

H = Holocene (< 10,000 years old)
W = Wisconsin (ca. 89 to 10 ka)
I = Illinoian
P = Pleistocene Undifferentiated
EP = Early Pleistocene
MPI = Middle Pleistocene
LP = Late Pleistocene
Q = Quaternary Undifferentiated
CZ = Cenozoic Undifferentiated

2. Origin / Surficial Process

A. Hillslope
r = residuum (in situ regolith)
c = colluvium (mass wasting)
ds = debris slide
rf = rock fall or topple
B. Valley Bottom
a = stream alluvium (normal flow)
hcf = hyperconcentrated flow
df = debris flow
sw = slackwater deposition
C. Lacustrine
l = lacustrine deposit, undiff.
lb = lake-bottom deposit
ld = lacustrine deltaic
D. Other
g = glaciofluvial, undifferentiated
go = glacial outwash
e = eolian
co = collapse (solution)
cr = cryoturbation
x = anthropogenic disturbance
f = artificial fill
rk = bedrock (process n/a)

3. Landform Units

A. Hillslope
n = nose
sl = side slope
h = hollow
vener = < 2m of regolith
blanket = > 2 m of regolith
bf = boulder field
bs = boulder stream
pg = patterned ground
tis = talus deposits

Table 5-2. Surficial Map Criteria for the Central Appalachians (after Kite, 1994).

3. Landform Units (Cont.)

B. Valley Bottom
ch = channel
fp = floodplain (RI < 2-3 yr)
t = terrace (t₁, t₂ ... t_n; height AMRL)
f = fan
f-t = fan terrace (t₁, t₂ ... t_n; height AMRL)
a = apron (footslope deposit)
lo = lobe
lv = levee
ox = oxbow, abandoned channel
C. Other
ft = flow track (debris flows)
hm = hummocky topography
rb = rock-block slide deposits
x = excavated, fill, disturbed ground
d = delta
du = dune

4. Material (Composition and Texture)

b = boulders (>256 mm; clast supported)
c = cobbles (64-256 mm; clast supported)
p = pebbles (4-64 mm; clast supported)
g = gravel (>2 mm; clast supported)
sg = mixed sand and gravel
s = sand (0.05-2.0 mm)
st = silt (0.002-0.05 mm)
cy = clay (<0.002 mm)
l = loam (mix of sand, silt, clay)
d = diamiction undifferentiated
bbd = very bouldery diamiction
bd = bouldery diamiction
cd = cobbly diamiction
pd = pebbly diamiction
ds = sandy matrix diamiction
dt = silty matrix diamiction
dy = clayey-matrix diamiction
rk = bedrock (modify with lithology)
rs = rotten stone, saprolite
tr = travertine
tu = tufa
ma = marl
og = organic-rich sediment
w = water
u = unknown

B. Type II Criteria: 2-D Surface Features

1. Karst

bv = blind valley
ca = cave (human entry)
Active cave passage
Abandoned cave passage
dv = dry valley
kw = karst window
sk = sinkhole (doline)
skst = sinking stream
ks = karst spring
2. Hillslope

hs = headscar
ds = debris-slide scar
ls = landslide scar undifferentiated
rs = rotational slide (slump) scar
ts = translational slide scar
rb = rock-block slide scar
tc = terracettes
3. Other

wf = water fall
w = water, lake, reservoir
4. Spring

wt = wetland, undifferentiated
wh = wetland, heath
wm = wetland, marsh
ws = swamp
quarry (with highwall)
gravel pit
deep mine opening
strip mine (with highwall)
mine subsidence zone
rc = rock city

Scarp
Meander scroll on floodplain
Lacustrine strandline

C. Type III Criteria: - Data Reference Points

Sandwich symbols showing stratigraphy
Depth to bedrock (drilling or seismic data)
Minimum depth to bedrock (log data)
Test hole / boring
Well
RE = refusal (in test boring)
Hand-auger hole, shovel hole,
Fossil locality
Paleocurrent direction
Observation Point

Hillslope Units after Hack and Goodlett (1960)

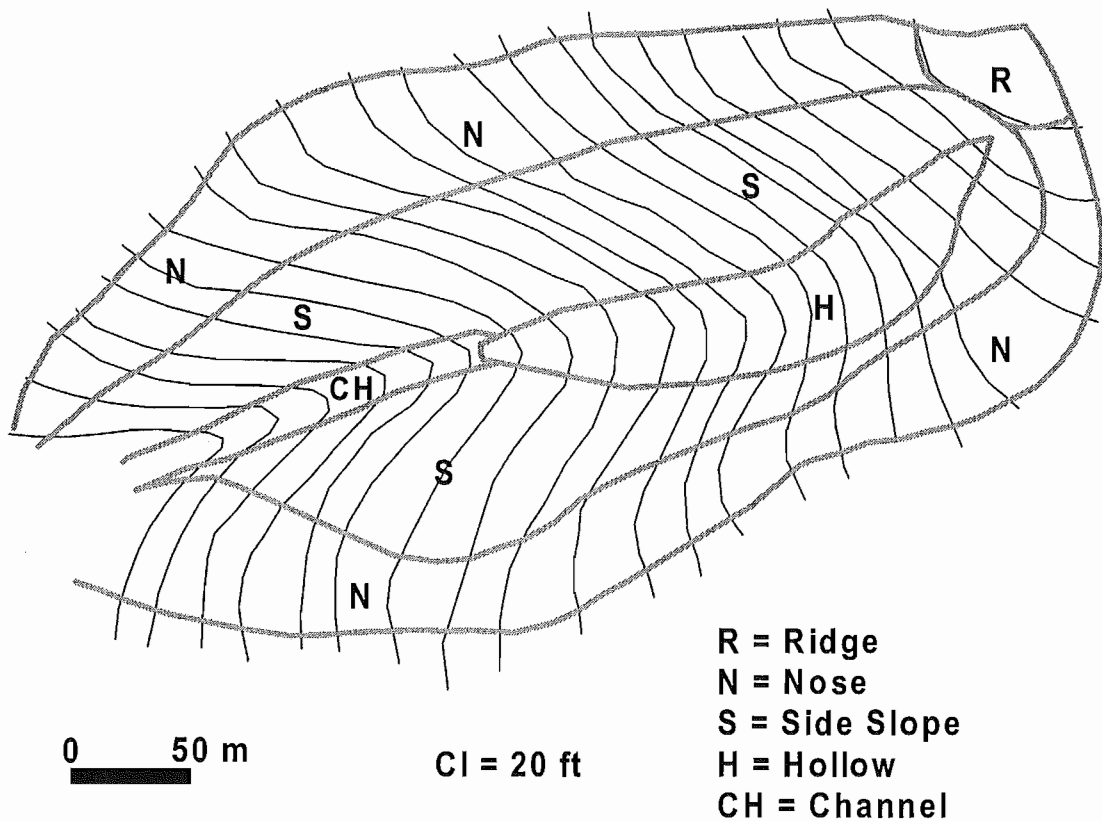




Figure 5-1. Hillslope landform elements after Hack and Goodlett (1960). Net transport flow paths are divergent on nose, convergent in hollows, and parallel on side slopes (Reneau and others, 1989). Noses represent drainage divides between zero- to first-order tributaries. Ridge crests serve as drainage divides between higher-order watersheds.

Qr	Quaternary Residuum	Qt2	Quaternary Terrace Alluvium (2-4 m)
Qc1	Quaternary Colluvium - Side slopes/noses	Qt3	Quaternary Terrace Alluvium (4-6 m)
Qc2	Quaternary Colluvium - Hollows	Hf	Historic Fan Deposits (at present grade)
	Holocene Channel Alluvium	Qf2	Quaternary Fan-Terrace Deposits (4-6 m)
	Historic Debris Slide / Flow Scar	Qf3	Quaternary Fan-Terrace Deposits (6-8 m)
Hfp2	Holocene Floodplain Alluvium (1-2 m)	Qf4	Quaternary Fan-Terrace Deposits (8-10 m)
Qt1	Quaternary Terrace Alluvium (2 m)	Qap	Quaternary Apron Deposits

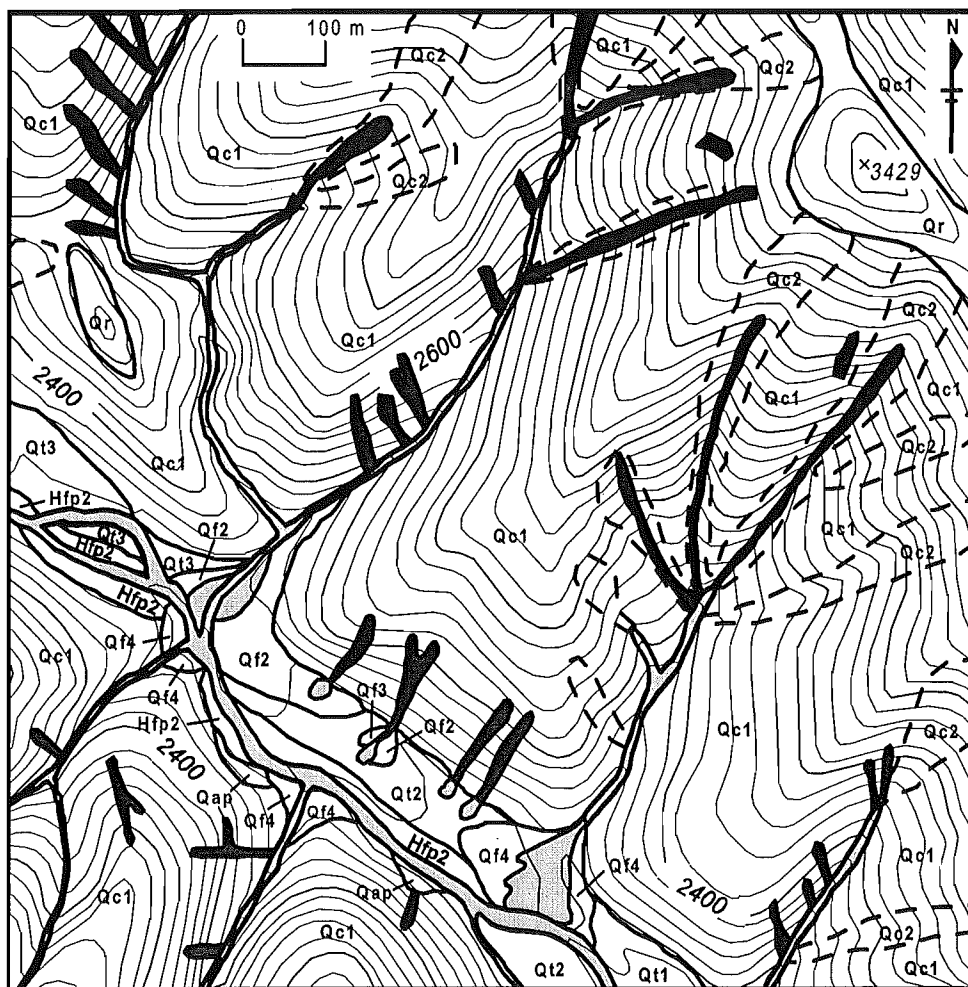
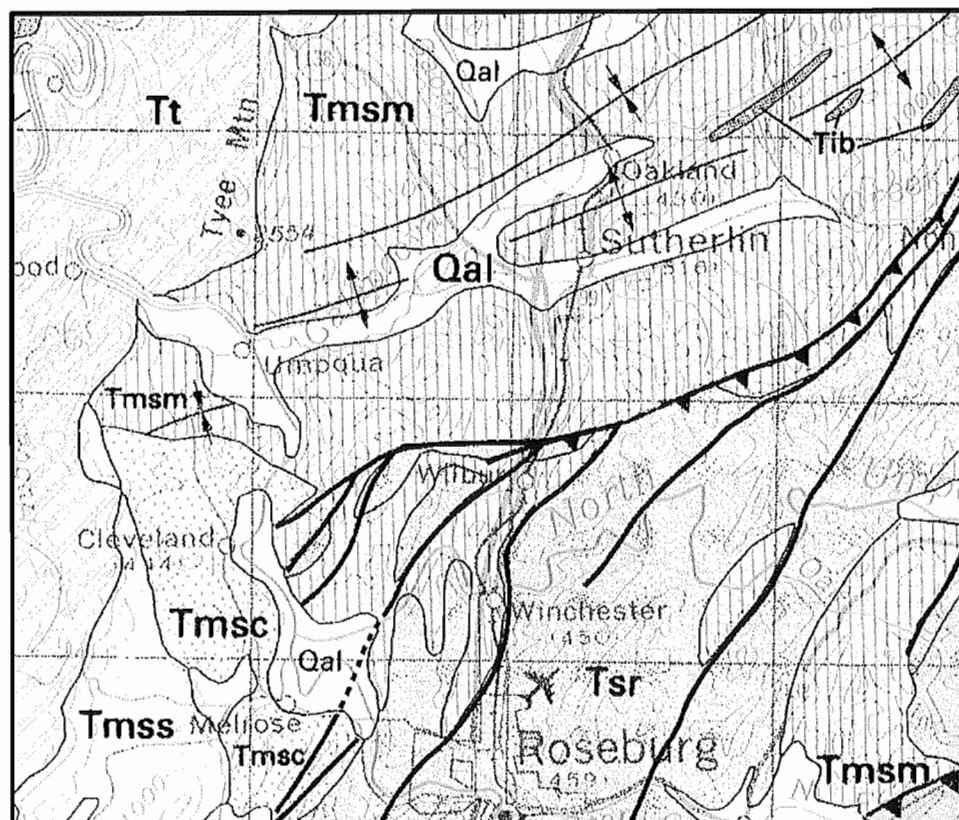
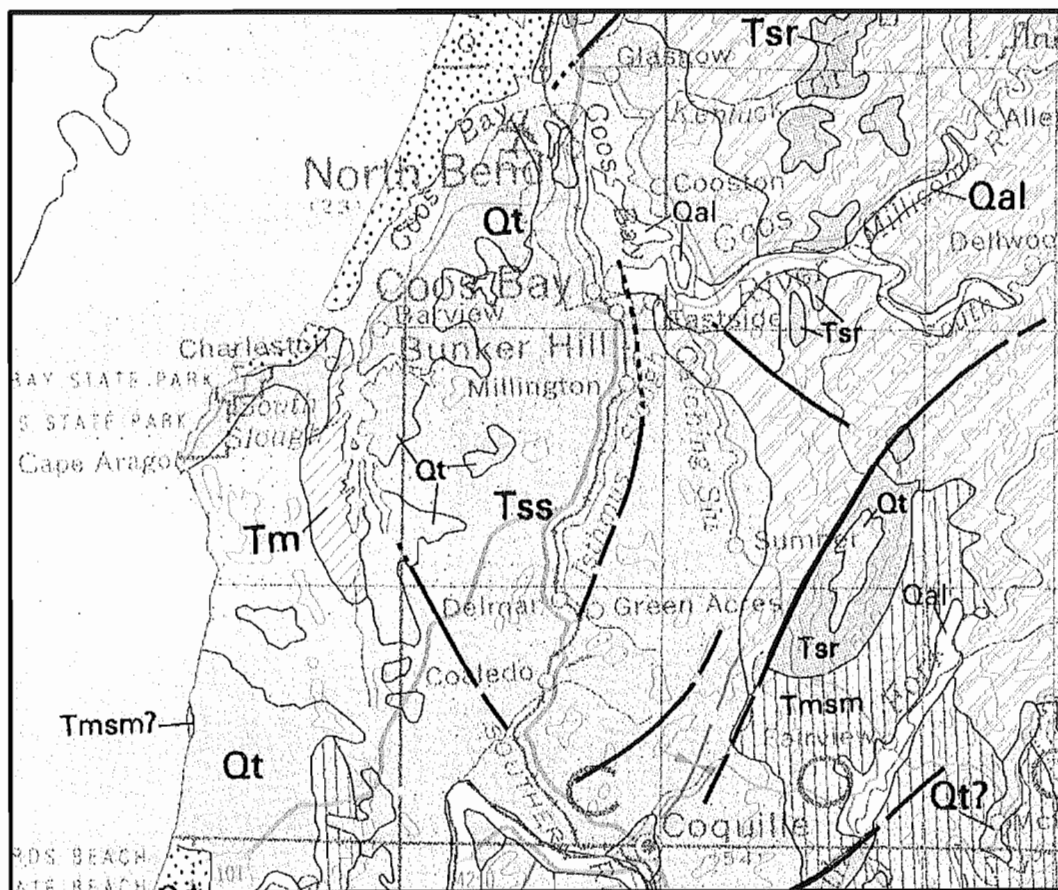


Figure 5-7. Portion of the surficial geology map for the Little River area, Augusta County, Virginia. Features were originally mapped at a scale of 1:9,600 (Taylor and Kite, 1998). Refer to Table 5-3 for an expanded explanation of map units. Contour interval = 40 ft.

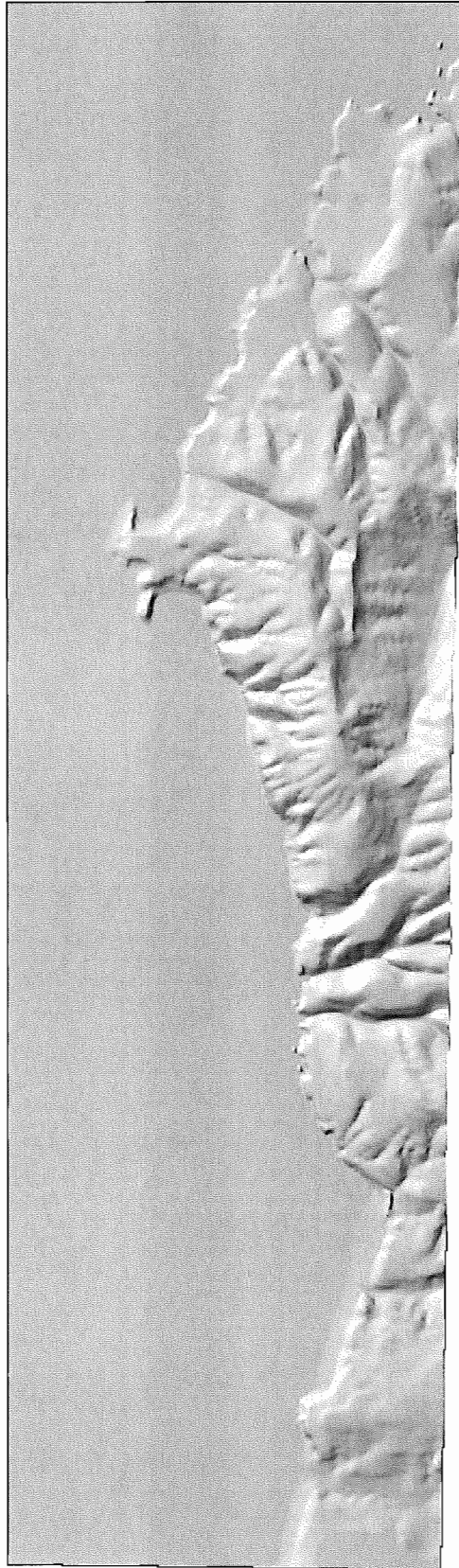
100

119

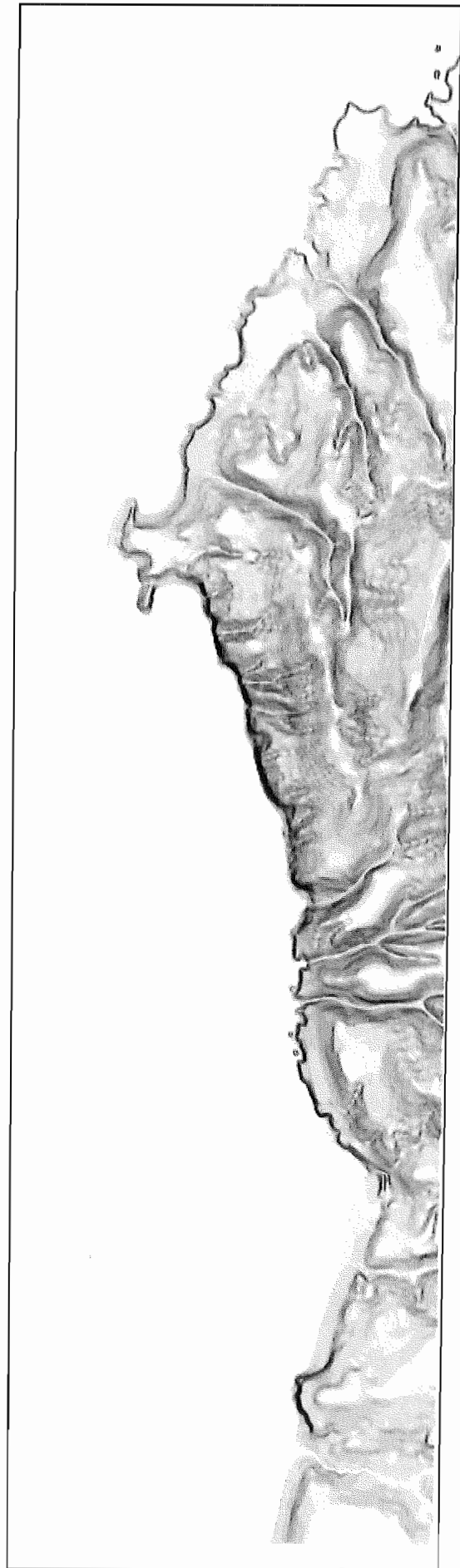
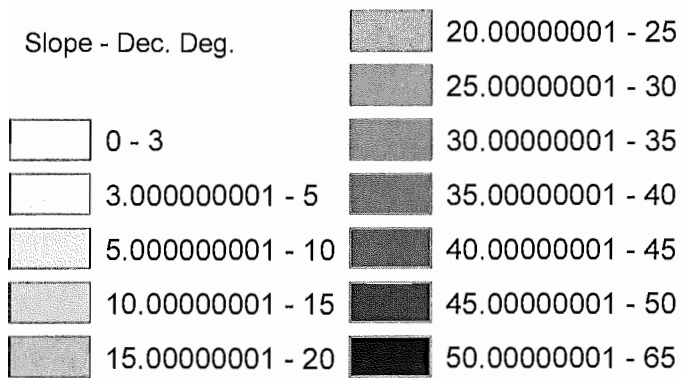
Geologic Maps of the Sunset Bay-Garden Valley Field Stops (from Walker and McLeod State Map)



10-M Hillshade Model of Cape Arago-Sunset Bay

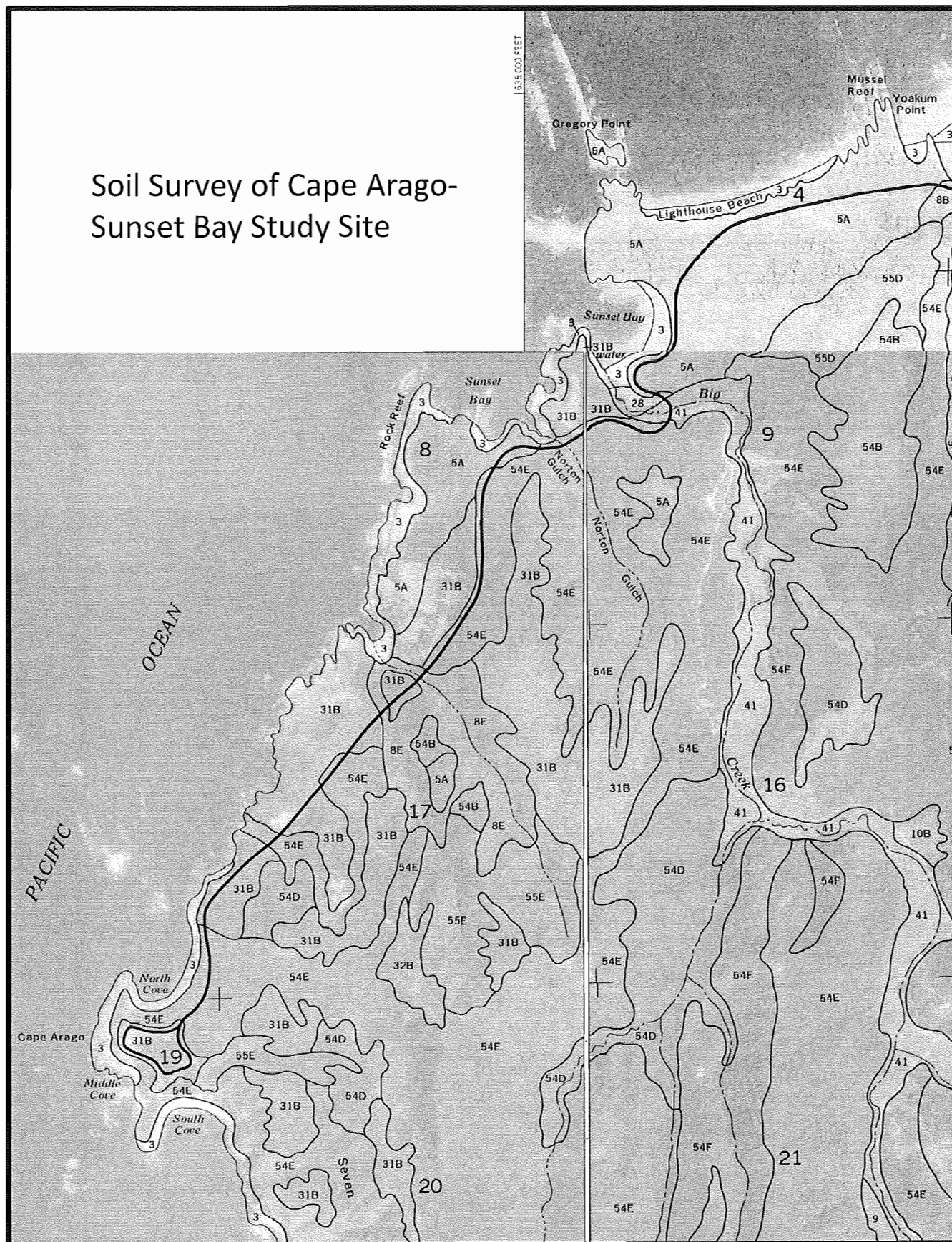


Cape Arago-Sunset Bay Slope Map

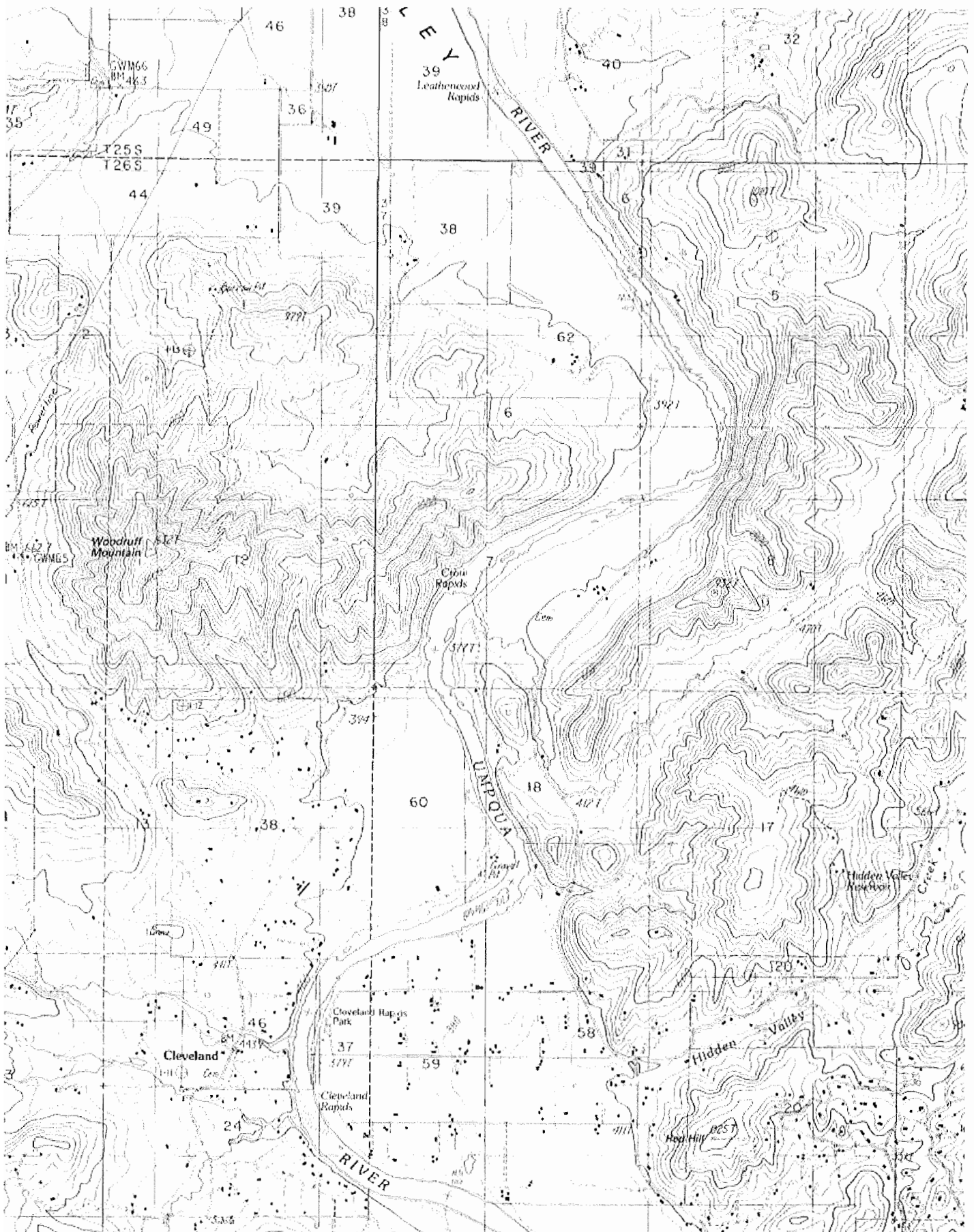


0 500 1,000 2,000 3,000 4,000 5,000 Meters

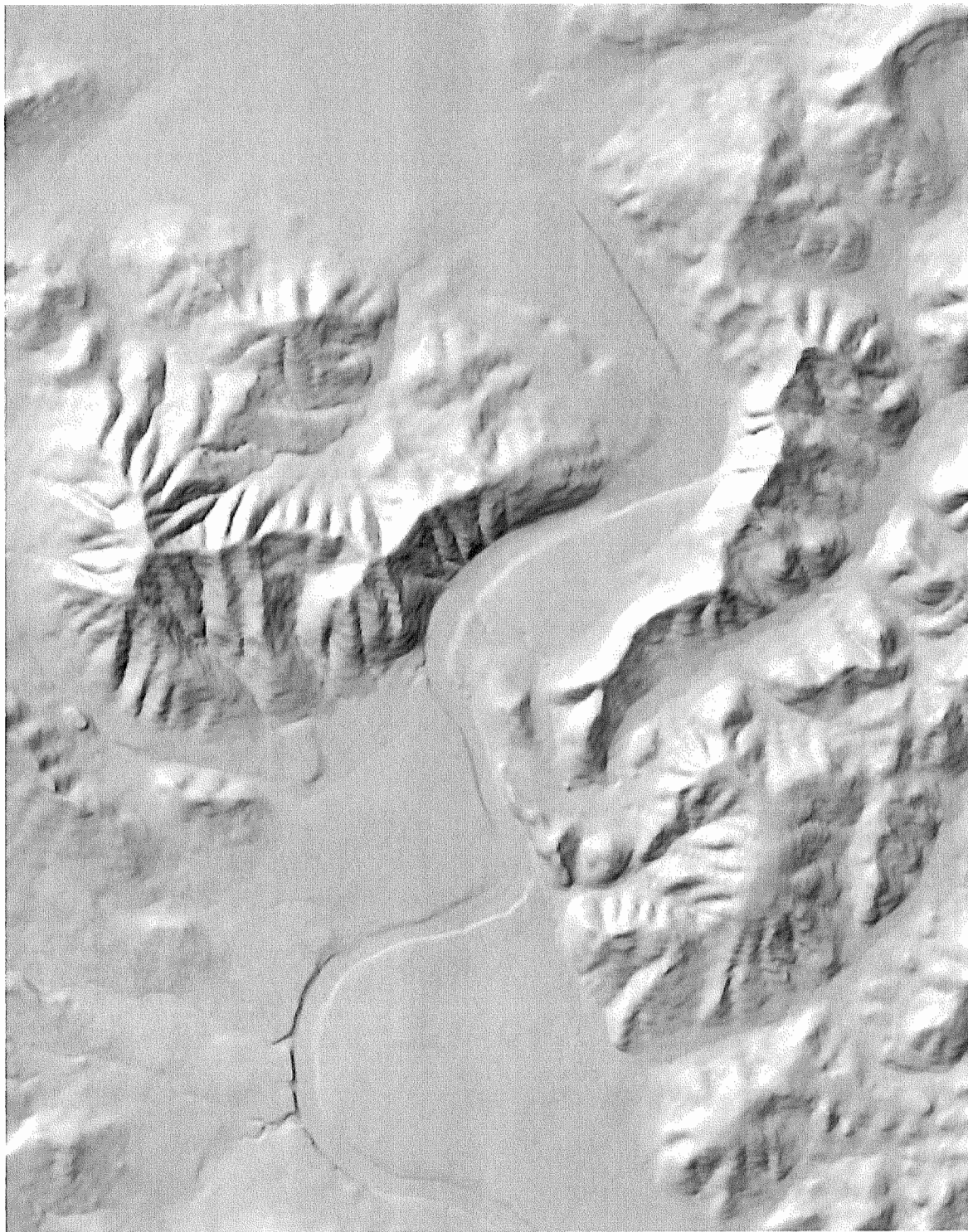
Soil Survey of Cape Arago-Sunset Bay Study Site



Garden Valley Road-Cut DRG



Hillshade Model of Garden Valley Outcrop

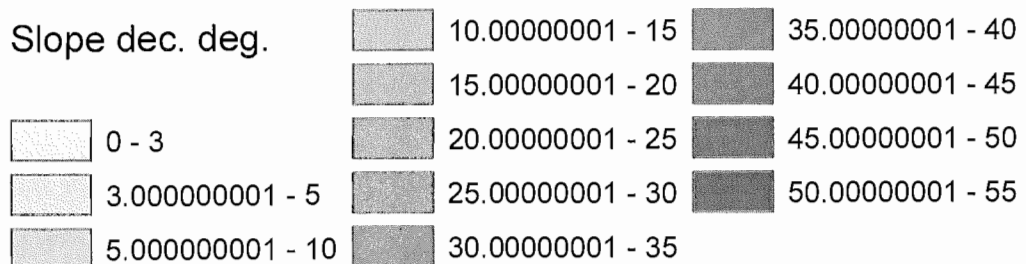


Slope Model of Garden Valley Outcrop

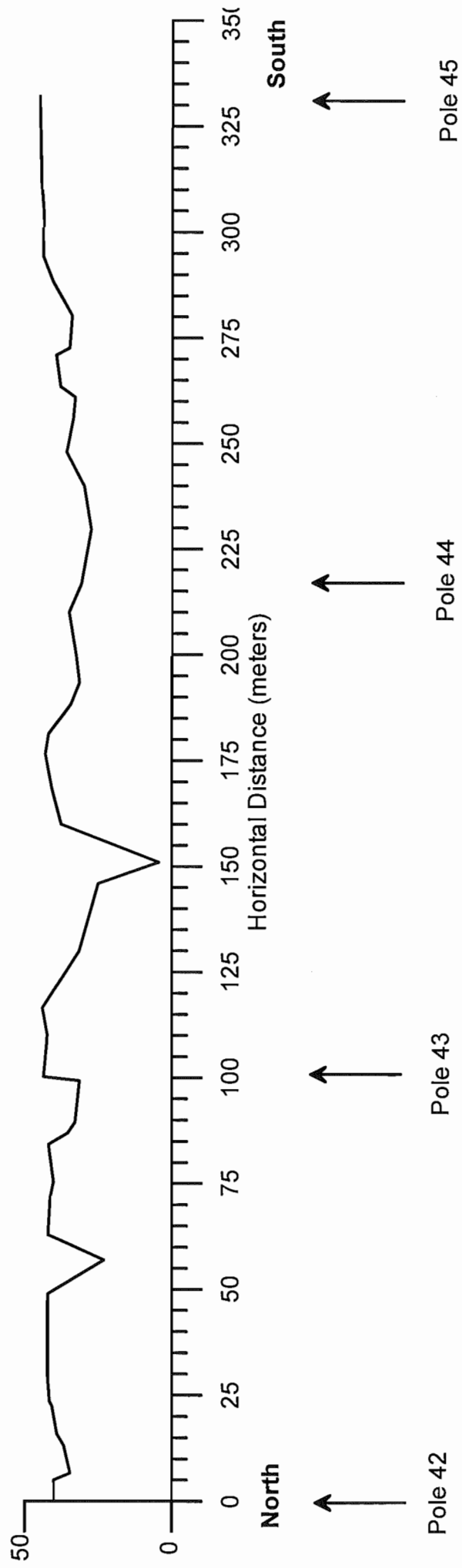


0 500 1,000 2,000 3,000 4,000 5,000 Meters

Slope dec. deg.



Garden Valley Transect



130A

Soil Survey of Coos County, Oregon

By John T. Haagen, Soil Conservation Service

Fieldwork by John T. Haagen, Mark S. Amara, Melvin D. Cheney, Jamie Kienzle, and
Fred Gelderman, Soil Conservation Service

United States Department of Agriculture, Soil Conservation Service,
in cooperation with
Oregon Agricultural Experiment Station

Coos County is in the southwestern part of Oregon. It has a total area of about 1,606 square miles, or 1,027,648 acres. Coquille, the county seat, is in the west-central part of the county, along the Coquille River. The population of the county in 1980 was about 63,200.

The eastern two-thirds of the county is steep, precipitous mountains. The west-central part is low, rolling to steep hills. A series of dissected marine terraces is along the southern coast, and an extensive dunefield is along the northern coast. The county is drained by the Coos and Coquille Rivers and their tributaries.

Timber is the main economic enterprise in the county. The climate and soils are favorable for production of Douglas fir, western hemlock, and other conifers. Agriculture is also important; it includes beef, sheep, and dairy operations.

Soil scientists determined that there are about 46 different named kinds of soil in Coos County. The soils have a wide range in texture, natural drainage, and other characteristics. In the northern and eastern three-fourths of the county, the soils are mostly well drained and loamy or clayey. Steepness of slope is the main limitation of these soils. The soils are well suited to timber. In the southwestern part of the county the soils are steep, wet, and clayey. They are subject to landslides. If well managed, the soils are well suited to pasture and timber. Along the coast the soils are gently sloping, are well drained, and are sandy throughout.

They are poorly suited to timber and pasture.

This survey area is adjacent to the Curry Area, Oregon, survey area (25). Descriptions and names of soils in this survey do not fully agree with those on soil maps for the Curry Area soil survey. Differences are the result of better knowledge of the soils, modifications of series concepts, or the extent of soils within the survey.

General Nature of the Survey Area

This section provides general information about the survey area. It briefly discusses history and development; physiography, relief, and drainage; and climate.

History and Development

Dr. Nathan Douthit, professor of history, Southwestern Oregon Community College, and Mark S. Amara, soil conservationist, Soil Conservation Service, prepared this section.

In the late 18th century the Coos County area was inhabited by five Indian groups. The Lower Umpqua Indians inhabited the area north of Tenmile Lake. The territory of the Hanis Indians extended from Tenmile Lake to the vicinity of Empire, on Coos Bay. They include all of the upper estuary, sloughs, and river systems of Coos Bay. The Milluk, or Lower Coquille, Indians occupied the lower reaches of the Coquille River from Beaver Slough to Bandon and along the coast as far north as Cape Arago. They also occupied

131

General Soil Map Units

The general soil map at the back of this publication shows broad areas that have a distinctive pattern of soils, relief, and drainage. Each map unit on the general soil map is a unique natural landscape. Typically, a map unit consists of one or more major soils or miscellaneous areas and some minor soils or miscellaneous areas. It is named for the major soils or miscellaneous areas. The soils or miscellaneous areas making up one unit can occur in other units but in a different pattern.

The general soil map can be used to compare the suitability of large areas for general land uses. Areas of suitable soils or miscellaneous areas can be identified on the map. Likewise, areas that are not suitable can be identified.

Because of its small scale, the map is not suitable for planning the management of a farm or field or for selecting a site for a road or building or other structure. The soils in any one map unit differ from place to place in slope, depth, drainage, and other characteristics that affect management.

The general map units in this survey have been grouped into general kinds of landscape for broad interpretive purposes. Each of the broad groups and the map units in each group are described in the following pages.

Map Unit Descriptions

Soils on Dunes, in Deflation Basins, and on Marine Terraces

This group consists of two map units. It makes up about 7 percent of the survey area.

1. Dune Land-Waldport-Heceta

Dune land and sandy, excessively drained and poorly drained soils that formed in eolian material; on sand dunes and in deflation basins

This map unit is on dune ridges and in deflation

basins. Barren dune ridges generally are linear and are oriented west to east. The north-facing slopes are short and steep, and the south-facing slopes are longer and moderately steep. Older vegetated dunes are hilly and are gently sloping to steep. A nearly level deflation basin is between the dune ridges and the ocean (fig. 1). Elevation ranges from 0 to 160 feet. Slopes range from 0 to 70 percent. The average annual precipitation is 50 to 70 inches, the average annual air temperature is 51 to 53 degrees F, and average frost-free period is 200 to 240 days.

This unit makes up about 3 percent of the survey area. It is about 30 percent Dune land, 29 percent Waldport soils, and 18 percent Heceta soils. The rest is components of minor extent.

Dune land is barren ridges of sand on the leeward side of deflation basins. It is also in scattered areas within the older wooded dunes, where the vegetation has been removed. Areas of Dune land are dark yellowish brown fine sand throughout.

Waldport soils are excessively drained. They are on stabilized sand dunes on the leeward side of deflation basins. These soils have a dark grayish brown fine sand surface layer and a dark yellowish brown fine sand subsoil.

Heceta soils are poorly drained. They are in deflation basins. These soils have a very dark grayish brown fine sand surface layer and a mottled, grayish brown sand subsoil.

Of minor extent in this unit are somewhat poorly drained Yaquina soils on low terraces; well drained Netarts soils on old stabilized sand dunes; very poorly drained Clatsop soils, Fluvaquents, and Histosols on tidal flats; and coastal Beaches.

This unit is used mainly for recreation, timber production, and wildlife habitat. About 10 percent of the unit is used as homesites.

The hazard of soil blowing, the hazard of ground water pollution, and droughtiness are the main limitations for recreational and urban development. Maintaining plant cover prevents soil blowing. Sewer

132



Figure 1.—Area of general soil map unit 1. Heceta soils in nearly level deflation basin in background; barren Dune land in foreground.

systems should be used to prevent contamination of ground water. Irrigation is needed to maintain lawn grasses and shrubs.

The soils in this unit are poorly suited to timber production. Productivity is very low because of the high winds and very low soil fertility. The vegetation is dominantly shore pine; some Douglas fir is in protected areas.

2. Bullards-Bandon-Blacklock

Well drained and poorly drained, loamy and sandy soils that formed in marine sediment; on marine terraces

This map unit is on a series of dissected marine terraces that parallel the coast and extend inland 2 to 4 miles. Most areas of this unit are drained by small streams that flow directly into the ocean. Elevation

133

ranges from 25 to 600 feet. Slopes range from 0 to 50 percent. The average annual precipitation is 50 to 80 inches, the average annual air temperature is 51 to 53 degrees F, and the frost-free period is 200 to 240 days.

This unit makes up about 4 percent of the survey area. It is about 58 percent Bullards soils, 20 percent Bandon soils, and 18 percent Blacklock soils. The rest is soils of minor extent.

Bullards soils are well drained. They are in the more highly dissected areas of marine terraces and on steep slopes along drainageways. These soils have a very dark grayish brown sandy loam surface layer and a dark reddish brown to strong brown gravelly sandy loam subsoil.

Bandon soils are well drained. They are in broad, gently sloping to moderately sloping areas of marine terraces. These soils have a dark grayish brown sandy loam surface layer and a dark reddish brown to strong brown sandy loam subsoil that is cemented below a depth of 30 inches.

Blacklock soils are poorly drained. They are in nearly level depressional areas of marine terraces. These soils have a black fine sandy loam surface layer and a mottled, strong brown to yellowish brown sand subsoil that is cemented below a depth of 15 inches.

Of minor extent are well drained Nehalem soils and poorly drained Nestucca soils on flood plains and poorly drained Joeney soils on older marine terraces.

This unit is used mainly for timber production and as wildlife habitat and homesites. Some areas are used for pasture and cranberry production.

Slow permeability, slope, and droughtiness are the main limitations. Septic tank filter fields do not function properly where the subsoil is cemented or wet. Slope restricts development in some areas. Irrigation is required for maximum production of pasture grasses and for maintenance of lawns and shrubs.

The soils in this unit are suited to timber production. Productivity is low because of low soil fertility and high winds from the Pacific Ocean. As a result, these soils are not intensively managed for timber production. The dominant tree species are Douglas fir, Sitka spruce, shore pine, and Port Orford cedar.

Soils on Flood Plains and Terraces

This group consists of two map units. It makes up about 5 percent of the survey area.

3. Coquille-Nestucca-Langlois

Somewhat poorly drained and very poorly drained, silty and clayey soils that formed in alluvium; on flood plains

This map unit is on flood plains along the lower reaches of major rivers and coastal streams. It is subject to flooding during high tides. Elevation ranges from 0 to 40 feet. Slopes range from 0 to 3 percent. The average annual precipitation is 50 to 80 inches, the average annual air temperature is 51 to 53 degrees F, and the frost-free period is 200 to 240 days.

This map unit makes up about 3 percent of the survey area. It is about 22 percent Coquille soils, 19 percent Nestucca soils, and 14 percent Langlois soils. The rest is soils of minor extent.

Coquille soils are very poorly drained. They are in nearly level areas of flood plains. These soils have a very dark grayish brown silt loam surface layer over dark grayish brown and olive gray silty clay loam.

Nestucca soils are somewhat poorly drained. They are in depressional areas. These soils have a mottled, dark brown silt loam surface layer and a mottled, dark grayish brown silty clay loam subsoil.

Langlois soils are very poorly drained. They are in depressional areas. They have a mottled dark grayish brown silty clay loam surface layer over dark grayish brown and dark gray silty clay and clay.

Of minor extent in this unit are well drained Nehalem soils on slightly higher elevations of flood plains; poorly drained, clayey Chetco soils and loamy Willanch soils in depressional areas; and very poorly drained Brallier soils in old stream channels.

This unit is used mainly for hay and pasture.

The main limitations are the susceptibility of the surface layer to compaction, wetness, the hazard of flooding, and high humidity. Grazing when the soil is wet results in compaction of the surface layer and poor tilth. Drainage is needed for maximum production of pasture grasses. Flooding restricts grazing in winter. High humidity and frequent periods of rainfall prevent the curing of high-quality hay.

4. Kirkendall-Chismore-Wintley

Well drained and somewhat poorly drained, silty and clayey soils that formed in alluvium; on flood plains and stream terraces

This map unit is on flood plains and terraces along the upper reaches of major rivers and streams. The flood plains are subject to frequent periods of flooding in fall and winter. Elevation ranges from 20 to 750 feet. Slopes range from 0 to 30 percent. The average annual precipitation is 60 to 90 inches, the average annual air temperature is 50 to 53 degrees F, and the frost-free period is 180 to 220 days.

This unit makes up about 2 percent of the survey

134



Figure 2.—Area of general soil map unit 5.

area. It is about 36 percent Kirkendall soils, 22 percent Chismore soils, and 19 percent Wintley soils. The rest is soils of minor extent.

Kirkendall soils are well drained. They are on flood plains. These soils have a dark brown silt loam surface layer and a dark brown and brown silt loam subsoil.

Chismore soils are somewhat poorly drained. They are on intermediate terraces. These soils have a very dark grayish brown silt loam surface layer and a mottled, brown and yellowish brown silty clay loam subsoil.

Wintley soils are well drained. They are on older high terraces. These soils have a dark brown silt loam surface layer and a strong brown silty clay and silty clay loam subsoil.

Of minor extent in this unit are poorly drained

Quosatana soils on flood plains; poorly drained Zyzug soils and well drained Ellertsen soils on low terraces; somewhat excessively drained Gaudy Variant soils, well drained Meda soils, and poorly drained Pyburn soils on intermediate terraces; and moderately well drained McCurdy soils on high terraces.

This unit is used mainly for hay and pasture and homesite development. Most areas of this unit have been cleared. Beef and dairy cattle are the main livestock enterprises. Homesites are mainly on terraces.

Susceptibility of the surface layer to compaction, droughtiness in summer, flooding, and high humidity are the main limitations of this unit for hay and pasture. Grazing when the soil is wet results in compaction of the surface layer and poor tilth. Irrigation is needed for maximum production of pasture grasses. Flooding

135

restricts grazing on flood plains in winter. High humidity and frequent periods of rainfall prevent the production of high-quality hay.

Wetness and slow permeability are the main limitations of this unit for homesite development. Septic tank absorption fields may not function properly during rainy periods.

Soils on Low Hills

This group consists of four map units. It makes up about 27 percent of the survey area.

5. Rinearson-Etelka

Well drained and moderately well drained silty and clayey soils that formed in colluvium and residuum derived from sedimentary rock

This map unit is on low foothills on the west side of the Klamath Mountains (fig. 2). Slopes generally are long and irregular. Areas of Rock outcrop and slumps are common. Elevation ranges from 50 to 1,800 feet. Slopes range from 0 to 70 percent. The average annual precipitation is 60 to 85 inches, the average annual air temperature is 50 to 54 degrees F, and the frost-free period is 180 to 240 days.

This unit makes up about 5 percent of the survey area. It is about 72 percent Rinearson soils and 15 percent Etelka soils. The rest is soils of minor extent.

Rinearson soils are well drained. They are on steep side slopes and on rounded ridgetops. These soils have a dark reddish brown silt loam surface layer and a reddish brown and dark reddish brown silty clay loam subsoil.

Etelka soils are moderately well drained. They are on ridgetops, benches, and low gradient side slopes. These soils have a dark grayish brown silt loam surface layer. The upper part of the subsoil is dark brown silty clay loam, and the lower part is mottled, olive brown silty clay.

Of minor extent in this unit are deep, well drained, gravelly Remote soils on steep side slopes; deep, well drained Orford soils on broad ridgetops; moderately deep, well drained, gravelly Digger soils on steep side slopes; and somewhat poorly drained Whobrey soils on benches.

This unit is used for timber production, wildlife habitat, and pasture. About 20 percent of the unit has been cleared for pasture. The main livestock enterprises are beef cattle and sheep. The susceptibility of the surface layer to compaction and landslide potential are the main limitations. Grazing when the soil

is wet results in compaction of the surface layer. Forage production is low in summer because of droughtiness. Livestock facilities should be placed in areas that are not subject to landslides.

The soils in this unit are suited to trees. Productivity is moderate. Using wheeled vehicles causes compaction of the surface layer. Cable yarding systems damage the soil less. Roadcuts may increase the hazard of landsliding and slumping if road systems are not carefully planned and constructed. The dominant tree species are Douglas fir, Port Orford cedar, western hemlock, and western redcedar.

6. Etelka-Whobrey

Moderately well drained and somewhat poorly drained, clayey soils that formed in colluvium and residuum derived from sedimentary rock

This map unit is on low foothills on the north side of the Klamath Mountains (fig. 3). Hilltops generally are broad and have irregular and short to long slopes because of numerous landslides and slumps. Elevation ranges from 100 to 1,800 feet. Slopes range from 7 to 60 percent. The average annual precipitation is 60 to 80 inches, the average annual air temperature is 50 to 54 degrees F, and the average frost-free period is 180 to 220 days.

This unit makes up about 6 percent of the survey area. It is about 45 percent Etelka soils and 19 percent Whobrey soils. The rest is components of minor extent.

Etelka soils are moderately well drained. They are on broad ridgetops and foot slopes. These soils have a dark grayish brown silt loam surface layer. The upper part of the subsoil is dark brown silty clay loam, and the lower part is mottled, olive brown silty clay.

Whobrey soils are somewhat poorly drained. They are in depressional areas on broad ridgetops and on benches. These soils have a brown and dark brown silt loam surface layer and a mottled, dark yellowish brown silt loam subsoil. Below this is mottled, very dark gray clay.

Of minor extent in this unit are well drained, gravelly Remote and Digger soils on steep side slopes, well drained Preacher soils on ridgetops, and Rock outcrop.

This unit is used for timber production, wildlife habitat, and pasture. About 35 percent of the unit has been cleared for pasture. The main livestock enterprise is raising sheep. Most of the cleared areas are on hilltops and lower foot slopes. The steeper side slopes are dominantly in timber. Slope, the hazard of erosion, susceptibility of the surface layer to compaction, and landslide potential are the main limitations. Grazing

136

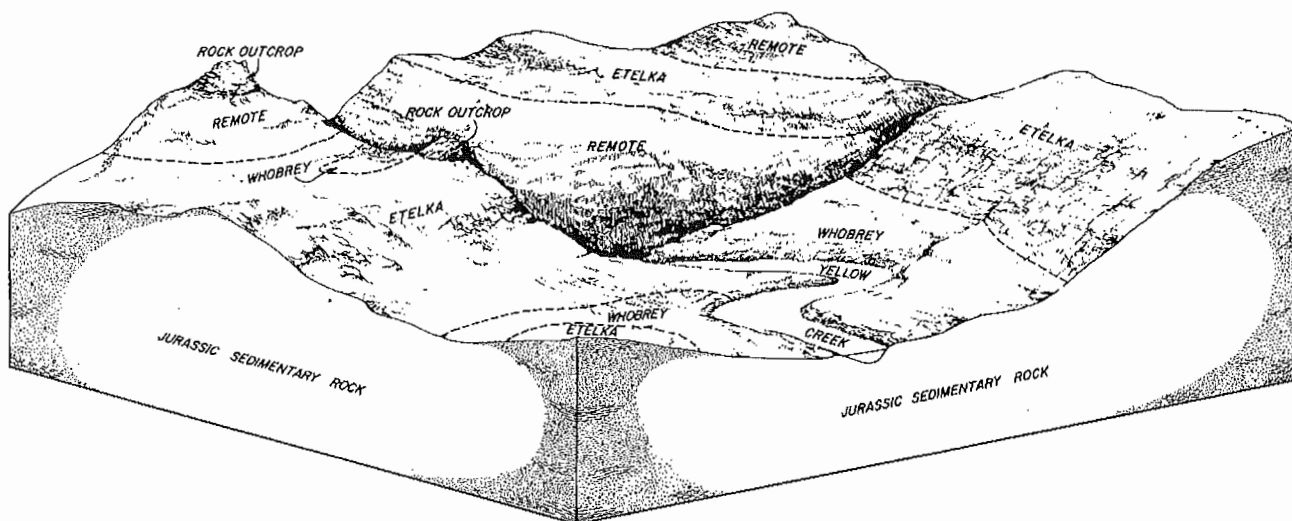


Figure 3.—Cross section of part of the Klamath Mountains, showing relationship of soils, relief, and parent material in general soil map unit 6.

when the soil is wet results in compaction of the surface layer. Livestock facilities should be placed in areas that are not subject to landslides.

The soils in this unit are suitable for trees. Use of wheeled vehicles for harvesting timber causes compaction of the surface layer. Cable yarding systems damage the soil less and are safer in the steeper areas. Erosion is a hazard along logging roads and skid trails, and maintenance costs in these areas are higher because of the landslide potential. The dominant tree species are Douglas fir, grand fir, and Port Orford cedar.

7. Templeton-Salander

Well drained, loamy soils that formed in colluvium derived from sedimentary rock

This map unit is on low foothills on the west side of the Coast Range. The ridgetops are rounded and have moderate, uniform side slopes. Most of this unit is drained by small intermittent streams that drain into sloughs and major streams. Elevation ranges from 50 to 800 feet. Slopes range from 0 to 75 percent. The average annual precipitation is 60 to 80 inches, the average annual air temperature is 51 to 53 degrees F, and the frost-free period is 200 to 240 days.

This unit makes up about 11 percent of the survey area. It is about 69 percent Templeton soils and 17 percent Salander soils. The rest is soils of minor extent.

Templeton soils are well drained. They are on

ridgetops and side slopes. These soils have a very dark brown and dark brown silt loam surface layer and a reddish brown to strong brown silty clay loam subsoil.

Salander soils are well drained. They are on side slopes. These soils have a dark reddish brown silt loam surface layer and a dark reddish brown and reddish brown silty clay loam subsoil.

Of minor extent are well drained Geisel and Millicoma soils on hilltops and side slopes; well drained, sandy Bullards soils on escarpments of marine terraces; poorly drained Joeney soils on marine terraces; and poorly drained Nestucca soils and well drained Nehalem soils on flood plains.

This unit is used mainly for timber production and wildlife habitat. Some areas are used for pasture and homesite development. About 10 percent of the unit has been cleared for pasture. The main livestock enterprises are beef and dairy cattle. Susceptibility of the surface layer to compaction, depth to bedrock, slow permeability, and slope are the main limitations. Grazing when the soil is wet results in compaction of the surface layer and poor tilth. Use of the soils in this unit as homesites is limited by the steepness of slope. Septic tank absorption fields may function poorly because of the slow permeability and shallow depth of the soils.

The soils in this unit are suited to trees. Productivity is high. Susceptibility of the surface layer to compaction, steepness of slope, and the hazard of erosion are the main limitations. Using standard

wheeled and tracked equipment causes compaction of the surface layer. Cable yarding systems damage the soil less and are safer in the steeper areas. Erosion is a hazard along logging roads and skid trails. The dominant tree species are Douglas fir, Sitka spruce, western hemlock, and western redcedar.

8. Honeygrove-Blachly-Dement

Well drained, clayey soils that formed in colluvium and residuum derived from sedimentary and igneous rock

This map unit is on low rounded foothills on the west side of the Coast Range. The hills and ridges are more rounded in the lower lying areas near major drainageways but are steeper and more irregular in the higher lying areas. Elevation ranges from 20 to 1,000 feet. Slopes range from 0 to 70 percent. The average annual precipitation is 55 to 85 inches, the average annual air temperature is 50 to 53 degrees F, and the frost-free period is 140 to 240 days.

This unit makes up about 5 percent of the survey area. It is about 33 percent Honeygrove soils, 31 percent Blachly soils, and 31 percent Dement soils. The rest is soils of minor extent.

Honeygrove soils are well drained. They are on broad ridgetops and moderate side slopes. These soils have a dark reddish brown silty clay loam surface layer and a subsoil of dark red and red clay over gravelly clay.

Blachly soils are well drained. They are on broad ridgetops and benches. They have a very dusky red silty clay loam surface layer and a dark red and yellowish red silty clay and silty clay loam subsoil.

Dement soils are well drained. They are on ridgetops and side slopes. These soils have a very dark grayish brown silt loam surface layer and a reddish brown silty clay loam subsoil.

Of minor extent are extremely gravelly Harrington soils on steep side slopes, loamy Preacher soils on benches and side slopes, moderately deep, gravelly Bohannon soils on steep side slopes, and well drained Kirkendall soils on flood plains.

This unit is used mainly for timber production and wildlife habitat. It is also used for pasture and homesite development. About 20 percent of the unit has been cleared for pasture. Homesites and pasture are mainly on the Dement and Honeygrove soils.

Susceptibility of the surface layer to compaction, slope, and moderately slow permeability are the main limitations. Grazing when the soil is wet results in compaction of the surface layer and poor tilth.

Steepness of slope limits the installation of septic tank absorption fields. Absorption fields may not function properly during rainy periods because of the moderately slow permeability of the subsoil.

The soils in this unit are suited to trees. Productivity is moderately high. Susceptibility of the surface layer to compaction and the hazard of erosion are the main limitations. Using standard wheeled and tracked equipment causes compaction of the surface layer. Cable yarding systems damage the soil less and are safer in the steeper areas. Erosion is a hazard along logging roads and skid trails. The dominant tree species are Douglas fir, western hemlock, western redcedar, and grand fir.

Soils on Mountains

This group consists of five map units. It makes up about 61 percent of the survey area.

9. Milbury-Bohannon-Umpcoos

Moderately deep and shallow, gravelly and loamy soils that formed in colluvium derived from sedimentary rock

This map unit on is strongly dissected areas of mountains. It has long, uniform slopes and very narrow ridgetops. Benches are present in some areas. Most areas of the unit are drained by small intermittent streams that have steep gradients. Elevation ranges from 100 to 2,500 feet. Slopes range from 30 to 80 percent. The average annual precipitation is 60 to 100 inches, the average annual air temperature is 45 to 53 degrees F, and the frost-free period is 110 to 200 days.

This unit makes up about 13 percent of the survey area. It is about 40 percent Milbury soils, 27 percent Bohannon soils, and 22 percent Umpcoos soils. The rest is components of minor extent.

Milbury soils are moderately deep. They are on midslopes and upper side slopes. These soils have a black very gravelly sandy loam surface layer and a very dark grayish brown and dark brown very cobbly loam subsoil.

Bohannon soils are moderately deep. They are on concave midslopes and lower side slopes. These soils have a very dark brown loam surface layer and a dark yellowish brown gravelly loam subsoil.

Umpcoos soils are shallow. They are on convex side slopes adjacent to areas of Rock outcrop and on narrow ridgetops. These soils have a dark grayish brown very gravelly sandy loam surface layer and a brown very gravelly sandy loam subsoil.

Of minor extent are deep Preacher and Blachly soils

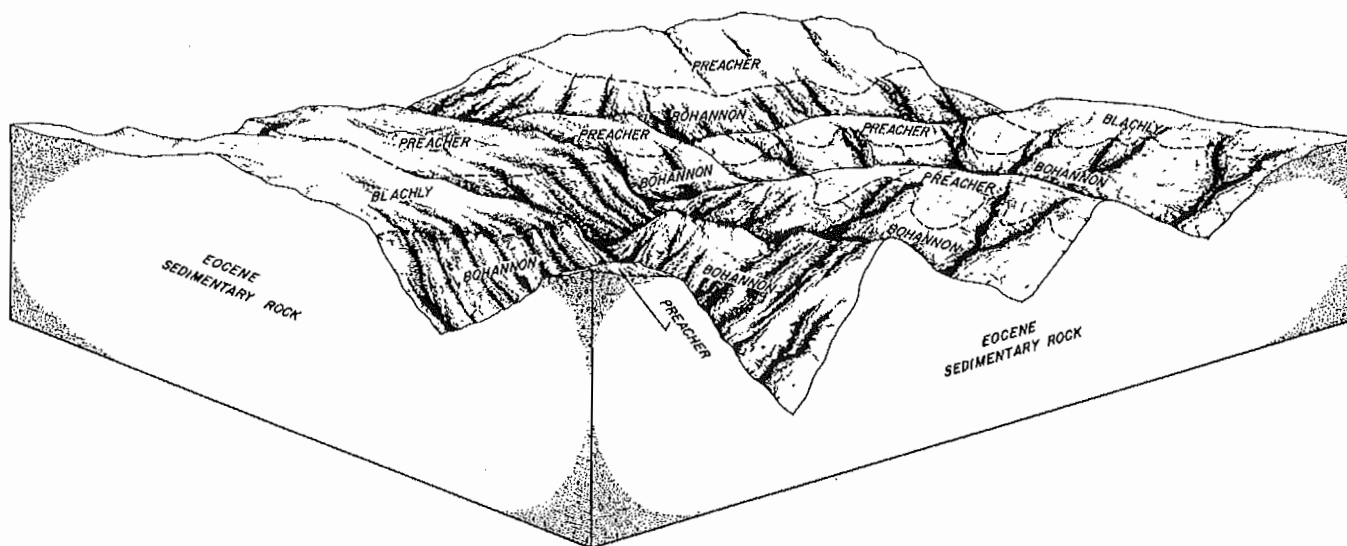


Figure 4.—Cross section of part of the deeply dissected Coast Range, showing relationship of soils, relief, and parent material in general soil map unit 10.

on slump benches, well drained Gardiner soils on flood plains, and Rock outcrop.

This unit is used for timber production and wildlife habitat.

The main limitations are steepness of slope and the hazard of erosion. Steepness of slope restricts the use of logging equipment. Erosion is a hazard along logging roads and skid trails. Productivity is moderately high. The dominant tree species are Douglas fir and western hemlock.

10. Preacher-Bohannon

Deep and moderately deep, moderately steep to very steep, gravelly and loamy soils that formed in colluvium and residuum derived from sedimentary rock

This unit consists of high mountains (fig. 4). The areas along major drainageways are very steep, and the ridgetops are broad and moderately steep. Slump benches are common in the steeper areas. Elevation ranges from 250 to 3,800 feet. Slopes range from 3 to 90 percent. The average annual precipitation is 60 to 100 inches, the average annual air temperature is 45 to 53 degrees F, and the frost-free period is 110 to 200 days.

This map unit makes up about 23 percent of the survey area. It is about 48 percent Preacher soils and 32 percent Bohannon soils. The rest is components of minor extent.

Preacher soils are deep. They are on side slopes and ridgetops. These soils have a very dark grayish brown and dark brown loam surface layer and a dark yellowish brown clay loam subsoil.

Bohannon soils are moderately deep. They are on the steep side slopes. These soils have a very dark brown and dark brown loam surface layer and a dark yellowish brown gravelly clay loam subsoil.

Of minor extent in this unit are the deep, well drained Blachly soils on ridgetops and slump benches, moderately deep Milbury soils on very steep side slopes, shallow Umpcoos soils on narrow ridgetops, and Rock outcrop.

This unit is used for timber production and wildlife habitat. The main limitations are steepness of slope, susceptibility of the surface layer to compaction, and the hazard of erosion. Steepness of slope restricts the use of logging equipment. Using standard wheeled and tracked equipment causes compaction of the surface layer. Cable yarding systems damage the soil less and are safer in the steeper areas. Erosion is a hazard along logging roads and skid trails. Productivity is high. The dominant tree species are Douglas fir, western hemlock, and western redcedar (fig. 5).

11. Digger-Preacher-Remote

Deep and moderately deep, moderately steep to very steep, gravelly and loamy soils that formed in colluvium and residuum derived from sedimentary rock

about 1.5 to 3.5 inches. Effective rooting depth is 12 to 24 inches. Runoff is very slow, and the hazard of water erosion is slight. The water table fluctuates from 6 inches above the surface to 30 inches below the surface from October to May.

This unit is used mainly for timber production and wildlife habitat. Areas of the Bandon soil are also used for pasture, recreation, and homesite development.

The Bandon soil is suited to the production of Douglas fir. Among the other species that grow on this soil are Sitka spruce, western hemlock, red alder, and western redcedar. The understory vegetation is mainly salal, evergreen huckleberry, western brackenfern, and Pacific waxmyrtle.

The Blacklock soil is suited to the production of shore pine. Among the other species that grow on this soil are Sitka spruce, western hemlock, and Port Orford cedar. The understory vegetation is mainly salal, evergreen huckleberry, Pacific rhododendron, manzanita, and slough sedge.

On the basis of a 100-year site curve, the mean site index for Douglas fir is 137 on the Bandon soil. At the culmination of the mean annual increment (CMAI), the production of 60-year-old Douglas fir trees 1.5 inches in diameter or more at breast height is 140 cubic feet per acre per year. On the basis of a 50-year site curve, the mean site index for Douglas fir is 105.

On the basis of a 100-year site curve, the mean site index for shore pine is 90 on the Blacklock soil. At the culmination of the mean annual increment (CMAI), the production of 60-year-old shore pine trees 1.5 inches in diameter or more at breast height is 79 cubic feet per acre per year.

High winds from the Pacific Ocean may seriously limit the growth of trees on this unit unless the trees are in a protected area.

The main limitations for the management of timber on this unit are the hazard of windthrow, seasonal wetness on the Blacklock soil, and plant competition on the Bandon soil. Windthrow is a hazard when the soil is wet and winds are strong. Tree roots are restricted by the cemented layer in the soils. The seasonal high water table in the Blacklock soil limits the use of equipment during wet periods. When openings are made in the canopy, invading brushy plants can delay natural reforestation. Undesirable plants reduce natural or artificial reforestation unless intensive site preparation and maintenance are provided. Reforestation can be accomplished by planting Douglas fir seedlings on the Bandon soil and shore pine seedlings on the Blacklock soil. Tree seedlings on the Blacklock soil have only a

moderate rate of survival because of the seasonal high water table.

If this unit is used for pasture, the main limitations are the droughtiness of the Bandon soil in summer and the wetness of the Blacklock soil. Supplemental irrigation is needed for maximum production on the Bandon soil. Sprinkler irrigation is a suitable method of applying water. Use of this method permits the even, controlled application of water. Water should be applied in amounts sufficient to wet the root zone but small enough to minimize the leaching of plant nutrients. Applications of water should be adjusted to the available water capacity, the water intake rate, and the crop needs. Drainage is needed for maximum production. Water on or near the surface can be removed with open ditches or tile drains. Fertilizer is needed to ensure optimum growth of grasses and legumes. Grasses respond to nitrogen, and legumes respond to sulfur and phosphorus. Proper stocking rates and pasture rotation help to keep the pasture in good condition and to protect the soil from erosion.

If this unit is used for recreational development, the main limitations are the very slow permeability of the Bandon soil and the wetness and very slow permeability of the Blacklock soil. Water perched above the cemented layer may limit the use of recreational facilities to dry periods. Drainage should be provided for paths and trails. Wetness can be reduced by ripping the cemented layer in the Bandon soil and by installing open ditches or tile drains in the Blacklock soil.

If this unit is used for homesite development, the main limitations are the very slow permeability of the soils and the hazard of erosion. Use of septic tank absorption fields is limited by the very slow permeability. Because of the cemented layer, onsite sewage disposal systems often fail or do not function properly during periods of high rainfall. The limitation of very slow permeability may be overcome by increasing the size of the absorption field.

Erosion is a hazard in the steeper areas. Only the part of the site that is used for construction should be disturbed. The risk of erosion is increased if the soil is left exposed during site development. Revegetating disturbed areas around construction sites as soon as feasible helps to control erosion. Structures to divert runoff are needed if buildings and roads are constructed.

This map unit is in capability subclass VIw.

3—Beaches. Beaches consists of areas of loose sand and shell fragments that have been worked and

140

reworked by waves, tides, and wind and are still subject to such action. Most of these areas are along the shore of the Pacific Ocean, but small areas are along the estuaries of major streams that flow into the ocean. Slope is 1 to 8 percent. Areas of beaches are barren of vegetation. Elevation is 0 to 10 feet.

Typically, areas of Beaches are sand, but gravel may be exposed during storms in winter. A few areas of Beaches at the base of sea cliffs are covered with rounded cobbles and stones.

Included in this unit are small areas of Waldport and Bullards soils and Rock outcrop. Included areas make up about 15 percent of the total acreage.

This unit is used for recreation activities such as surf fishing, beachcombing, and clam digging.

This map unit is in capability subclass VIIIw.

4D—Blachly silty clay loam, 0 to 30 percent slopes. This deep, well drained soil is on broad ridgetops and benches of mountains. It formed in colluvium derived dominantly from sedimentary rock or basalt. The native vegetation is mainly conifers, shrubs, forbs, and hardwoods. Elevation is 250 to 2,500 feet. The average annual precipitation is 60 to 100 inches, the average annual air temperature is 45 to 53 degrees F, and the average frost-free period is 140 to 220 days.

Typically, the surface layer is very dusky red and dark reddish brown silty clay loam 7 inches thick. The upper 45 inches of the subsoil is dark red and yellowish red silty clay, and the lower 8 inches is yellowish red silty clay loam.

Included in this unit are small areas of Dement, Honeygrove, and Preacher soils. Included areas make up about 20 percent of the total acreage. The percentage varies from one area to another.

Permeability of this Blachly soil is moderately slow. Available water capacity is about 7.0 to 8.5 inches. Effective rooting depth is 60 inches or more. Runoff is medium, and the hazard of water erosion is moderate.

This unit is used mainly for timber production and wildlife habitat.

This unit is suited to the production of Douglas fir. Among the other species that grow on this unit are western hemlock, red alder, and bigleaf maple. The understory vegetation is mainly vine maple, salal, red huckleberry, western swordfern, and oxalis.

On the basis of a 100-year site curve, the mean site index for Douglas fir is 160. At the culmination of the mean annual increment (CMAI), the production of 60-year-old Douglas fir trees 1.5 inches in diameter or more at breast height is 170 cubic feet per acre per year. On the basis of a 50-year site curve, the mean

site index for Douglas fir is 126.

The main limitations for the management of timber on this unit are the susceptibility of the surface layer to compaction, the hazard of erosion, and plant competition. Using standard wheeled and tracked equipment when the soil is moist causes rutting and compaction. Puddling can occur when the soil is wet. Using low-pressure ground equipment reduces damage to the soil and helps to maintain productivity.

Proper design of road drainage systems and care in the placement of culverts help to control erosion. Cut and fill areas are subject to erosion unless treated. Seeding, mulching, benching, and compacting the soil can reduce erosion. Unsurfaced roads and skid trails are sticky when wet or moist, and they may be impassable during rainy periods. Logging roads require suitable surfacing for year-round use. Rock for road construction is not readily available in this unit.

When openings are made in the canopy, invading brushy plants can delay natural reforestation. Undesirable plants can reduce natural or artificial reforestation unless intensive site preparation and maintenance are provided. Reforestation can be accomplished by planting Douglas fir seedlings.

This map unit is in capability subclass VIe.

4E—Blachly silty clay loam, 30 to 50 percent slopes. This deep, well drained soil is on broad ridgetops and benches of mountains. It formed in colluvium derived dominantly from sedimentary rock or basalt. The native vegetation is mainly conifers, shrubs, forbs, and hardwoods. Elevation is 250 to 2,500 feet. The average annual precipitation is 60 to 80 inches, the average annual air temperature is 45 to 53 degrees F, and the average frost-free period is 140 to 220 days.

Typically, the surface layer is very dusky red and dark reddish brown silty clay loam 7 inches thick. The upper 45 inches of the subsoil is dark red and yellowish red silty clay, and the lower 8 inches is yellowish red silty clay loam.

Included in this unit are small areas of Preacher, Dement, Honeygrove, and Remote soils. Included areas make up about 20 percent of the total acreage. The percentage varies from one area to another.

Permeability of this Blachly soil is moderately slow. Available water capacity is about 7.0 to 8.5 inches. Effective rooting depth is 60 inches or more. Runoff is rapid, and the hazard of water erosion is high.

This unit is used mainly for timber production and wildlife habitat.

This unit is suited to the production of Douglas fir. Among the other species that grow on this unit are

141

western hemlock, red alder, and bigleaf maple. The understory vegetation is mainly vine maple, salal, red huckleberry, western swordfern, and oxalis.

On the basis of a 100-year site curve, the mean site index for Douglas fir is 160. At the culmination of the mean annual increment (CMAI), the production of 60-year-old Douglas fir trees 1.5 inches in diameter or more at breast height is 170 cubic feet per acre per year. On the basis of a 50-year site curve, the mean site index for Douglas fir is 126.

The main limitations for the management of timber on this unit are the susceptibility of the surface layer to compaction, the hazard of erosion, steepness of slope, and plant competition. The main limitation for the harvesting of timber is steepness of slope. Using standard wheeled and tracked equipment when the soil is moist causes rutting and compaction. Puddling can occur when the soil is wet. Cable yarding systems are safer, damage the soil less, and help to maintain productivity.

Proper design of road drainage systems and care in the placement of culverts help to control erosion. Cut and fill areas are subject to erosion unless treated. Seeding, mulching, benching, and compacting the soil can reduce erosion. Unsurfaced roads and skid trails are sticky when wet or moist, and they may be impassable during rainy periods. Rock for road construction is not readily available in this unit. Material cast to the side when building roads can damage vegetation. It is also a potential source of sedimentation. End hauling of waste material minimizes damage to the vegetation downslope and reduces the potential for sedimentation.

When openings are made in the canopy, invading brushy plants can delay natural reforestation. Undesirable plants reduce natural or artificial reforestation unless intensive site preparation and maintenance are provided. Reforestation can be accomplished by planting Douglas fir seedlings.

This map unit is in capability subclass VIe.

5A—Blacklock fine sandy loam, 0 to 3 percent slopes. This deep, poorly drained soil is in depressional areas of marine terraces. It formed in sandy marine deposits. The native vegetation is mainly conifers, shrubs, forbs, and sedges. Elevation is 25 to 350 feet. The average annual precipitation is 55 to 75 inches, the average annual air temperature is 51 to 53 degrees F, and the average frost-free period is 200 to 240 days.

Typically, the surface is covered with a mat of organic litter 1 inch thick. The surface layer is black and very dark gray fine sandy loam and loamy fine sand 9

inches thick. The subsurface layer is gray loamy fine sand 4 inches thick. The upper 2 inches of the subsoil is black mucky loam, and the lower 37 inches is mottled, strong brown to yellowish brown, cemented sand. The substratum to a depth of 75 inches or more is mottled, light olive brown, red, and brown sand (fig. 6).

Included in this unit are small areas of Bandon and Bullards soils. Also included are small areas of soils that are similar to this Blacklock soil but do not have a cemented layer and have a clayey substratum. Included areas make up about 25 percent of the total acreage. The percentage varies from one area to another.

Permeability of this Blacklock soil is moderate above the cemented layer, very slow through it, and moderately rapid below it. Available water capacity is about 1.5 to 3.5 inches. Effective rooting depth is 12 to 24 inches. Runoff is very slow, and the hazard of water erosion is slight. The water table fluctuates from 6 inches above the surface to 30 inches below the surface from October to May.

This unit is used mainly for timber production and wildlife habitat. It is also used for cranberry production and recreation.

This unit is suited to the production of shore pine. Among the other species grown on the soil in this unit are Sitka spruce, western hemlock, and Port Orford cedar. The understory vegetation is mainly salal, evergreen huckleberry, Pacific rhododendron, manzanita, and slough sedge.

On the basis of a 100-year site curve, the mean site index for shore pine is 90. At the culmination of the mean annual increment (CMAI), the production of 60-year-old shore pine trees 1.5 inches in diameter or more at breast height is 79 cubic feet per acre per year. High winds from the Pacific Ocean may seriously limit the growth of trees unless they are in a protected area.

The main limitations for the management of timber on this unit are seasonal wetness and the hazard of windthrow. The seasonal high water table limits the use of equipment to dry periods. Because roots are restricted by the cemented layer, trees commonly are subject to windthrow.

Reforestation can be accomplished by planting shore pine, Sitka spruce, and western hemlock. Tree seedlings have only a moderate rate of survival because of the seasonal high water table.

Irrigation and drainage are needed if the soil in this unit is intensively managed for cranberry production. Fields are prepared by removing the soil material above the cemented layer and replacing it with about 10 inches of sandy soil material. The top of the cemented

142

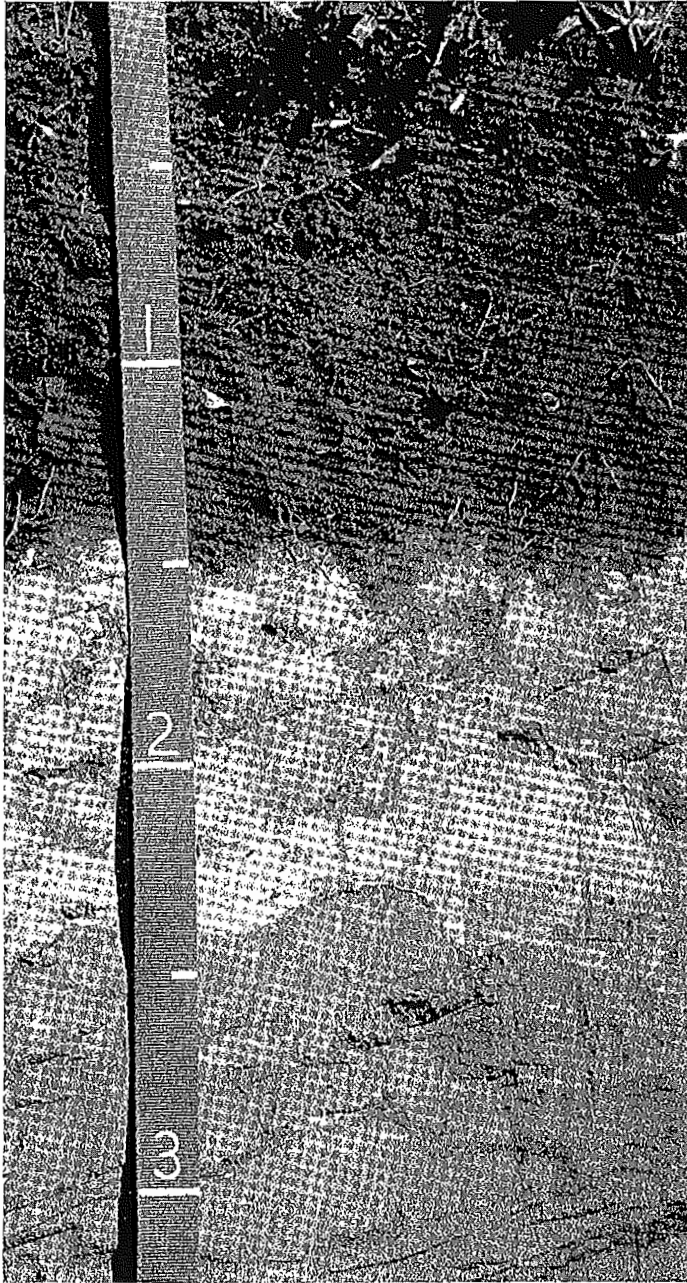


Figure 6.—Typical profile of Blacklock fine sandy loam, 0 to 3 percent slopes, showing cemented subsoil.

layer should be graded toward the edge of the field to provide internal drainage. Open ditches and dikes are needed around the edge of fields to provide drainage and to control the water level; however, open ditches should not extend into the cemented layer.

Sprinkler irrigation is an efficient method of applying

water during the dry period in summer. Sprinklers can also be used to control the temperature during summer, to prevent frost damage during winter, and to apply fertilizer, pesticides, and herbicides.

The very slow permeability of the cemented layer facilitates water management by preventing excessive seepage and reduces losses of fertilizer and soil amendments. Excess seepage may occur in the sandy substratum. Yields vary greatly depending on the management practices used.

If this unit is used for recreational development, the main limitations are wetness and the very slow permeability. Water perched above the cemented layer may limit the use of recreational facilities to 3 or 4 months during the dry period. Drainage should be provided for paths and trails. Septic tank absorption fields do not function properly because of the seasonal high water table and the cemented layer. If sanitary facilities are constructed on this unit, holding tanks or effluent treatment systems should be used.

This map unit is in capability subclass VIw.

5B—Blacklock fine sandy loam, 3 to 7 percent slopes. This deep, poorly drained soil is in depressional areas on marine terraces. It formed in sandy marine deposits. The native vegetation is mainly conifers, shrubs, forbs, and sedges. Elevation is 25 to 350 feet. The average annual precipitation is 55 to 75 inches, the average annual air temperature is 51 to 53 degrees F, and the average frost-free period is 200 to 240 days.

Typically, the surface is covered with a mat of organic litter 1 inch thick. The surface layer is black and very dark gray fine sandy loam 9 inches thick. The subsurface layer is gray fine sandy loam 4 inches thick. The upper 2 inches of the subsoil is black mucky loam, and the lower 37 inches is mottled, strong brown to yellowish brown, cemented sand. The substratum to a depth of 75 inches or more is mottled, light olive brown sand.

Included in this unit are small areas of Bandon, Bullards, and Heceta soils. Included areas make up about 25 percent of the total acreage. The percentage varies from one area to another.

Permeability of this Blacklock soil is moderate above the cemented layer, very slow through it, and moderately rapid below it. Available water capacity is about 1.5 to 3.5 inches. Effective rooting depth is 12 to 24 inches. Runoff is very slow, and the hazard of water erosion is slight. The water table fluctuates from 6 inches above the surface to 30 inches below the surface from October to May.

This unit is used mainly for timber production and

inches thick. The subsoil is dark reddish brown, dark brown, and strong brown gravelly sandy loam 34 inches thick. The substratum to a depth of 60 inches or more is yellowish brown sand.

Included in this unit are small areas of Blacklock and Bandon soils. Also included are small areas of Templeton soils. Included areas make up about 25 percent of the total acreage.

Permeability of this Bullards soil is moderate. Available water capacity is about 4.0 to 5.5 inches. Effective rooting depth is 60 inches or more. Runoff is slow, and the hazard of water erosion is slight. The hazard of soil blowing is severe.

This unit is used mainly for timber production, wildlife habitat, and homesite development. It is also used for pasture and recreation.

This unit is suited to the production of Douglas fir. Among the other species that grow on this unit are Sitka spruce, western hemlock, western redcedar, shore pine, and red alder. The understory vegetation is mainly evergreen huckleberry, creambush oceanspray, salal, Pacific rhododendron, cascara, and western swordfern.

On the basis of a 100-year site curve, the mean site index for Douglas fir is 132. At the culmination of the mean annual increment (CMAI), the production of 60-year-old Douglas fir trees 1.5 inches in diameter or more at breast height is 133 cubic feet per acre per year. On the basis of a 50-year site curve, the mean site index for Douglas fir is 105.

The main limitations for the management of timber on this unit are the hazard of windthrow and plant competition. Careful use of wheeled and tracked equipment reduces the disturbance of the protective layer of duff. Maintaining the understory is essential in controlling erosion. Logging roads require suitable surfacing for year-round use. Rock for road construction is not readily available in this unit.

Windthrow is a hazard when the soil is wet and winds are strong. When openings are made in the canopy, invading brushy plants can delay natural reforestation. Undesirable plants reduce natural or artificial reforestation unless intensive site preparation and maintenance are provided. Reforestation can be accomplished by planting Douglas fir, Sitka spruce, and western hemlock seedlings.

If this unit is used for homesite development, the main limitation is droughtiness in summer. In summer, irrigation is needed for lawn grasses, shrubs, vines, shade trees, and ornamental trees.

If this unit is used for pasture, the main limitation is droughtiness in summer. Supplemental irrigation is needed for maximum production. Sprinkler irrigation is a

suitable method of applying water. Use of this method permits the even, controlled application of water. Water should be applied in amounts sufficient to wet the root zone but small enough to minimize the leaching of plant nutrients. Applications of water should be adjusted to the available water capacity, the water intake rate, and the crop needs.

Fertilizer is needed to ensure optimum growth of grasses and legumes. Grasses respond to nitrogen, and legumes respond to sulfur and phosphorus. Proper stocking rates and pasture rotation help to keep the pasture in good condition and to protect the soil from erosion. Periodic mowing and clipping help to maintain uniform growth, discourage selective grazing, and reduce clumpy growth.

This unit is well suited to recreational development. It has few limitations.

This map unit is in capability subclass IIIe.

8C—Bullards sandy loam, 7 to 12 percent slopes.

This deep, well drained soil is on dissected marine terraces. It formed in mixed eolian and marine deposits. The native vegetation is mainly conifers, shrubs, forbs, and hardwoods. Elevation is 50 to 600 feet. The average annual precipitation is 55 to 75 inches, the average annual air temperature is 51 to 53 degrees F, and the average frost-free period is 200 to 240 days.

Typically, the surface is covered with a mat of undecomposed organic matter 3 inches thick. The surface layer is very dark grayish brown sandy loam 7 inches thick. The subsoil is dark reddish brown, dark brown, and strong brown gravelly sandy loam 34 inches thick. The substratum to a depth of 60 inches or more is yellowish brown sand.

Included in this unit are small areas of Bandon and Templeton soils. Also included are small areas of Blacklock soils. Included areas make up about 25 percent of the total acreage.

Permeability of this Bullards soil is moderate. Available water capacity is about 4.0 to 5.5 inches. Effective rooting depth is 60 inches or more. Runoff is medium, and the hazard of water erosion is moderate. The hazard of soil blowing is severe.

This unit is used mainly for timber production, wildlife habitat, and homesite development. It is also used for pasture and recreation.

This unit is suited to the production of Douglas fir. Among the other species that grow on this unit are Sitka spruce, western hemlock, western redcedar, shore pine, and red alder. The understory vegetation is mainly evergreen huckleberry, creambush oceanspray, salal, Pacific rhododendron, cascara, and western swordfern.

144

On the basis of a 100-year site curve, the mean site index for Douglas fir is 132. At the culmination of the mean annual increment (CMAI), the production of 60-year-old Douglas fir trees 1.5 inches in diameter or more at breast height is 133 cubic feet per acre per year. On the basis of a 50-year site curve, the mean site index for Douglas fir is 105.

The main limitations for the management of timber on this unit are the hazard of windthrow and plant competition. Careful use of wheeled and tracked equipment reduces the disturbance of the protective layer of duff.

Proper design of road drainage systems and care in the placement of culverts help to control erosion. Logging roads require suitable surfacing for year-round use. Rock for road construction is not readily available in this unit.

Windthrow is a hazard when the soil is wet and winds are strong. When openings are made in the canopy, invading brushy plants can delay natural reforestation. Undesirable plants reduce natural or artificial reforestation unless intensive site preparation and maintenance are provided. Reforestation can be accomplished by planting Douglas fir, Sitka spruce, and western hemlock seedlings.

If this unit is used for homesite development, the main limitations are slope and droughtiness in summer. Absorption lines should be installed on the contour. In summer, irrigation is needed for lawn grasses, shrubs, vines, shade trees, and ornamental trees.

If this unit is used for pasture, the main limitation is droughtiness in summer. Supplemental irrigation is needed for maximum production. Sprinkler irrigation is a suitable method of applying water. Use of this method permits the even, controlled application of water. Water should be applied in amounts sufficient to wet the root zone but small enough to minimize the leaching of plant nutrients. Applications of water should be adjusted to the available water capacity, the water intake rate, and the crop needs.

Fertilizer is needed to ensure optimum growth of grasses and legumes. Grasses respond to nitrogen, and legumes respond to sulfur and phosphorus. Proper stocking rates and pasture rotation help to keep the pasture in good condition and to protect the soil from erosion. Periodic mowing and clipping help to maintain uniform growth, discourage selective grazing, and reduce clumpy growth.

If this unit is used for recreational development, the main limitation is steepness of slope. Slope may restrict some kinds of activities and increase the cost of constructing facilities.

This map unit is in capability subclass IIIe.

8D—Bullards sandy loam, 12 to 30 percent s

This deep, well drained soil is on dissected marine terraces. It formed in mixed eolian and marine deposits. The native vegetation is mainly conifers, shrubs, and hardwoods. Elevation is 50 to 600 feet. The average annual precipitation is 55 to 75 inches, the average annual air temperature is 51 to 53 degrees Fahrenheit, and the average frost-free period is 200 to 240 days.

Typically, the surface is covered with a mat of undecomposed organic matter 3 inches thick. The surface layer is very dark grayish brown sandy loam 1 to 2 inches thick. The subsoil is dark reddish brown, reddish brown, and strong brown gravelly sandy loam 34 inches thick. The substratum to a depth of 60 inches or more is yellowish brown sand (fig. 7).

Included in this unit are small areas of Bandon and Templeton soils. Also included are small areas of Blacklock soils in depressional areas. Included areas make up about 25 percent of the total acreage.

Permeability of this Bullards soil is moderate. Available water capacity is about 4.0 to 5.5 inches. Effective rooting depth is 60 inches or more. Runoff is medium, and the hazard of water erosion is moderate. The hazard of soil blowing is severe.

This unit is used mainly for timber production, wildlife habitat, and pasture. It is also used for recreation.

This unit is suited to the production of Douglas fir. Among the other species that grow on this unit are Sitka spruce, western hemlock, western redcedar, white pine, and red alder. The understory vegetation includes evergreen huckleberry, creambush oceanspray, Pacific rhododendron, cascara, and western snowberry.

On the basis of a 100-year site curve, the mean site index for Douglas fir is 132. At the culmination of the mean annual increment (CMAI), the production of 60-year-old Douglas fir trees 1.5 inches in diameter or more at breast height is 133 cubic feet per acre per year. On the basis of a 50-year site curve, the mean site index for Douglas fir is 105.

The main limitations for the management of timber on this unit are the hazard of erosion, the hazard of windthrow, and plant competition. Careful use of wheeled and tracked equipment reduces the disturbance of the protective layer of duff. Steep paths, skid trails, and firebreaks are subject to erosion and gullying unless they are provided with adequate water bars or are protected by plant cover, or by proper design of road drainage systems and careful placement of culverts help to control erosion. Logging roads require suitable surfacing for year-round use.

145



Figure 7.—Typical profile of Bullards sandy loam, 12 to 30 percent slopes, showing sand substratum. Tape is marked in 2.5-inch increments.

Rock for road construction is not readily available in this unit.

Windthrow is a hazard when the soil is wet and winds are strong. When openings are made in the canopy, invading brushy plants can delay natural reforestation. Undesirable plants reduce natural or artificial reforestation unless intensive site preparation and maintenance are provided. Reforestation can be accomplished by planting Douglas fir, Sitka spruce, and western hemlock seedlings.

If this unit is used for pasture, the main limitation is droughtiness in summer. Supplemental irrigation is needed for maximum production. Sprinkler irrigation can be used in the less sloping areas of the unit. Use of this method permits the even, controlled application of water, reduces runoff, and minimizes the risk of erosion. Applications of water should be adjusted to the available water capacity, the water intake rate, and the crop needs. Fertilizer is needed to ensure optimum growth of grasses and legumes. Grasses respond to nitrogen, and legumes respond to sulfur and phosphorus. Proper stocking rates and pasture rotation help to keep the pasture in good condition and to protect the soil from erosion.

If this unit is used for recreational development, the main limitations are steepness of slope and the hazard of erosion. Slope limits the type of recreational facilities that are suited to the unit. The risk of erosion is increased if the soil is left exposed during site development. Erosion and sedimentation can be controlled and the beauty of the area enhanced by maintaining adequate plant cover.

This map unit is in capability subclass IVe.

8E—Bullards sandy loam, 30 to 50 percent slopes.

This deep, well drained soil is on dissected marine terraces. It formed in mixed eolian and marine deposits. The native vegetation is mainly conifers, shrubs, forbs, and hardwoods. Elevation is 50 to 600 feet. The average annual precipitation is 55 to 75 inches, the average annual air temperature is 51 to 53 degrees F, and the average frost-free period is 200 to 240 days.

Typically, the surface is covered with a mat of undecomposed organic matter 3 inches thick. The surface layer is very dark grayish brown sandy loam 7 inches thick. The subsoil is dark reddish brown, dark brown, and strong brown gravelly sandy loam 34 inches thick. The substratum to a depth of 60 inches or more is yellowish brown sand.

Included in this unit are small areas of Templeton soils. Included areas make up about 20 percent of the total acreage. The percentage varies from area to area.

146

Permeability of this Bullards soil is moderate. Available water capacity is about 4.0 to 5.5 inches. Effective rooting depth is 60 inches or more. Runoff is rapid, and the hazard of water erosion is high. The hazard of soil blowing is severe.

This unit is used mainly for timber production and wildlife habitat. It is also used for recreation.

This unit is suited to the production of Douglas fir. Among the other species that grow on this unit are Sitka spruce, western hemlock, western redcedar, shore pine, and red alder. The understory vegetation is mainly evergreen huckleberry, creambush oceanspray, salal, Pacific rhododendron, cascara, and western swordfern.

On the basis of a 100-year site curve, the mean site index for Douglas fir is 132. At the culmination of the mean annual increment (CMAI), the production of 60-year-old Douglas fir trees 1.5 inches in diameter or more at breast height is 133 cubic feet per acre per year. On the basis of a 50-year site curve, the mean site index for Douglas fir is 105. High winds from the Pacific Ocean may seriously limit the growth of trees unless they are in a protected area.

The main limitations for the management of timber on this unit are steepness of slope, the hazard of erosion, the hazard of windthrow, and plant competition. Careful use of wheeled and tracked equipment reduces the disturbance of the protective layer of duff. Highlead or other logging systems that fully or partially suspend logs damage the soil less and generally are less costly than tractor systems.

Proper design of road drainage systems and care in the placement of culverts help to control erosion. Cut and fill areas are subject to erosion unless treated. Seeding, mulching, benching, and compacting the soil can reduce erosion. Logging roads require suitable surfacing for year-round use. Rock for road construction is not readily available in this unit. Steep yarding paths, skid trails, and firebreaks are subject to rilling and gullying unless they are provided with adequate water bars or are protected by plant cover, or both.

Windthrow is a hazard when the soil is wet and winds are strong. When openings are made in the canopy, invading brushy plants can delay natural reforestation. Undesirable plants reduce natural or artificial reforestation unless intensive site preparation and maintenance are provided. Reforestation can be accomplished by planting Douglas fir, Sitka spruce, and western hemlock seedlings.

If this unit is used for recreational development, the main limitations are slope and the hazard of erosion. Slope limits the use of areas of this unit mainly to a few paths and trails, which should extend across the slope.

The risk of erosion is increased if the soil is left exposed during site development. Revegetating disturbed areas around construction sites as soon as feasible helps to control erosion.

This map unit is in capability subclass VIe.

9—Chetco silty clay loam. This deep, very poorly drained soil is on flood plains and deltas. It formed in alluvium. Slope is 0 to 3 percent. The native vegetation is mainly conifers, shrubs, forbs, and hardwoods. Elevation is 0 to 40 feet. The average annual precipitation is 60 to 80 inches, the average annual air temperature is 51 to 53 degrees F, and the average frost-free period is 200 to 240 days.

Typically, the surface layer is very dark grayish brown silty clay loam 10 inches thick. The subsoil is mottled, dark gray silty clay 14 inches thick. The substratum to a depth of 60 inches or more is mottled, dark gray clay.

Included in this unit are small areas of Coquille and Nestucca soils. Also included are small areas of Langlois soils. Included areas make up about 25 percent of the total acreage.

Permeability of this Chetco soil is very slow. Available water capacity is about 5.0 to 8.5 inches. Effective rooting depth is 60 inches or more for water-tolerant plants, but it is limited by the water table for non-water-tolerant plants. Runoff is very slow, and the hazard of water erosion is slight. This soil is subject to frequent periods of flooding during prolonged periods of rainfall. Channeling and deposition are common along streambanks. The water table fluctuates between the surface and a depth of 18 inches in October to May.

This unit is used mainly for hay and pasture and wildlife habitat.

The vegetation in areas not cultivated is mainly Sitka spruce, western redcedar, western hemlock, and red alder. The understory vegetation is mainly western swordfern, evergreen huckleberry, slough sedge, soft rush, and skunkcabbage.

If this unit is used for hay and pasture, the main limitations are the susceptibility of the surface layer to compaction, wetness, droughtiness in summer, the hazard of flooding, and, for the curing of hay, high humidity. Grazing when the soil is moist results in compaction of the surface layer and poor tilth. Compaction limits the movement of air and water in the soil and restricts the growth of roots; it can seriously reduce the productivity of the soil. Grazing should be delayed until the soil has drained sufficiently and is firm enough to withstand trampling by livestock.

Drainage and irrigation are needed for maximum

that are similar to this Honeygrove soil but have bedrock at a depth of 30 to 40 inches. Included areas make up about 25 percent of the total acreage.

Permeability of this Honeygrove soil is moderately slow. Available water capacity is about 8.5 to 9.5 inches. Effective rooting depth is 60 inches or more. Runoff is rapid, and the hazard of water erosion is high.

This unit is used mainly for timber production and wildlife habitat.

This unit is suited to the production of Douglas fir. Among the other species that grow on this unit are western hemlock, western redcedar, Port Orford cedar, and red alder. The understory vegetation is mainly salal, vine maple, evergreen huckleberry, creambush oceanspray, western swordfern, and western brackenfern.

On the basis of a 100-year site curve, the mean site index for Douglas fir is 165. At the culmination of the mean annual increment (CMAI), the production of 60-year-old Douglas fir trees 1.5 inches in diameter or more at breast height is 176 cubic feet per acre per year. On the basis of a 50-year site curve, the mean site index for Douglas fir is 122.

The main limitations for the management of timber on this unit are the hazard of erosion, steepness of slope, and plant competition. Steepness of slope restricts the use of wheeled and tracked equipment on skid trails. Cable yarding generally is safer and disturbs the soil less.

Proper design of road drainage systems and care in the placement of culverts help to control erosion. Cuts and fills are subject to erosion unless treated. Seeding, mulching, benching, and compacting the soil can reduce erosion. Steep yarding paths, skid trails, and firebreaks are subject to rilling and gullying unless they are provided with adequate water bars or are protected by plant cover, or both. Unsurfaced roads and skid trails are slippery when moist or wet, and they may be impassable during rainy periods. Logging roads require suitable surfacing for year-round use. Rock for road construction is not readily available in this unit.

When openings are made in the canopy, invading brushy plants can delay natural reforestation. Undesirable plants reduce natural or artificial reforestation unless intensive site preparation and maintenance are provided. Reforestation can be accomplished by planting Douglas fir seedlings.

This map unit is in capability subclass VIe.

31B—Joenev very fine sandy loam, 0 to 7 percent slopes. This deep, poorly drained soil is on marine terraces. It formed in marine deposits. The native

vegetation is mainly conifers, shrubs, forbs, and hardwoods. Elevation is 150 to 550 feet. The average annual precipitation is 60 to 65 inches, the average annual air temperature is 51 to 53 degrees F, and the average frost-free period is 200 to 240 days.

Typically, the surface is covered with a mat of leave and needles 1 inch thick. The surface layer is light gray and gray very fine sandy loam 10 inches thick. The upper 2 inches of the subsoil is dark reddish brown very fine sandy loam, and the lower 12 inches is mottled, reddish yellow and brownish yellow loam and silt loam. The substratum to a depth of 41 inches or more is mottled, brownish yellow and light gray silty clay loam.

Included in this unit are small areas of Templeton soils. Also included are small areas of soils that are similar to this Joenev soil but have a sandy substratum. Included areas make up about 25 percent of the total acreage.

Permeability of this Joenev soil is moderately slow. Available water capacity is about 2 to 4 inches. Effective rooting depth is 60 inches for water-tolerant plants, but it is limited by the water table for non-water tolerant plants. Runoff is very slow, and the hazard of water erosion is slight. The water table fluctuates between the surface and a depth of 18 inches below the surface from November to March.

This unit is used mainly for timber production and wildlife habitat.

This unit is suited to the production of Sitka spruce. Among the other species that grow on this unit are western redcedar and western hemlock. The understory vegetation is mainly evergreen huckleberry, Pacific rhododendron, salal, sedges, and rushes.

On the basis of a 100-year site curve, the mean site index for Sitka spruce is 120. At the culmination of the mean annual increment (CMAI), the production of 50-year-old Sitka spruce trees 1.5 inches in diameter or more at breast height is 156 cubic feet per acre per year.

The main limitations for the management of timber on this unit are the hazard of windthrow, seedling mortality, and plant competition. The seasonal high water table limits the use of equipment to dry periods.

Proper design of road drainage systems and care in the placement of culverts help to control erosion. Cuts and fills are subject to erosion unless treated. Seeding, mulching, benching, and compacting the soil can reduce erosion. Unsurfaced roads and skid trails are soft when wet or moist, and they may be impassable during rainy periods. Logging roads require suitable surfacing for year-round use. Rock for road construction is not readily available in this unit.

148

Windthrow is a hazard when the soil is wet and winds are strong. Tree seedlings have only a moderate rate of survival because of the seasonal high water table. When openings are made in the canopy, invading brushy plants can delay natural reforestation. Undesirable plants prevent adequate natural or artificial reforestation unless intensive site preparation and maintenance are provided. Reforestation can be accomplished by planting Douglas fir, Sitka spruce, and western redcedar seedlings.

This map unit is in capability subclass IVw.

32B—Joenev-Templeton complex, 0 to 7 percent slopes. This map unit is in undulating areas of dissected marine terraces. The native vegetation is mainly conifers, shrubs, forbs, and hardwoods. Elevation is 150 to 550 feet. The average annual precipitation is 60 to 65 inches, the average annual air temperature is 51 to 53 degrees F, and the average frost-free period is 200 to 240 days.

This unit is 40 percent Joenev very fine sandy loam and 30 percent Templeton silt loam. The Joenev soil is in concave, nearly level depressional areas, and the Templeton soil is in convex, gently sloping areas on marine terrace escarpments. The components of this unit are so intricately intermingled that it was not practical to map them separately at the scale used.

Included in this unit are small areas of soils that are similar to this Joenev soil but have a thin cemented pan. In the vicinity of Beaver Hill are small areas of soils that are similar to the Templeton soil but that formed in marine sediment, have mottles in the subsoil, and have a sandy substratum. These soils are less productive than the Templeton soils. Included areas make up about 30 percent of the total acreage.

The Joenev soil is deep and poorly drained. It formed in marine deposits. Typically, the surface is covered with a mat of leaves and needles 1 inch thick. The surface layer is light gray and gray very fine sandy loam 10 inches thick. The upper 2 inches of the subsoil is dark reddish brown very fine sandy loam, and the lower 12 inches is mottled, reddish yellow and brownish yellow loam and silt loam. The substratum to a depth of 41 inches or more is mottled, brownish yellow and light gray silty clay loam.

Permeability of the Joenev soil is moderately slow. Available water capacity is about 2 to 4 inches. Effective rooting depth is 60 inches for water-tolerant plants, but it may be limited by the water table for non-water-tolerant plants. Runoff is very slow, and the hazard of water erosion is slight. The water table fluctuates between the surface and a depth of 18 inches

below the surface from November to March.

The Templeton soil is deep and well drained. It formed in colluvium and residuum derived dominantly from sedimentary rock. Typically, the surface layer is very dark brown and dark brown silt loam 16 inches thick. The subsoil is reddish brown, yellowish red, and strong brown silty clay loam 26 inches thick. Soft, weathered, fractured siltstone is at a depth of 42 inches. In some areas the dark-colored surface layer is less than 10 inches thick.

Permeability of the Templeton soil is moderate. Available water capacity is about 8.0 to 17.5 inches. Effective rooting depth is 40 to 60 inches. Runoff is slow, and the hazard of water erosion is slight.

This unit is used mainly for timber production and wildlife habitat.

This unit is suited to the production of Sitka spruce. Among the other species that grow on the unit are western redcedar, western hemlock, red alder, and Douglas fir. The understory vegetation is mainly evergreen huckleberry, Pacific rhododendron, salal, sedges, and rushes.

On the basis of a 100-year site curve, the mean site index for Sitka spruce is 120 on the Joenev soil. At the culmination of the mean annual increment (CMAI), the production of 50-year-old Sitka spruce trees 1.5 inches in diameter or more at breast height is 156 cubic feet per acre per year.

On the basis of a 100-year site curve, the mean site index for Sitka spruce is 169 on the Templeton soil. At the culmination of the mean annual increment (CMAI), the production of 50-year-old Sitka spruce trees 1.5 inches in diameter or more at breast height is 255 cubic feet per acre per year.

High winds from the Pacific Ocean may seriously limit the growth of trees on this unit unless they are in a protected area.

The main limitations for the management of timber on this unit are the susceptibility of the surface layer of the Templeton soil to compaction, the hazard of windthrow and seedling mortality on the Joenev soil, and plant competition. Using standard wheeled and tracked equipment when the soil is moist causes rutting and compaction. Displacement of the surface layer occurs most readily when the soil is dry. Puddling can occur when the soil is wet. Using low-pressure ground equipment damages the soil less and helps to maintain productivity. The seasonal high water table in the Joenev soil limits the use of equipment to dry periods.

Proper design of road drainage systems and care in the placement of culverts help to control erosion. Unsurfaced roads and skid trails are soft and slippery

149



Figure 11.—Hay in an area of Kirkendall silt loam.

when wet or moist, and they may be impassable during rainy periods. Logging roads require suitable surfacing for year-round use. Rock for road construction is not readily available in this unit.

Because roots are restricted by the seasonal high water table in the Joeney soil, trees commonly are subject to windthrow. Tree seedlings have only a moderate rate of survival because of the seasonal high water table. When openings are made in the canopy, invading brushy plants can delay natural reforestation. Undesirable plants prevent adequate natural or artificial reforestation unless intensive site preparation and maintenance are provided. Reforestation can be accomplished by planting Sitka spruce, western hemlock, or Douglas fir seedlings.

This map unit is in capability subclass IVw.

33—Kirkendall silt loam. This deep, well drained soil is on flood plains. It formed in mixed alluvium. Slopes are 0 to 3 percent. The native vegetation is mainly

conifers, shrubs, forbs, and hardwoods. Elevation is 2 to 750 feet. The average annual precipitation is 60 to 80 inches, the average annual air temperature is 50 to 55 degrees F, and the average frost-free period is 180 to 220 days.

Typically, the surface layer is dark brown silt loam 4 to 6 inches thick. The subsoil is dark brown and brown silt loam 35 inches thick. The substratum to a depth of 6 inches or more is mottled, brown silt loam.

Included in this unit are small areas of poorly drained and very poorly drained soils. Also included are small areas of soils that are similar to this Kirkendall soil but have a sandy loam subsoil and soils, in Eden Valley that are similar to this Kirkendall soil but are at an elevation of 2,300 feet. Included areas make up about 20 percent of the total acreage.

Permeability of this Kirkendall soil is moderately slow. Available water capacity is about 7.5 to 12.5 inches. Effective rooting depth is 60 inches or more. Runoff is slow, and the hazard of water erosion is slight. This

are provided with adequate water bars or are protected by plant cover, or both.

Windthrow is a hazard when the soil is wet and winds are strong. The high content of rock fragments in the soil increases seedling mortality. To compensate for the higher mortality that can be expected, larger trees or more trees than normal can be planted. When openings are made in the canopy, invading brushy plants can delay natural reforestation. Reforestation can be accomplished by planting Douglas fir seedlings. This map unit is in capability subclass VIe.

53E—Serpentano very stony loam, 35 to 70 percent slopes.

This deep, well drained soil is on sideslopes and ridgetops of mountains. It formed in colluvium and residuum derived dominantly from serpentinite and peridotite. The native vegetation is mainly conifers, hardwoods, shrubs, forbs, and grasses. Elevation is 1,500 to 3,900 feet. The average annual precipitation is 90 to 100 inches, the average annual air temperature is 45 to 51 degrees F, and the average frost-free period is 110 to 180 days.

Typically, the surface is covered with a mat of partially decomposed needles and leaves 3 inches thick. The surface layer is dark brown very stony loam 5 inches thick. The subsoil is dark brown gravelly and cobbly loam 13 inches thick. The substratum is yellowish brown very gravelly and extremely stony loam 28 inches thick. Partially weathered serpentinite is at a depth of 46 inches.

Included in this unit are small areas of Umpcoos and note soils. Also included are small areas of Preacher s. Included areas make up about 20 percent of the total acreage. The percentage varies from one area to another.

Permeability of this Serpentano soil is moderate. Available water capacity is about 4 to 7 inches.

Effective rooting depth is 40 to 60 inches. Runoff is direct, and the hazard of water erosion is high.

This unit is used for timber production and wildlife habitat.

This unit is suited to the production of Douglas fir. Among the other species that grow on this unit are Port wine cedar, western redcedar, tanoak, and Pacific ironwood. The understory vegetation is mainly Pacific hollyhock, manzanita, salal, western swordfern, low huckleberry, and red huckleberry.

On the basis of a 100-year site curve, the mean site index for Douglas fir is 120. At the culmination of the 100-year annual increment (CMAI), the production of 60-year-old Douglas fir trees 1.5 inches in diameter or greater at breast height is 115 cubic feet per acre per

year. On the basis of a 50-year site curve, the mean site index for Douglas fir is 97.

The main limitations for the management of timber on this unit are the hazard of erosion, steepness of slope, the hazard of windthrow, and seedling mortality. Highlead or other cable logging systems are most suitable. Stones on the surface cause breakage of timber and hinder yarding.

Proper design of road drainage systems and care in the placement of culverts help to control erosion. Cuts and fills are subject to erosion unless treated. Seeding, mulching, benching, and compacting the soil can reduce erosion. Logging roads require suitable surfacing for year-round use. Rock for road construction is readily available in this unit. Steep yarding paths, skid trails, and firebreaks are subject to rilling and gullying unless they are provided with adequate water bars or are protected by plant cover, or both. Locating roads on midslopes results in large cuts and fills and thus removes land from production. Material cast to the side when building roads can damage vegetation. It is also a potential source of sedimentation. End hauling of waste material minimizes damage to the vegetation downslope and reduces the potential for sedimentation.

Windthrow is a hazard when the soil is wet and winds are strong. The high content of rock fragments in the soil increases seedling mortality. To compensate for the higher mortality that can be expected, larger trees or more trees than normal can be planted. When openings are made in the canopy, invading brushy plants can delay natural reforestation. Reforestation can be accomplished by planting Douglas fir seedlings.

This map unit is in capability subclass VIIe.

54B—Templeton silt loam, 0 to 7 percent slopes.

This deep, well drained soil is on ridgetops and benches of mountains. It formed in colluvium and residuum derived dominantly from sedimentary rock. The native vegetation is mainly conifers, shrubs, forbs, and hardwoods. Elevation is 50 to 450 feet. The average annual precipitation is 60 to 70 inches, the average annual air temperature is 51 to 53 degrees F, and the average frost-free period is 200 to 240 days.

Typically, the surface layer is very dark brown and dark brown silt loam 16 inches thick. The subsoil is reddish brown, yellowish red, and strong brown silty clay loam 26 inches thick. Soft, weathered and fractured siltstone is at a depth of 42 inches. In some areas the dark-colored surface layer is less than 10 inches thick.

Included in this unit are small areas of Geisel soils and deep gravelly loam. Also included are areas of

soils, mainly between Beaver Hill and south slough, that are similar to this Templeton soil but formed in marine sediment on coastal terraces. In some areas these soils have mottles in the subsoil and have a sandy substratum. Included areas make up about 25 percent of the total acreage. The percentage varies from one area to another.

Permeability of this Templeton soil is moderate. Available water capacity is about 8.0 to 17.5 inches. Effective rooting depth is 40 to 60 inches. Runoff is slow, and the hazard of water erosion is slight.

This unit is used mainly for timber production and wildlife habitat. It has potential for homesite development and livestock grazing.

This unit is suited to the production of Sitka spruce. Among the other species that grow on this unit are western hemlock, Douglas fir, Port Orford cedar, western redcedar, and red alder. The understory vegetation is mainly salal, evergreen huckleberry, Pacific rhododendron, western swordfern, and Oregon oxalis.

On the basis of a 100-year site curve, the mean site index for Sitka spruce is 169. At the culmination of the mean annual increment (CMAI), the production of 50-year-old Sitka spruce trees 1.5 inches in diameter or more at breast height is 255 cubic feet per acre per year. On the basis of a 100-year site curve, the mean site index for Douglas fir is 170. High winds from the Pacific Ocean may seriously limit the growth of trees unless they are in a protected area.

The main limitations for the production of timber on this unit are the susceptibility of the surface layer to compaction, plant competition, and the hazard of windthrow. Using standard wheeled and tracked equipment when the soil is moist causes rutting and compaction. Displacement of the surface layer occurs most readily when the soil is dry. Puddling can occur when the soil is wet. Using low-pressure ground equipment damages the soil less and helps to maintain productivity.

Proper design of road drainage systems and care in the placement of culverts help to control erosion. Unsurfaced roads and skid trails are slippery when wet or moist, and they may be impassable during rainy periods. Logging roads require suitable surfacing for year-round use. Rock for road construction is not readily available in this unit. Sitka spruce, a shallow rooted species, commonly is subject to windthrow.

When openings are made in the canopy, invading brushy plants can delay natural reforestation. Undesirable plants prevent adequate natural or artificial reforestation unless intensive site preparation and

maintenance are provided. Reforestation can be accomplished by planting Sitka spruce, western hemlock, and Douglas fir seedlings.

This unit is well suited to livestock grazing. In summer, droughtiness limits the choice of forage plants and limits production. Irrigation generally is impractical because of an inadequate water supply.

Fertilizer is needed to ensure optimum growth of grasses and legumes. Grass-legume pastures respond to sulfur, phosphorus, and molybdenum. Using a good fertilization program increases the production of forage in winter. Proper stocking rates and pasture rotation help to keep the pasture in good condition. Periodic mowing and clipping help to maintain uniform growth, discourage selective grazing, and reduce clumpy growth.

If this unit is used for homesite development, absorption lines should be installed on the contour. Preserving the existing plant cover during construction helps to control erosion. Topsoil can be stockpiled and used to reclaim areas disturbed during construction. In summer, supplemental irrigation is needed for lawn grasses and vegetable gardens.

This unit is in capability subclass IIIe.

54D—Templeton silt loam, 7 to 30 percent slopes

This deep, well drained soil is on side slopes of mountains. It formed in colluvium and residuum derived dominantly from sedimentary rock. The native vegetation is mainly conifers, shrubs, forbs, and hardwoods. Elevation is 50 to 800 feet. The average annual precipitation is 60 to 70 inches, the average annual air temperature is 51 to 53 degrees F, and the average frost-free period is 200 to 240 days.

Typically, the surface layer is very dark brown and dark brown silt loam 16 inches thick. The subsoil is reddish brown, yellowish red, and strong brown silty clay loam 26 inches thick. Soft, weathered and fractured siltstone is at a depth of 42 inches. In some areas the dark-colored surface layer is less than 10 inches thick.

Included in this unit are small areas of Salander soils. Included areas make up about 25 percent of the total acreage. The percentage varies from one area to another.

Permeability of this Templeton soil is moderate. Available water capacity is about 8.0 to 17.5 inches. Effective rooting depth is 40 to 60 inches. Runoff is medium, and the hazard of water erosion is moderate.

This unit is used mainly for timber production and wildlife habitat. It is also used for livestock grazing at homesite development.

152

nit is well suited to the production of Douglas
g the other species that grow on this unit are
hemlock, western redcedar, Sitka spruce,
and red alder. The understory vegetation is
the maple, thimbleberry, creambush
ay, red huckleberry, western swordfern, and
illium.

basis of a 100-year site curve, the mean site
Sitka spruce is 180. At the culmination of the
annual increment (CMAI), the production of 50-
Sitka spruce trees 1.5 inches in diameter or
least height is 270 cubic feet per acre per
the basis of a 100-year site curve, the mean
for Douglas fir is 170.

main limitations for the management of timber on
are the susceptibility of the surface layer to
on, the hazard of erosion, plant competition,
hazard of windthrow. Using standard wheeled
ed equipment when the soil is moist causes
id compaction. Displacement of the surface
urs most readily when the soil is dry. Puddling
r when the soil is wet. Using low-pressure
quipment reduces damage to the soil and
maintain productivity.

design of road drainage systems and care in
ment of culverts help to control erosion. Cuts
are subject to erosion unless treated. Seeding,
benching, and compacting the soil can reduce
Unsurfaced roads and skid trails are slippery
or moist, and they may be impassable during
ods. Logging roads require suitable surfacing
ound use. Rock for road construction is not
available in this unit. Steep yarding paths, skid
l firebreaks are subject to rilling and gullyng
ey are provided with adequate water bars or
cted by plant cover, or both. Sitka spruce, a
oted species, commonly is subject to
v.

openings are made in the canopy, invading
ants can delay natural reforestation.
ole plants prevent adequate natural or artificial
ion unless intensive site preparation and
nce are provided. Reforestation can be
shed by planting Sitka spruce, Douglas fir, and
hemlock seedlings.

nit is well suited to livestock grazing. In
droughtiness limits the choice of forage plants
production. Irrigation generally is impractical
of an inadequate water supply.

er is needed to ensure optimum growth of
nd legumes. Grass-legume pastures respond
phosphorus, and molybdenum. Using a good

fertilization program increases the production of forage
in winter. Proper stocking rates, pasture rotation, and
restricted grazing during wet periods help to keep the
pasture in good condition.

If this unit is used for homesite development, the
main limitations are slope and depth to bedrock.
Absorption lines should either be placed in the more
gently sloping areas of this unit or in adjoining areas of
soils that are not so steep.

Extensive cutting and filling generally are required to
provide nearly level construction sites. Building roads in
the less sloping areas of this unit reduces the amount of
cutting and filling required. Roads should be provided
with surface drainage. Cuts and fills are susceptible to
erosion. Revegetating disturbed areas around
construction sites as soon as possible helps to control
erosion. In summer, supplemental irrigation is needed
for lawn grasses and vegetable gardens.

This map unit is in capability subclass VIe.

54E—Templeton silt loam, 30 to 50 percent slopes.

This deep, well drained soil is on side slopes of
mountains. It formed in colluvium and residuum derived
dominantly from sedimentary rock. The native
vegetation is mainly conifers, shrubs, forbs, and
hardwoods. Elevation is 50 to 800 feet. The average
annual precipitation is 60 to 80 inches, the average
annual air temperature is 51 to 53 degrees F, and the
average frost-free period is 200 to 240 days.

Typically, the surface layer is very dark brown and
dark brown silt loam 16 inches thick. The subsoil is
reddish brown, yellowish red, and strong brown silty
clay loam 26 inches thick. Soft, weathered and
fractured siltstone is at a depth of 42 inches. In some
areas the dark-colored surface layer is less than 10
inches thick.

Included in this unit are small areas of Geisel soils
and deep gravelly loam. Included areas make up about
25 percent of the total acreage. The percentage varies
from one area to another.

Permeability of this Templeton soil is moderate.
Available water capacity is about 8.0 to 17.5 inches.
Effective rooting depth is 40 to 60 inches. Runoff is
rapid, and the hazard of water erosion is high.

This unit is used mainly for timber production and
wildlife habitat.

This unit is suited to the production of Sitka spruce.
Among the other species that grow on this unit are
western hemlock, Douglas fir, Port Orford cedar,
western redcedar, and red alder. The understory
vegetation is mainly salal, evergreen huckleberry,

153

Pacific rhododendron, western swordfern, and Oregon oxalis.

On the basis of a 100-year site curve, the mean site index for Sitka spruce is 180. At the culmination of the mean annual increment (CMAI), the production of 50-year-old Sitka spruce trees 1.5 inches in diameter or more at breast height is 270 cubic feet per acre per year. On the basis of a 100-year site curve, the mean site index for Douglas fir is 170. High winds from the Pacific Ocean may seriously limit the growth of trees unless they are in a protected area.

The main limitations for the management of timber on this unit are the susceptibility of the surface layer to compaction, steepness of slope, the hazard of erosion, plant competition, and the hazard of windthrow. The main limitation for the harvesting of timber is steepness of slope. Using standard wheeled and tracked equipment when the soil is moist causes rutting and compaction. Displacement of topsoil occurs most readily when the soil is dry. Puddling can occur when the soil is wet. Cable yarding systems are safer, damage the soil less, and help to maintain productivity.

Proper design of road drainage systems and care in the placement of culverts help to control erosion. Cuts and fills are subject to erosion unless treated. Seeding, mulching, benching, and compacting the soil can reduce erosion. Unsurfaced roads and skid trails are slippery when wet or moist, and they may be impassable during rainy periods. Logging roads require suitable surfacing for year-round use. Rock for road construction is not readily available in this unit. Steep yarding paths, skid trails, and firebreaks are subject to rilling and gullyng unless they are provided with adequate water bars or are protected by plant cover, or both. Road location and maintenance costs are greater in the more steeply sloping areas. Material cast to the side when building roads can damage vegetation. It is also a potential source of sedimentation. End hauling of waste material minimizes damage to the vegetation downslope and reduces the potential for sedimentation. Sitka spruce, a shallow rooted species, is subject to windthrow.

When openings are made in the canopy, invading brushy plants can delay natural reforestation. Undesirable plants prevent adequate natural or artificial reforestation unless intensive site preparation and maintenance are provided. Reforestation can be accomplished by planting Sitka spruce, western hemlock, and Douglas fir seedlings.

This map unit is in capability subclass VIe.

54F—Templeton silt loam, 50 to 70 percent slopes.
This deep, well drained soil is on side slopes of

mountains. It formed in colluvium and residuum derived dominantly from sedimentary rock. The native vegetation is mainly conifers, shrubs, forbs, and hardwoods. Elevation is 50 to 800 feet. The average annual precipitation is 60 to 70 inches, the average annual air temperature is 51 to 53 degrees F, and the average frost-free period is 200 to 240 days.

Typically, the surface layer is very dark brown and dark brown silt loam 16 inches thick. The subsoil is reddish brown, yellowish red, and strong brown silty clay loam 26 inches thick. Soft, weathered and fractured siltstone is at a depth of 42 inches. In some areas the dark-colored surface layer is less than 10 inches thick.

Included in this unit are small areas of Millicoma and Salander soils in the northwestern part of the survey area. Included areas make up about 15 percent of the total acreage. The percentage varies from one area to another.

Permeability of this Templeton soil is moderate. Available water capacity is about 8.0 to 17.5 inches. Effective rooting depth is 40 to 60 inches. Runoff is rapid, and the hazard of water erosion is high.

This unit is used for timber production and wildlife habitat.

This unit is suited to the production of Douglas fir. Among the other species that grow on this unit are western hemlock, western redcedar, and red alder. The understory vegetation is mainly creambush oceanspray evergreen huckleberry, red huckleberry, salal, western swordfern, and vine maple.

On the basis of a 100-year site curve, the mean site index for Sitka spruce is 180. At the culmination of the mean annual increment (CMAI), the production of 60-year-old Sitka spruce trees 1.5 inches in diameter or more at breast height is 270 cubic feet per acre per year. On the basis of a 100-year site curve, the mean site index for Douglas fir is 170.

The main limitations for the management of timber on this unit are the susceptibility of the surface layer to compaction, steepness of slope, the hazard of erosion, plant competition, and the hazard of windthrow. Highlead or other cable logging systems are most suitable.

Proper design of road drainage systems and care in the placement of culverts help to control erosion. Cuts and fills are subject to erosion unless treated. Seeding, mulching, benching, and compacting the soil can reduce erosion. Unsurfaced roads and skid trails are slippery when wet or moist, and they may be impassable during rainy periods. Logging roads require suitable surfacing for year-round use. Rock for road construction is not

154

readily available in this unit. Steep yarding paths, skid trails, and firebreaks are subject to rilling and gullying unless they are provided with adequate water bars or are protected by plant cover, or both. Locating roads on midslopes results in large cuts and fills and thus removes land from production. Material cast to the side when building roads can damage vegetation. It is also a potential source of sedimentation. End hauling of waste material minimizes damage to the vegetation downslope and reduces the potential for sedimentation. Sitka spruce, a shallow rooted species, is subject to windthrow.

When openings are made in the canopy, invading brushy plants can delay natural reforestation. Undesirable plants prevent adequate natural or artificial reforestation unless intensive site preparation and maintenance are provided. Reforestation can be accomplished by planting Douglas fir seedlings.

This map unit is in capability subclass VIIc.

55D—Templeton-Bullards complex, 3 to 30 percent slopes. This map unit is on ridgetops and side slopes of mountains and strongly dissected marine terraces. The native vegetation is mainly conifers, shrubs, forbs, and hardwoods. Elevation is 50 to 600 feet. The average annual precipitation is 60 to 70 inches, the average annual air temperature is 51 to 53 degrees F, and the average frost-free period is 200 to 240 days.

This unit is 45 percent Templeton silt loam and 30 percent Bullards sandy loam. The Templeton soil is in convex areas on side slopes where recent marine and eolian deposits have been eroded away, and the Bullards soil is in convex areas on ridgetops and on west-facing side slopes. The components of this unit are so intricately intermingled that it was not practical to map them separately at the scale used.

Included in this unit are small areas of deep, well drained, gravelly soils and moderately deep, loamy soils. Also included are small areas of deep, poorly drained, loamy soils. Included areas make up about 25 percent of the total acreage.

The Templeton soil is deep and well drained. It formed in colluvium and residuum derived dominantly from sedimentary rock. Typically, the surface layer is very dark brown and dark brown silt loam 16 inches thick. The subsoil is reddish brown, yellowish red, and strong brown silty clay loam 26 inches thick. Soft, weathered and fractured siltstone is at a depth of 42 inches. In some areas the dark-colored surface layer is less than 10 inches thick.

Permeability of the Templeton soil is moderate. Available water capacity is about 8.0 to 17.5 inches.

Effective rooting depth is 40 to 60 inches. Runoff is medium, and the hazard of water erosion is moderate.

The Bullards soil is deep and well drained. It formed in mixed eolian and marine deposits. Typically, the surface is covered with a mat of undecomposed organic litter 3 inches thick. The surface layer is very dark grayish brown sandy loam 7 inches thick. The subsoil is dark reddish brown, dark brown, and strong brown gravelly sandy loam 34 inches thick. The substratum to a depth of 60 inches or more is yellowish brown sand.

Permeability of the Bullards soil is moderate. Available water capacity is about 4.0 to 5.5 inches. Effective rooting depth is 60 inches or more. Runoff is medium, and the hazard of water erosion is moderate.

This unit is used mainly for timber production and wildlife habitat.

This unit is suited to the production of Sitka spruce and Douglas fir. Among the other species that grow on the unit are western hemlock, Port Orford cedar, western redcedar, shore pine, and red alder. The understory vegetation is mainly salal, evergreen huckleberry, creambush oceanspray, Pacific rhododendron, cascara, western swordfern, and oxalis.

On the basis of a 100-year site curve, the mean site index for Sitka spruce is 180 on the Templeton soil. At the culmination of the mean annual increment (CMAI), the production of 50-year-old Sitka spruce trees 1.5 inches in diameter or more at breast height is 255 cubic feet per acre per year. On the basis of a 100-year site curve, the mean site index for Douglas fir is 170.

On the basis of a 100-year site curve, the mean site index for Douglas fir is 132 on the Bullards soil. At the culmination of the mean annual increment (CMAI), the production of 60-year-old Douglas fir trees 1.5 inches in diameter or more at breast height is 133 cubic feet per acre per year. On the basis of a 50-year site curve, the mean site index for Douglas fir is 105.

High winds from the Pacific Ocean may seriously limit the growth of trees on this unit unless they are in a protected area.

The main limitations for the management of timber on this unit are the susceptibility of the surface layer of the Templeton soil to compaction, the hazard of erosion, the hazard of windthrow, and plant competition. Using standard wheeled and tracked equipment when the soil is moist causes rutting and compaction. Displacement of the surface layer occurs most readily when the soil is dry. Puddling can occur when the soil is wet. Using low-pressure ground equipment damages the soil less and helps to maintain productivity.

Proper design of road drainage systems and care in the placement of culverts help to control erosion. Cuts

155

and fills are subject to erosion unless treated. Seeding, mulching, benching, and compacting the soil can reduce erosion. Unsurfaced roads and skid trails are slippery when wet or moist, and they may be impassable during rainy periods. Logging roads require suitable surfacing for year-round use. Rock for road construction is not readily available in this unit. Road location and maintenance costs are greater in the more steeply sloping areas.

Windthrow is a hazard when the soil is wet and winds are strong. When openings are made in the canopy, invading brushy plants can delay natural reforestation. Undesirable plants reduce natural or artificial reforestation unless intensive site preparation and maintenance are provided. Reforestation can be accomplished by planting Sitka spruce, western hemlock, and Douglas fir seedlings.

This map unit is in capability subclass VIe.

55E—Templeton-Bullards complex, 30 to 50 percent slopes. This map unit is on ridgetops and side slopes of mountains and strongly dissected marine terraces. The native vegetation is mainly conifers, shrubs, forbs, and hardwoods. Elevation is 50 to 500 feet. The average annual precipitation is 60 to 70 inches, the average annual air temperature is 51 to 53 degrees F, and the average frost-free period is 200 to 240 days.

This unit is 55 percent Templeton silt loam and 25 percent Bullards sandy loam. The Templeton soil is in convex areas on side slopes where recent marine and eolian deposits have been eroded away, and the Bullards soil is in convex areas on ridgetops and in the more gently sloping areas on west-facing side slopes. The components of this unit are so intricately intermingled that it was not practical to map them separately at the scale used.

Included in this unit are small areas of deep, well drained, gravelly soils. Included areas make up about 20 percent of the total acreage.

The Templeton soil is deep and well drained. It formed in colluvium and residuum derived dominantly from sedimentary rock. Typically, the surface layer is very dark brown and dark brown silt loam 16 inches thick. The subsoil is reddish brown, yellowish red, and strong brown silty clay loam 26 inches thick. Soft, weathered and fractured siltstone is at a depth of 42 inches. In some areas the dark-colored surface layer is less than 10 inches thick.

Permeability of the Templeton soil is moderate. Available water capacity is about 8.0 to 17.5 inches. Effective rooting depth is 40 to 60 inches. Runoff is

rapid, and the hazard of water erosion is high.

The Bullards soil is deep and well drained. It forms in mixed eolian and marine deposits. Typically, the surface is covered with a mat of undecomposed organic litter 3 inches thick. The surface layer is very dark grayish brown sandy loam 7 inches thick. The subsoil is dark reddish brown, dark brown, and strong brown gravelly sandy loam 34 inches thick. The substratum a depth of 60 inches or more is yellowish brown sand.

Permeability of the Bullards soil is moderate. Available water capacity is about 4.0 to 5.5 inches. Effective rooting depth is 60 inches or more. Runoff is rapid, and the hazard of water erosion is high.

This unit is used mainly for timber production and wildlife habitat.

This unit is suited to the production of Sitka spruce and Douglas fir. Among the other species that grow in this unit are western hemlock, Port Orford cedar, western redcedar, shore pine, and red alder. The understory vegetation is mainly salal, evergreen huckleberry, creambush oceanspray, Pacific rhododendron, cascara, western swordfern, and oxal.

On the basis of a 100-year site curve, the mean site index for Sitka spruce is 180 on the Templeton soil. At the culmination of the mean annual increment (CMAI), the production of 50-year-old Sitka spruce trees 1.5 inches in diameter or more at breast height is 255 cubic feet per acre per year. On the basis of a 100-year site curve, the mean site index for Douglas fir is 170.

On the basis of a 100-year site curve, the mean site index for Douglas fir is 132 on the Bullards soil. At the culmination of the mean annual increment (CMAI), the production of 60-year-old Douglas fir trees 1.5 inches in diameter or more at breast height is 133 cubic feet per acre per year. On the basis of a 50-year site curve, the mean site index for Douglas fir is 105.

High winds from the Pacific Ocean may seriously limit the growth of trees on this unit unless they are protected area.

The main limitations for the management of timber in this unit are the susceptibility of the surface layer of Templeton soil to compaction, steepness of slope, the hazard of erosion, the hazard of windthrow, and plant competition. The main limitation for the harvesting of timber is steepness of slope. Using standard wheel and tracked equipment when the soil is moist cause rutting and compaction. Displacement of topsoil occurs most readily when the soil is dry. Puddling can occur when the soil is wet. Cable yarding systems are safe damage the soil less, and help to maintain productivity.

Proper design of road drainage systems and care in the placement of culverts help to control erosion. C

156

and fills are subject to erosion unless treated. Seeding, mulching, benching, and compacting the soil can reduce erosion. Unsurfaced roads and skid trails are slippery when wet or moist, and they may be impassable during rainy periods. Logging roads require suitable surfacing for year-round use. Rock for road construction is not readily available in this unit. Material cast to the side when building roads can damage vegetation. It is also a potential source of sedimentation. End hauling of waste material minimizes damage to the vegetation downslope and reduces the potential for sedimentation.

Windthrow is a hazard when the soil is wet and winds are strong. When openings are made in the canopy, invading brushy plants can delay natural reforestation. Undesirable plants reduce natural or artificial reforestation unless intensive site preparation and maintenance are provided. Reforestation can be accomplished by planting Sitka spruce, western hemlock, and Douglas fir seedlings.

This map unit is in capability subclass VIe.

56E—Templeton-Millicoma complex, 12 to 50

percent slopes. This map unit is on ridgetops and side slopes of mountains. The native vegetation is mainly conifers, shrubs, forbs, and hardwoods. Elevation is 50 to 800 feet. The average annual precipitation is 70 to 80 inches, the average annual air temperature is 51 to 53 degrees F, and the average frost-free period is 200 to 240 days.

This unit is 55 percent Templeton silt loam and 30 percent Millicoma gravelly loam. The Templeton soil is in convex areas on ridgetops and on the more gently sloping side slopes, and the Millicoma soil is on side slopes. The components of this unit are so intricately intermingled that it was not practical to map them separately at the scale used.

Included in this unit are small areas of Salander soils. Also included are small areas of soils that are similar to the Millicoma soil but have less than 35 percent rock fragments in the subsoil. Included areas make up about 15 percent of the total acreage. The percentage varies from one area to another.

The Templeton soil is deep and well drained. It formed in colluvium and residuum derived dominantly from sedimentary rock. Typically, the surface layer is very dark brown and dark brown silt loam 16 inches thick. The subsoil is reddish brown, yellowish red, and strong brown silty clay loam 26 inches thick. Soft, weathered and fractured siltstone is at a depth of 42 inches.

Permeability of the Templeton soil is moderate. Available water capacity is about 8.0 to 17.5 inches.

Effective rooting depth is 40 to 60 inches. Runoff is rapid, and the hazard of water erosion is high.

The Millicoma soil is moderately deep and well drained. It formed in colluvium derived dominantly from sandstone. Typically, the surface is covered with a mat of undecomposed needles, leaves, and twigs 3 inches thick. The surface layer is very dark brown and very dark grayish brown gravelly loam 18 inches thick. The subsoil is dark brown very gravelly loam 17 inches thick. Partially weathered sandstone is at a depth of 35 inches.

Permeability of the Millicoma soil is moderately rapid. Available water capacity is about 3 to 6 inches. Effective rooting depth is 20 to 40 inches. Runoff is rapid, and the hazard of water erosion is high.

This unit is used mainly for timber production and wildlife habitat.

This unit is suited to the production of Sitka spruce and Douglas fir. Among the other species that grow on the unit are western hemlock, western redcedar, and red alder. The understory vegetation is mainly salal, salmonberry, cascade Oregongrape, western swordfern, and vine maple.

On the basis of a 100-year site curve, the mean site index for Sitka spruce is 180 on the Templeton soil. At the culmination of the mean annual increment (CMAI), the production of 50-year-old Sitka spruce trees 1.5 inches in diameter or more at breast height is 270 cubic feet per acre per year. On the basis of a 100-year site curve, the mean site index for Douglas fir is 170.

On the basis of a 100-year site curve, the mean site index for Sitka spruce is 169 on the Millicoma soil. At the culmination of the mean annual increment (CMAI), the production of 50-year-old Sitka spruce trees 1.5 inches in diameter or more at breast height is 255 cubic feet per acre per year. On the basis of a 100-year site curve, the mean site index for Douglas fir is 145.

The main limitations for the management of timber on this unit are the susceptibility of the surface layer of the Templeton soil to compaction, steepness of slope, the hazards of erosion and windthrow, and plant competition. The main limitation for the harvesting of timber is steepness of slope. Using standard wheeled and tracked equipment when the soil is moist causes rutting and compaction. Puddling can occur when the soil is wet. Cable yarding systems are safer, damage the soil less, and help to maintain productivity. Low-pressure ground equipment can be used in the more gently sloping areas of this unit.

Proper design of road drainage systems and care in the placement of culverts help to control erosion. Cuts and fills are subject to erosion unless treated. Seeding,

157

SUNSET BAY GEOMORPHIC MAPPING PROJECT

Dr. Taylor – ES322 Geomorphology

INTRODUCTION

Geologic mapping has a long tradition in the United States, dating to the western expeditions of Powell in the late 1800's (Powell, 1882; 1888). The National Geologic Mapping Act of 1992 recognized the importance of geologic mapping as a tool for resource evaluation, environmental protection, and natural hazards assessment. As a cartographic subset, surficial maps provide representation of the critical links between bedrock geology, climate, tectonics, vegetation, and surficial processes.

The purpose of this field-based exercise is to gain an understanding of mapping concepts as they are applied to the surficial deposits and landforms manifested at the Earth's surface. This exercise focuses on landforms and processes in the vicinity of Sunset Bay, Coos County, Oregon.

SURFICIAL MAPPING APPROACH

Surficial mapping will employ a four-fold scheme in which units are delineated on the basis of age, origin (process), landform, and material (texture). The technique emphasizes the link between landforms, materials, and processes in a landscape dominated by tectonic uplift, hillslopes, mass wasting, and fluvial/coastal erosion.

Large-scale landform units are classified into hillslope and valley-bottom features. Hillslope landforms are subdivided into ridges and side slopes. Valley-bottoms are subdivided into channels, floodplains, terraces, and fans. Hillslope deposits include residuum and colluvial diamicton. Fluvial deposits are typically clast supported, moderately sorted, and imbricated due to deposition by turbulent streamflow. Debris flows result in poorly-sorted diamictons with crude internal stratification. Dating of surficial deposits is problematic, hence traditional stratigraphy-based techniques are largely not applicable. The four-fold mapping protocol circumvents the need for formal stratigraphic nomenclature.

SOIL SURVEYS AS A REFERENCE FOR LANDSCAPE ANALYSIS

Soils represent the weathered mantle of unconsolidated surficial material that covers land surfaces. They are comprised of a mixture of mineral and organic matter derived from the physical, chemical, and biologic weathering of bedrock. The Natural Resource Conservation Service (NRCS) is the federal agency that is primarily responsible for the analysis and preservation of this valuable resource. As a result, county soil surveys and soil maps have been prepared for most regions of the U.S. These surveys provide an important data set for geomorphic analysis of landforms and surficial materials.

The main controlling factors that contribute to soil formation are: 1) climate, 2) organic activity (animals / plants), 3) relief / topography, 4) parent material, and 5) time (CLORPT). Climate refers to amount of rainfall and temperature. Organic activity refers to style of plant growth, microbial activity, and burrowing organisms. Relief / topography refers to the steepness of slope. Parent material refers to the source of weathered material upon which the soils are formed (e.g. bedrock = igneous, sedimentary, metamorphic; surficial regolith = colluvium). Time refers to the residence time of the soil material, essentially the length of time that the soil has been forming without physical interruption. All of these factors contribute to soil characteristics.

Soil surveys are conducted by using topographic maps, air photos, ground surveys, soils excavations, and geologic maps. Soil map units are delineated primarily on the basis of material composition (i.e. texture of the soil) and topographic configuration (steepness of slope, flood-prone

areas, etc.). Other parameters include color and soil chemistry. Soil maps are typically published on air photos and created for individual counties and conservation districts. A brief comparison of soils and topographic maps suggests that soils are not randomly distributed, but are intimately related to topography and geomorphic setting. Landforms and geomorphic processes often influence the physical and chemical properties of soils. Hence, if we know the soil and its characteristics we may be able to begin to understand the geomorphic system.

PROCEDURES AND TASKS

Part 1. Geomorphic Mapping

- (1) Drive to Sunset Bay, Coos County, Oregon... or take a class field trip as the case may be.
- (2) We will spend the afternoon at Sunset Bay. The following resources are available to support your observations: (a) topographic map of Cape Arago-Sunset Bay area, (2) 10-m hillshade model, (3) slope model, and (4) relevant excerpts from the NRCS Coos County Soil Survey.
- (3) The first step is to orient yourself to the area, examine all available maps and directly observe the landscape around you, answer the following questions:
 - a. List and describe the upland (ridge, hillslopes) and lowland (valley bottoms, beaches) landforms that you observe.
 - b. List and describe the dominant erosional processes evident in the area. Think of all the agents of erosion, and how they are working at this site.
 - c. List and describe the range of surficial deposits ("regolith") that occur in this area. In your description include texture (grain size) and sorting of surficial material). Make observations of material color as well.
- (4) Examine the topographic and slope maps. Using the topographic map as a base, use colored pencils to shade landform elements based on slope. Use the following color code and slope classes:

a. 0 to 10 degrees	Yellow
b. 10 to 20 degrees	Green
c. 20 to 30 degrees	Blue
d. > 30 degrees	Red

(USE topo map on p. 124)
- (5) Once you've color-shaded your map, use a heavy pencil or pen to draw "contacts" or black line land-unit boundaries between your shaded areas.
- (6) Compare your color-coded topographic slope map to the Coos County soil survey for the area. Fill in the following table combining observations from these two data sources:

A. Yellow Land-Unit Zone (0-10 degrees)

Soil Unit Code (number + name)	Landforms	Materials (texture, sorting)	Processes (transport agent)	Age
_____	_____	_____	_____	_____
_____	_____	_____	_____	_____
_____	_____	_____	_____	_____
_____	_____	_____	_____	_____
_____	_____	_____	_____	_____

B. Green Land-Unit Zone (10-20 degrees)

Soil Unit Code (number + name)	Landforms	Materials (texture, sorting)	Processes (transport agent)	Age
_____	_____	_____	_____	_____
_____	_____	_____	_____	_____
_____	_____	_____	_____	_____
_____	_____	_____	_____	_____
_____	_____	_____	_____	_____

C. Blue Land-Unit Zone (20-30 degrees)

Soil Unit Code (number + name)	Landforms	Materials (texture, sorting)	Processes (transport agent)	Age
_____	_____	_____	_____	_____
_____	_____	_____	_____	_____
_____	_____	_____	_____	_____
_____	_____	_____	_____	_____
_____	_____	_____	_____	_____

160

D. Red Land-Unit Zone (>30 degrees)

Soil Unit Code (number + name)	Landforms	Materials (texture, sorting)	Processes (transport agent)	Age
_____	_____	_____	_____	_____
_____	_____	_____	_____	_____
_____	_____	_____	_____	_____
_____	_____	_____	_____	_____
_____	_____	_____	_____	_____

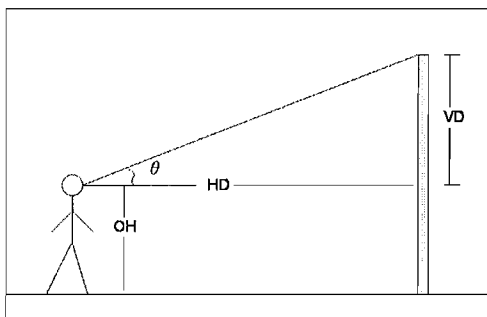
(7) Complete your draft geomorphic map by combining slope observations with soil-landform-material observations. Using a marker or dark pencil, refine your color-shaded areas to include subdivisions based on the soils-landform-process observations. Subdivide color zones with heavy dashed-lines, and label your geomorphic units within each color zone with one of the following designations:

- Qr – residuum, Quaternary in age, undifferentiated (ridge tops, in-place regolith)
- Qc - colluvium, Quaternary in age, undifferentiated (hillslopes and footslopes)
- Qal - alluvium, Quaternary in age, undifferentiated (river deposits, valleys, channels, floodplains)
- Qt – marine terrace, Quaternary in age, undifferentiated (abandoned, elevated beach zones)
- Hb – beach zone, Holocene in age (present day beach zones)
- Qd – dune deposits, Quaternary in age, undifferentiated (wind-blown, sand dunes)

Part 2 - Landform and Soil Sampling Exercise – North End of Sunset Bay

A. At the north end of Sunset Bay, there is an elevated upland bench that bounds the beach. Examine the area on the topographic map, on your geomorphic map, and on the slope-hillshade-soils maps. Working in teams, conduct the following tasks.

B. At the beach level, using a Brunton compass-pace-tape, and trigonometric techniques, determine the approximate height of the upland bench above active beach level **in meters and feet**. Refer to the figure below for a guide on how to complete this calculation.



OH = ocular height, VD = vertical distance from eyes to top of object, HD = horizontal distance from eyes to object, θ = angle of inclination between eyes and top of object:

	$\tan \theta = VD / HD$	Total Height of Object = OH + VD
Ocular Height _____		
HD _____		
θ _____		Total Height (ft) _____
VD _____		Total Height (m) _____

C. Hike up to the top of the bench, at the north end of Sunset Bay. Using the soil auger, collect a series of samples at about 20 to 25 cm increments, to a total depth of approximately 150 centimeters. See how far you can drive the auger into the regolith materials. Carefully empty the bucket auger samples out on the ground in organized, linear fashion, from top to bottom for observation. Keep track of the depth increments of each extraction using a meter stick and the sample rod.

Once we make field observations, we will ziplock-bag and label the samples for transport back to the Geology Lab. Depending on time, in the field, or follow-up in the lab, use your soil observation skills / tools to describe the soil samples for each increment. Refer to the soil-observation reference materials provided in the field guide. Fill in the table below.

Depth Interval (cm)	Color (moist)	Consistency (moist)	Texture	Other Observations
_____	_____	_____	_____	_____
_____	_____	_____	_____	_____
_____	_____	_____	_____	_____
_____	_____	_____	_____	_____
_____	_____	_____	_____	_____
_____	_____	_____	_____	_____
_____	_____	_____	_____	_____
_____	_____	_____	_____	_____
_____	_____	_____	_____	_____
_____	_____	_____	_____	_____
_____	_____	_____	_____	_____

D. Soil Interpretation

Question 1: Table 2 below is a summary of soils data collected for marine surfaces throughout the southern Oregon region. By comparing your soils observations to Table 2, what is your best approximation of soil development stage for the Sunset Bay surface soil?

TABLE 2. DEVELOPMENT STAGES OF SOILS ON ELEVATED MARINE TERRACES ALONG THE CENTRAL AND SOUTHERN OREGON COAST

Development stage	Depth to Cox (m)	B horizon hue	Bt thickness (cm)	Maximum B horizon texture* (% clay) ^b	Maximum clay films ^c
1	0.8-1.4	7.5-10YR	0	sil, l, sl (<30)	1-3npfpo
2	1.0-1.4	7.5YR	<50	sicl, cl, scl (30-40)	2-3n-mkpfpo
3	1.0-1.7	7.5YR	<50	sicl, cl, scl (30-40)	2-3mkpfpo
4	1.4-1.8	5-7.5YR	50-100	sicl, sic, cl, c (35-42)	3-4mkpfpo
5	1.9-2.8	5-7.5YR	100-200	sic, c (40-58)	3-4mk-kpfpo
6	2.6-4.5	5YR	>200	sic, c (40-65)	3-4mk-kpfpo
7	3.2->4.5	2.5YR	>200	sic, c (45-65)	3-4mk-kpfpo

*l, loam; sl, sandy loam; sil, silt loam; sicl, silty clay loam; sic, silty clay; cl, clay loam; scl, sandy clay loam; c, clay. Abbreviations follow Soil Survey Staff (1951).

^bNotations for clay films; number denotes extent of ped faces covered by film; v1, <5%; 1, 5%-25%; 2, 25%-50%; 3, 50%-90%; >90%; n, thin; mk, moderately thick; k, thick; pf, film on ped face; po, film lines the pores. Abbreviations follow Soil Survey Staff (1951).

^cWe estimated percent clay for each horizon at each soil locality during field work. We have confidence in our ability to estimate clay content in the field because we obtained a significant correlation ($r^2 = 0.66$; $p \leq 0.01$) between percent clay estimated in the field and percent clay measured in the laboratory (28 samples).

Question 2: Based on your geomorphic mapping, soil sampling, and review of the Coos County Soil Survey, what is the type of landform that you sampled at the north end of Sunset Bay?

Question 3: Explain how this surface formed? How old is this surface, i.e. the time since it was eroded and formed at sea level?

Question 4: Using your surface height calculation in 8 B above and age estimate, calculate rate of surface elevation change in mm/yr. Calculate again in meters / thousand years. Show all of your work. (NOTE: 17m is the whiskey run surface at 80,000 yrs old)

Question 5: Is the Oregon coast at Sunset Bay uplifting or subsiding over time? What forces may be driving this phenomena?

Question 6: How does the Quaternary tectonic setting of the Oregon Coast relate to that manifested in the Tertiary bedrock outcrops and structured exposed on the beach at Sunset Bay? Are similar processes operating today as they did in the Eocene or Oligocene? What is your evidence one way or another?

G322 Lab Exercise
Neotectonic and Coastal Processes of Oregon

Part I. Pre-Lab Questions

Use your notes, textbook, wall maps, and reading assignments to answer the following questions.

A. Match the Following Coastal Locations with the terms on the Right. List all that apply.

_____	1. Oregon Coast	Passive Margin Tectonics (inactive)
_____	2. Washington Coast	Active Margin Tectonics - subduction
_____	3. Southern California Coast	Active Margin Tectonics - transform
_____	4. Northern California Coast	Active Margin Tectonics - rifting / spreading
_____	5. Aleutian Islands of Alaska	Emergent Coastline
_____	6. Southeast Alaskan Coast	Submergent Coastline
_____	7. Gulf of Mexico - Texas	Active Subsidence
_____	8. Central Atlantic / U.S.	Active Uplift

B. Thinking Questions

9. The last major glaciation (i.e. a pervasive cold-wet climate regime) in the northern hemisphere was at it's peak 18,000 to 20,000 years ago. 100's to 1000' of feet of Ice covered much of Canada and the northern tier of the U.S.

A. From what major hydrologic source does the precipitation that forms glacial ice originate?

B. Describe how this moisture is cycled into glacial ice (what are the processes associated with this part of the hydrologic cycle).

C. What happens to global sea level during a major glacial climate? What happens to global sea level during a major interglacial (i.e. warm / melting) climate?

D. What happens to land surface elevation at convergent tectonic boundaries (i.e. subduction zones), especially where accretionary tectonics is prevalent?

E. What happens to land surface elevation at passive tectonic boundaries, where sediment accumulates over time (think about what happens to water saturated sediment as it accumulates, becoming thicker over time, under increasing weight).

10. If global sea level is rising at a rate of 2 mm/yr, at a passive continental margin, how long will it take for sea level to rise 5 m? Show your math work.

11. If global sea level is rising at a rate of 5 mm/yr, and an active tectonic coastline is experiencing uplift at a rate of 5 mm/yr, what will be the net relative rate of sea level change at this location? Show your math work.
12. If global sea level is rising at a rate of 3 mm /yr, and a passive margin coastline is actively subsiding at a rate of 5 mm /yr, what will be the net relative rate of sea level change at this location? Show your math work. Is this coastline best characterized as "emergent" or "submergent"?
13. If global sea level is rising at a rate of 1 mm/yr and an active tectonic coastline is experiencing uplift at a rate of 5 mm/yr, what will be the net relative rate of sea level change at this location? Show your math work. Is this coastline best characterized as "emergent" or "submergent"?
14. List two dominant oceanic processes associated with the Oregon Coast.
15. List two dominant tectonic processes associated with the Oregon Coast.
16. List three geologic hazards that you can think of, associated with the Oregon Coast (think about the news reports that you hear every year).
17. In terms of temperature as related to the physics of volume expansion / contraction (think hot air balloon), which condition would have a greater volume, warm sea water or cold sea water?
18. In terms of density driven currents: warm sea water is _____ (more dense or less dense?) compared to cold sea water. Therefore, warm sea water will tend to _____ (rise or sink), and cold sea water will tend to _____ (rise or sink?).
19. Similarly, in terms of density-driven motion in rock material: hot, young oceanic crust is _____ (more dense or less dense?) compared to cold, old oceanic crust. Therefore, hot, young oceanic crust will tend to (rise or sink?), and cold, old oceanic crust will tend to _____ (rise or sink?).
20. Question for you: What would happen to global sea level under conditions of very rapid seafloor spreading? Why?

What would happen to global sea level under conditions of very slow seafloor spreading? Why?

Part 5. Neotectonics of the Oregon Coast

Western Oregon is the site of plate tectonic convergence, with subduction of the Juan de Fuca plate beneath the North American plate. This convergent zone is associated with accretionary tectonics, compressional strain, and Cascade arc volcanism. As such, neotectonic deformation, crustal motion, and differential uplift/subsidence of the Oregon coast must be reconciled with any geomorphic model of the region.

Historic crustal motion of the Earth is measured via re-leveling surveys of surface elevation (re-leveling = re-measurement of land surface elevation over time), or with satellite positioning systems (GPS = global positioning system). Longer term uplift of coastal areas is reconstructed by examination of wave-cut terraces and coast terrace deposits, with related application of geologic dating techniques.

Mitchell and others (1994) examined historic re-leveling data of surface elevations along a transect extending from northern California to Washington. They combined the re-leveling data with tide gauge measurements to determine net relative vertical ground motion velocities for coastal regions of the Pacific Northwest. Table 4 is a summary of historical ground motion velocity data for a south-to-north transect, arranged by latitude (degrees north); positive velocities = uplift, negative velocities = crustal subsidence.

Task 7 Using the data in Table 4, plot a south-to-north transect of historic ground motion velocity (y axis) vs. latitude (x axis). Use the blank profile paper provided in Figure 7 (alternatively, create the profile using the chart wizard in microsoft Excel). List the geographic names of the data localities above the profile, for reference.

Question 5-1. Identify regions of coastal PNW that are experiencing rapid historic uplift. Identify regions of coastal PNW that are experiencing no net uplift, or subsidence. Do you see any spatial patterns in terms of uplift / stability / subsidence along the south-to-north transect?

Question 5-2. Assuming that sea level is presently rising, what can you conclude about the rate of tectonic uplift, and rate of sea level rise for the Newport, OR area?

Question 5-3. Examine a tectonic map of the PNW (see the "fractured surface" map on the wall of the lab room). Identify the area of highest rates of tectonic uplift on your profile, and locate that area on the tectonic map. Comment on the relationship between the type of tectonic boundary(ies) and the highest rates of coastal uplift in the PNW.

Question 5-4. Which areas of the coastal transect would you expect to find the highest, and most well-developed flights of coastal terraces? Which areas would you expect to find the most well-developed coast-terrace soils? Why? Draw sketches to support your answer.

Task 8. Figure 8 is a map of interpolated uplift rates for select points in the Pacific Northwest (west of the Cascades). Draw contour lines on the map data connecting points of equal uplift rates. Use a contour interval = 1 mm/year. Using colored pencils, color code the neotectonic domains using the following classification scheme (i.e. color all regions of the map according to uplift rate):

uplift 0-1 mm /yr	blue
uplift 2-3 mm/yr	yellow
uplift 4-5 mm/yr	red

Question 5-5. Identify the zone of highest uplift. What type of tectonic process is occurring in this region.

Question 5-6. Locate Monmouth, OR on the map. What is our historic rate of uplift on campus? Which part of western Oregon is associated with the highest rates of uplift?

Question 5-7. What is the rate of uplift in the Puget Sound region? What other isostatic process(es) must be accounted for in the Puget Sound region, and to the north of that point.

Task 8. Table 5 is a listing of data collected from uplifted marine terraces in southern Oregon. The terraces are formed by wave-base erosion, at or below sea level. They are elevated along the Oregon coast through the process of relative uplift over time. The age of the terrace is derived by numerically dating preserved marine deposits. The original depth of the wave-cut platform is reconstructed from fossil organisms. Paleo-sea level (compared to modern sea level) is derived from the global marine sea level record.

Complete the data in Table 5 by using Microsoft Excel. Download the table from the class web site and use the spreadsheet math functions to determine parameters in columns e, f, and g (total tectonic uplift and average uplift rate). To help in resolving the parameters, draw a cross-sectional sketch of modern sea level, paleo-sea level, original depth of terrace, and present elevation. Calculate the total tectonic uplift that the terrace has experienced, combine that with the age data to determine the long-term average rate of uplift on the southern Oregon Coast.

Question 5-8. How do the long term average uplift rates in Table 5 compare with the historic uplift rates presented in Table 4, and Figures 7-8? Explain the differences or similarities that you observe.

Question 5-9. In looking at degree of soils development on the Whiskey Run, Cape Blanco, and Pioneer terraces; explain which terraces would have more well-developed soils, and which less. Describe the physical and chemical characteristics of the soils that you would expect to see when visiting all three of the localities.

Question 5-10. If you were asked to find these marine terraces on a map and in the field, what types of topographic and geologic evidence would you look for (how would you go about doing this from scratch)? Explain how county soils surveys would help in this process.

Table 3A. Reconstructed Global Sea Level Data for the Late Pleistocene (data reconstructed from coral assemblages in Tahiti, New Guindea, Barbados).

Calendar Age (kyr BP)	Reconstructed Relative Sea Level Compared to Modern (meters)
3.0	-0.07
5.8	-0.60
6.8	-4.19
7.3	-6.90
7.8	-11.43
8.2	-15.46
9.0	-22.71
9.5	-29.89
10.1	-39.79
10.5	-43.03
11.0	-48.90
11.5	-55.47
12.2	-61.60
12.8	-68.48
13.3	-74.56
13.9	-79.86
14.3	-93.12
14.6	-96.44
14.9	-98.87
16.8	-109.32
17.8	-112.38
18.4	-116.09
19.0	-118.24

Figure 5D. Reconstructed Global Sea Level Curve for the Late Pleistocene.

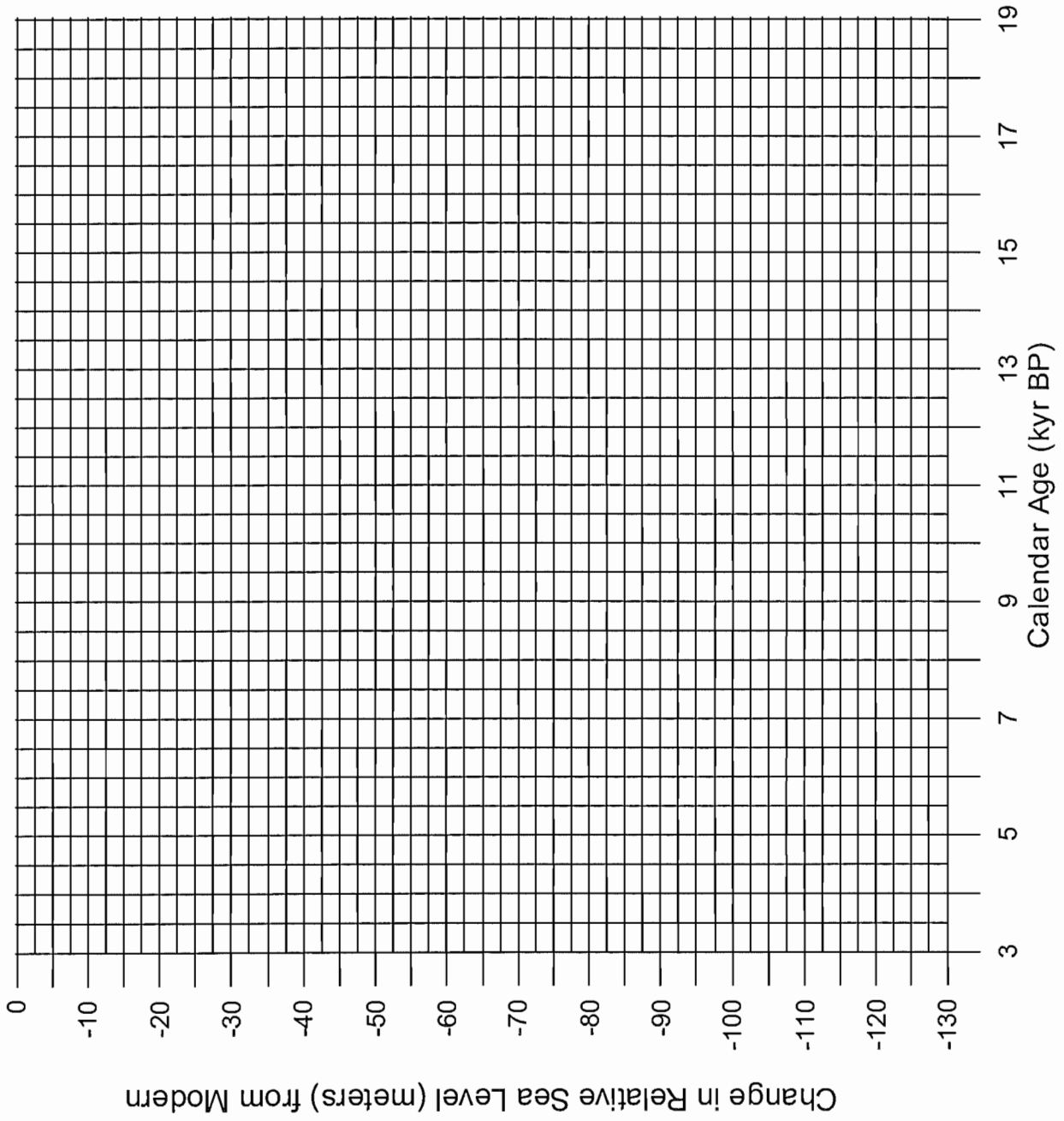


Figure 5E. Profile of the Continental Shelf, West of Newport Oregon.

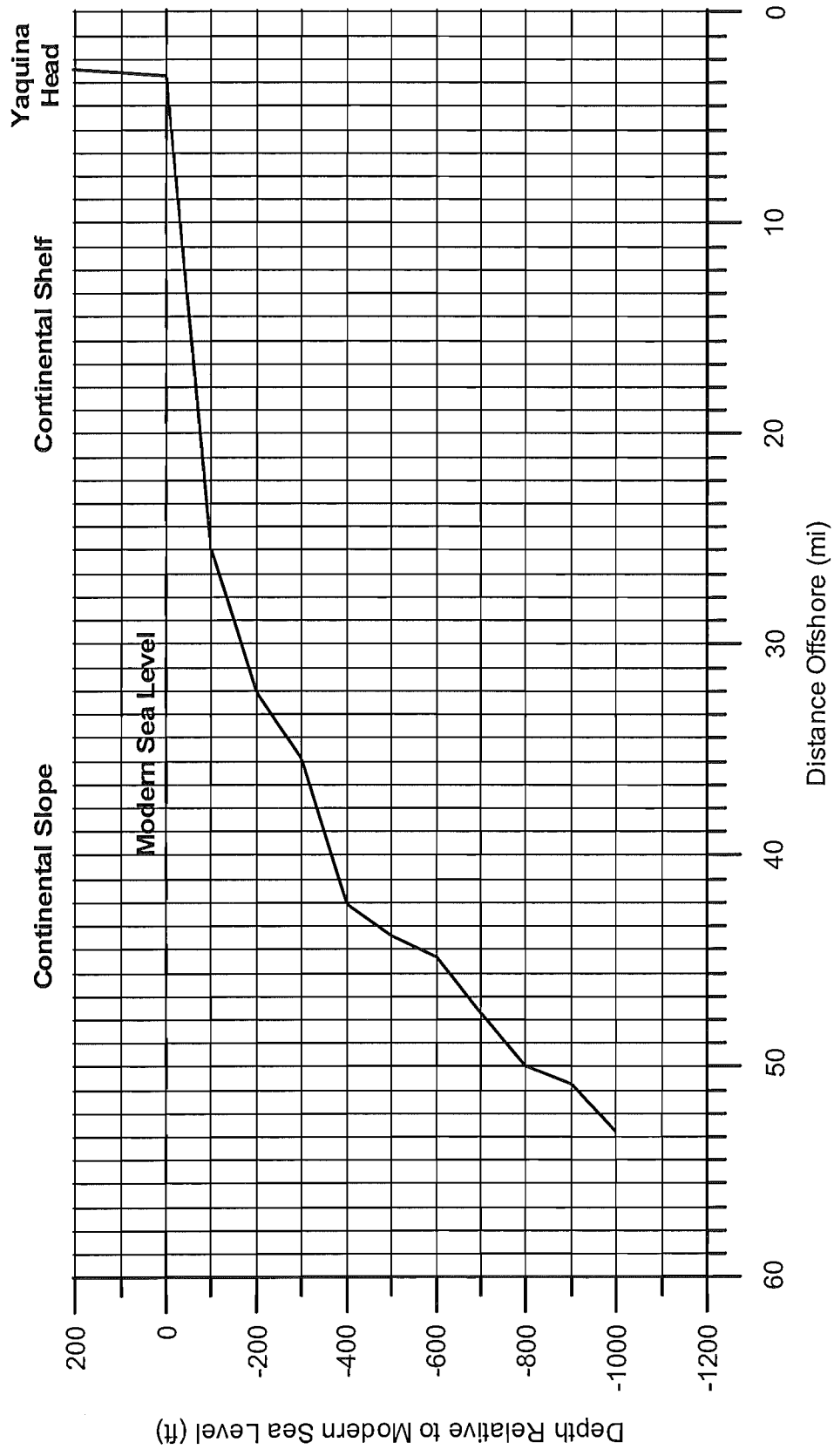


Table 4. Average Vertical Ground Motion Velocities for a South-to-North Transect Along the Coast of the Pacific Northwest

(Data derived from Mitchell et al., 1994 via releveling surveys).
 (Note: positive velocity = uplift, negative velocity = subsidence)
 c:wou:geomorph:f00:coastlab:neotect.xls / coastup

Latitude (degrees N)	Historic Average Vertical Ground Motion Velocity (mm/yr)	Approximate Geographic Location
39.5	1.2	Fort Bragg, CA
39.6	1.5	
39.7	1.8	
39.9	3.0	
40.0	4.1	
40.2	4.5	Garberville, CA
40.4	5.1	
40.6	5.4	
40.7	5.2	
40.9	4.9	Arcata, CA
41.0	4.8	
41.0	4.4	
41.0	3.8	
41.1	3.5	
41.2	3.3	
41.3	3.1	
41.4	2.8	
41.5	2.8	
41.7	2.8	
41.8	2.8	
41.9	2.9	
42.0	3.3	
42.1	3.8	Brookings, OR
42.1	4.0	
42.2	4.1	
42.3	4.1	
42.3	3.6	
42.4	3.3	
42.5	3.1	Gold Beach, OR
42.6	3.0	
42.7	3.0	
42.8	3.4	
42.9	3.7	
43.0	4.4	
43.1	4.4	
43.2	4.1	Bandon, OR
43.2	3.7	
43.3	3.4	
43.4	3.0	
43.5	2.5	
43.8	1.4	Reedsport, OR

Table 4. Average Vertical Ground Motion Velocities for a South-to-North Transect Along the Coast of the Pacific Northwest

(Data derived from Mitchell et al., 1994 via releveing surveys).
 (Note: positive velocity = uplift, negative velocity = subsidence)
 c:wou:geomorph:f00:coastlab:neotect.xls / coastup

Latitude (degrees N)	Historic Average Vertical Ground Motion Velocity (mm/yr)	Approximate Geographic Location
44.0	0.9	Florence, OR
44.2	0.6	
44.3	0.2	
44.4	0.0	
44.6	-0.1	Newport, OR
44.7	-0.2	
44.9	-0.2	Lincoln City, OR
45.2	-0.3	
45.5	-0.4	Tillamook, OR
45.6	-0.1	
45.7	0.2	
45.9	0.5	
45.9	1.2	
46.0	1.5	Seaside, OR
46.1	1.6	
46.1	1.5	
46.2	1.0	
46.4	0.4	
46.5	0.0	Willapa, WA
46.7	-0.6	
46.8	-0.8	
47.0	-1.0	Aberdeen, WA
47.2	-1.1	
47.3	-1.2	
47.4	-1.1	Queets, WA
47.6	-0.7	
47.7	-0.4	
47.7	0.3	
47.8	1.1	
47.9	1.8	La Push, WA
48.0	2.6	
48.1	3.2	Lake Ozette, WA

Figure 7. Plot of South-to-North Average Uplift Rate Profiles Along the Coast of the Pacific Northwest

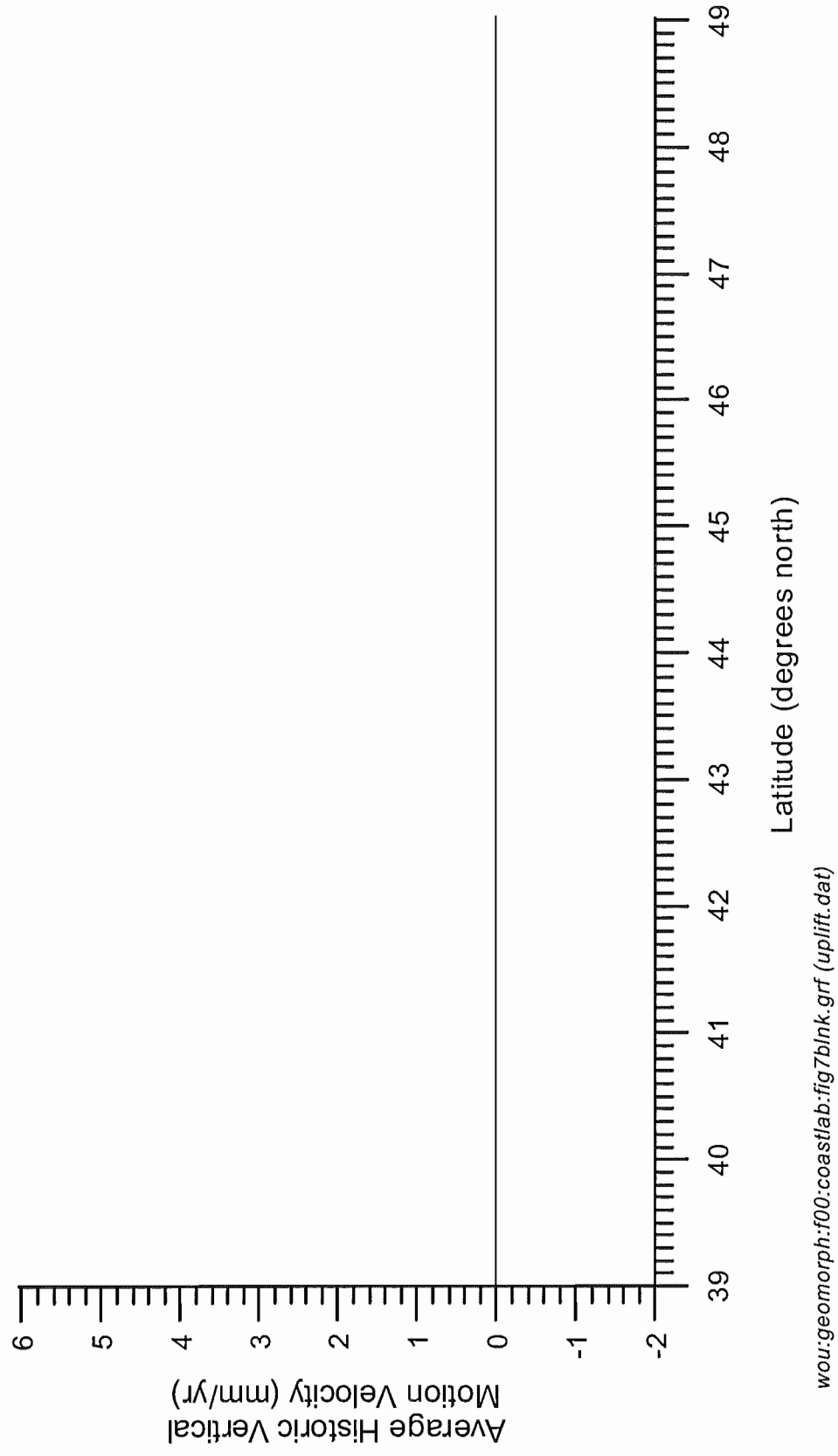


Figure 8. Map of Interpolated Uplift Rates for the Pacific Northwest, West of the Cascade Range (data derived from Mitchell et al., 1994)

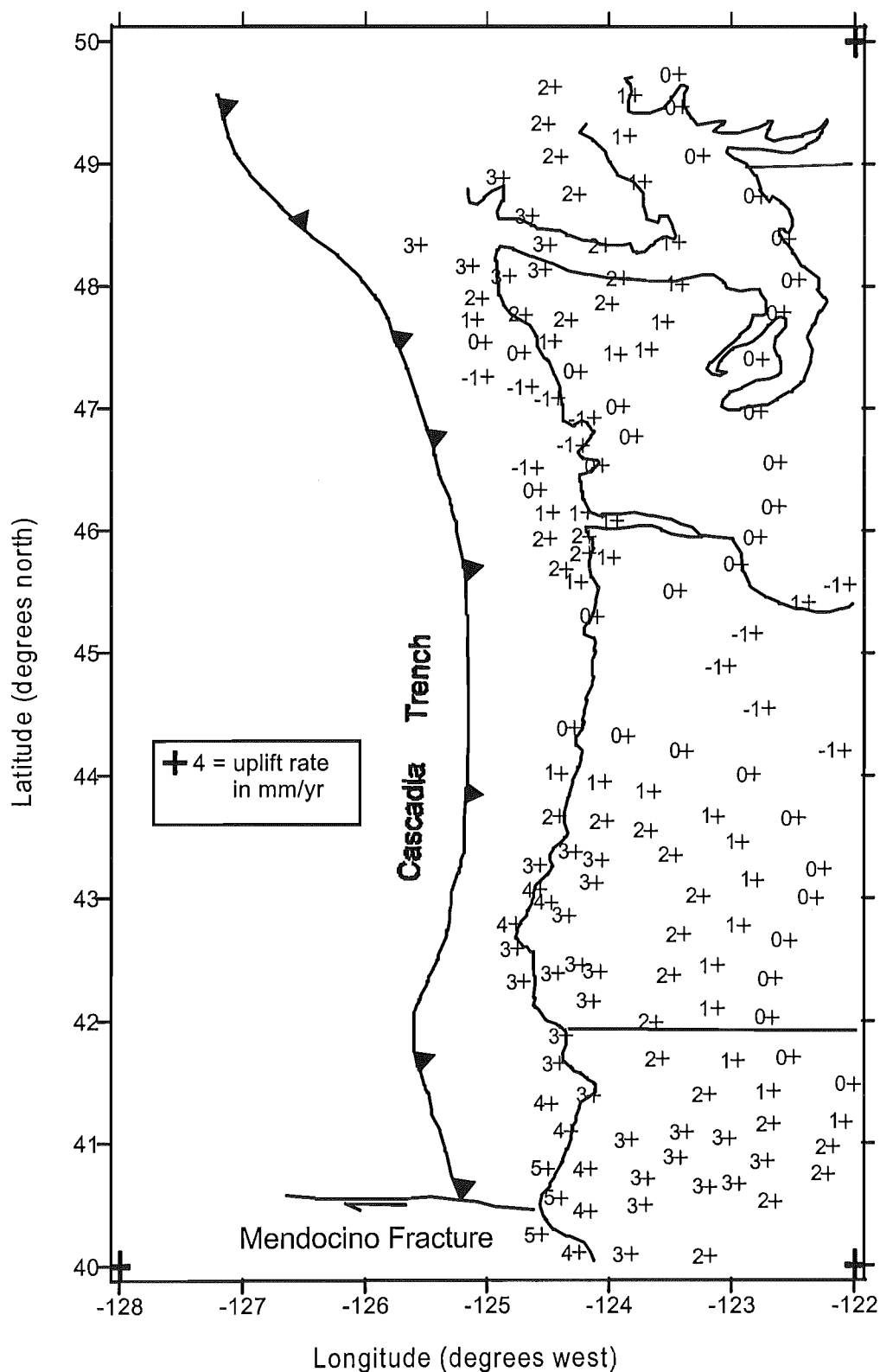


Table 5. Worksheet Calculation of Late Quaternary Uplift Rates in the PNW, as Derived from Marine Terrace Data (data derived from Muhs et al., 1990).

Terrace Name	Location	Terrace Age (ka)	Present Elevation (m)	Original Depth of Wave-Cut Platform (meters)	Paleo-Sea Level (meters)	Total Tectonic Uplift (meters)	Average Uplift Rate (m/kyr)	Average Uplift Rate (mm/yr)
		<i>a</i>	<i>b</i>	<i>c</i>	<i>d</i>	<i>e</i>	<i>f</i>	<i>g</i>
Whiskey Run	Coquille Point, OR	80	17	14	-19			
Whiskey Run	Coquille Point, OR	80	17	48	-19			
Whiskey Run	Coquille Point, OR	80	17	14	-5			
Whiskey Run	Coquille Point, OR	80	17	48	-5			
Cape Blanco	Cape Blanco, OR	80	53	10	-19			
Cape Blanco	Cape Blanco, OR	80	53	28	-19			
Cape Blanco	Cape Blanco, OR	80	53	10	-5			
Cape Blanco	Cape Blanco, OR	80	53	28	-5			
Pioneer	Cape Blanco, OR	105	57	26	-9			
Pioneer	Cape Blanco, OR	105	57	90	-9			
Pioneer	Cape Blanco, OR	105	57	26	-2			
Pioneer	Cape Blanco, OR	105	57	90	-2			

Explanation of Data:

Column a: "ka" = kiloans = 1000's of years ago (how long ago the wave-cut platform was formed)

Column b: "present elevation" = present day elevation of coastal terrace above sea level

Column c: "original depth" = original depth of wave-cut platform below sea level, at time of wave erosion

Column d: "paleo-sea level" = level of sea, relative to present, at time wave-cut platform was eroded

Column e: total tectonic uplift of wave-cut platform from time in column a to present.

Column f: tectonic uplift rate of terrace in meters per 1000 yrs

Column g: tectonic uplift rate of terrace in millimeters per yr

c:\wou\geomorph:f00:coastlab:neotect.xls / table 5 terrace data

REFERENCE TABLES

APPENDIX 7

Table for length conversion

Unit	mm	cm	m	km	in	ft	yd	mi
1 millimeter	1	0.1	0.001	10^{-6}	0.0397	0.00328	0.00109	6.21×10^{-7}
1 centimeter	10	1	0.01	0.0001	0.3937	0.0328	0.0109	6.21×10^{-6}
1 meter	1000	100	1	0.001	39.37	3.281	1.094	6.21×10^{-4}
1 kilometer	10^6	10^5	1000	1	39,370	3281	1093.6	0.621
1 inch	25.4	2.54	0.0254	2.54×10^{-5}	1	0.0833	0.0278	1.58×10^{-5}
1 foot	304.8	30.48	0.3048	3.05×10^{-4}	12	1	0.333	1.89×10^{-4}
1 yard	914.4	91.44	0.9144	9.14×10^{-4}	36	3	1	5.68×10^{-4}
1 mile	1.61×10^6	1.01×10^5	1.61×10^3	1.6093	63,360	5280	1760	1

APPENDIX 8

Table for area conversion

Unit	cm ²	m ²	km ²	ha	in ²	ft ²	yd ²	mi ²	ac
1 sq. centimeter	1	0.0001	10^{-10}	10^{-8}	0.155	1.08×10^{-3}	1.2×10^{-4}	3.86×10^{-11}	2.47×10^{-8}
1 sq. meter	10^4	1	10^{-6}	10^{-4}	1550	10.76	1.196	3.86×10^{-7}	2.47×10^{-4}
1 sq. kilometer	10^{10}	10^6	1	100	1.55×10^8	1.076×10^7	1.196×10^6	0.3861	247.1
1 hectare	10^8	10^4	0.01	1	1.55×10^7	1.076×10^6	1.196×10^5	3.861×10^{-3}	2.471
1 sq. inch	6.452	6.45×10^{-4}	6.45×10^{-10}	6.45×10^{-8}	1	6.94×10^{-3}	7.7×10^{-4}	2.49×10^{-10}	1.574×10^{-7}
1 sq. foot	929	0.0929	9.29×10^{-8}	9.29×10^{-6}	144	1	0.111	3.587×10^{-8}	2.3×10^{-5}
1 sq. yard	8361	0.8361	8.36×10^{-7}	8.36×10^{-5}	1296	9	1	3.23×10^{-7}	2.07×10^{-4}
1 sq. mile	2.59×10^{10}	2.59×10^6	2.59	259	4.01×10^9	2.79×10^7	3.098×10^6	1	640
1 acre	4.04×10^7	4047	4.047×10^{-3}	0.4047	6.27×10^6	43,560	4840	1.562×10^{-3}	1

APPENDIX 9

Table for volume conversion

Unit	mL	liters	m ³	in ³	ft ³	gal	ac-ft	million gal
1 milliliter	1	0.001	10^{-6}	0.06102	3.53×10^{-5}	2.64×10^{-4}	8.1×10^{-10}	2.64×10^{-10}
1 liter	10^3	1	0.001	61.02	0.0353	0.264	8.1×10^{-7}	2.64×10^{-7}
1 cu. meter	10^6	1000	1	61,023	35.31	264.17	8.1×10^{-4}	2.64×10^{-4}
1 cu. inch	16.39	1.64×10^{-2}	1.64×10^{-5}	1	5.79×10^{-4}	4.33×10^{-3}	1.218×10^{-8}	4.329×10^{-9}
1 cu. foot	28,317	28.317	0.02832	1728	1	7.48	2.296×10^{-5}	7.48×10^{-6}
1 U.S. gallon	3785.4	3.785	3.78×10^{-3}	231	0.134	1	3.069×10^{-6}	10^6
1 acre-foot	1.233×10^9	1.233×10^6	1233.5	75.27×10^6	43,560	3.26×10^5	1	0.3260
1 million gallons	3.785×10^9	3.785×10^6	3785	2.31×10^8	1.338×10^5	10^6	3.0684	1

APPENDIX 10

Table for time conversion

Unit	sec	min	hours	days	years
1 second	1	1.67×10^{-2}	2.77×10^{-4}	1.157×10^{-5}	3.17×10^{-8}
1 minute	60	1	1.67×10^{-2}	6.94×10^{-4}	1.90×10^{-6}
1 hour	360	60	1	4.17×10^{-2}	1.14×10^{-4}
1 day	8.64×10^4	1440	24	1	2.74×10^{-3}
1 year	3.15×10^7	5.256×10^5	8760	365	1

Unit	Equivalent ^{1,2}			
	feet per day	kilometers per hour	miles per hour	meters per second
feet per day	1	1.27×10^{-5}	1.157×10^{-5}	3.528×10^{-6}
kilometers per hour	7.874×10^4	1	0.6214	0.2778
feet per second	8.64×10^4	1.097	0.6818	0.3048
miles per hour	1.267×10^5	1.609	1	0.447
meters per second	2.835×10^5	3.6	2.237	1

Mass

Unit	Equivalent ^{1,2}					
	ounce	pound	kilogram	metric slug	short ton	long ton
ounce	1	6.25×10^{-2}	2.835×10^{-2}	1.943×10^{-3}	3.125×10^{-5}	2.79×10^{-5}
pound	16	1	0.4536	4.625×10^{-2}	5×10^{-4}	4.464×10^{-4}
kilogram	35.28	2.205	1	0.102	6.852×10^{-2}	9.842×10^{-4}
metric slug	345.9	21.62	9.807	1	92.51	9.651×10^{-3}
slug	514.7	32.17	14.59	1.49	62.17	1.436×10^{-2}
short ton	3.2×10^4	2,000	907.2	92.51	1	0.8929
ton	3.529×10^4	2,205	1,000	102	1.103	1
long ton	3.584×10^4	2,240	1,016	103.7	1.12	1

Force

Unit	Equivalent ^{1,2}		
	dyne	newton	pound _{force}
dynes	1	1×10^{-5}	2.248×10^{-6}
newtons	1×10^5	1	0.2248
pound _{force}	4.448×10^5	4.448	1
kilogram _{force}	9.807×10^5	9.807	2.205

Density

Unit	Equivalent ^{1,2}			
	pounds per cubic inch	pounds per cubic foot	pounds per gallon	grams per liter
pounds per cubic inch	1	1,728	231	2,768 $\times 10^4$
pounds per cubic foot	5.787×10^{-4}	1	0.1337	16.02
pounds per gallon	4.33×10^{-3}	7.481	1	119.8
grams per cubic centimeter	3.61×10^{-3}	62.43	8.345	1,000
grams per liter	3.61×10^{-3}	6.24×10^{-2}	8.35×10^{-3}	1

APPENDIX 9.A. Conversion Tables

Length

Unit	Equivalent ^{1,2}				
	millimeters	inches	feet	meters	kilometers
millimeters	1	3.937×10^{-2}	3.281×10^{-3}	1×10^{-3}	1×10^{-6}
inches	25.4	1	8.33×10^{-2}	2.54×10^{-2}	2.54×10^{-5}
feet	304.8	12	1	0.3048	3.048×10^{-4}
meters	1,000	39.37	3.281	1	1×10^{-3}
kilometers	1×10^6	3.937×10^4	3,281	1,000	1
miles	1.609×10^6	6.336×10^4	5,280	1,609	1

Area

Unit	Equivalent ^{1,2}						
	square inches	square feet	square meters	hectares	acres	square kilometers	square miles
square inches	1	6.944×10^{-3}	6.453×10^{-4}	1.594×10^{-8}	1.594×10^{-8}	6.453×10^{-10}	2.491×10^{-10}
square feet	144	1	9.29×10^{-2}	2.296×10^{-5}	2.296×10^{-5}	9.29×10^{-8}	3.587×10^{-8}
square meters	1,550	10.76	1	2.471×10^{-4}	2.471×10^{-4}	1×10^{-6}	3.861×10^{-7}
hectares	6.773×10^6	4.36×10^4	10,000	1	1	1×10^{-4}	3.861×10^{-5}
acres	1.55×10^7	1.076×10^5	2.471×10^4	1	1	0.001	3.861×10^{-5}
square kilometers	1.55×10^9	1.076×10^7	1×10^6	100	259	1	0.3861
square miles	4.014×10^9	2.788×10^7	2.59×10^6	259	640	2.59	1

Volume

Unit	Equivalent ^{1,2}						
	cubic inches	liters	gallons	cubic feet	cubic yards	cubic meters	acre-ft
cubic inches	1	1.639×10^{-2}	1.329×10^{-3}	5.777×10^{-4}	2.143×10^{-5}	1.639×10^{-5}	1.329×10^{-8}
liters	61.02	1	0.2642	3.531×10^{-2}	1.358×10^{-3}	0.001	8.108×10^{-7}
gallons	231.0	3.785	1	0.1337	4.951×10^{-3}	3.785×10^{-3}	3.068×10^{-6}
cubic feet	1,728	28.32	7.481	1	3.704×10^{-2}	2.832×10^{-2}	2.296×10^{-5}
cubic yards	4.666×10^4	764.6	202.0	27	1	0.7646	6.198×10^{-4}
cubic meters	6.102×10^4	1,000	264.2	35.31	1.358	1	8.108×10^{-4}
acre-ft	7.537×10^7	1.233×10^6	3.259×10^5	4.356×10^4	1,613	1,233	1

Discharge (flow rate, volume/time)

Unit	Equivalent ^{1,2}			
	gallons per minute	liters per second	acre-feet per day	cubic meters per day
gallons per minute	1	6.309×10^{-2}	4.419×10^{-3}	2.228×10^{-3}
liters per second	15.85	1	7.005×10^{-2}	3.531×10^{-2}
acre-feet per day	226.3	14.28	1	0.5042
cubic feet per second	448.8	28.32	1.983	2.447
cubic meters per day	1.369×10^4	8.64×10^3	6.051×10^4	3.051×10^4

128

TABLE 4.1 English and SI Units

$$1 \text{ N} = 1 \text{ kg} \cdot \text{m} / \text{sec}^2$$

Parameter	English Unit	SI Unit	Conversion Factor	Dimensional Formula
Force	pound (lb)	newton (N)	1 lb = 4.448 N	ML/T^2
Mass	slug	kilogram (kg)	1 slug = 14.594 kg	M
Length	foot (ft)	meter (m)	1 ft = 0.3048 m	L
Time	second (s)	second	1 s = 1 s	T
Density	slug/ft ³	kg/m ³	1 slug/ft ³ = 515.4 kg/m ³	M/L^3
Specific weight	lb/ft ³	N/m ³	1 lb/ft ³ = 157.1 N/m ³	M/L^2T^2
Pressure	lb/ft ²	N/m ²	1 lb/ft ² = 47.88 N/m ²	M/LT^2
Dynamic viscosity	lb-s/ft ²	N-s/m ²	1 lb-s/ft ² = 47.88 N-s/m ²	M/LT
Bulk modulus	lb/ft ²	N/m ²	1 lb/ft ² = 47.88 N/m ²	M/LT^2

$g = \text{Acceleration due to Gravity} = 9.8 \text{ m/sec}^2$

Equations for areas and volumes

Circumference of circle = $3.1416 \times \text{dia} = 6.2832 \times \text{radius}$

Area of circle = $0.7854 \times (\text{dia})^2 = 3.1416 \times (\text{radius})^2$

Area of sphere = $3.1416 \times (\text{dia})^2$

Volume of sphere = $0.5236 \times (\text{dia})^3$

Area of triangle = $0.5 \times \text{base} \times \text{height}$

Area of trapezoid = $0.5 \times \text{sum of the two parallel sides} \times \text{height}$

Area of square, rectangle, or parallelogram = $\text{base} \times \text{height}$

Volume of pyramid = $\text{area of base} \times 1/3 \text{ height}$

Volume of cone = $0.2618 \times (\text{dia of base})^2 \times \text{height}$

Volume of cylinder = $0.7854 \times \text{height} \times (\text{dia})^2$

Pressure

Unit	Equivalent ^{1,2}										
	pounds per square inch	pounds per square foot	atmospheres	kilograms per square centimeter	kilograms per square meter	inches of water (68°F)	feet of water (68°F)	inches of mercury (32°F)	millimeters of mercury (32°F)	bars	kilo Pascals
pounds per square inch	1	144	6.805×10^{-2}	7.031×10^{-2}	703.1	27.73	2.311	2.036	51.72	6.895×10^{-2}	6.895
pounds per square foot	6.945×10^{-3}	1	4.73×10^{-4}	4.88×10^{-4}	4.882	0.1926	1.605×10^{-2}	1.414×10^{-2}	0.3591	4.79×10^{-4}	4.79×10^{-3}
atmospheres	14.7	2,116	1	1.033	1.033×10^4	407.5	33.96	29.92	760	1.013	101.3
kilograms per square centimeter	14.22	2,048	0.9678	1	1×10^4	394.4	32.87	28.96	735.6	0.9807	98.07
kilograms per square meter	1.422×10^{-3}	0.2048	9.678×10^{-3}	0.001	1	3.944×10^{-2}	3.287×10^{-3}	2.896×10^{-3}	7.356×10^{-2}	9.807×10^{-3}	9.807×10^{-3}
inches of water (68°F)	3.609×10^{-2}	5.197	2.454×10^{-3}	2.53×10^{-3}	25.38	1	8.333×10^{-2}	7.343×10^{-2}	1.865	2.49×10^{-3}	0.249
feet of water (68°F)	0.4328	62.32	2.945×10^{-3}	3.043×10^{-3}	304.3	12	1	0.8812	22.38	2.984×10^{-2}	2.984
inches of mercury (32°F)	0.4912	70.73	3.342×10^{-2}	3.453×10^{-2}	345.3	13.62	1.135	1	25.4	3.386×10^{-2}	3.386
millimeters of mercury (32°F)	1.934×10^{-2}	2.785	1.316×10^{-2}	1.36×10^{-2}	13.6	0.5362	4.468×10^{-2}	3.937×10^{-2}	1	1.333×10^{-1}	0.1333
bars	14.5	2,089	0.9869	1.02	1.02×10^4	402.2	33.51	29.53	750.1	1	100
kilo Pascals	0.145	20.89	9.869×10^{-3}	1.02×10^{-2}	102	4.022	0.3351	0.2953	7.501	0.01	1

Appendix 9.A. Continued

1.709

FORMULAS

Composition of Forces

The resultant of two forces acting at an angle upon a given point is equal to the diagonal of a parallelogram of which the two force vectors are sides. The equilibrant equals the magnitude of the resultant, but acts in the opposite direction.

Accelerated Motion

$v = at$, or $v = gt$
 v is final velocity; a is acceleration, or g is acceleration due to gravity; t is time

Accelerated Motion

$s = \frac{1}{2}at^2$ or $s = \frac{1}{2}gt^2$
 s is total distance; a is acceleration, or g is acceleration due to gravity; t is time

Accelerated Motion

$v = \sqrt{2as}$, or $v = \sqrt{2gs}$
 v is final velocity; a is acceleration, or g is acceleration due to gravity; s is total distance

Newton's Second Law of Motion

$F = ma$
 F is force; m is mass; a is acceleration

Impulse and Momentum

$Fl = mv$
 F is force; t is time; the product Fl is impulse; m is mass; v is velocity; the product mv is momentum

Centrifugal Force

Centrifugal Force = $\frac{mv^2}{r}$
 m is mass; v is velocity; r is radius of path

Work

$W = Fs$
 W is work; F is force; s is distance

Potential Energy

$$P.E. = mgh$$

P.E. is potential energy; m is mass; g is acceleration due to gravity; h is vertical distance

Kinetic Energy

$$K.E. = \frac{1}{2}mv^2$$

K.E. is kinetic energy; m is mass; v is velocity

PHYSICAL CONSTANTS

$C = 2.9979 \times 10^8 \text{ m/s}$
 $G = 6.6720 \times 10^{-11} \text{ m}^2 \cdot \text{s}^{-2} \cdot \text{kg}^{-1}$
 $e = 1.6022 \times 10^{-19} \text{ C}$
 $\epsilon/m_e = 1.7588 \times 10^{11} \text{ C} \cdot \text{kg}^{-1}$
 $F = 9.6485 \times 10^4 \text{ C} \cdot \text{mol}^{-1}$
 $V_m = 22.4138 \times 10^{-3} \text{ m}^3 \cdot \text{mol}^{-1}$
 $h = 6.6262 \times 10^{-34} \text{ J} \cdot \text{s}$
 $R = 8.3144 \text{ J} \cdot \text{mol}^{-1} \cdot \text{K}^{-1}$
 $N_A = 6.0220 \times 10^{23} \text{ mol}^{-1}$
 Atomic Mass Unit $\mu = 1.6606 \times 10^{-27} \text{ kg}$
 $M_e = 9.1094 \times 10^{-31} \text{ kg}$
 1 Kilogram Calorie (Nutrition Calorie) = 4,1868 Kilojoules
 1 BTU = 1,0551 kJ

RELATIONS BETWEEN COMMON UNITS

LENGTH

1 in = 2.540 cm
 1 ft = 30.48 cm
 1 micron (μ) = 0.00001 m = 0.001 mm = 10^{-6} m
 1 millimicron ($m\mu$) = 10^{-9} m
 1 Angstrom Unit = 10^{-10} m

VOLUME

1 liter = 1000 cm³ = 61.024 in³ = 1.05671 qt.

MASS

1 lb = 453.59 g
 1 kg = 2,204.6 lb

ANGLES

1 circumference = 360° = 2π radians
 1 radian = 57.2958°

DENSITY

1 g/cm³ = 62.4 lb/ft³

WORK OR ENERGY

1 ft-lb = 1.356 X 10³ ergs
 1 joule = 10⁷ ergs
 1 B.T.U. = 4.186 X 10³ ergs
 1 B.T.U. = 777.8 ft-lb = 252.2 g cal

POWER

1 H.P. = 33,000 ft-lb/min
 = 550 ft-lb/sec = 746 watts
 1 watt = 1 joule/second

ELECTRICAL UNITS

1 ampere = 10³ ab amps = 3 X 10⁹ ESU
 1 volt = 10⁸ EMU = 1/3 X 10⁹ ESU
 1 coulomb = 10⁹ EMU = 3 X 10⁹ ESU
 1 ohm = 10⁹ EMU = 9 X 10¹¹ ESU
 1 farad = 10⁹ EMU = 9 X 10¹¹ ESU
 1 henry = 10⁹ EMU = 9 X 10¹¹ ESU

CHEMISTRY

SYMBOLS OF SOME PARTICLES

electron	-e	deuteron	² H
neutron	n ⁰	triton	³ H
proton	¹ H	alpha particle	⁴ He ²⁺

OXIDATION STATE OF SOME RADICALS

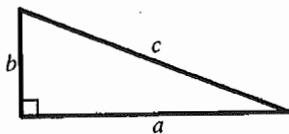
CH ₃ COO	ClO ₂	H ₂ PO ₄	NO ₂
CO ₃	CrO ₄	H ₂ O ₂	OH
C ₂ O ₄	HCO ₃	Hg ₂	PO ₄
ClO	HPO ₄	MnO ₂	PO ₃
ClO ₂	H ₂ SO ₄	NH ₄	SO ₃
ClO ₃		NO ₂	SO ₂

PERIODIC TABLE OF THE ELEMENTS

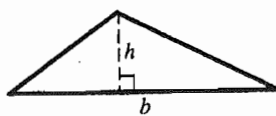
Atomic weights conform to the 1961 values of the Commission on Atomic Weights.

KEY															
Atomic Mass (Weight) — 12.01115															
Symbol — C															
Atomic Number — 6															
GROUPS															
IIIA		IVA		VA		VIA		VIIA		0					
1		2		3		4		5		6		7			
1.00794		4.0026						H		He					
3		4		5		6		7		8		9			
5.9815		28.086		30.9738		32.064		35.453		39.948					
Al		Si		P		S		Cl		Ar					
13		14		15		16		17		18					
69.72		72.59		74.9216		78.96		79.904		83.80					
Ga		Ge		As		Se		Br		Kr					
31		32		33		34		35		36					
114.82		118.69		121.75		127.60		126.9044		131.30					
In		Sn		Sb		Te		I		Xe					
50		51		52		53		54		55					
207.19		208.980		(210)		(210)		(222)		Rn					
82		83		84		85		86		87					
82.50		164.930		167.26		186.934		173.04		174.97					
Dy		Ho		Er		Tm		Yb		Lu					
67		68		69		70		71		72					
(249)		(254)		(253)		(256)		(254)		(257)					
Cf		Es		Fm		Md		No		Lw					
98		99		100		101		102		103					

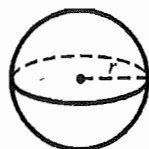
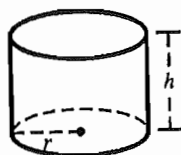
GEOMETRIC FORMULAS



Right Triangle



Any Triangle



● Triangles

Pythagorean Theorem $a^2 + b^2 = c^2$

Area $A = \frac{1}{2}bh$

● Circles

Area $A = \pi r^2$

Circumference $C = 2\pi r$

● Cylinders

Surface Area $S = 2\pi r^2 + 2\pi rh$

Volume $V = \pi r^2 h$

● Cones

Surface Area $S = \pi r^2 + \pi r \sqrt{r^2 + h^2}$

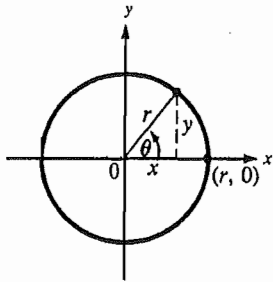
Volume $V = \frac{1}{3}\pi r^2 h$

● Spheres

Surface Area $S = 4\pi r^2$

Volume $V = \frac{4}{3}\pi r^3$

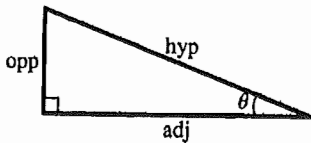
TRIGONOMETRIC FUNCTIONS AND LAWS



● Definitions Based on the Circle

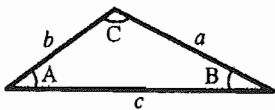
$$\begin{aligned}\cos \theta &= \frac{x}{r} & \sec \theta &= \frac{r}{x} \\ \sin \theta &= \frac{y}{r} & \csc \theta &= \frac{r}{y} \\ \tan \theta &= \frac{y}{x} & \cot \theta &= \frac{x}{y}\end{aligned}$$

For the unit circle, $r = 1$



● Definitions Based on the Right Triangle

$$\begin{aligned}\cos \theta &= \frac{\text{adj}}{\text{hyp}} & \sec \theta &= \frac{\text{hyp}}{\text{adj}} \\ \sin \theta &= \frac{\text{opp}}{\text{hyp}} & \csc \theta &= \frac{\text{hyp}}{\text{opp}} \\ \tan \theta &= \frac{\text{opp}}{\text{adj}} & \cot \theta &= \frac{\text{adj}}{\text{opp}}\end{aligned}$$



● Law of Sines

$$\frac{\sin A}{a} = \frac{\sin B}{b} = \frac{\sin C}{c}$$

● Law of Cosines

$$\begin{aligned}a^2 &= b^2 + c^2 - 2bc \cos A \\ \cos A &= \frac{b^2 + c^2 - a^2}{2bc}\end{aligned}$$

182

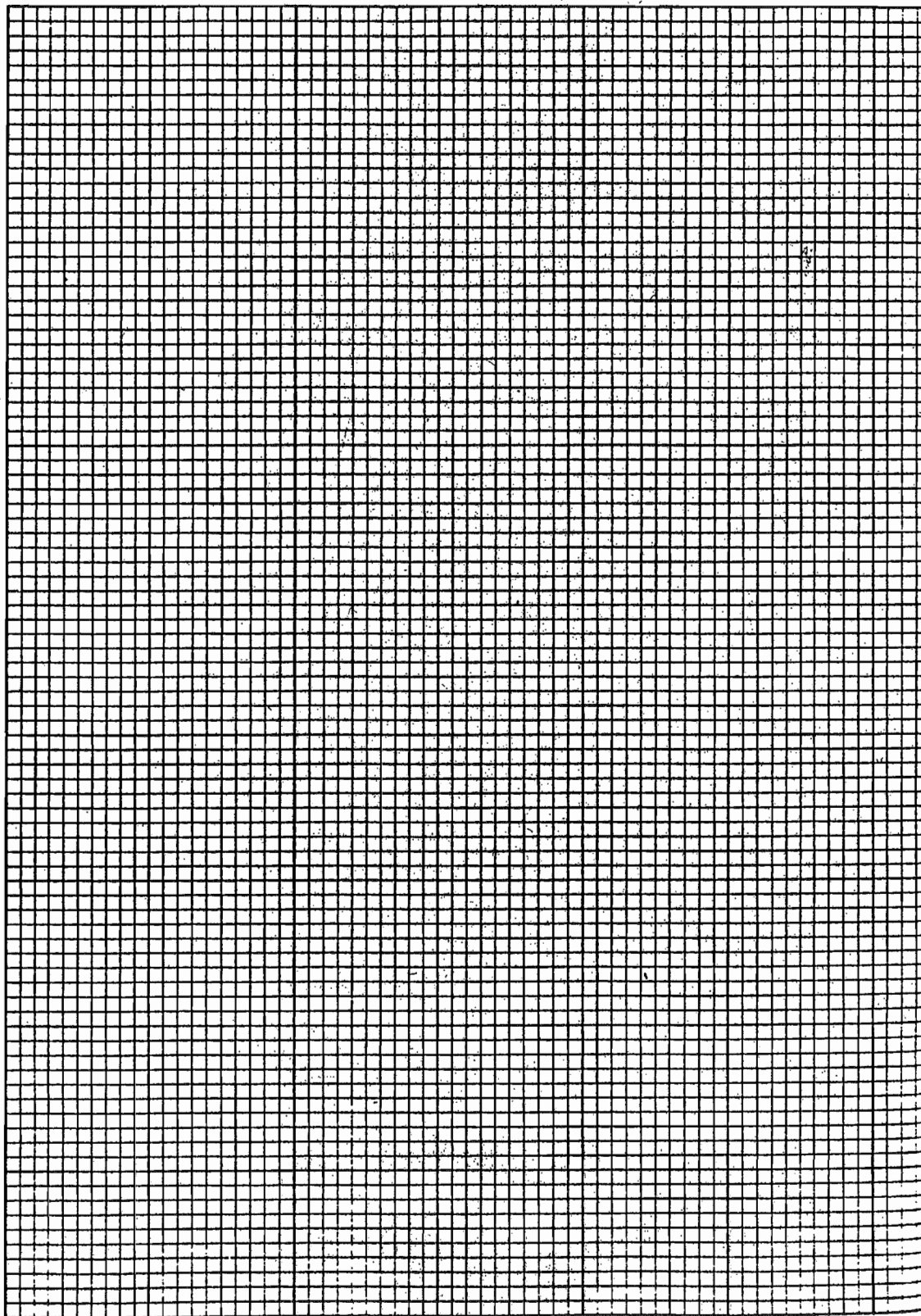
Blank Pages for Field Notes

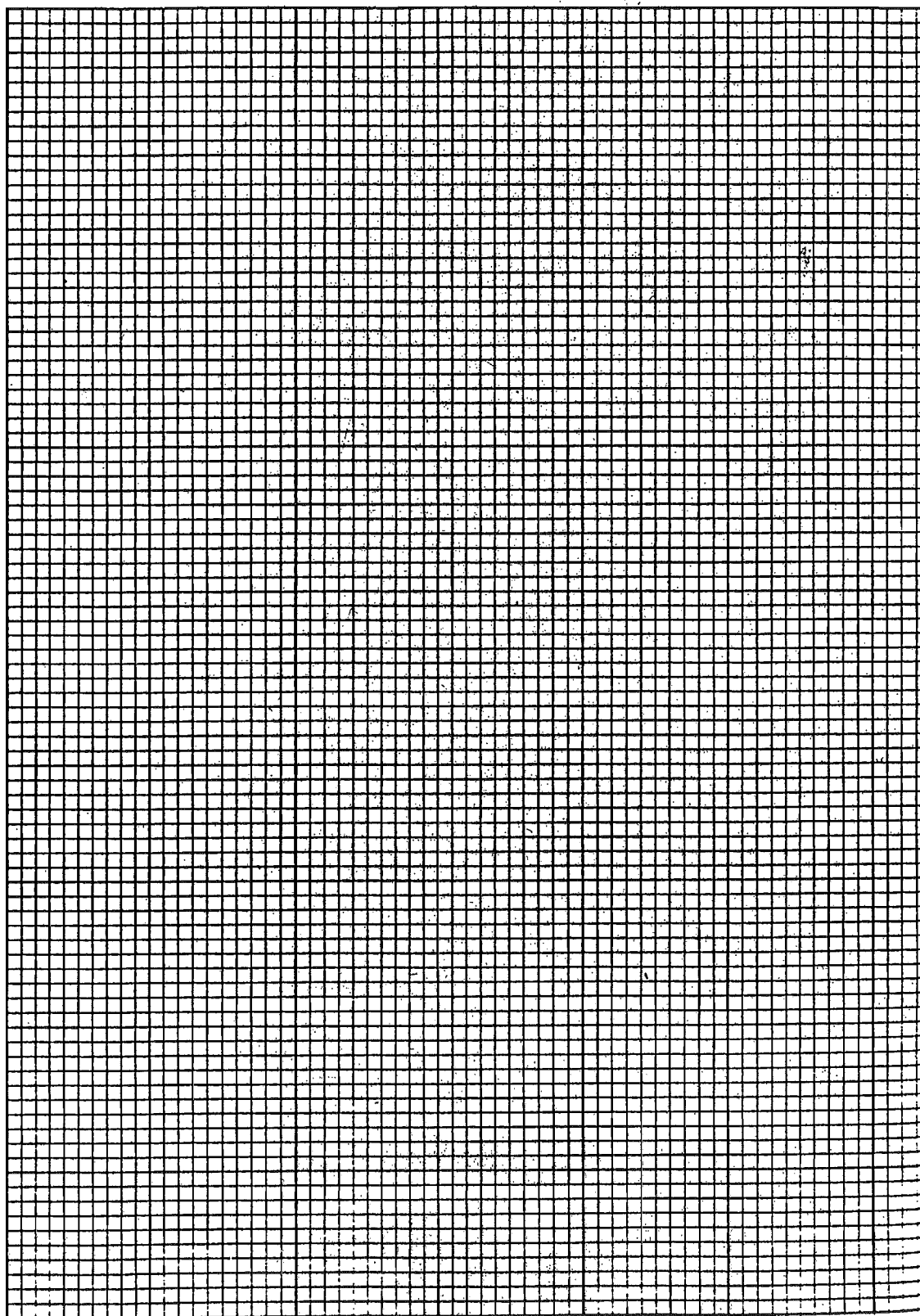
103

~~211~~

218

258





23